JOURNAL OF RESEARCH of the National Bureau of Standards—A. Physics and Chemistry
Vol. 73A, No. 5, September-October 1969

Conversion of Existing Calorimetrically Determined Thermodynamic Properties to the Basis of the International Practical Temperature Scale of 1968

Thomas B. Douglas

Institute for Basic Standards, National Bureau of Standards, Washington, D.C. 20234

(June 20, 1969)

Formulas are derived for converting the relative enthalpy, heat capacity, entropy, and Gibbs energy from the basis of one practical temperature scale to the basis of another, when these properties on either scale have been derived from calorimetric measurements of enthalpy as though that scale were the thermodynamic one. These formulas are directly applicable for converting certain other properties as well. The conversion relates the values of the property at the same numerical temperature on both scales. The formulas, given as exact infinite series, are applicable to widely differing scales, one of which may vary linearly with a temperature-measuring quantity such as electrical resistance. However, great simplification is well within most calorimetric accuracy when the conversion is from the International Practical Temperature Scale of 1948 to the corresponding scale of 1968, which has recently replaced it, provided the heat capacity is not changing abnormally rapidly, as in a transition region. For convenient application to conversion between these two scales, relatively simple numerical equations are derived giving the differences between the two scales at temperatures from 90 K to 10,000 K. The problem of avoiding the introduction of discontinuities with temperature in converted tables, arising from the existing discontinuities in the temperature derivative of the differences between the two scales, is discussed.

Key words: Existing property tables; IPTS–48; IPTS–68; practical-scale differences; temperature-scale conversion; thermodynamic properties.

1. Introduction

The International Practical Temperature Scale of 1968 ("IPTS–68") was adopted in 1968 [1][1] as a replacement for the corresponding scale of 1948 (amended edition of 1960) ("IPTS–48"). The IPTS–68 serves the same general purposes as the IPTS–48, but better: its specification is more consistent with current experimental capabilities for reproducing temperature, it more closely approximates the thermodynamic temperature scale, and it extends the temperature range downward (from approximately 90 K in the IPTS–48 to approximately 14 K in the IPTS–68).

The great preponderance of quantitative macroscopic properties of matter vary appreciably with temperature. As a consequence, it will be of interest and concern as to the extent to which numerous existing values of these properties, expressed in reference to temperatures on the IPTS–48 or an earlier scale, would change if referred to temperatures on the IPTS–68. In the case of the most accurate values it will be desirable to make the actual conversion—for the sake of future consistency, for facilitating direct comparison with future values expressed in reference to the IPTS–68, and for better thermodynamic accuracy when this is significant. In what will undoubtedly be the more common case of less accurate values, one will want to know the magnitudes of the errors neglected if such a conversion is not made. Incidentally, tables of thermodynamic properties of ideal gases derived statistical-mechanically from molecular-constant data

[1] Figures in brackets indicate the literature references at the end of this paper.

are based on the thermodynamic temperature scale (as well as on the values of the physical constants used), and are hence independent of any practical temperature scale.

This article is limited to a consideration of the more common thermodynamic properties derived from calorimetric data—enthalpy, heat capacity, entropy, and Gibbs (free) energy—with particular attention to the substitution of the IPTS–68 for the IPTS–48 as a temperature basis. The differences between these two scales (listed numerically in table 4 of this article) are not so large but that very simple procedures which have been previously used,[2] and which are virtually self-evident, are adequate within the accuracy of most existing calorimetric data. However, it seems worthwhile to outline systematically the rigorous conversion procedures, which may be required not only in regions of sharp transitions but also in those cases where the correction terms are large, as when one is converting from an arbitrary temperature scale such as one related very simply (for convenience) to thermometer resistance, thermocouple electromotive force, or radiative brightness.

In section 2, conversion formulas (exact as infinite series) are derived for converting the thermodynamic properties named above to the basis of a new temperature scale, in terms of the difference between the two scales as a continuous function of temperature. The thermodynamic properties are assumed to be based on experimental measurements of enthalpy increments that span the entire temperature range of interest. Thus the correction to be applied to an enthalpy increment involves merely associating it with different boundary temperatures, but the corrections to the properties derived from the enthalpy (heat capacity, entropy, etc.) involve in addition what is essentially a repetition of the differentiation or integration as if the new temperature scale, not the old, corresponds to true thermodynamic temperatures. The formulas derived convert the properties at a given temperature on the old scale to those at the same numerical value of temperature on the new scale, thus preserving the "round" temperature values of most tables. When, instead, it is desired to make conversion to a fixed-point temperature whose values are different on the two scales, the additional step simply involves the variation of the given property with temperature on one of the scales, and can be readily carried out by standard thermodynamic procedures.

Some non-calorimetric properties may be converted to the basis of the new temperature scale using the same formulas derived in this article. For example, if the linear coefficient of thermal expansion is defined as $(1/l)\ (dl/dt)$, then this coefficient or $\ln l$ can replace C_p or H, respectively.

In section 2.5 it is shown what modifications are needed when extrapolation of calorimetric data to 0 K has been effected by such means as the well-known "T^3" law. Simple approximate correction formulas, obtained by dropping all terms of the exact infinite series that are of no practical value when the conversion is from the IPTS–48 to the IPTS–68 and outside sharp-transition regions, are given in section 2.6.

In section 3, a numerical equation giving the difference between the IPTS–68 and the IPTS–48 ($T_{68}-T_{48}$, or $t_{68}-t_{48}$) as a function of temperature is derived for each of the four temperature ranges above the oxygen boiling point (approximately 90 K) that are defined separately by the IPTS–68. Values of $T_{68}-T_{48}$ and its first temperature derivative, calculated from these equations, are tabulated up to 10,000 K in section 3.6, for use in the formulas of section 2; the values of $T_{68}-T_{48}(=t_{68}-t_{48})$ agree perfectly with a recently published tabulation [1]. Though the IPTS–68 is defined from 13.81 to 90.188 K, the IPTS–48 was not, so the two scales cannot be compared in this temperature range. (Tentative differences in this range between the IPTS–68 and each of four "national" scales are being published, but it is stated that these differences may undergo changes of up to several millikelvins when the national scales are finally compared accurately to the IPTS–68 [3].)

The first temperature derivative of $T_{68}-T_{48}$ is continuous at the ice point (0 °C), but has sharp discontinuities at the "antimony" and gold points (approximately 631 and 1064 °C) which will

[2] E.g., several years ago the author derived corrections to convert the thermodynamic properties of mercury from the basis of practical temperature scales to what was at that time regarded as the best available approximation to the scale of thermodynamic temperatures [2].

introduce corresponding small discontinuities at these temperatures into a heat capacity-temperature function that has previously been smoothed. This problem is discussed in section 3.5. where suggested "smoothing" equations to eliminate these discontinuities are derived.

2. Derivation of General Conversion Formulas

2.1. Enthalpy (H)

The conversion formula derived in this section for enthalpy (and those derived in sections 2.2–2.6 for other properties as well) are for clarity expressed specifically in terms of conversion from the IPTS–48 to the IPTS–68. Because these formulas (in sections 2.1–2.5) are exact, any other pair of continuous temperature scales may be used instead. For example, one of these scales might be defined as some linear function of thermometer resistance or thermocouple electromotive force.

The formulation is given in terms of what is now called the International Practical Kelvin (absolute) temperature (T), which is numerically greater than the International Practical Celsius temperature (t) by 273.15. This constant was adopted for the IPTS–68 [1], and for the IPTS–48 in 1954. (Between 1948 and 1954 this constant was not officially defined, but was usually taken as 273.16.) Thus we shall always use

$$T_{68} = t_{68} + 273.15 \tag{1}$$

and

$$T_{48} = t_{48} + 273.15, \tag{2}$$

designating the value of the temperature on either IPTS as Kelvin or Celsius interchangeably as may prove convenient.

We shall often find it convenient to refer specifically to a pair of temperatures [3] (referred to as temperatures 1 and 2 and symbolized by single prime and double prime, respectively), and consider the case of converting the enthalpy (or any other property) from its value on the basis of the IPTS–48 at temperature 1 to its value on the basis of the IPTS–68 at temperature 2. As stated in the introduction (sec. 1), these two temperatures will be related to each other such that numerically

$$T''_{68} = T'_{48}. \tag{3}$$

Since such thermodynamic properties as enthalpy cannot be assigned absolute values and therefore are usually expressed numerically as the magnitude in excess of the enthalpy at a reference temperature, it will be convenient to use the symbol H to represent this relative enthalpy. Because it simplifies the treatment, the reference temperature is to be restricted to one having the same value on both temperature scales (e.g., 273.16 K, but not 298.15 K). The situation under discussion may be clarified somewhat by reference to figures 1 and 2, which are schematic and are not to be taken as implying a given sign or magnitude of $(T'_{68} - T'_{48})$ or $(T''_{68} - T''_{48})$.

The relative enthalpy will be assumed to be given by heat measurements at constant pressure, but it will be convenient to omit the indication of the constancy of pressure from derivatives of enthalpy. The lack of both a single and a double prime will imply a temperature unspecified in relation to temperatures 1 and 2. For convenience we shall abbreviate according to the further definitions:

$$C_p^{68} \equiv dH/dT_{68}; \tag{4}$$

$$C_p^{48} \equiv dH/dT_{48}; \tag{5}$$

$$\mu[=\mu(T_{68})] \equiv T_{68} - T_{48} \text{ at a given temperature.} \tag{6}$$

[3] Subsequent use of the word "temperature" instead of "temperature value" is restricted to mean "hotness."

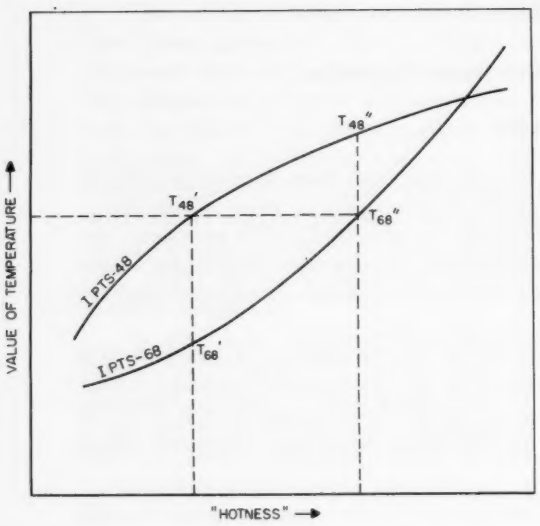

FIGURE 1. *Schematic example illustrating the relation of* T_{48} *and* T_{68} *to "hotness."*

(The thermodynamic or *any* other temperature scale whose temperature values continually increase with increasing "hotness" may be used as a quantitative measur of "hotness.")

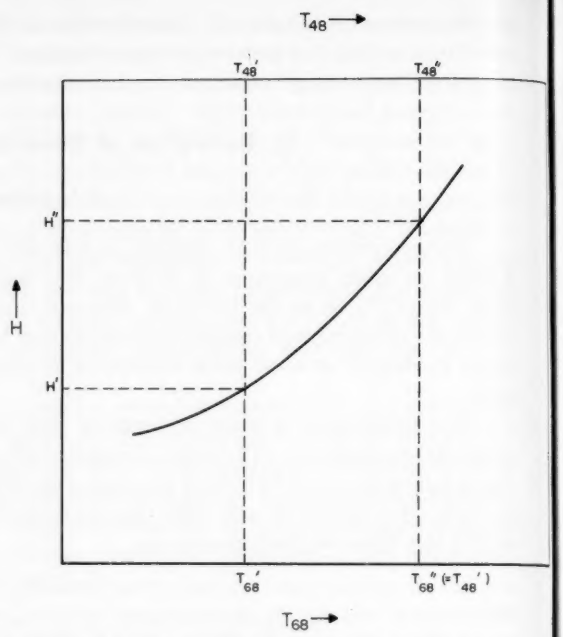

FIGURE 2. *Schematic example illustrating the conventions used in converting relative enthalpy* (H) *from the basis of one temperature scale (e.g.,* T_{48}*) to that of another scale (e.g.,* T_{68}*).*

H' (at T'_{48}) is converted to H'' (at T''_{68}).

In more specific form for future reference, eq (6) can of course be written

$$\mu' = T'_{68} - T'_{48} \tag{7}$$

or

$$\mu'' = T''_{68} - T''_{48}. \tag{8}$$

From eq (3) and (8),

$$\mu'' = T'_{48} - T''_{48}. \tag{9}$$

From eq (6),

$$\frac{dT_{48}}{dT_{68}} = 1 - \frac{d\mu}{dT_{68}}, \tag{10}$$

and therefore

$$\frac{dT_{68}}{dT_{48}} = \frac{1}{1 - \frac{d\mu}{dT_{68}}}. \tag{11}$$

The Taylor expansion of $H(T_{48})$ about H' is [remembering eq (5)]

$$H = H' + (T_{48} - T'_{48})\ (C_\beta^{48})' + \frac{1}{2}\ (T_{48} - T'_{48})^2 \left(\frac{dC_\beta^{48}}{dT_{48}}\right)' + \frac{1}{6}\ (T_{48} - T'_{48})^3 \left(\frac{d^2C_\beta^{48}}{dT_{48}^2}\right)' + \ldots \tag{12}$$

Substituting H'' for H and T''_{48} for T_{48} in eq (12), then replacing $(T''_{48} - T'_{48})$ from eq (9), gives the desired enthalpy correction δH,

$$\delta H = H'' - H' = -\mu''(C_p^{48})' + \frac{1}{2}(\mu'')^2\left(\frac{dC_p^{48}}{dT_{48}}\right)' - \frac{1}{6}(\mu'')^3\left(\frac{d^2C_p^{48}}{dT_{48}^2}\right)' + \ldots . \quad (13)$$

Equation (13) is in a convenient form: H and its derivatives with respect to T_{48} are presumed known (or evaluable) at the round value of temperature $T_{48} = T'_{48}$, whereas μ is assumed to be known as a function of T_{68} and so can readily be evaluated at the temperature where $T_{68} = T''_{68}$ $(= T'_{48})$, also a round value of temperature.

Equation (13) is exact (as an infinite series). However, of the rhs (right-hand side), only the first term is, usually, not negligible in practice (see sec. 2.6).

Reverting temporarily to the usual definition of the symbol H as representing absolute enthalpy at some one temperature, let us exemplify enthalpy relative to that at a temperature where $\mu \neq 0$ by $H - H_{298.15}$. Obviously $\delta(H - H_{298.15}) \equiv \delta(H - H_c) - \delta(H_{298.15} - H_c)$. Each of the two terms of the right-hand side be evaluated separately from eq (13) with reference to a temperature c (say, 0 K) where $\mu = 0$.

2.2 Heat Capacity (C_p)

The Taylor expansion of heat capacity as a function of T_{48} about $(C_p^{48})'$ is [after replacing C_p^{48} by $(C_p^{48})''$, T_{48} by T''_{48}, and then $(T''_{48} - T'_{48})$ from eq (9)]

$$(C_p^{48})'' = (C_p^{48})' - \mu''\left(\frac{dC_p^{48}}{dT_{48}}\right)' + \frac{1}{2}(\mu'')^2\left(\frac{d^2C_p^{48}}{dT_{48}^2}\right)' - \ldots . \quad (14)$$

From eq (4), (5), and (11),

$$(C_p^{48})'' = (C_p^{68})''\left[\frac{1}{1 - \left(\frac{d\mu}{dT_{68}}\right)''}\right]. \quad (15)$$

Substituting for $(C_p^{48})''$ from eq (15) into eq (14) and then solving for $(C_p^{68})'' - (C_p^{48})'$ gives the desired heat-capacity correction δC_p,

$$\delta C_p = (C_p^{68})'' - (C_p^{48})' = -\left(\frac{d\mu}{dT_{68}}\right)''(C_p^{48})' + \left[1 - \left(\frac{d\mu}{dT_{68}}\right)''\right]\left[-\mu''\left(\frac{dC_p^{48}}{dT_{48}}\right)' + \frac{1}{2}(\mu'')^2\left(\frac{d^2C_p^{48}}{dT_{48}^2}\right)' - \ldots\right]. \quad (16)$$

Equation (16) is exact (as an infinite series). In practice, $\left|\frac{d\mu}{dT_{68}}\right| \ll 1$, so that the factor $\left[1 - \left(\frac{d\mu}{dT_{68}}\right)''\right]$ may be replaced by 1 (approximate).

2.3. Absolute "Third-Law" Entropy (S)

We wish to find the equivalent of $(S^{68})'' - (S^{48})'$, each term of which is taken to represent entropy relative to that at 0 K (*absolute* entropy if the Third Law of Thermodynamics holds) and is evaluated from the enthalpy data at its respective indicated temperature value on the assumption that the respective indicated IPTS represents the thermodynamic temperature.

Since both $(S^{68})''$ and $(S^{48})'$ involve integration down to 0 K, it is convenient to formulate them separately, then take the difference. Consider dS^{68} and dS^{48} over a definite infinitesimal temperature range, dH being a fixed experimentally determined quantity. Then

$$dS^{68} = \frac{dH}{T_{68}} \quad (17)$$

and

$$dS^{48} = \frac{dH}{T_{48}}. \quad (18)$$

Replacing dH from eq (5) and T_{68} from eq (6), eq (17) becomes

$$dS^{68}=\left(\frac{C_p^{48}}{T_{48}+\mu}\right)dT^{48}. \tag{19}$$

Integrating eq (19),

$$(S^{68})''=\int_0^{T_{48}}\left(\frac{C_p^{48}}{T_{48}+\mu}\right)dT_{48}+(S^{68})''-(S^{68})' \tag{20}$$

Similarly using eq (5), the integration of eq (18) gives

$$(S^{48})'=\int_0^{T_{48}}\frac{C_p^{48}}{T_{48}}dT_{48}. \tag{21}$$

Subtracting eq (21) from eq (20),

$$(S^{68})''-(S^{48})'=-\int_0^{T_{48}}\frac{\mu C_p^{48}dT_{48}}{T_{48}(T_{48}+\mu)}+(S^{68})''-(S^{68})' \tag{22}$$

$(S^{68})''-(S^{48})'$ is the desired correction ($\equiv\delta S$), but it remains (a) to formulate $\mu(T_{48})$ from the presumably known $\mu(T_{68})$ for use in eq (22), and (b) to substitute for $(S^{68})''-(S^{68})'$ in terms of known quantities, remembering that S^{48} and its derivatives with respect to T_{48} are known at $T_{48}=T'_{48}$, whereas μ and its derivatives with respect to T_{68} are known at $T_{68}=T''_{68}$, numerically the same value of temperature.

Expanding $\mu(T_{48})$ about μ'', then setting $\mu=\mu'$,

$$\mu'=\mu''+(T'_{48}-T''_{48})\left(\frac{d\mu}{dT_{48}}\right)''+\frac{1}{2}(T'_{48}-T''_{48})^2\left(\frac{d^2\mu}{dT_{48}^2}\right)''+\ldots. \tag{23}$$

Substituting from eq (9), eq (23) gives

$$\mu'=\mu''\left[1+\left(\frac{d\mu}{dT_{48}}\right)''\right]+\frac{1}{2}(\mu'')^2\left(\frac{d^2\mu}{dT_{48}^2}\right)''+\ldots. \tag{24}$$

Using eq (11), we can write

$$\frac{d\mu}{dT_{48}}\equiv\frac{d\mu}{dT_{68}}\frac{dT_{68}}{dT_{48}}=\frac{\dfrac{d\mu}{dT_{68}}}{1-\dfrac{d\mu}{dT_{68}}}. \tag{25}$$

Differentiating eq (25) with respect to T_{48} gives

$$\frac{d^2\mu}{dT_{48}^2}=\frac{\dfrac{d^2\mu}{dT_{68}^2}}{\left(1-\dfrac{d\mu}{dT_{68}}\right)^3}. \tag{26}$$

Substituting from eq (25) and (26) for the derivatives in eq (24) gives

$$\mu'=\frac{\mu''}{1-\left(\dfrac{d\mu}{dT_{68}}\right)''}+\frac{\dfrac{1}{2}\left(\dfrac{d^2\mu}{dT_{68}^2}\right)''(\mu'')^2}{\left[1-\left(\dfrac{d\mu}{dT_{68}}\right)''\right]^3}+\ldots \tag{27}$$

We are assuming μ to be available in the form $\mu(T_{68})$. Consider any given value of T_{48} in the integrand of eq (22); if we temporarily call it T'_{48} (not to be confused with the T'_{48} which forms the upper limit of integration), then the μ to be associated with it is, of course, μ at $T_{48}=T'_{48}$, or μ'. This μ' can be obtained from eq (27), since, in view of eq (3), the corresponding μ'' is μ at $T_{68}=T''_{68}=T'_{48}$. Hence the μ to use in the integrand of eq (22) is μ' of eq (27), where μ'' and its derivatives with respect to T_{68} are evaluated, with T_{68} then replaced by T_{48}. Expressed more concisely, where ψ designates a definite function defined by the rhs of eq (27):

$$\left.\begin{aligned}\mu' &= \psi(T''_{68});\\ \mu(T_{48}) &= \psi(T_{48}).\end{aligned}\right\} \tag{28}$$

Although eq (27) as an infinite series is exact, in practice $\left|\frac{d\mu}{dT_{68}}\right| \ll 1$, $\mu\left|\frac{d^2\mu}{dT_{68}^2}\right| \ll 1$, etc., so that

$$\mu' \simeq \mu''. \tag{29}$$

Turning to the formulation of $(S^{68})''-(S^{68})'$ [needed in using eq (22)], let us expand $S^{68}(T_{48})$ about $(S^{68})'$. Then successively replacing S^{68} by $(S^{68})''$, T_{48} by T''_{48}, and $T''_{48}-T'_{48}$ from eq (9), we get

$$(S^{68})''-(S^{68})' = -\mu''\left(\frac{dS^{68}}{dT_{48}}\right)' + \frac{1}{2}(\mu'')^2\left(\frac{d^2S^{68}}{dT_{48}^2}\right)' - \cdots \tag{30}$$

From eq (19)

$$\frac{dS^{68}}{dT_{48}} = \frac{C_P^{48}}{T_{48}+\mu}, \tag{31}$$

and differentiating eq (31),

$$\frac{d^2S^{68}}{dT_{48}^2} = \left(\frac{1}{T_{48}+\mu}\right)\frac{dC_P^{48}}{dT_{48}} - \frac{C_P^{48}}{(T_{48}+\mu)^2}\left(1+\frac{d\mu}{dT_{48}}\right). \tag{32}$$

From eq (25),

$$1+\frac{d\mu}{dT_{48}} = \frac{1}{1-\dfrac{d\mu}{dT_{68}}}. \tag{33}$$

Equations (31)–(33) convert eq (30) into

$$(S^{68})''-(S^{68})' = -\frac{\mu''(C_P^{48})'}{T'_{48}+\mu'}\left\{1+\frac{\frac{1}{2}\mu''}{[T'_{48}+\mu']\left[1-\left(\frac{d\mu}{dT_{68}}\right)'\right]}\right\} + \frac{\frac{1}{2}(\mu'')^2}{T'_{48}+\mu'}\left(\frac{dC_P^{48}}{dT_{48}}\right)' + \cdots \tag{34}$$

Finally, substituting for $(S^{68})''-(S^{68})'$ into eq (22) from eq (34) gives the desired entropy correction δS,

$$\delta S = (S^{68})''-(S^{48})' = -\int_0^{T_{48}} \frac{\mu C_P^{48}\,dT_{48}}{T_{48}(T_{48}+\mu)} - \frac{\mu''(C_P^{48})'}{T'_{48}+\mu'}\left\{1+\frac{\frac{1}{2}\mu''}{[T'_{48}+\mu']\left[1-\left(\frac{d\mu}{dT_{68}}\right)'\right]}\right\} + \frac{\frac{1}{2}(\mu'')^2}{T'_{48}+\mu'}\left(\frac{dC_P^{48}}{dT_{48}}\right)' + \cdots, \tag{35}$$

where, if eq (29) is not a sufficiently good approximation, $\mu(T_{48})$ in the integrand can be evaluated as μ' from eq (27) [in view of eq (28)], and where μ' and $\left(\frac{d\mu}{dT_{68}}\right)'$ can also be found from eq (27).

The contribution of any first-order process (such as a heat of transition, fusion, or vaporization) to $C_P^{48}dT_{48}$ in eq (35) is indeterminate, and must be replaced by dH, whose integral is the heat of that process.

Equation (35) as an infinite series is exact, but it does assume calorimetric evaluation of $C_P^{48}(T_{48})$ all the way down to 0 K. When this assumption is invalid, see section 2.5.

2.4. Other Thermodynamic Functions

The other thermodynamic functions commonly used in chemical thermodynamics can be readily converted from the basis of one temperature scale to that of another using the corrections found above (secs. 2.1 and 2.3) for the enthalpy, H, and the absolute entropy, S. For example, consider the enthalpy function H/T, more explicitly written $(H_T-H_0)/T$ when H is understood to represent the enthalpy at temperature T relative to the enthalpy at absolute zero. Using eq (3) and our previous notation, the correction $\delta(H/T)$ is given by

$$\delta\left(\frac{H}{T}\right)=\frac{H''}{T''_{68}}-\frac{H'}{T'_{48}}=\frac{H''-H'}{T'_{48}} \tag{36}$$

or simply the correction to the enthalpy, divided by the value of the Kelvin temperature. The correction δG to the Gibbs energy is given by

$$\delta G=(G^{68})''-(G^{48})'=[H''-T''_{68}(S^{68})'']-[H'-T'_{48}(S^{48})']=H''-H'-T'_{48}[(S^{68})''-(S^{48})'], \tag{37}$$

where H and G are both understood to be relative to the enthalpy H at some one temperature which has the same value on both temperature scales. The correction $\delta(-G/T)$ to the "free-energy function" $-(G_T-H_0)/T$, when the latter is abbreviated to $-G/T$, is analogous to eq (36):

$$\delta\left(-\frac{G}{T}\right)=\left[-\frac{(G^{68})''}{T''_{68}}\right]-\left[-\frac{(G^{48})'}{T'_{48}}\right]=-\frac{[(G^{68})''-(G^{48})']}{T'_{48}}, \tag{38}$$

where $-[(G^{68})''-(G^{48})']$ is given by eq (37).

2.5. Modifications of Conversion Procedure when Significant Extrapolation to 0 K was Made Using a Theoretical Relation

In evaluating thermodynamic functions based on 0 K, the heat capacity is measured to as low a temperature as practical and then extrapolation to 0 K is carried out on some more or less simple theoretical basis. The following treatment of the conversion to the basis of a new temperature scale will be exemplified by the use of the simple "T^3" law. If the extrapolation has been from such a low temperature that the heat capacity at all lower temperatures is very small, the modifications are of little importance. However, a great many heat-capacity investigations have involved experimental measurements only down to the triple point of nitrogen (or oxygen), and it is desirable to know whether the required modifications are significant in preserving a given degree of accuracy.

The "T^3" law gives for the fundamental thermodynamic properties

$$(C_P)_T=cT^3 \tag{39}$$

$$H_T-H_0=\int_0^T (C_P)_T dT=\frac{1}{4}cT^4=\frac{1}{4}(C_P)_T T \tag{40}$$

$$S_T=\int_0^T \frac{(C_P)_T}{T}dT=\frac{1}{3}cT^3=\frac{1}{3}(C_P)_T \tag{41}$$

where the constant c is dependent on the substance involved. Equation (41) as written assumes the validity of the Third Law of Thermodynamics in the case in question.

According to the Debye theory the constant c is given by

$$c=\frac{12}{5}\pi^4 R/\theta_D^3 \tag{42}$$

per gram-atom, where θ_D is the Debye characteristic temperature. However, c is rarely evaluated from eq (42) independently of the heat-capacity data, because the "T^3" law expressed by eq (39) and (42) is only approximate: for any given substance the value of θ_D depends on the property from which it is derived. It also varies with temperature when derived from a given property such as heat capacity, and the "T^3" law may "fail" well below the highest temperature at which it is desired to apply eq (39).

Let us use the T in eq (39)–(41) to represent the temperature on any scale assumed to be the thermodynamic one. In what follows it will be assumed that extrapolation to 0 K using the "T^3" law was from a temperature a which is T_{48}^a on the IPTS–48 and T_{68}^a on the IPTS–68, that measurements of enthalpy giving heat capacity are available at the temperatures above temperature a, and that a temperature b (where $T_{48}=T_{48}^b$ and $T_{68}=T_{68}^b$) is such that $T_{68}^b=T_{48}^a$ [analogous to eq (3)]. As before, it is desired to find the correction converting a thermodynamic property on the basis of IPTS–48 and at $T_{48}=T'_{48}$ to the basis of IPTS–68 and at $T_{68}=T''_{68}=T'_{48}$, where $T'_{48}\geq T_{48}^a$ and $T''_{68}\geq T_{68}^b$. The temperature ranges of interest are represented by these various symbols in the schematic diagram of figure 3. It will be assumed that c is assigned values such that the heat capacity given by eq (39) agrees with the experimental value of $(C_P^{48})^a$ if IPTS–48 is the basis, and with that of $(C_P^{68})^b$ if IPTS–68 is the basis.

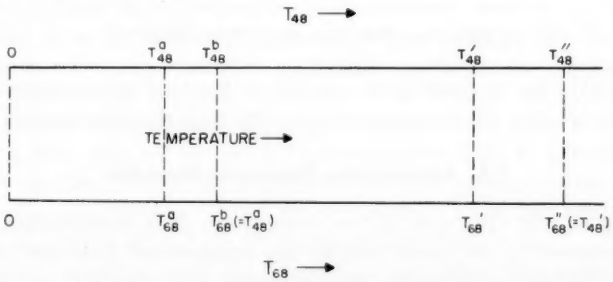

FIGURE 3. *Temperature ranges of interest when extrapolation to 0 K was made using a theoretical relation (schematic).*

As before, the desired correction to the enthalpy (this time specified to be relative to that at 0 K) is $H''-H'$, which can be found as the sum of the corrections to the enthalpy increment above T_{68}^b(or T_{48}^a) and the correction to the enthalpy increment below this temperature:

$$\delta H=H''-H'\equiv[(H''-H')-(H^b-H^a)]+[H^b-H^a]. \tag{43}$$

The two parenthesized terms of eq (43) are separately calculable from eq (13), using the heat-capacity data on the IPTS–48 and $\mu(T_{68})$. The second bracketed term in eq (43) is, from eq (40),

$$\begin{aligned}[H^b-H^a]&=\tfrac{1}{4}(C_P^{68})^b T_{68}^b-\tfrac{1}{4}(C_P^{48})^a T_{48}^a\\&=\tfrac{1}{4}[(C_P^{68})^b-(C_P^{48})^a]T_{48}^a\ ,\end{aligned} \tag{44}$$

since $T_{68}^b=T_{48}^a\cdot[(C_P^{68})^b-(C_P^{48})^a]$ is derivable from eq (16) after replacing temperatures 1 and 2 by a and b respectively.

There is no modification to the heat capacity correction $[(C_p^{68})''-(C_p^{48})']$ given by eq (16) ($T''_{68} \geq T^b_{68}$ and $T'_{48} \geq T^a_{48}$), since the heat capacity in the experimental range is assumed to depend on temperature only in the manner observed experimentally.

As before, the desired correction to the entropy (taken as zero at 0 K because the Third Law of Thermodynamics is assumed) is $(S^{68})''-(S^{48})'$, and

$$\delta S=(S^{68})''-(S^{48})' \equiv [(S^{68})''-(S^{68})^b] - [(S^{48})'-(S^{48})^a]+[(S^{68})^b-(S^{48})^a]. \tag{45}$$

From eq (9) (with subscripts changed correspondingly),

$$T^b_{48}=T^a_{48}-\mu^b. \tag{46}$$

If eq (20) is modified by replacing the lower limit of integration by T^b_{48}, given by eq (46), it becomes

$$(S^{68})''-(S^{68})^b=\int_{T^b_{48}-\mu^b}^{T''_{68}} \left(\frac{C_p^{48}}{T_{48}+\mu}\right) dT_{48}+(S^{68})''-(S^{68}) \tag{47}$$

where $(S^{68})''-(S^{68})'$ is given, as before, by eq (34). Similarly, modifying the lower integration limit to T^a_{48}, eq (21) becomes

$$-[(S^{48})'-(S^{48})^a]=-\int_{T^a_{48}}^{T'_{48}} \frac{C_p^{48}}{T_{48}}\, dT_{48}. \tag{48}$$

From eq (41),

$$[(S^{68})^b-(S^{48})^a]=\tfrac{1}{3}[(C_p^{68})^b-(C_p^{48})^a], \tag{49}$$

where $[C_p^{68})^b-(C_p^{48})^a]$ can be found from eq (16) for the two temperatures involved. The substitution from eq (47)–(49) into the last member of eq (45) then gives the desired entropy correction.

2.6. Approximate Conversion Formulas

Instead of using eq (13), (16), and (35) (or those in sec. 2.5) the enthalpy, heat capacity, and entropy may be corrected by the much simpler but approximate formulas below with sufficient accuracy for most purposes—even for the most accurate data except in the case of sharp transitions, and except possibly at very low temperatures. It should be realized, however, that the approximate formulas of this section may not be sufficiently accurate when applied to two temperature scales differing more widely from each other than the IPTS–48 and IPTS–68; in such cases, additional terms of the exact equations of the preceding sections are needed. Incidentally, it is well to point out that when the enthalpy data are sufficiently precise to justify the higher-order correction terms containing temperature derivatives of the heat capacity, it will often be simpler instead to repeat the treatment of the original unsmoothed data after replacing the boundary temperatures of each enthalpy increment in terms of the new temperature scale.

We define

$$\delta X \equiv (X^{68})_{T_{68}=T_0}-(X^{48})_{T_{48}=T_0}. \tag{50}$$

($X \equiv C_P$, or H or S relative to that at a temperature where $\mu=0$. The superscript "68" or "48" indicates the temperature scale with respect to which the given value of X was determined.)

$$\mu \equiv T_{68}-T_{48}=t_{68}-t_{48}. \tag{51}$$

All properties are those at T_0, the nominal value of T_{68} where the corrected property is desired,

unless otherwise stated. The property values in the rhs of each equation below are as determined on the IPTS–48, and either dT_{48} or dT_{68} can be used for dT [dropping the last term of eq (10)].

From eq (13), the only term of importance, usually, is the first, so

$$\delta H = -\mu C_P. \tag{52}$$

From eq (52),

$$\delta C_P = \delta\left(\frac{dH}{dT}\right) = \frac{d}{dT}\delta H = -C_P\frac{d\mu}{dT} - \mu\frac{dC_P}{dT}. \tag{53}$$

Considering the correction to the absolute entropy, we can first write [using eq (53)]:

$$\frac{d}{dT}(\delta S) = \delta\left(\frac{dS}{dT}\right) = \delta\left(\frac{C_P}{T}\right) = \frac{\delta C_P}{T} = -\frac{\mu}{T}\frac{dC_P}{dT} - \frac{C_P}{T}\frac{d\mu}{dT}. \tag{54}$$

But

$$\frac{d}{dT}\left(-\int_0^T \frac{\mu C_P dT}{T^2} - \frac{\mu C_P}{T}\right) \equiv -\frac{\mu}{T}\frac{dC_P}{dT} - \frac{C_P}{T}\frac{d\mu}{dT}. \tag{55}$$

Since the last members of eq (54) and (55) are identical, we can write

$$\delta S = -\int_0^T \frac{\mu C_P dT}{T^2} - \frac{\mu C_P}{T}, \tag{56}$$

of which the second member approximates the only important terms in eq (35).

The last member of eq (53) represents the only two terms of eq (16) that are usually of importance; and of these two terms, the first is probably nearly always the much more important (except, of course, when $d\mu/dT$ is accidentally very close to zero). According to this term, the relative (fractional) correction to the heat capacity is approximately equal in magnitude to $d\mu/dT$. According to table 4, this does not exceed 0.3 percent below 3000 K. The relative correction to the absolute entropy [eq (56)] tends to be considerably smaller, owing to partial cancellation within the integral and to the magnified weighting by the factor $1/T^2$ of low temperatures where the differences between the IPTS–48 and the IPTS–68 are relatively small.

The corresponding equations that are accurate to the same approximation when the "T^3" law is used below absolute temperature τ, with the "T^3" and experimental heat capacities required to agree at this temperature, are easily found from section 2.5. Thus, where δH and δS in the rhs are given by eq (52) and (56) respectively:

$$\delta H = \tfrac{1}{4}\tau(\delta C_P)_\tau + (\delta H) - (\delta H)_\tau; \tag{57}$$

δC_P is given by eq (53); (58)

$$\delta S = \tfrac{1}{3}(\delta C_P)_\tau + (\delta S) - (\delta S)_\tau. \tag{59}$$

3. The Numerical Differences Between the International Practical Temperature Scales of 1948 and 1968

The temperature ranges separately defined by the two scales are treated individually in sections 3.1–3.4 (headed by the respective temperature ranges expressed on the IPTS–68), and equations are derived giving numerically the differences $\mu(\equiv T_{68} - T_{48} = t_{68} - t_{48})$ between the IPTS–68 and the IPTS–48 in these respective ranges, with sufficient accuracy for most practical purposes.

3.1. 90.188 to 273.15 K (−182.962 to 0 °C)

The realization of both scales is specified to be by the resistance of a suitable platinum thermometer over the entire temperature range from approximately 90 to 904 K (−183 to 631 °C). Since both scales are so defined as to preserve the highest practical continuity over this whole temperature range, their specifications below the ice point depend on those above the ice point. Therefore it will be necessary to consider together the definitions of the two scales in these two regions of temperature.

Using W to represent the ratio of the measured resistance of a particular thermometer at some temperature to its resistance at 0 °C,[4] the specified functions may be written:

IPTS-48 (t_{48}, −182.97 to 0 °C) (Callendar-van Dusen equation) [4]:

$$W = 1 + \alpha(1 + 0.01\ \delta_{48})t_{48} - 10^{-4}\alpha\delta_{48}t_{48}^2 - 10^{-8}\alpha\beta t_{48}^3(100 - t_{48}). \tag{60}$$

IPTS-68 (t_{68}, −182.962 to 0 °C) [1]:

$$W = W_r^* + a_4 t_{68} + c_4 t_{68}^3(t_{68} - 100). \tag{61}$$[5]

IPTS-48 (t_{48}, 0 to 630.5 °C) (Callendar equation) [4]:

$$W = 1 + \alpha(1 + 0.01\delta_{48})t_{48} - 10^{-4}\alpha\delta_{48}t_{48}^2 \tag{62}$$

IPTS-68 (t_{68}, 0 to 630.74 °C) [1]:

$$t' = \frac{1}{\alpha}(W - 1) + \delta_{68}\left(\frac{t'}{100}\right)\left(\frac{t'}{100} - 1\right). \tag{63}$$

which when rearranged is

$$W(t') = 1 + \alpha\,(1 + 0.01\delta_{68})t' - 10^{-4}\alpha\delta_{68}(t')^2. \tag{63a}$$

where t' is defined (as a monotonic function) by the equation

$$t_{68} = t' + 0.045\left(\frac{t'}{100}\right)\left(\frac{t'}{100} - 1\right)\left(\frac{t'}{419.58} - 1\right)\left(\frac{t'}{630.74} - 1\right). \tag{64}$$

The functions $W(t_{48})$ and $W(t_{68})$ differ somewhat from one thermometer to another, and the con-

TABLE 1. *Fixed points used for calibration of platinum resistance thermometers using eq (60)–(64)*

Fixed point	Temperature value	
	IPTS-48 [4, 5]	IPTS-68 [1]
	°C	°C
Normal boiling point of oxygen	−182.970	−182.962
Triple point of water	0.01	0.01
Normal boiling point of water	100	100
Normal boiling point of sulfur	[a] 444.600	.....
Normal freezing point of zinc	[a] 419.505	419.58

[a] For IPTS-48, the "sulfur" point was an official defining fixed point, but the substitution of the "zinc" point and the temperature listed for it were recommended.

[4] Actually, a temperature whose value is exactly 0 °C on one of the two scales has a value trivially different (by 5×10^{-6} °C) on the other scale.

[5] In ref. [1], W_r^* is written as $W_{(T-T_{90})}(T_{90})$.

stants appearing in eq (60)–(63a) are determined for a particular thermometer by measuring W at the fixed points listed in table 1. W_t^*, which appears in eq (61), is a single-valued reference function given by the equation

$$t_{68} = \sum_{i=1}^{20} A_i [\ln W_t^*(T_{68})]^i, \tag{65}$$

with the 20 constants $A_1 \ldots A_{20}$ defined numerically and having 16 significant figures each [1].

Since the correction to the heat capacity is approximately proportional to $d\mu/dT$ [eq (53)], we shall be concerned as to whether the latter and its temperature derivative are continuous at 0 °C, above and below which both $W(T_{48})$ and $W(T_{68})$ are each defined differently by the above equations. Among W, T_{48}, and T_{68} there is only one independent variable, so we can write

$$\frac{d\mu}{dT_{68}} = \frac{d(T_{68} - T_{48})}{dT_{68}} = 1 - \frac{dT_{48}}{dT_{68}} = 1 - \frac{dW}{dT_{68}} \Big/ \frac{dW}{dT_{48}}. \tag{66}$$

It is clear [from eq (60) and (62)] that dW/dT_{48} and d^2W/dT_{48}^2 are continuous at 0 °C, but the situation for the corresponding derivatives involving T_{68} is not obvious. From eq (66), $d\mu/dT_{68}$ and $d^2\mu/dT_{68}^2$ are continuous at 0 °C if and only if dW/dT_{68} and d^2W/dT_{68}^2 also are.

It turns out that the two derivatives of W involving T_{68} as defined by eq (61), (63a), and (64) are not identically continuous at 0 °C. The statement has been made, however, that they are continuous at 0 °C for what may be regarded as a typical thermometer having the following constants [1] (using asterisks for this special case):

$$a_4^* = c_4^* = 0;\ \alpha^* = 3.9259668(10^{-3});\ \delta_{68}^* = 1.496334. \tag{67}$$

This continuity may be readily demonstrated, as shown below. Incidentally, the corresponding function $W^*(T_{68})$ [$\equiv W_t^*$ at and below 0 °C; $\equiv W^*(t')$ at and above 0 °C] may alternatively be regarded as the standard reference function defining t_{68} from −182.962 to 630.74 °C.

Since $W_t^* = 1$ at $T_{68} = 273.15$, it was found, using eq (65) and the numerical values of the constants A_i, that at 0 °C

$$\frac{dW_t^*}{dT_{68}} = 1 \Big/ \frac{dT_{68}}{dW_t^*} = \frac{1}{A_1} = 3.98650632(10^{-3}) \tag{68}$$

and

$$\frac{d^2W_t^*}{dT_{68}^2} = -\frac{d^2T_{68}}{dW_t^{*2}} \Big/ \left(\frac{dT_{68}}{dW_t^*}\right)^3 = \frac{A_1 - 2A_2}{A_1^3} = -1.2261330(10^{-6}). \tag{69}$$

Similarly, it was found, using eq (63a), (64), and (67), that at 0 °C

$$\frac{dW^*(t')}{dT_{68}} = \frac{dW^*(t')}{dt'} \Big/ \frac{dt_{68}}{dt'} = 3.98650630(10^{-3}) \tag{70}$$

and

$$\frac{d^2W^*(t')}{dT_{68}^2} = \frac{d^2W^*(t')}{dt'^2} \Big/ \left(\frac{dt_{68}}{dt'}\right)^2 - \frac{dW^*(t')}{dt'} \left(\frac{d^2t_{68}}{dt'^2}\right) \Big/ \left(\frac{dt_{68}}{dt'}\right)^3 = -1.2261327(10^{-6}). \tag{71}$$

The values of eq (68) and (70) differ by a factor of $1 + 5(10^{-9})$, and those of eq (69) and (71) by a factor of $1 + 2(10^{-7})$. Though the pertinent magnitudes are such that at 0 °C the fractional discontinuity in $d\mu/dT_{68}$ is many times as great as that in dW/dT_{68}, these discrepancies are too small to be of any practical significance and are very likely to be so for all resistance thermometers meeting the standards imposed by the IPTS–68.

For a given resistance thermometer, α has the same value in eq (60), (62), (63), and (63a), because it depends only on the resistances at 0 and 100 °C, which designate the same [4] (see footnote 4) respective temperatures on the IPTS–48 and the IPTS–68. However, $\delta_{48} \neq \delta_{68}$, because of the difference in the two values of temperature for the zinc (or sulfur) point (table 1). At the zinc point $t_{48} = 419.505$ and $t' = t_{68} = 419.58$. Substituting these values and that of δ_{68}^* from eq (67) into eq (62) and (63a) and equating the two expressions for W give

$$\delta_{48}^* = 1.49135723. \tag{72}$$

Since W also is a continuous function of temperature, W and its derivatives may replace H and its derivatives in eq (13) to give an equation from which $\mu(t_{68})$ may be derived,

$$W'' - W' = -\mu'' \left(\frac{dW}{dt_{48}}\right)' + \frac{1}{2}(\mu'')^2 \left(\frac{d^2W}{dt_{48}^2}\right)' - \ldots . \tag{73}$$

In rhs of eq (73) all terms except the first may with sufficient accuracy be neglected (the ratio of the second term to the first does not exceed 0.00004 between −182.962 and 630.74 °C), giving

$$\mu'' = (W' - W'')/\left(\frac{dW}{dt_{48}}\right)'. \tag{74}$$

Using for W the standard reference function defined by eq (60)–(65) with the parameter values of eq (67) and (72), we shall derive from eq (74) numerical functions for $\mu(t_{68})$, in this section for the range $t_{68} = -182.962$ to 0 °C and in the next section for the range $t_{68} = 0$ to 630.74 °C.

Since eq (74) expresses μ at temperature 2, for temperatures at or below 0 °C W' and $(dW/dt_{48})'$ are found from eq (60), (67), and (72), then replacing t_{48}' by t_{68}'' by eq (1)–(3), and W'' from eq (61) and (67). [The value of β is found from eq (60) applied at the oxygen boiling point, where W has the value of W_t^* at $T_{68} = 90.188$ K and where $t_{48} = -182.970$ (table 1).] The final equation is

$$\mu = \frac{250.97\ [1 + 3.9845170(10^{-3})t_{68} - 5.855019(10^{-7})t_{68}^2 + 4.35717(10^{-12})(100 - t_{68})t_{68}^3 - W_t^*]}{1 - 2.9389(10^{-4})t_{68} + 4.3741(10^{-9})(75 - t_{68})t_{68}^2}$$

$$[t_{68} = -182.962 \text{ to } 0\ ^\circ\text{C}]. \tag{75}$$

3.2. 273.15 to 903.89 K (0 to 630.74 °C)

For temperatures at and above 0 °C, eq (74) is applied similarly as was done in section 3.1 for the lower temperature range. W' and $(dW/dt_{48})'$ are found from eq (62), replacing t_{48}' by t_{68}'', and W'' from eq (63a). For replacing t' in eq (63a) in terms of t_{68}, eq (64) may be written

$$t_{68} = t' + \varphi(t'), \tag{76}$$

where

$$\varphi(t') \equiv 0.045 \left(\frac{t'}{100}\right)\left(\frac{t'}{100} - 1\right)\left(\frac{t'}{419.58} - 1\right)\left(\frac{t'}{630.74} - 1\right). \tag{77}$$

Expanding $\varphi(t')$ to two terms about $\varphi(t_{68})$ and then replacing $\varphi(t')$ from eq (76) gives

$$t' = t_{68} - \frac{\varphi(t_{68})}{1 + \dfrac{d\varphi(t_{68})}{dt_{68}}}. \tag{78}$$

(The magnitude of $d\varphi(t_{68})/dt_{68}$ never exceeds about 0.001.) Neglecting a term [in $\varphi(t_{68})$] whose magnitude never exceeds approximately 0.00002 °C, the result is

$$\mu=\frac{0.01\ (\delta_{68}-\delta_{48})t_{68}(0.01t_{68}-1)}{1+0.01\ \delta_{48}-0.0002\ \delta_{48}t_{68}}+\varphi(t_{68}). \tag{79}$$

Substituting the values of δ_{68} and δ_{48} for the reference function [eq (67) and (72)] gives the final numerical equation,

$$\mu=\frac{4.904(10^{-7})t_{68}(t_{68}-100)}{1-2.939(10^{-4})t_{68}}+\varphi(t_{68}), \qquad [t_{68}=0 \text{ to } 630.74\ ^\circ\text{C}] \tag{80}$$

where $\varphi(t_{68})$ is given by eq (77) on replacing t' by t_{68}. Differentiation of eq (80) gives

$$\frac{d\mu}{dt_{68}}=\frac{-4.904(10^{-5})[1-0.02t_{68}+2.939(10^{-6})t_{68}^2]}{[1-2.939(10^{-4})t_{68}]^2}+\frac{d\varphi(t_{68})}{dt_{68}}. \qquad [t_{68}=0 \text{ to } 630.74\ ^\circ\text{C}] \tag{81}$$

3.3. 903.89 to 1,337.58 K (630.74 to 1,064.43 °C)

Temperature in this range is measured by a platinum-versus-rhodium-platinum thermocouple of suitable specifications, the temperature being defined on the IPTS–48 [4] by

$$E=a'+b't_{48}+c't_{48}^2, \tag{82}$$

and on the IPTS–68 [1] by

$$E=a+bt_{68}+ct_{68}^2. \tag{83}$$

In these equations E is the electromotive force of the thermocouple, and the six constants $a' \ldots c$ are evaluated by calibration at the three fixed points listed in table 2. The IPTS–68 specifies that E shall have the respective values listed in the last column of table 2, within specified tolerances. We may regard these nominal values as defining for each of the two scales a "standard" emf-temperature function to which the emf of a given thermocouple may be corrected through its calibration.

The right-hand sides of eq (82) and (83) may be equated, then t_{48} replaced by $(t_{68}-\mu)$ [eq (1), (2), and (6)]. The result on solving for μ may be written

$$\mu=\frac{(a'-a)+(b'-b)t_{68}+(c'-c)t_{68}^2}{b'+2c't_{68}-c'\mu}. \tag{84}$$

The term $-c'\mu$ in the denominator is virtually negligible, but μ in this term may be replaced by $-1.616+0.002864t_{68}$, which fits the three values of table 2 within 0.01 °C. After using the values

TABLE 2. *Fixed points used for calibration of* Pt/Pt–10% Rh *thermocouples using eq (82) and (83)*

Fixed point	Defined temperature		Nominal electromotive force (IPTS–68) [1]
	IPTS–48 [4]	IPTS–68 [1]	
	°C	°C	μV
Calibrated Pt resistance thermometer	630.5		
Calibrated Pt resistance thermometer	(a)	630.74	5534
Normal freezing point of silver	960.8	961.93	9117
Normal freezing point of gold	1063.0	1064.43	10300

[a] According to eq (80), $t_{48}=630.538$ °C when $t_{68}=630.74$ °C.

of temperature and electromotive force listed in table 2 to solve eq (82) and (83) for the six constants a' . . . c, their substitution into eq (84) gives the numerical equation

$$\mu = \frac{-1.3145 + 1.5016(10^{-3})t_{68} + 1.5625(10^{-6})t_{68}^2}{1 + 4.101(10^{-4})t_{68}},$$

$$[t_{68} = 630.74 \text{ to } 1064.43 \text{ °C}] \qquad (85)$$

Differentiation of eq (85) gives

$$\frac{d\mu}{dt_{68}} = \frac{2.0407(10^{-3})[1 + 1.53135(10^{-3})t_{68} + 3.1400(10^{-7})t_{68}^2]}{[1 + 4.101(10^{-4})t_{68}]^2},$$

$$[t_{68} = 630.74 \text{ to } 1064.43 \text{ °C}] \qquad (86)$$

3.4. 1,337.58 K (1,064.43 °C) to 10,000 K

Above the freezing point of gold both the IPTS–48 and the IPTS–68 define the temperature by the Planck Radiation Law, according to which, at wavelength λ and in the range $d\lambda$, the ratio of the spectral intensity at the absolute thermodynamic temperature T to that at the absolute themodynamic temperature of freezing gold, $T(\text{Au})$, is

$$\frac{\exp\left[\frac{c_2}{\lambda T(\text{Au})}\right] - 1}{\exp\left[\frac{c_2}{\lambda T}\right] - 1}, \qquad (87)$$

where c_2 is the so-called second radiation constant. The definition of T_{48} is obtained by making the replacements $T = T_{48}$, $c_2 = 1.438$ cm kelvin, and $T(\text{Au}) = 1336.15$ K in (87) [4], and the definition of T_{68} by the substitutions $T = T_{68}$, $c_2 = 1.4388$ cm kelvin, and $T(\text{Au}) = 1337.58$ K [1]. These functions for the two scales may, of course, be equated; when the equation is solved for T_{48} and this then subtracted from T_{68}, it gives $T_{68} - T_{48}$, or $\mu(T_{68})$, exactly. A simpler numerical equation results by expanding some of the exponentials and dropping negligible terms; when the representative wavelength of optical pyrometers $\lambda = 6.5(10^{-5})$ cm is substituted, the result is

$$\mu = 5.56(10^{-4})T_{68} + 3.84(10^{-7})(1 - e^{-22135/T_{68}})T_{68}^2,$$

$$[T_{68} = 1{,}337.58 \text{ to } 10{,}000] \qquad (88)$$

Up to 10,000 K eq (88) is insensitive to wavelength, and the error in μ does not exceed about 0.1 kelvin.

Differentiation of eq (88) gives

$$\frac{d\mu}{dT_{68}} = 5.56(10^{-4}) + 7.68(10^{-7})T_{68} - [8.5(10^{-3}) + 7.68(10^{-7})T_{68}]e^{-22135/T_{68}},$$

$$[T_{68} = 1{,}337.58 \text{ to } 10{,}000] \qquad (89)$$

3.5. Discontinuities in the Temperature Derivatives of $t_{68} - t_{48}$ at 630.74 and 1,064.43 °C

Though both the IPTS–48 and the IPTS–68 treat the "resistance thermometer" temperature range differently below and above 0 °C, the two scales are highly continuous at this temperature and no discontinuity in $t_{68} - t_{48}$ $(= \mu)$ and its first two temperature derivatives exists, as demonstrated in section 3.1. This is not true where the "thermometer" and "thermocouple" ranges join (630.74 °C), nor where the "thermocouple" and "pyrometer" ranges join (1,064.43 °C). Though μ is continuous at these two temperatures, $d\mu/dt_{68}$ is not, the discontinuity having a magnitude of about 0.001 in both cases.

TABLE 3. *Comparison of the difference in the value of temperature, and its temperature derivative, given by the IPTS of 1968 and the IPTS of 1948 (a) as the two scales are defined and (b) as smoothed in the regions of discontinuity.*

$T_{68}(K)$	$T_{68}-T_{48}$ (kelvins)		$d(T_{68}-T_{48})/dT_{68}$	
	As defined	Smoothed	As defined	Smoothed
840	[a] +0.113	.....	[f] +0.0009	.....
850	.123	[d] +0.123	.0010	[d] +0.0011
860	.134	.135	.0012	.0013
870	.146	.150	.0013	.0016
880	.160	.166	.0015	.0018
890	.176	.185	.0017	.0020
900	[a] .194	.205	.0019	.0021
903.89	[a, b] .202	.214	[f] .0020 [g] .0027	.0022
910	[b] .218	.227	.0027	.0023
920	.245	.251	.0027	.0024
940	.300	.301	.0027	.0026
960	.354	[d] .354	.0027	[d] .0027
980	[b] .409	.....	[g] .0027	.....
.....	.....	.....	.....	.....
1260	[b] 1.202	.....	[g] .0029	.....
1280	1.261	[c] 1.261	.0029	[c] .0029
1300	1.319	1.316	.0029	.0027
1320	[b] 1.378	1.368	.0029	.0025
1337.58	[b, c] 1.430	1.410	[g] .0030 [h] .0016	.0023
1350	[c] 1.45	1.44	.0016	.0022
1375	1.49	[e] 1.49	.0016	[e] .0019
1400	[c] 1.53	.....	[h] .0016	.....

[a] Eq (80). [c] Eq (88). [e] Eq (91). [g] Eq (86).
[b] Eq (85). [d] Eq (90). [f] Eq (81). [h] Eq (89).

Though these discontinuities reflect small corresponding discontinuities at these two temperatures in the IPTS–48 or the IPTS–68 or both, it is not the purpose here to discuss this question. The principal *additional* discontinuity introduced when calorimetric thermodynamic properties are converted from the basis of one temperature scale to that of the other is when the heat capacity-temperature function has been smoothed prior to this conversion: the conversion will introduce an approximately 0.1 percent discontinuity. Such an effect is virtually within the precision of the best present-day calorimetry at temperatures as high as 631 °C, but it may be desirable to avoid it in the systematic conversion of many existing tables.

An obvious simple expedient is to replace the functions $\mu(t_{68})$, over a temperature range extending below and above each temperature of discontinuity, by a function which provides continuity with the pertinent original functions in both μ and $d\mu/dt_{68}$ at the ends of the modified range. That the extent of such a modified range is normally an arbitrary decision is evident from consideration of the idealized simple case (sometimes approximated in reality) in which the heat capacity shows a discontinuity at one temperature but otherwise no change with temperature: How should one join the two disconnected segments smoothly? However, when the effect is as small as in the present case, this question can hardly be important.

The procedure outlined above was followed to derive simple polynomial "smooth" equations for the temperature ranges 570 to 690 °C and 1000 to 1120 °C. These equations are as follows.

356-078 O-69—2

$$\mu = 0.1162 + 9.153(10^{-4})(t_{68} - 570) + 1.3328(10^{-5})(t_{68} - 570)^2$$
$$- 3.192(10^{-8})(t_{68} - 570)^3 \qquad [t_{68} = 570 \text{ to } 690\ ^\circ\text{C}] \qquad (90)$$

$$\mu = 1.241 + 2.92(10^{-3})(t_{68} - 1000) - 4.092(10^{-6})(t_{68} - 1000)^2$$
$$- 7.222(10^{-9})(t_{68} - 1000)^3 \qquad [t_{68} = 1000 \text{ to } 1120\ ^\circ\text{C}] \qquad (91)$$

These two equations and their first derivatives are compared in table 3 with the equations which it is proposed they displace in the temperature ranges indicated above when converting values that were previously smoothed with respect to temperature on the IPTS–48. When no such smoothing was done, eq (90) and (91) should not be used.

3.6. Tabulated Values of $(T_{68} - T_{48})$ and $d(T_{68} - T_{48})/dT_{68}$ at Round Temperatures of T_{68} From 90 to 10,000 K

Values of $T_{68} - T_{48} (\equiv \mu)$ and $d(T_{68} - T_{48})/dT_{68}$ $(= d\mu/dt_{68})$, computed from the equations derived in sections 3.1–3.4 [μ from eq (75), (80), (85), and (88); $d\mu/dt_{68}$ from eq (81). (86), and (89)], are tabulated at round temperatures (T_{68}) in table 4. Below 0 °C, $d(T_{68} - T_{48})/dT_{68}$ was taken by averaging successive pairs of differences of values of $T_{68} - T_{48}$ tabulated at intervals of 1 kelvin. Double entries are included for those temperatures for which the equations for the adjacent temperature ranges give different values (see discussion in sec. 3.5).

A similar table of $T_{68} - T_{48}$ covering the range −180 to 4000 °C has been published [1]. The two tables agree exactly, to the number of significant figures given in each.

TABLE 4. *Approximate difference in the value of temperature, and its temperature derivative, given by the International Practical Temperature Scales of 1968 and 1948*

(The unit of temperature is the kelvin. For both scales, $T(\text{K}) = t(^\circ\text{C}) + 273.15$.)

T_{68}	$T_{68} - T_{48}$	$d(T_{68} - T_{48})/dT_{68}$	T_{68}	$T_{68} - T_{48}$	$d(T_{68} - T_{48})/dT_{68}$	T_{68}	$T_{68} - T_{48}$	$d(T_{68} - T_{48})/dT_{68}$
90	+0.0076	+0.0022	128	−0.0135	0.00000	220	+0.0299	−0.00038
90.188	.0080	.0021	130	−.0134	+.00015	225	.0278	−.00045
91	.0095	.0017	132	−.0129	.00028	230	.0254	−.00051
92	.0110	.0013	134	−.0122	.00041	235	.0227	−.00056
93	.0121	.0008	136	−.0113	.00052	240	.0198	−.00059
94	.0127	.0005	138	−.0102	.00062	245	.0168	−.00061
95	.0130	.0002	140	−.0088	.00071	250	.0137	−.00062
96	.0130	−.0001	142	−.0073	.00079	255	.0105	−.00062
97	.0128	−.0004	144	−.0057	.00086	260	.0074	−.00061
98	.0123	−.0006	146	−.0039	.00092	265	.0044	−.00058
99	.0116	−.0008	148	−.0020	.00096	270	.0016	−.00054
100	.0108	−.00089	150	.0000	.00100	273.15	.0000	−.00050
102	.0088	−.00112	155	+.0050	.00103	275	−.0009	−.00047
104	.0064	−.00124	160	.0102	.00102	280	−.0031	−.00041
106	.0038	−.00130	165	.0152	.00096	285	−.0050	−.00035
108	.0012	−.00130	170	.0197	.00087	290	−.0066	−.00029
110	−.0013	−.00125	175	.0238	.00075	295	−.0079	−.00023
112	−.0038	−.00116	180	.0272	.00061	298.15	−.0085	−.00020
114	−.0060	−.00106	185	.0299	.00047	300	−.0089	−.00018
116	−.0080	−.00092	190	.0318	.00032	305	−.0096	−.00013
118	−.0097	−.00078	195	.0331	.00017	310	−.0101	−.00008
120	−.0111	−.00063	200	.0336	.00005	315	−.0104	−.00003
122	−.0122	−.00046	205	.0335	−.00009	320	−.0105	+.00001
124	−.0129	−.00030	210	.0328	−.00020	325	−.0103	.00006
126	−.0134	−.00015	215	.0316	−.00029	330	−.0099	.00009

TABLE 4. *Approximate difference in the value of temperature, and its temperature derivative, given by the International Practical Temperature Scales of 1968 and 1948*—Continued

(The unit of temperature is the kelvin. For both scales, $T(K) = t(°C) + 273.15$.)

T_{68}	$T_{68} - T_{48}$	$d(T_{68} - T_{48})/dT_{68}$	T_{68}	$T_{68} - T_{48}$	$d(T_{68} - T_{48})/dT_{68}$	T_{68}	$T_{68} - T_{48}$	$d(T_{68} - T_{48})/dT_{68}$
335	−0.0093	+0.00013	700	+0.075	0.0000	1320	+1.378	+0.0029
340	−.0086	.00016	710	.074	.0000	1337.58	1.430	[b] .0030 / [c] .0016
345	−.0077	.00020	720	.074	.0000	1350	1.45	.0016
350	−.0066	.00023	730	.074	.0000	1375	1.49	.0016
355	−.0054	.00026	740	.075	+.0001			
360	−.0041	.00028	750	.076	.0001	1400	1.53	.0016
365	−.0026	.00030	760	.077	.0001	1425	1.57	.0017
370	−.0010	.00033	770	.079	.0002	1450	1.61	.0017
373.15	.0000	.00034	780	.081	.0003	1475	1.66	.0017
375	+.0006	.00035	790	.084	.0003	1500	1.70	.0017
380	.0024	.00036	800	.088	.0004	1525	1.74	.0017
385	.0043	.00038	810	.093	.0005	1550	1.78	.0017
390	.0062	.00039	820	.098	.0006	1575	1.83	.0018
395	.0082	.00041	830	.105	.0007	1600	1.87	.0018
400	.0103	.00042	840	.113	.0009	1625	1.92	.0018
410	.0146	.00044	850	.123	.0010	1650	1.96	.0018
420	.0190	.00045	860	.134	.0012	1675	2.01	.0018
430	.0235	.00045	870	.146	.0013	1700	2.05	.0019
440	.0280	.00045	880	.160	.0015	1725	2.10	.0019
450	.0325	.00045	890	.176	.0017	1750	2.15	.0019
460	.0369	.00044	900	.194	.0019	1775	2.20	.0019
470	.0413	.00043	903.89	.202	[a] .0020 / [b] .0027	1800	2.24	.0019
480	.0454	.00041				1825	2.29	.0020
490	.0494	.00039	910	.218	.0027	1850	2.34	.0020
500	.0532	.00037	920	.245	.0027	1875	2.39	.0020
510	.057	.0003	940	.300	.0027	1900	2.44	.0020
520	.060	.0003	960	.354	.0027	1925	2.49	.0020
530	.063	.0003	980	.409	.0027	1950	2.54	.0021
540	.066	.0003	1000	.464	.0028	1975	2.60	.0021
550	.068	.0002	1020	.519	.0028	2000	2.65	.0021
560	.070	.0002	1040	.575	.0028	2050	2.75	.0021
570	.072	.0002	1060	.631	.0028	2100	2.86	.0022
580	.074	.0001	1080	.687	.0028	2150	2.97	.0022
590	.075	.0001	1100	.743	.0028	2200	3.08	.0022
600	.076	.0001	1120	.800	.0028	2250	3.19	.0023
610	.076	.0001	1140	.857	.0028	2300	3.31	.0023
620	.077	.0000	1160	.914	.0029	2350	3.43	.0024
630	.077	.0000	1180	.971	.0029	2400	3.55	.0024
640	.077	.0000	1200	1.029	.0029	2450	3.67	.0024
650	.077	.0000	1220	1.086	.0029	2500	3.79	.0025
660	.076	.0000	1235.08	1.130	.0029	2600	4.0	.003
670	.076	.0000	1240	1.144	.0029	2700	4.3	.003
680	.076	.0000	1260	1.202	.0029	2800	4.6	.003
690	.075	.0000	1280	1.261	.0029	2900	4.8	.003
692.73	.075	.0000	1300	1.319	.0029	3000	5.1	.003

See footnotes at end of table p. 470.

TABLE 4. *Approximate difference in the value of temperature, and its temperature derivative, given by the International Practical Temperature Scales of 1968 and 1948*—Continued

(The unit of temperature is the kelvin. For both scales, $T(K) = t(°C) + 273.15$.)

T_{68}	$T_{68} - T_{48}$	$d(T_{68} - T_{48})/dT_{68}$	T_{68}	$T_{68} - T_{48}$	$d(T_{68} - T_{48})/dT_{68}$	T_{68}	$T_{68} - T_{48}$	$d(T_{68} - T_{48})/dT_{68}$
3100	+5.4	+0.003	4100	+8.7	+0.004	5500	+14.	+0.005
3200	5.7	.003	4200	9.1	.004	6000	17.	.005
3300	6.0	.003	4300	9.4	.004	6500	19.	.005
3400	6.3	.003	4400	9.8	.004	7000	22.	.005
3500	6.6	.003	4500	10.2	.004	7500	25.	.006
3600	7.0	.003	4600	10.6	.004	8000	27.	.006
3700	7.3	.003	4700	11.0	.004	8500	30.	.006
3800	7.6	.004	4800	11.4	.004	9000	33.	.006
3900	8.0	.004	4900	11.8	.004	9500	37.	.006
4000	8.3	.004	5000	12.3	.004	10,000	40.	.006

[a] Eq (81).
[b] Eq (86).
[c] Eq (89).

John L. Riddle read the entire manuscript and made several helpful suggestions.

4. References

[1] The International Practical Temperature Scale of 1968, Metrologia **5**, 35 (1969).
[2] Douglas, T. B., Ball, A. F., and Ginnings, D. C., J. Research NRS **46**, 334 (1951) RP2204.
[3] Bedford, R. E., Durieux, M., Muijlwijk, R., and Barber, C. R., Relationships between the International Practical Temperature Scale of 1968 and the NBS–55, NPL–61, PRMI–54, and PSU–54 temperature scales in the range from 13.81 to 90.188 K. Metrologia **5**, 47 (1969).
[4] Stimson, H. F., The International Temperature Scale of 1948, J. Research NBS **42**, 209 (1949) RP1962.
[5] Temperature: Its Measurement and Control in Science and Industry, Vol. **3**, ed. Herzfeld, C. M., Part 1, ed. Brickwedde, F. G. (Reinhold Publ. Corp. New York, N.Y., 1962), pp. 62–63.

(Paper 73A5–563)

JOURNAL OF RESEARCH of the National Bureau of Standards—A. Physics and Chemistry
Vol. 73A, No. 5, September-October 1969

Measured Enthalpy and Derived Thermodynamic Properties of Alpha Beryllium Nitride, Be_3N_2, from 273 to 1200 K[1]

Thomas B. Douglas and William H. Payne[2]

Institute for Basic Standards, National Bureau of Standards, Washington, D.C. 20234

(June 9, 1969)

The relative enthalpy of a sample of alpha beryllium nitride, Be_3N_2, of 95 percent purity was precisely measured over the temperature range 273 to 1173 K using a drop calorimetric method. Corrections were applied for the impurities, and the resulting heat capacity–temperature function was required to join smoothly that from recent precise NBS adiabatic calorimetry which covered the range 20 to 315 K. The enthalpy, heat capacity, entropy, and Gibbs free-energy function were computed from empirical functions of temperature and tabulated from 273 to 1200 K.

Key words: Beryllium nitride; drop calorimetry; enthalpy data; light-element compounds; refractory crystals; thermodynamic properties.

1. Introduction

In a research program for the past several years at the National Bureau of Standards, the thermodynamic properties of numerous light-element compounds have been under investigation. One of the simplest of these compounds, beryllium nitride (Be_3N_2), is the subject of the present paper. Several investigators [1, 2, 3][3] have determined the structure of the crystalline form which is stable at relatively low temperatures ("alpha") (bcc lattice with a D5, or "anti-Mn_2O_3", structure). It has been reported to undergo a phase transition at 1400 °C to a hexagonal structure ("beta"), it being stated that its conversion to the alpha form has not been observed [3]. The melting point lies at or above 2000 °C, and even at somewhat lower temperatures it decomposes reversibly to an appreciable extent into its elements. Its decomposition equilibrium has recently been studied from 1450 to 1650 K by a torsion-effusion method [4], and the resulting value for its heat of formation is in very good agreement with two independent calorimetric determinations of the same property [5, 6].

The present paper reports enthalpy measurements on α-Be_3N_2 over the temperature range 273 to 1173 K. Recent precise heat-capacity measurements at the National Bureau of Standards from 20 to 315 K [7] define the heat capacity, as well as the enthalpy and entropy relative to 0 K, in the overlap region near room temperature. Another series of low-temperature heat-capacity measurements (25 to 310 K), which are in good agreement, has been reported [8]. The only high-temperature enthalpy measurements that have been reported are three which covered the temperature range 273 to 773 K [9].

2. Sample

The sample of beryllium nitride was prepared specifically for the NBS calorimetric measurements by the Brush Beryllium Co., of Cleveland, Ohio, by reacting pure nitrogen and beryllium powder at elevated temperatures and crushing the product to particle sizes between 0.3 and 0.8 mm. The material received was thoroughly mixed and preserved in an atmosphere of dry argon. A speciment was subjected to x-ray examination at the Bureau, showing only the cubic (alpha) form within the detection limits of this method.

Another specimen (of about 3.7 g) was weighed into a sample container of 80 Ni-20 Cr for the enthalpy measurements, and was thereafter kept in a desiccator, or in an atmosphere of dry helium during the measurements. The sample container was deliberately closed not quite gas-tight, in order to allow any chemically bound hydrogen present to escape as water vapor or ammonia during heating. The sample mass did in fact fluctuate by several tenths of a percent during the initial 5 hrs of heating (at 400 to 600 °C), and the enthalpy measurements made then were discarded. Thereafter the mass of the sample remained constant

[1] Research sponsored by the Advanced Research Projects Agency, U.S. Department of Defense, under Order No. 20, and by the Air Force Office of Scientific Research, Office of Aerospace Research, U.S. Air Force, under AFOSR Contract No. ISSA 68–0004.

[2] Present address: Science Information Exchange, 1730 M St., N.W., Washington, D.C. 20036.

[3] Figures in brackets indicate the literature references at the end of this paper.

within a range of about 0.1 percent. Despite the efforts to exclude moisture and oxygen, undoubtedly appreciable hydrolysis and possibly also oxidation of the sample occurred during the initial changes in sample mass, and therefore the chemical composition on which the corrections for impurities were based was calculated solely from the analyses of the sample performed after the completion of the enthalpy measurements.

The results of the analyses of the sample, carried out in the Analytical Chemistry Division of the Bureau after the enthalpy measurements, are recorded in table 1. Each individual analysis for beryllium and nitrogen was made on an aliquot portion of the sample in solution in dilute hydrochloric acid, the beryllium being precipitated by ammonium hydroxide and weighed as BeO, and the nitrogen being determined by the Kjeldahl method with standardization against ammonium dihydrogen phosphate. Of the numerous elements searched for spectrochemically, only those detected are listed in the table.

TABLE 1. *Chemical and spectrochemical analyses of the sample*

Elements	Individual analyses	Mean
	Weight %	*Weight %*
	(a) By chemical analysis	
Be	[a] 48.63, [a] 48.67	[b] 48.57
N	48.07, 48.13, 48.23	48.14
	(b) By qualitative spectrochemical analysis	
Al	0.001 − 0.01	
Ca	< 0.001	
Cr	0.001 − 0.01	
Cu	< 0.001	
Fe	0.01 − 0.1	
Mg	0.001 − 0.01	
Mn	< 0.001	
Ni	0.001 − 0.01	
Si	0.01 − 0.1	
Ti	0.001 − 0.01	

[a] Uncorrected for the metallic elements listed below.
[b] This value includes a correction of −0.08 percent to account for the oxides of the 10 elements listed under (b) below which were assumed to have been weighed as BeO.

The heating of the sample to approximately constant weight is believed to have simplified the problem of interpreting its subsequent analysis by allowing the reasonable assumption that water and ammonia (even as hydrates or ammoniates) were absent. The small amounts of foreign metallic elements found were assumed to be present in half the respective maximum amounts indicated in table 1, and, when assumed furthermore to be present in the form of their most stable oxides, account for 0.22 weight percent of the sample. The remainder is assumed to have been composed entirely of Be_3N_2, BeO, and, because of the method of preparation of the sample, possibly some Be metal (or an amount of subnitride or suboxide that would evolve an equal amount of hydrogen when treated with dilute acid). Although the sample was not analyzed for oxygen, the average beryllium and nitrogen analyses in table 1 correspond to definite percentages of Be_3N_2 and BeO, plus several tenths of a percent of Be metal.

However, it seems more likely that much less (if any) Be metal was present. The original sample showed only 0.10 ± 0.01 percent, the sample on which the NBS low-temperature calorimetry had been conducted showed only 0.04 ± 0.00 percent, and the small amount of water and possibly oxygen that must have been initially in contact with the specimen used in the present calorimetry would be expected to have oxidized most of these small amounts of the free metal at the elevated temperatures. It was therefore assumed that the remaining 99.78 percent of the sample was composed wholly of Be_3N_2 and BeO, and that either the beryllium or the nitrogen analysis (or both) was somewhat in error. This is equivalent to assuming that the true weight percentages of these two elements are related according to

$$\%N = 3.8904 \times \%Be - 139.87. \quad (1)$$

According to table 1 and the analysis of the original sample, the beryllium analysis was several times as precise as the nitrogen analysis (very possibly because of the much smaller amount of sample used in each Kjeldahl analysis and the greater chance for error from the distillation and titration of this method). One might therefore conclude that the beryllium analysis was more accurate; and, according to eq (1) it would need to be, in order to establish the percentage of Be_3N_2 with a given accuracy. It may be added that the above-mentioned analyses of the original sample and the sample that had undergone low-temperature calorimetry showed similar discrepancies, and consequently afforded no clue to the ambiguity under discussion here.

It was decided to assume, somewhat arbitrarily, that the sample contained 48.39 percent Be and 48.40 percent N, which are respectively 0.18 percent below and 0.26 percent above the corresponding mean values in table 1. (If the mounts of foreign elements were nearer the maxima in the table, the Be discrepancy would be smaller.) This leads to the final assumed sample composition shown in table 2. The heat capacities of Be_3N_2 and BeO *per unit mass* are sufficiently close to each other as to render the uncertainty in the finally corrected thermal values smaller from this arbitrariness of assumed composition than from other sources.

3. Enthalpy Measurements

The enthalpy measurements were made using the "drop" method, which, as used in this laboratory, is described in detail in a recent publication [10]. Briefly, the method is as follows. The sample in its container is suspended inside a vertical thick-wall silver pipe in a furnace until it has had time to reach the temperature of the silver. It is then dropped into a Bunsen ice calorimeter, which measures precisely the heat evolved by the sample and container in cooling

to 0 °C (273.15 K). In order to account for the enthalpy change of the container itself and the small amount of heat lost from its surface during the drop, a separate measurement is made on the empty container at the same furnace temperature.

TABLE 2. *Assumed chemical composition of the sample*

Substance	Weight percent	Substance	Weight percent
Be_3N_2	95.11 } [a]	Fe_2O_3	0.07
BeO	4.67 } [a]	MgO	.008
Be metal	0.00 } [a]	NiO	.006
Al_2O_3	.009	SiO_2	.11
Cr_2O_3	.007	TiO_2	.008
		Total:	100.00

[a] Equivalent to 48.39 percent Be and 48.40 percent N.

In the case of beryllium nitride, the furnace (i.e., the silver-pipe) temperature was measured by two Pt/Pt-10 percent Rh thermocouples. One of the thermocouples was calibrated before the enthalpy measurements by the NBS Pyrometry Laboratory, and after the enthalpy measurements by comparison in the furnace with another similarly calibrated thermocouple. The thermocouple calibration during the enthalpy measurements changed by less than 0.1 kelvin during the whole series of enthalpy measurements.

The heats observed in individual measurements are listed (in joules) in the second and third columns of table 3. These values are for the actual sample and container used, except that corrections have been applied for very small unavoidable departures from the "standard" masses of parts of the container, but not for impurities in the sample. For each furnace temperature the values are given in chronological order, although the different furnace temperatures were run in somewhat random order. As always with this method, the times in the furnace adequate for

TABLE 3. *Relative enthalpy of beryllium nitride,* Be_3N_2

Furnace temperature,[a] t	Individual enthalpy measurements		Net enthalpy of Be_3N_2 [d]		Mean obs.–calculated
	Container plus sample [b, c]	Empty container	Mean observed [e]	Calc. from equations	
°C	J	J	J mol^{-1}	J mol^{-1}	J mol^{-1}
99.75	.....	671.45	6,979	6,980	−1
	1,140.69	673.67			
	1,142.95	667.64			
	1,143.11	667.72			
	.....	673.50			
	.....	671.99			
199.65	2,452.3	1,391.6	15,710	15,744	−34
	2,452.2	1,390.6			
299.80	3,875.4	2,132.0	25,821	25,786	+35
	3,875.8	2,131.8			
399.65	5,374.0	2,910.5	36,574	36,615	−41
	5,380.3	2,904.2			
	5,373.6	2,903.5			
499.40	6,933.0	3,691.2	47,983	47,988	−5
	6,935.5	3,693.5			
	6,938.1	3,697.8			
	.....	3,698.5			
599.50	8,556.0	.....	59,781	59,812	−31
	8,553.9	4,518.2			
	8,548.4	4,515.2			
	8,556.4	.....			
700.00	10,255.6	5,387.1	72,056	72,012	+44
	10,253.1	5,389.8			
800.40	12,000.8	6,301.4	84,430	84,480	−50
	12,000.8	6,298.2			
	12,003.3	.....			
900.75	13,780.8	7,222.0	97,194	97,193	+1
	13,787.5	7,225.2			
	13,793.0	7,225.1			
	13,790.1	.....			

[a] International Practical Temperature Scale of 1968 [13].
[b] Sample mass = 3.7440 g.
[c] Uncorrected for sample impurity.
[d] Molecular weight = 55.050. Enthalpy relative to that at 0 °C.
[e] Corrected for sample impurity.

reaching thermal equilibrium were predetermined from preliminary measurements at one temperature with deliberately inadequate times, and checked by choosing substantially different times for each set of duplicate measurements (without detecting any trend of the results with time).

The net mean observed enthalpy of the sample at each furnace temperature (relative to that at 0 °C) is given in the fourth column of table 3, and was obtained by converting the difference of the means of the second and third columns to a molar basis. These net molar enthalpies have been corrected for the sample impurities (assuming additivity) as given in table 2, the total correction amounting to very nearly +0.7 percent at each furnace temperature, on the basis of replacing the impurities by the same mass of beryllium nitride. (The corrections for BeO are based on accurate measurements on this substance in this laboratory [11]; the very small corrections for the remaining impurities were made using the adequate assumption that their enthalpy changes over a given temperature interval are the same as for the same number of gram-atoms of Be_3N_2.)

The "calculated" values of enthalpy referred to in the last two columns of table 3 are the smoothed, finally adopted values arrived at as described in section 4.

4. Derivation of Thermodynamic Functions

The mean "observed" values of the enthalpy of beryllium nitride (table 3, column 4) were smoothed by using them to determine (by the method of least squares, using equal weighting) the linear coefficients of several alternative empirical functions of temperature. The equation adopted is identical with eq (5) below (except with the constant term adjusted to make the function vanish at 273.15 K).

Such a formulation is adequate to represent such monotonic enthalpy values within their uncertainties. But when the relative enthalpy has been measured over temperature intervals no smaller than 100 kelvins, as here, it cannot be relied on to provide accurate interpolation (such as for heat capacity) near the ends of the temperature range covered, owing to the empirical nature of the equation—particularly at the low-temperature end, where the heat capacity-temperature curve of a typical solid shows the greatest curvature. Nevertheless, experience in this laboratory has shown that for transition-free solids whose enthalpy has been measured relative to 273.15 K, this "end-effect" uncertainty in the heat capacity is usually minor at and above 298 K.

Fortunately, Furukawa and Reilly [7] have recently measured the heat capacity of beryllium nitride from 20 to 315 K, with a precision of ±0.01 percent between 50 and 300 K. It was decided to adopt in this paper their values for its heat capacity, enthalpy, and entropy from 273.15 to 298.15 K, to adopt the above-mentioned enthalpy equation only above 400 K, and to derive a new equation for the interval 298.15 to 400 K. The new enthalpy equation was taken simply as a quartic polynomial in $(T-400)$, with its five constants required to provide continuity in the enthalpy (relative to 0 K) at 298.15 K, and in the heat capacity and its temperature derivative at 298.15 and 400 K. The constant term of the enthalpy equation for use *above* 400 K was then adjusted so as to provide continuity in the enthalpy at this temperature. It will be noted that the above procedure was not explicitly required to represent the observed enthalpies, but it does so within their precision, as is shown by the last column of table 3. The nature of the fit, for the three regions of temperature covered by the present investigation, is shown in figure 1 as percentage deviations from the adopted heat capacities. Furukawa and Reilly's maximum deviation (at 315 K) is +0.15 percent, which constitutes an injustice to their precision, but not to their absolute accuracy, which is limited by some ambiguity in the composition of their sample.

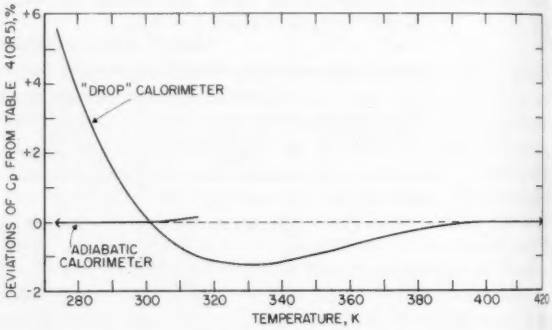

FIGURE 1. *Deviations of heat capacity, derived separately from the adiabatic calorimetry of Furukawa and Reilly* [7] *and from the "drop" calorimetry of the present work, from the final values of table 4 (or 5).*

The dotted portion of the base line (298.15 to 400 K) corresponds to equation (3).

The following numerical equations, which resulted from the above procedure, give the final values of the enthalpy (H), heat capacity (C_p), and entropy (S) of alpha beryllium nitride adopted in this paper for the temperature interval 298.15 to 1200 K. The enthalpy is relative to that at 0 K, and the entropy is absolute if the value at 0 K is zero (presumably so in the case of beryllium nitride). The units are joules per mole for energy (with 1 mol = 55.050 g), and kelvins (International Practical Temperature Scale of 1968 [13]) for the absolute temperature T.

298.15–400 K:

$$H^\circ - H_0^\circ = 15690.33 - 204.00263T + 0.9489086\ T^2 - 1.5025526\ (10^{-3})T^3 + 9.779786\ (10^{-7})T^4 \quad (2)$$

$$C_p^\circ = -204.0026 + 1.8978172T - 4.5076578\ (10^{-3})T^2 + 3.911914\ (10^{-6})T^3 \quad (3)$$

$$S^\circ = 796.6989 - 204.00263\ \ln T + 1.8978172T - 2.253829\ (10^{-3})T^2 + 1.303971\ (10^{-6})T^3 \quad (4)$$

[4] "ln" indicates the natural logarithm (base e).

400-1200 K:

$$H^\circ - H_0^\circ = -352093.01 + 73.838107T + 1.3979455\ (10^{-2})T^2 + 4.6161343\ (10^4)\ln T + 2.8241611\ (10^7)T^{-1} - 1.931104\ (10^9)T^{-2} \quad [4](5)$$

$$C_p^\circ = 73.8381 + 2.79589\ (10^{-2})T + 4.616134\ (10^4)T^{-1} - 2.824161\ (10^7)T^{-2} + 3.862208\ (10^9)T^{-3} \quad (6)$$

$$S^\circ = -349.9251 + 73.83810 \ln T + 2.79589\ (10^{-2})T - 4.616134\ (10^4)T^{-1} + 1.412081\ (10^7)T^{-2} - 1.287403\ (10^9)T^{-3} \quad [4](7)$$

[4] "ln" indicates the natural logarithm (base e).

Values from Furukawa and Reilly [7] below 298.15 K and from eqs (2)–(7) above 298.15 K are listed in table 4, the Gibbs free-energy function $-(G^\circ - H_0^\circ)/T$ being computed from the thermodynamic relation

$$-(G^\circ - H_0^\circ)/T = S^\circ - (H^\circ - H_0^\circ)/T. \quad (8)$$

For convenience, table 4 is repeated as table 5 except in terms of the defined calorie (≡4.1840 joules) instead of the joule, since the defined calorie is commonly used in the calculations of chemical thermodynamics.

5. Comparison With Other Work; Estimates of Accuracy

The heat capacity of beryllium nitride is shown as a function of temperature in figure 2, where the solid curve represents the values of table 4, and the open circles represent the unsmoothed drop-calorimetry values $\Delta H/\Delta t$ for the nine successive intervals of temperature (from table 3, columns 1 and 4). Each unsmoothed value has been corrected for curvature by subtracting $(d^2C_p/dt^2)(\Delta t)^2/24$ [calculated from eq (3) or (6)] and assigned to the mean temperature of its interval. The mean deviation of the points from the curve is 0.45 percent. However, the enthalpy, not heat capacity, was determined experimentally, and "observed" heat capacity calculated in this way is dependent on the size of the temperature interval of enthalpy measurement, and hence is only roughly indicative of the experimental imprecision.

Satoh [9] used an ice calorimeter, and reported three measurements of the enthalpy of beryllium nitride, relative to 0 °C, at 99.5, 303.3, and 500.3 °C. His values, which he corrected for the 1.87 percent of impurity, are respectively 2.1, 0.5, and 2.2 percent higher than the corresponding values from table 4 or 5. The "observed" heat capacities similarly calculated from his enthalpies are shown as filled circles in figure 2, and the dotted line represents the linear equation derived by Kelley [12] to represent these results. Obviously Satoh's heat capacities are in good agreement with the present work up to above 300 °C, but the extrapolation of the straight line to considerably higher temperatures would, of course, lead to large errors.

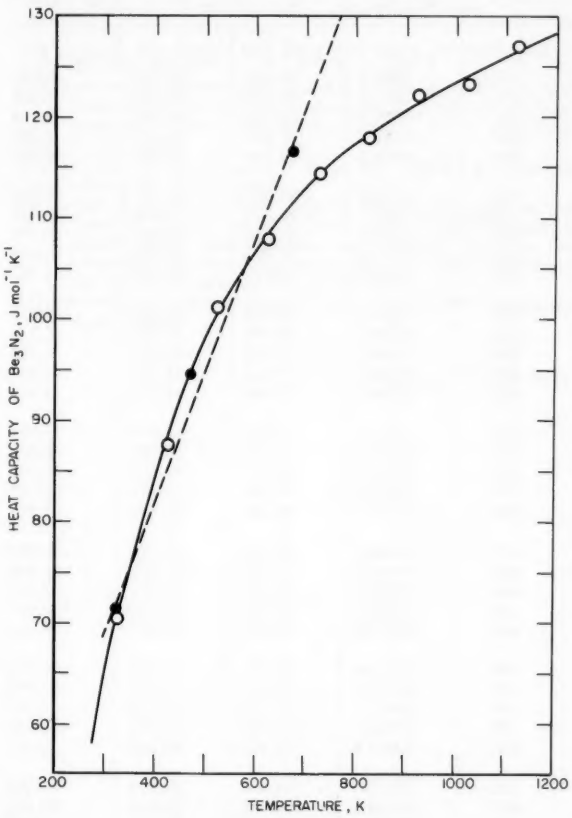

FIGURE 2. *Heat capacity of* Be_3N_2(c).
This work: ——, smoothed; ○, unsmoothed.
Satoh [9]: – – –, smoothed by Kelley [12]; ●, unsmoothed.

The principal sources of systematic error in the present work are the uncertainties in the sample composition and in the furnace temperatures. The uncertainty in the heat capacities derived from the drop calorimetry arising from the corrections for sample impurities is estimated as 0.2 percent—equivalent to assuming that the beryllium analysis in table 1 might be correct. The uncertainty in the thermocouple calibration was stated to be no greater than 0.5 kelvin, and it is believed that the uncertainty in measuring furnace temperature introduced a systematic error of less than 0.1 percent into the heat capacities. The general overall uncertainty in the heat-capacity values of tables 4 and 5 above 298.15 K is estimated as 0.7 percent.

The values of $S^\circ_{298.15}$ and $(H^\circ_{298.15} - H^\circ_0)$ given by Furukawa and Reilly [7] are 34.42 ±0.3 J mol^{-1} K^{-1} and 7123.7 J mol^{-1}, respectively, and the other values of entropy and enthalpy in tables 4 and 5 are based

TABLE 4. *Thermodynamic functions for beryllium nitride* (Be_3N_2) *solid phase (in terms of* **JOULES** *per mole)*

(1 mole = 55.050 g; International Practical Temperature Scale of 1968)

T	$H^\circ - H_0^\circ$	C_p°	S°	$-(G^\circ - H_0^\circ)/T$
K	J mol^{-1}	J mol^{-1} K^{-1}	J mol^{-1} K^{-1}	J mol^{-1} K^{-1}
273.15	5585.2	58.195	29.033	8.590
275	5693.2	58.706	29.430	8.728
280	5989.8	60.066	30.497	9.104
285	6294.0	61.400	31.572	9.489
290	6604.0	62.718	32.652	9.883
295	6920.8	64.007	33.736	10.276
298.15	7123.7	64.810	34.418	10.527
300	7244.0	65.275	34.820	10.673
305	7573.5	66.498	35.909	11.078
310	7908.9	67.675	37.000	11.487
315	8250.2	68.808	38.092	11.901
320	8596.9	69.900	39.184	12.319
330	9306.4	71.976	41.367	13.166
340	10036.0	73.924	43.545	14.027
350	10784.6	75.769	45.715	14.902
360	11551.1	77.533	47.874	15.788
370	12335.0	79.242	50.022	16.684
380	13135.9	80.917	52.158	17.590
390	13953.3	82.582	54.281	18.503
400	14787.5	84.262	56.393	19.424
410	15638.6	85.923	58.494	20.351
420	16505.9	87.519	60.584	21.284
430	17388.8	89.049	62.661	22.222
440	18286.6	90.516	64.725	23.165
460	20124.8	93.262	68.810	25.061
480	22015.6	95.774	72.834	26.968
500	23954.4	98.072	76.791	28.882
520	25937.1	100.173	80.678	30.799
540	27960.1	102.097	84.496	32.718
560	30019.9	103.862	88.241	34.634
580	32113.6	105.485	91.914	36.546
600	34238.5	106.981	95.516	38.452
620	36392.1	108.363	99.047	40.350
640	38572.3	109.643	102.508	42.238
660	40777.2	110.833	105.900	44.116
680	43005.1	111.941	109.225	45.983
700	45254.4	112.978	112.485	47.836
720	47523.8	113.951	115.682	49.677
740	49812.0	114.866	118.817	51.503
760	52118.1	115.729	121.891	53.315
780	54440.9	116.546	124.908	55.112
800	56779.6	117.323	127.869	56.894
820	59133.5	118.062	130.775	58.661
840	61501.9	118.769	133.628	60.412
860	63884.1	119.446	136.431	62.147
880	66279.6	120.096	139.185	63.867
900	68687.8	120.723	141.891	65.571
950	74761.4	122.202	148.458	69.762
1000	80906.3	123.579	154.761	73.855
1050	87118.0	124.879	160.823	77.853
1100	93393.2	126.119	166.661	81.758
1150	99729.2	127.316	172.294	85.572
1200	106124.2	128.479	177.737	89.300

H_0° and S_0° are, respectively, the enthalpy and entropy at 0 K and 1 atm pressure. Values below 300 K are taken from G. T. Furukawa and M. L. Reilly [7].

TABLE 5. *Thermodynamic functions for beryllium nitride* (Be_3N_2) *solid phase (in terms of* **CALORIES** *per mole)*

(1 cal = 4.1840 J; 1 mole = 55.050 g; International Practical Temperature Scale of 1968)

T	$H^\circ - H_0^\circ$	C_p°	S°	$-(G^\circ - H_0^\circ)/T$
K	cal mol^{-1}	cal mol^{-1} K^{-1}	cal mol^{-1} K^{-1}	cal mol^{-1} K^{-1}
273.15	1334.9	13.909	6.939	2.053
275	1360.7	14.031	7.034	2.086
280	1431.6	14.356	7.289	2.176
285	1504.3	14.675	7.546	2.268
290	1578.4	14.990	7.804	2.362
295	1654.1	15.298	8.063	2.456
298.15	1702.6	15.490	8.226	2.516
300	1731.4	15.601	8.322	2.551
305	1810.1	15.893	8.582	2.648
310	1890.3	16.175	8.843	2.746
315	1971.8	16.445	9.104	2.844
320	2054.7	16.707	9.365	2.944
330	2224.3	17.203	9.887	3.147
340	2398.7	17.668	10.408	3.353
350	2577.6	18.109	10.926	3.562
360	2760.8	18.531	11.442	3.773
370	2948.1	18.939	11.956	3.988
380	3139.5	19.340	12.466	4.204
390	3334.9	19.738	12.973	4.422
400	3534.3	20.139	13.478	4.642
410	3737.7	20.536	13.980	4.864
420	3945.0	20.918	14.480	5.087
430	4156.0	21.283	14.976	5.311
440	4370.6	21.634	15.470	5.537
460	4809.9	22.290	16.446	5.990
480	5261.8	22.891	17.408	6.445
500	5725.2	23.440	18.353	6.903
520	6199.1	23.942	19.283	7.361
540	6682.6	24.402	20.195	7.820
560	7174.9	24.824	21.090	8.278
580	7675.3	25.212	21.968	8.735
600	8183.2	25.569	22.829	9.190
620	8697.9	25.899	23.673	9.644
640	9219.0	26.205	24.500	10.095
660	9746.0	26.490	25.311	10.544
680	10278.5	26.755	26.105	10.990
700	10816.1	27.002	26.885	11.433
720	11358.5	27.235	27.649	11.873
740	11905.4	27.454	28.398	12.310
760	12456.5	27.660	29.133	12.743
780	13011.7	27.855	29.854	13.172
800	13570.7	28.041	30.561	13.598
820	14133.3	28.218	31.256	14.020
840	14699.3	28.386	31.938	14.439
860	15268.7	28.548	32.608	14.854
880	15841.2	28.704	33.266	15.265
900	16416.8	28.854	33.913	15.672
950	17868.4	29.207	35.482	16.673
1000	19337.1	29.536	36.989	17.652
1050	20821.7	29.847	38.438	18.607
1100	22321.5	30.143	39.833	19.541
1150	23835.9	30.429	41.179	20.452
1200	25364.3	30.707	42.480	21.343

H_0° and S_0° are, respectively, the enthalpy and entropy at 0 K and 1 atm pressure. Values below 300 K are taken from G. T. Furukawa and M. L. Reilly [7].

on these values. For the same quantities the JANAF table [6] gives 34.13 J mol^{-1} K^{-1} (0.8 percent lower) and 7075 J mol^{-1} (0.7 percent lower), which are based on the measurements of Justice [8].

The sample of beryllium nitride was analyzed chemically by Rolf A. Paulson and spectrochemically by Elizabeth K. Hubbard, both of the Analytical Chemistry Division of the Bureau.

6. References

[1] Stackelberg, M., and Paulus, R., Z. physik. Chem. **B22,** 305 (1933).
[2] Chiotti, P., J. Am. Ceram. Soc. **35,** 123 (1952).
[3] Eckerlin, P., and Rabenau, A., Z. anorg. allgem. Chem. **304,** 218 (1960).
[4] Yates, R. E., Greenbaum, M. A., and Farber, M., J. Phys. Chem. **68,** 2682 (1964).
[5] Gross, P., Hayman, C., Greene, P. D., and Bingham, J. T., Trans. Faraday Soc. **62,** 2719 (1966).
[6] JANAF Thermochemical Tables, Second Addendum (PB 168 370-2), Clearinghouse, U.S. Department of Commerce, Springfield, Va., Aug. 1967 (table for α-Be_3N_2, dated Mar. 31, 1967).
[7] Furukawa, G. T., and Reilly, M. L., unpublished data.
[8] Justice, B. H., (see ref. [6]).
[9] Satoh, S., Sci. Papers Inst. Phys. and Chem. Research (Tokyo) **34,** 888 (1938).
[10] Experimental Thermodynamics, Vol. I, McCullough, J. P., and Scott, D. W., Ed. (Butterworths, London, 1968) (Ch. 8, High-temperature Drop Calorimetry, Douglas, T. B., and King, E. G., p. 293).
[11] Victor, A. C., and Douglas, T. B., J. Res. NBS **67A** (Phys. and Chem.) No. 4, 325 (1963).
[12] Kelley, K. K., Bur. Mines Bulletin 584, Contributions to the Data on Theoretical Metallurgy. XIII. High-Temperature Heat-Content, Heat-Capacity, and Entropy Data for the Elements and Inorganic Compounds, U.S. Government Printing Office, Washington, D.C., 1960, p. 25.
[13] International Practical Temperature Scale of 1968, Metrologia **5,** 35 (1969).

(Paper 73A5-564)

JOURNAL OF RESEARCH of the National Bureau of Standards—A. Physics and Chemistry
Vol. 73A, No. 5, September–October 1969

Measured Enthalpy and Derived Thermodynamic Properties of Solid and Liquid Lithium Tetrafluoroberyllate, Li_2BeF_4, from 273 to 900 K[1]

Thomas B. Douglas and William H. Payne[2]

Institute for Basic Standards, National Bureau of Standards, Washington, D.C. 20234

(May 20, 1969)

The enthalpy of a sample of lithium tetrafluoroberyllate, Li_2BeF_4, of 98.6 percent purity was measured relative to 273 K at eleven temperatures from 323 to 873 K. Corrections were applied for the impurities and for extensive premelting below the melting point (745 K). The enthalpy and heat capacity, and the entropy and Gibbs free-energy function relative to the undetermined value of $S^\circ_{298.15}$, were computed from empirical functions of temperature derived from the data, and are tabulated from 273 to 900 K.

Key words: Drop calorimetry; enthalpy data; lithium beryllium fluoride; lithium tetrafluoroberyllate; premelting; thermodynamic properties.

1. Introduction

As part of a long-term research program at the National Bureau of Standards on the thermodynamic properties of the simpler light-element compounds, the measurements of high-temperature enthalpy have included several well-defined substances which may be regarded as double oxides or double fluorides of two metals. Such results have been published in two papers for $BeO \cdot Al_2O_3$ ($BeAl_2O_4$) and $BeO \cdot 3Al_2O_3$ ($BeAl_6O_{10}$) [1],[3] are being obtained for $3LiF \cdot AlF_3$ (Li_3AlF_6), and are presented in this paper for $2LiF \cdot BeF_2$ (Li_2BeF_4). The standard heats of formation and heat capacities of some "double" compounds of this type are very nearly the same as the values calculated additively from the parent binary compounds (in the same state), but in other cases there are considerable differences.

The United States molten salt reactor program has in recent years provided several notable demonstrations of feasible examples. In nearly any foreseeable thermal reactor of this type, the solvent for the fissile and/or fertile material is an LiF-BeF_2 mixture of composition near that of Li_2BeF_4 [2]. Accordingly, the thermodynamic properties of this compound are of great practical importance in this developing technology.

The temperature-composition phase diagram of the condensed phases of the LiF–BeF_2 system has been investigated in a number of laboratories. The version in a fairly recent compilation of phase diagrams [3] is based on the results of two groups of workers [4, 5]. Another composite diagram [6] is based on the results of the above workers, as well as on those from two other publications [7, 8] and additional work unpublished at that time. A more recent version of the phase diagram, which is in essential agreement with the two already mentioned, is reproduced here as figure 1; it is based largely on a comprehensive study at the Oak Ridge National Laboratory [9]. One group of workers [5] reported a compound $LiF \cdot 2BeF_2$ not found in other laboratories. There is general agreement, however, on the existence of the two solid compounds in the LiF–BeF_2 system indicated in figure 1. It will be noted that Li_2BeF_4, the compound of interest in this paper, is not quite congruent-melting, showing a peritectic point. The liquid field is continuous, but when it has the stoichiometric composition of Li_2BeF_4 it may be regarded as the liquid phase of this compound.

Crystalline Li_2BeF_4 exhibits an unusually small volume change when it melts (no more than 2 or 3 percent [10]). This is attributed to the existence of two continuous void channels penetrating the unit cell of the crystal, an unusual feature revealed by a recent quantitative structure determination [11]. A consequence of this feature is that the crystal density of Li_2BeF_4 is about 15 percent less than that computed additively from the two component binary fluorides. An investigation of the thermodynamic activities of

[1] Research sponsored by the Advanced Research Projects Agency, U.S. Department of Defense, under ARPA Order No. 20, and by the Air Force Office of Scientific Research, Office of Aerospace Research, U.S. Air Force, under AFOSR Contract No. ISSA 68–0004.
[2] Present address: Science Information Exchange, 1730 M St., N.W., Washington, D.C. 20036.
[3] Figures in brackets indicate the literature references at the end of this paper.

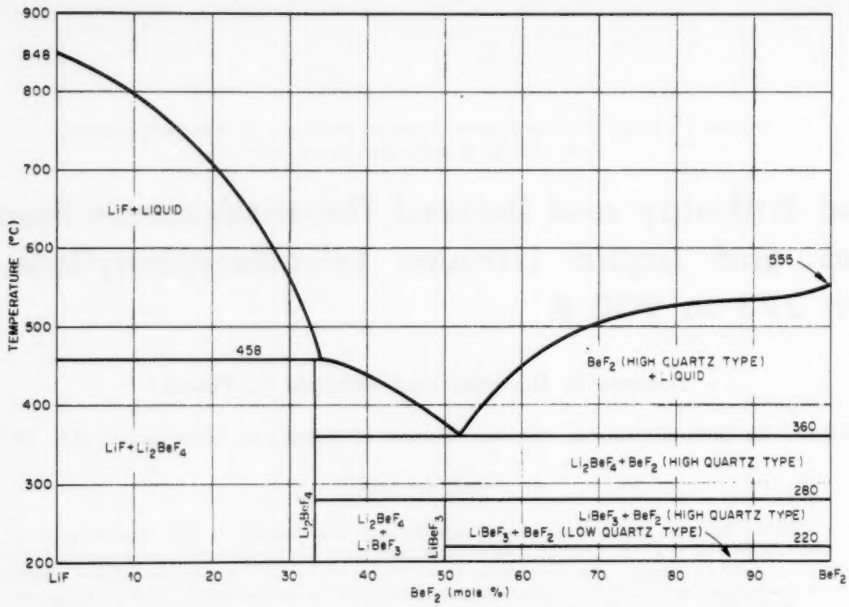

FIGURE 1. *The temperature-composition phase diagram of the LiF-BeF_2 system (from ref. [9]).*

the components of the liquid LiF–BeF_2 system has recently been published [12].

Besides the above solid compounds in the LiF–BeF_2 system, two gaseous compounds are known: from mass-spectrometric work the heats of formation at 900 K of $LiBeF_3(g)$ [13] and $Li_2BeF_4(g)$ [14] have been reported. The heat of formation of crystalline Li_2BeF_4 at 298 K also has been reported [15].

The measurements of enthalpy of Li_2BeF_4 reported in this paper cover the temperature range 0 to 600 °C. Because the sample was only 98.6 percent pure, there was extensive "premelting" in the region 400–470 °C, and the large corrections which this necessitated are sufficiently uncertain as to leave the derived heat of fusion much more uncertain than if the sample had been highly pure. In addition, no low-temperature heat-capacity measurements on Li_2BeF_4 are available to enable the calculation of values of absolute entropy from the data.

2. Sample

The sample of lithium tetrafluoroberyllate was prepared by the Oak Ridge National Laboratory, of Oak Ridge, Tenn., by heating together in calculated proportions LiF and BeF_2 to form a single liquid phase, followed by distillation of NH_4HF_2 from the material in order to replace any oxygen present by fluorine. According to subsequent petrographic and x-ray examinations at ORNL, the colorless crystalline sample consisted of a single phase within the detection limits of these methods.

After the sample was received, a portion of it (about 3.3 g) was encased in a container of pure silver and heated electrically in an efficient dry box for an hour at about 400 °C, in order to remove any volatile impurities that might have been produced by the accidental entrance of moisture during handling. The silver container was then sealed gas-tight by flame welding, and further enclosed within a container of 80 Ni–20 Cr as a further precaution against escape of the toxic sample by volatilization or leakage during the subsequent enthalpy measurements.

After the completion of the enthalpy measurements described in section 3, the sample was analyzed chemically and spectrochemically in the Analytical Chemistry Division of the Bureau. The results of the chemical analyses are given in table 1. The qualitative spectrochemical analysis indicated the presence of the following additional elements in the ranges of abundance stated as weight percentages: 0.001–0.01 percent each of Ag, Al, Cu, Fe, K, Mn, Na, Si, Ti, and Zr; 0.0001–0.001 percent each of Ba, Ni, and Pb. (Thirty-five other elements were sought but not detected.)

The deduction of the chemical composition of the sample was based entirely on table 1. It was assumed that the metals were present in their highest oxidation states, and the deficiency of fluorine in relation to the total equivalents of metal was assumed to be accounted for by oxygen, which was not analyzed for. Using the mean analyses given in the last column of table 1, this procedure accounted for 99.8 percent by weight of the sample. However, the percentage of fluorine is obviously the least precisely determined, so the percentage of this element was then taken to be 76.34 so that the percentages would add to exactly 100 percent. The corresponding elemental composition of the sample then becomes the same as that of table 2, which was used for correcting the thermal data to the basis of pure Li_2BeF_4 in the manner described in section 4.

TABLE 1. *Chemical analysis of the sample*

Element	Individual analyses	Mean
	Weight %	*Weight %*
Li	[a] 13.87, [a] 13.85	[b] 13.85
Be	9.36, 9.33	9.34
F	76.42, 75.90, 75.56, 75.91	75.95
Ca	< 0.01	0.005
Mg	0.01	.01
Cr	< 0.01	.005
Sr	0.02	.02

[a] Uncorrected for Ca, Mg, Cr, and Sr.
[b] This value includes a correction of −0.01 percent to account for the Ca, Mg, Cr, and Sr.

TABLE 2. *Assumed chemical composition of the sample*

Substance	Relative No. of moles	Substance	Relative No. of moles
Li_2BeF_4	1	SrF_2	0.0002
BeO	0.0269	CaF_2	.0001
BeF_2	.0121	CrF_3	.0001
MgF_2	.0004		

3. Enthalpy Measurements

The enthalpy measurements were made using the "drop" method, which, as used in this laboratory, is described in detail in a recent publication [16]. Briefly, the method is as follows. The sample in its container is suspended inside a vertical thick-wall silver pipe in a furnace until it has had time to reach the temperature of the silver. It is then dropped into a Bunsen ice calorimeter, which precisely measures the heat evolved by the sample and container in cooling to 0 °C (273.15 K). In order to account for the enthalpy change of the container itself and the small amount of heat lost from its surface during the drop, a separate measurement is made on the empty container at the same furnace temperature. In the present case the measurements with and without the sample present employed the same outer (80 Ni–20 Cr) container, but utilized different though entirely comparable inner containers of pure silver having identical masses.

For the present measurements the furnace temperature was measured by two Pt/Pt–10 percent Rh thermocouples (as a precaution against any sudden shifts in the differences between their readings, which did not occur). One of these thermocouples was calibrated before the enthalpy measurements by the NBS Pyrometry Laboratory, and it agreed with another similarly calibrated thermocouple when the two were compared in the furnace.

The heats observed in individual measurements are listed (in joules) in table 3 (columns 3 and 4). These values are for the actual sample and container used, except that corrections have been applied for very small unavoidable departures from the "standard" masses of parts of the container system, but not for impurities or premelting. For each furnace temperature the values are given in chronological order, although the different furnace temperatures were run in somewhat random order. As always with this method, the times in the furnace adequate for reaching thermal equilibrium were predetermined from preliminary measurements at one temperature with deliberately inadequate times. The times actually used are shown in column 2 of table 3. As a further precaution, considerably different times for duplicate measurements at most of the temperatures were deliberately chosen. A second precaution was to hold the sample for a few minutes at temperatures higher than the final ones, in the case of one measurement at 470.05 °C and one at 500.10 °C (see table 3), to hasten the slow process of fusion at these temperatures near the melting point. However, there is no correlation between columns 2 and 3 of the table that might suggest the appreciable lack of thermal equilibrium for any of the measurements.

The derivation of columns 5–9 of table 3 is discussed in the next section.

4. Treatment of the Data

The purpose of the present investigation was to determine thermodynamic properties (those derivable from enthalpy data) of pure Li_2BeF_4, not the actual sample measured nor even an odd composition of the LiF-BeF_2 system. It is convenient to correct the enthalpy data for the deviation of the sample composition from pure Li_2BeF_4 in two steps, firstly for the impurities indicated by table 2 and secondly for the "premelting" of the Li_2BeF_4 which they caused.

Figure 1 shows qualitatively the expected equilibrium behavior as the temperature is raised above 200 °C. No polymorphic transition of pure Li_2BeF_4 is indicated, but at the peritectic temperature it decomposes completely into a liquid richer in BeF_2 and a small amount of LiF(c), and several degrees higher (when the highest liquidus curve is crossed) all solid has disappeared and the liquid has regained the composition Li_2BeF_4. If the actual sample represented by table 2 behaved as Li_2BeF_4 with a small proportion of additional BeF_2, it was completely solid at and below 300 °C, but had successively increasing proportions of liquid at 400, 425, and 450 °C, and may have been all liquid at 470 °C.

After averaging the entries in column 3 of table 3 for each furnace temperature (column 1), subtracting the corresponding average for the empty container (column 4), and converting this net enthalpy to a molar basis (defining 1 mole as 1 gram-formula-weight of Li_2BeF_4), the total correction listed in column 5 for the impurities given in table 2 was applied on the basis of replacing the impurities by the same mass of Li_2BeF_4. The correction for BeO(c) was computed from accurate results obtained in this laboratory [17], that for BeF_2(c) was computed from results of drop calorimetry elsewhere [18], and that for the small amounts of the four additional fluorides was assumed

to be equivalent to the same number of atoms of BeF_2. A further impurity correction of −293 J (per mole of Li_2BeF_4) was applied above 300 °C: without knowing what fraction of the impurities was dissolved in the liquid solutions or what their heats of solution are, this minor correction was estimated as half the heat of fusion (derived below) of the amount of Li_2BeF_4 having the same number of atoms as the impurities.

The corrections for premelting can be predicted to be large, and in the absence of further experimental data (such as enthalpy measurements on another sample of somewhat different composition) no rigor-

TABLE 3. *Relative enthalpy of lithium tetrafluoroberyllate,* Li_2BeF_4

1. Furnace temperature,[a] t	2. Time sample in furnace	Individual enthalpy measurements		Corrections		Net enthalpy of Li_2BeF_4[g]		9. Mean obs.−calc.
		3. Container plus sample[b, c]	4. Empty container[d]	5. Impurities[e]	6. Premelting[f]	7. Mean observed[h]	8. Calc. from equations	
°C	*min*	*J*	*J*	*J mol*$^{-1}$	*J mol*$^{-1}$	*J mol*$^{-1}$	*J mol*$^{-1}$	*J mol*$^{-1}$
50.00	56	609.36	378.48	+21	0	6,837	6,763	+74
	60	610.57	380.12					
	.....	.....	780.65					
	.....	.....	782.95					
	.....	.....	777.97					
100.00	54	1,248.55	778.77	+34	0	13,849	13,898	−49
	59	1,247.71	778.77					
	.....	.....	781.65					
	.....	.....	782.12					
	.....	.....	782.78					
	.....	.....	1,601.1					
	44	2,592.9	1,603.7					
200.05	33	2,594.7	1,610.8	+67	0	29,296	29,296	0
	.....	.....	1,604.0					
	.....	.....	1,603.6					
	46	4,015.4	2,455.0					
300.05	30	4,015.1	2,455.8	+100	0	46,183	46,178	+5
	62	4,014.1	.....					
	44	5,562.8	3,341.6					
400.10	46	5,567.6	3,340.4	−134	−1,218	64,559	64,561	−2
	35	5,987.0	3,554.8					
425.10	48	5,988.5	3,553.7	−109	−2,276	69,408	69,387	+21
	58	6,496.7	3,791.7					
450.05	38	6,496.7	3,788.7	−50	−5,820	74,279	74,295	−16
	42	8,097.6	3,961.3					
470.05	[i] 86	8,096.6	3,963.2	+464	0	122,528	122,637	−106
	41	8,612.7	4,243.5					
500.10	[j] 78	8,617.6	4,240.5	+494	0	129,721	129,612	+109
	.....	.....	4,241.3					
	.....	.....	4,707.5					
	47	9,458.4	4,697.4					
550.10	76	9,457.6	4,708.2	+531	0	141,059	141,218	−159
	48	9,462.2	4,701.2					
	.....	.....	4,704.9					
	62	10,333.0	5,173.7					
600.15	39	10,332.5	5,176.4	+577	0	152,984	152,833	+151

[a] International Practical Temperature Scale of 1968 [20].
[b] Sample mass = 3.3463 g.
[c] Uncorrected for sample impurity.
[d] Before computing the mean net enthalpy of the sample, the mean of the values in this column for each of four temperatures was incremented by a small amount to agree with a smooth plot of $(H—H_{0\,°C})/t$ versus t for the empty container: −6.4 J at 400.10 °C, +3.9 J at 425.10 °C, −5.7 J at 450.05 °C, and +4.1 J at 470.05 °C.
[e] For all temperatures above 300.05 °C this column includes a correction of −293 J (per mole of Li_2BeF_4) for the assumed heat of fusion of the impurities (see text).
[f] See text.
[g] Molecular weight = 98.884. Enthalpy relative to that of the solid at 0 °C.
[h] Corrected for sample impurity and for premelting.
[i] Temperature of container plus sample first raised momentarily to 500 °C to hasten completion of fusion.
[j] Temperature of container plus sample held at 525–550 °C for first 10 min of heating period to insure completion of fusion.

ously accurate means of determining them is available. This fact made it desirable first to derive tentative enthalpy-temperature equations for the pure solid and liquid, later testing them for consistency with the best empirical estimation of the premelting corrections that could be devised.

The heats of the small amounts of solid-phase reproportionation below 400 °C (see fig. 1) were considered negligible, and the four mean observed enthalpies up to and including that at 300.05 °C (table 3, column 7) were used to derive (by the least-square method) the coefficients of an equation which was tentatively assumed to apply to pure solid Li_2BeF_4 up to its melting point [identical with eq (2), sec. 5, except referred to the enthalpy of the crystal at 0 °C]. (In an attempt to decrease the deviations, which are the first four entries in column 9 of the table, fits were tried using an additional term proportional to T^{-n}, with n varying from 0.5 to 4, but the standard deviations of fit were considerably greater.) The four mean observed enthalpies at and above 470.05 °C (table 3, column 7) vary almost linearly with temperature, and were similarly used to derive the coefficients of an equation assumed to apply to pure liquid Li_2BeF_4 relative to the solid at 0 °C [identical with eq (6), sec. 5, except that its constant term differs by the amount indicated by eq (2)]. Since these two enthalpy equations for the solid and the liquid are both based on the solid at the same temperature (0 °C), their difference represents the heat of fusion as a function of temperature. For simplicity, the incongruent melting of Li_2BeF_4 over the short temperature range from the peritectic temperature to the "freezing point" was ignored as though this incongruency were suppressed (fig. 1), and the liquidus curve below the peritectic temperature was extrapolated to a "congruent" melting point of 472 °C ($T_m = 745.2$ K).[4] At this temperature the heat of fusion of Li_2BeF_4, arrived at as described above, is 44,400 J mol^{-1} (equivalent to the reasonable value of 2.03 cal g-atom^{-1} K^{-1} for the entropy of fusion).

Since premelting over a range of some 70 kelvins is to be considered, its thermodynamic consideration should not involve unnecessary approximations applicable only to temperatures much nearer the melting point. It can be shown that if the impurities are insoluble in the main substance when it is solid but form ideal solutions with it when it is liquid, the enthalpy correction for premelting, per mole of main substance at absolute temperature T, is

$$\Delta H = -nL_f \Big/ \left\{ \exp \int_T^{T_m} [L_f(T)/RT^2]dT \right\} - 1. \qquad (1)$$

where T_m and L_f are respectively the absolute melting point and molar heat of fusion of the main substance, n being the number of moles of impurity in solution in the liquid part of one mole of the main substance, and R being the molar gas constant. Equation (1) is applicable also to non-ideal solutions if actual molecular weights are replaced by effective ones (which may change somewhat with temperature), but for electrolytic solutions such as the present one, it is difficult to say what these effective molecular weights are. However, taking the formula weight of Li_2BeF_4 as its molecular weight and, as above, $T_m = 745.2$ K, the constant value of n with which eq (1) gives the best fit of the mean observed corrected enthalpy values at 400.10, 425.10, and 450.05 °C to the above enthalpy equation for the solid (which is based wholly on observed values at lower temperatures) proved to be 0.03216. (This is about 80 percent of the sum of the moles of impurity in table 2.) The corresponding corrections for premelting are given in column 6 of table 3. [Corrections of roughly the same respective magnitudes can be calculated by ignoring eq (1) and using instead the "$Li_2BeF_4(c)$" liquidus curve of the phase diagram (fig. 1).]

It is striking that the three non-zero premelting corrections in table 3 are in magnitude many times the corresponding final deviations between the observed and equation values given in column 9. This good agreement for the calculated premelting corrections, while probably somewhat fortuitous, seems to justify regarding the tentative enthalpy equation for the solid [eq (2)] as a good representation of the enthalpy below the melting point. Nevertheless, it corresponds to a heat capacity increasing strictly linearly with temperature [eq (3)], whereas many pure ionic solids are now known to possess heat capacity-temperature curves with appreciable upward curvature near the melting point owing to lattice vacancies. Such an effect in Li_2BeF_4 would lead to a lower heat of fusion than that calculated in this paper.

5. Thermodynamic Functions

The following numerical equations, which resulted from the enthalpy equations derived from the data as outlined in section 4, gives the final values of the enthalpy (H), heat capacity (C_p), and entropy (S) of solid and liquid lithium tetrafluoroberyllate, Li_2BeF_4, adopted in this paper. Since enthalpy and heat-capacity data on this substance are not available below 273.15 K, the enthalpy and entropy are given relative to the respective values for the solid at the standard thermodynamic temperature 298.15 K, though the equations for the solid are valid (with increasing uncertainty, as mentioned later) down to 273.15 K. The units are joules per mole for energy (with 1 mole = 98.884 g), and kelvins (International Practical Temperature Scale of 1968 [20]) for the absolute temperature T.

Solid $Li_2BeF_4(c)$, 273.15–745.2 K:

$$H^\circ - H^\circ_{298.15} = -33698.8 + 90.7970T + 0.0745589T^2 \qquad (2)$$

$$C_p^\circ = 90.797 + 0.149118T \qquad (3)$$

$$S^\circ - S^\circ_{298.15} = -561.786 + 90.7970 \ln T + 0.149118T \qquad (4)[5]$$

[4] This temperature was estimated by consideration of the phase diagram of reference [6] as well as that of figure 1, and is uncertain by a few degrees.

[5] "ln" indicates the natural logarithm (base e).

356-078 O-69—3

Fusion, 745.2 K:

$$\Delta H_m^\circ = 44400; \qquad \Delta S_m^\circ = 59.58 \tag{5}$$

Liquid $Li_2BeF_4(l)$, 745.2–900 K:

$$H^\circ(l) - H^\circ_{298.15}(c) = -53187.0 + 232.0907T \tag{6}$$

$$C_p^\circ = 232.09 \tag{7}$$

$$S^\circ(l) - S^\circ_{298.15}(c) = -1325.550 + 232.0907 \ln T \tag{8}[5]$$

Values calculated from eqs (2)–(4) and (6)–(8) are listed in table 4, the Gibbs free-energy function relative to the entropy of the solid at 298.15 K being computed from the thermodynamic relation

$$[-(G^\circ - H^\circ_{298.15})/T - S^\circ_{298.15}] = [S^\circ - S^\circ_{298.15}] - [(H^\circ - H^\circ_{298.15})/T]. \tag{9}$$

For convenience, table 4 is repeated as table 5 except in terms of the defined calorie (= 4.1840 joules) instead of the joule, since the defined calorie is commonly used in the calculations of chemical thermodynamics.

While experimental data are presently lacking from which a reliable value for $S^\circ_{298.15}$ of the solid can be evaluated, an estimated value may be used with table 4 or 5 to provide estimated values of the absolute

TABLE 4. *Thermodynamic functions for lithium tetrafluoroberyllate (Li_2BeF_4) solid and liquid phases (in terms of* **JOULES** *per mole)*

(1 mole=98.884 g; International Practical Temperature Scale of 1968)

T	$H^\circ - H^\circ_{298}$	C_p°	$S^\circ - S^\circ_{298}$	$-(G^\circ - H^\circ_{298})/T - S^\circ_{298}$
K	J mol^{-1}	J mol^{-1} K^{-1}	J mol^{-1} K^{-1}	J mol^{-1} K^{-1}
Solid Phase				
273.15	−3335	131.53	−11.68	0.53
275	−3091	131.80	−10.79	.45
298.15	0	135.26	0	0
300	251	135.53	.84	.00
325	3686	139.26	11.83	.49
350	7214	142.99	22.29	1.68
375	10835	146.72	32.28	3.39
400	14549	150.44	41.87	5.49
425	18357	154.17	51.10	7.91
450	22258	157.90	60.02	10.56
475	26252	161.63	68.66	13.39
500	30339	165.36	77.04	16.36
525	34520	169.08	85.20	19.45
550	38794	172.81	93.15	22.62
575	43161	176.54	100.91	25.85
600	47621	180.27	108.51	29.14
625	52174	184.00	115.94	32.46
650	56820	187.72	123.23	35.81
675	61560	191.45	130.39	39.18
700	66393	195.18	137.42	42.57
725	71319	198.91	144.33	45.96
745.2	75367	201.92	149.84	48.70
Liquid Phase				
745.2	119767	232.09	209.42	48.70
750	120881	232.09	210.91	49.73
775	126683	232.09	218.52	55.06
800	132486	232.09	225.89	60.28
825	138288	232.09	233.03	65.41
850	144090	232.09	239.96	70.44
875	149892	232.09	246.68	75.38
900	155695	232.09	253.22	80.23

H°_{298} and S°_{298} are, respectively, the enthalpy and entropy of the solid at 298.15 K and 1 atm pressure.

[5] "ln" indicates the natural logarithm (base e).

TABLE 5. *Thermodynamic functions for lithium tetrafluoroberyllate (Li_2BeF_4) solid and liquid phases (in terms of* **CALORIES** *per mole)*

(1 cal=4.1840 J; 1 mole=98.884 g; International Practical Temperature Scale of 1968)

T	$H^\circ - H^\circ_{298}$	C_p°	$S^\circ - S^\circ_{298}$	$-(G^\circ - H^\circ_{298})/T - S^\circ_{298}$
K	cal mol^{-1}	cal mol^{-1} K^{-1}	cal mol^{-1} K^{-1}	cal mol^{-1} K^{-1}
Solid Phase				
273.15	−797	31.44	−2.79	0.13
275	−739	31.50	−2.58	.11
298.15	0	32.33	0	0
300	60	32.39	.20	.00
325	881	33.28	2.83	.12
350	1724	34.17	5.33	.40
375	2590	35.07	7.72	.81
400	3477	35.96	10.01	1.31
425	4387	36.85	12.21	1.89
450	5320	37.74	14.34	2.52
475	6274	38.63	16.41	3.20
500	7251	39.52	18.41	3.91
525	8250	40.41	20.36	4.65
550	9272	41.30	22.26	5.41
575	10316	42.19	24.12	6.18
600	11382	43.08	25.93	6.96
625	12470	43.98	27.71	7.76
650	13580	44.87	29.45	8.56
675	14713	45.76	31.16	9.37
700	15868	46.65	32.84	10.17
725	17046	47.54	34.50	10.98
745.2	18013	48.26	35.81	11.64
Liquid Phase				
745.2	28625	55.47	50.05	11.64
750	28891	55.47	50.41	11.89
775	30278	55.47	52.23	13.16
800	31665	55.47	53.99	14.41
825	33052	55.47	55.70	15.63
850	34438	55.47	57.35	16.84
875	35825	55.47	58.96	18.02
900	37212	55.47	60.52	19.18

H°_{298} and S°_{298} are, respectively, the enthalpy and entropy of the solid at 298.15 K and 1 atm pressure.

entropy and the Gibbs free-energy function. One compilation [19] has estimated for this constant 29.8 ± 2 cal mol^{-1} K^{-1} (124.7 $\pm$ 8 J mol^{-1} K^{-1}), taken as the sum of the entropies at this temperature of two moles of $LiF(c)$ and one mole of $BeF_2(c)$.

From a consideration of the sources of systematic error and the precision of the enthalpy values, the corrected heat capacities as given by eqs (3) and (7) and in tables 4 and 5 are estimated to have general uncertainties of ± 2 percent for the solid from 298 to 600 K and ± 3 percent for the liquid from 750 to 850 K. However, the error in the derived heat capacity may reach several percent near the lower end of the experimental range (below 298 K). Between 600 and 750 K the large, rather uncertain corrections for premelting introduce additional uncertainties for the solid and the heat of fusion which are difficult to estimate, but no additional uncertainty for the enthalpy of the liquid as given by eq (6), and very little for the entropy of the liquid as given by eq. (8).

The authors are pleased to acknowledge the help of several persons. Roy E. Thoma and his associates at the Oak Ridge National Laboratory prepared the sample and made the petrographic and x-ray examinations of it. The sample was analyzed in the Analytical Chemistry Division of the Bureau—chemically by Rolf A. Paulson and E. June Maienthal, and spectrochemically by Elizabeth K. Hubbard.

6. References

[1] Ditmars, D. A., and Douglas, T. B., J. Research NBS **71A**, 89, 97 (1967).

[2] Thoma, R. E., private communication (April 21, 1969),

[3] Phase Diagrams for Ceramists, Levin, E. M., Robbins, C. R., and McMurdie, H. F., The American Ceramic Society, Columbus, Ohio, 1964, p. 420 (fig. 1469).

[4] Jones, L. V., Etter, D. E., Hudgens, C. R., Huffman, A. A., Rhinehammer, T. B., Rogers, N. E., Tucker, P. A., and Wittenberg, L. J., J. Am. Ceram. Soc. **45**, 80 (1962).

[5] Roy, D. M., Roy, R., and Osborn, E. F., J. Am. Ceram. Soc. **37**, 300 (1954).

[6] Phase Diagrams of Nuclear Reactor Materials, Thoma, R. E., Ed., Report ORNL–2548 [TID–4500 (15th ed.)], Oak Ridge National Laboratory, Oak Ridge, Tenn., Nov. 20, 1959. p. 33.

[7] Novoselova, A. V., Simanov, Yu. P., and Yarembash, E. I., J. Phys. Chem. (U.S.S.R.) **26**, 1244 (1952).

[8] Speirs, J. L., "The Binary and Ternary Systems Formed by Calcium Fluoride, Lithium Fluoride, and Beryllium Fluoride: Phase Diagrams and Electrolytic Studies," Ph.D. thesis, Univ. of Michigan, Ann Arbor, Mich., May 29, 1952.

[9] Thoma, R. E., Insley, H., Friedman, H. A., and Hebert, G. M., J. Nuclear Materials **27**, 166 (1968).

[10] Sturm, B. J., and Thoma, R. E., Report ORNL–3789, Oak Ridge National Laboratory, Oak Ridge, Tenn. 1965, p. 83.

[11] Burns, J. H., and Gordon, E. K., Acta Cryst. **20**, 135 (1966).

[12] Mathews, A. L., and Baes, C. F., Inorg. Chem. **7**, 373 (1968).

[13] Berkowitz, J., and Chupka, W. A., Ann. N.Y. Acad. Sci. **79**, 1073 (1960).

[14] Buchler, A., and Stauffer, J. L., Symposium on Thermodynamics, Paper SM–66/26, Vienna, Austria, 1965.

[15] Gross, P., Admin. Report No. 5 [Contract AF 61(052)–863, 1 Jan. 1966–30 April 1966], Fulmer Research Inst., Stoke Poges, Buckinghamshire, England.

[16] Experimental Thermodynamics, Vol. I, McCullough, J. P., and Scott, D. W., Ed., Butterworths, London, 1968 (Ch. 8, "High-temperature Drop Calorimetry," Douglas, T. B., and King, E. G., p. 293).

[17] Victor, A. C., and Douglas, T. B., J. Research NBS **67A**, 325 (1963).

[18] Taylor, A. R., and Gardner, T. E., U.S. Bur. Mines Rept. Invest. 6664 (1965).

[19] JANAF Thermochemical Tables, Second Addendum (PB 168 370–2), Clearinghouse, U.S. Department of Commerce, Springfield, Va., Aug. 1967 (tables for crystalline and liquid Li_2BeF_4, dated June 30, 1966).

[20] International Practical Temperature Scale of 1968, Metrologia **5**, 35 (1969).

(Paper 73A5–565)

JOURNAL OF RESEARCH of the National Bureau of Standards—A. Physics and Chemistry
Vol. 73A, No. 5, September–October

Nonanalytic Vapor Pressure Equation With Data for Nitrogen and Oxygen

Robert D. Goodwin*

Institute for Basic Standards, National Bureau of Standards, Boulder, Colorado 80302

(June 10, 1969)

The specific heat of a two phase liquid-vapor system at constant volume apparently increases without limit at temperatures approaching the critical point, suggesting (via a thermodynamic relation) that the vapor pressure derivative d^2P/dT^2 may behave similarly. This nonanalytic behavior at the critical point is used in the present vapor pressure formula to gain simplicity and accuracy, as seen by use of data for nitrogen and oxygen.

Key words: Critical point; equation; formula; liquid; nitrogen; nonanalytic; oxygen; vapor pressure.

List of Symbols

A, B, C	constant coefficients.
a, b, c, d, e	constant coefficients.
Δ	$100 \cdot (P/P_{calc}-1)$.
ϵ	a nonintegral exponent, $1<\epsilon<2$.
$F(x)$	any function of T, nonanalytic at T_c.
P	pressure, 1 atm = 0.101325 MN/m².
P_c	critical-point pressure.
P_t	triple-point pressure.
T	temperature, K.
T_c	critical-point temperature.
T_t	triple-point temperature.

$x(T) \equiv (1-T_t/T)/(1-T_t/T_c)$.
$y(P) \equiv \log (P/P_t)/\log (P_c/P_t)$.

1. Introduction

An accurate vapor pressure equation is essential for computing thermodynamic properties of fluids, but a satisfactory function remains undiscovered [1].[1] To achieve accuracy for thermal property computations, many authors resort to polynomial representations of experimental vapor pressure data. This has the serious disadvantage that derivatives, dP/dT etc., may not be reliable.

A new approach to this problem resides in the proposal that d^2P/dT^2 be infinite at the critical point, as given by a term $P \sim -(T_c-T)^2 \cdot \log (T_c-T)$ where subscript c refers to the critical point [2]. Other work on critical phenomena [3] suggests that this pole also might be described by use of a nonintegral exponent ϵ in a term $(T_c-T)^\epsilon$, $1<\epsilon<2$.

Our particular need was for a reduced equation sufficiently simple to permit examination of existing data on fluorine. I have therefore used data only on the similar substances nitrogen and oxygen in the present work. Application of this equation to new data on fluorine will be reported independently [4].

2. Data and Method

I have examined nitrogen and oxygen for deviations from the basic vapor pressure equation,

$$\log (P) = a - b/T, \tag{1}$$

as have many previous workers. To normalize the variables, I eliminate the constants of (1) by use of triple-point and critical-point properties in the definitions.

$$x(T) \equiv (1-T_t/T)/(1-T_t/T_c),$$

$$y(P) \equiv \log (P/P_t)/\log (P_c/P_t),$$

where subscript t refers to the triple point. These variables range from zero to unity. Equation (1) now reads simply $y=x$, and we may conveniently examine plots of the deviations $(y-x)$ as a function of x. For each substance the plot is qualitatively a simple cubic, with roots $x_1=0$, $0<x_2<1$, $x_3=1$.

3. The Vapor Pressure Equation

Qualitative behavior of the above deviations is

$$(y-x) = A \cdot x \cdot (B-x) \cdot (1-x). \tag{2}$$

*Cryogenics Division, NBS Boulder Laboratories, Boulder, Colorado, 80302.
[1] Figures in brackets indicate the literature references at the end of this paper.

Precise oxygen vapor pressures [5] still cannot be represented accurately by (2). Addition of a nonanalytic term, $F(x)$, however, yields an accurate equation for nitrogen and oxygen,

$$y = x + A \cdot x \cdot (B-x) \cdot (1-x) + C \cdot F(x). \quad (3)$$

Equation (3) is converted to a working equation by multiplying the terms in brackets and collecting powers of x,

$$\log (P/P_t) = a \cdot x + b \cdot x^2 + c \cdot x^3 + d \cdot F(x). \quad (3a)$$

This equation is used throughout the following work. It is constrained to a given triple-point pressure, P_t. As vapor pressures in the mm Hg range have very low relative accuracy, figure 1a, this constraint is desirable and useful. If P_t is unknown and is to be estimated from the equation, we have the following option with no constraints,

$$\log (P) = a + b \cdot x + c \cdot x^2 + d \cdot x^3 + e \cdot F(x). \quad (3b)$$

Excellent representation of vapor pressure data for nitrogen and oxygen is obtained with either of the nonanalytic forms

$$F_1(x) = -(1-x)^2 \cdot \log (1-x), \quad (4a)$$

$$F_2(x) = x \cdot (1-x)^\epsilon \quad (4b)$$

where exponent ϵ is nonintegral, $1 < \epsilon < 2$. In the following we shall see that (4b) is better for oxygen as T approaches T_c. For nitrogen, data of the precision necessary to choose between (4a) and (4b) are not available, and hence I do not plot the nitrogen deviations in this report. Nitrogen results are given only to indicate that (3) is not unique for oxygen.

As a guide for comparing results given below, the most accurate vapor pressure equation currently available for oxygen probably is that of Hust and Stewart [9],

$$\log (P) = \sum_{i=0}^{7} A_i \cdot T^i, \quad (5)$$

with eight coefficients. We note absence of a term $1/T$. This is no oversight, as these authors intensively investigated many well-known forms [1].

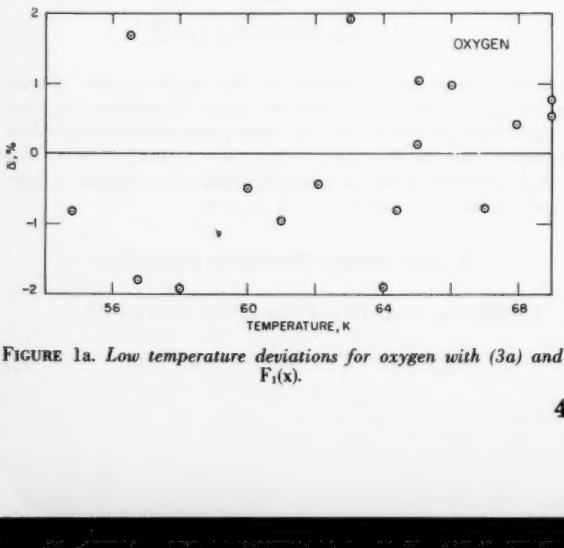

FIGURE 1a. *Low temperature deviations for oxygen with (3a) and* $F_1(x)$.

4. Some Results for Nitrogen and Oxygen

The nitrogen data used here are those selected by Strobridge [6], namely from [7] and [8]. The oxygen data are the same as selected by Hust [9], namely from [5]. Fixed-point constants used for the present work are in table 1. Results for eq (3a) are in table 2. Each column gives the form of $F(x)$, the derived critical-point pressure P_c, the relative critical-point slope, $[d\ln(P)/d\ln(T)]_c$, exponent ϵ and the coefficients, the number of datum pairs, NP, and the root mean square of individual, relative deviations, RMS.

Hoge [5] gives about 218 data for oxygen. For table 2, some imprecise low-temperature data were eliminated to yield an rms deviation of 0.06 percent. For all 218 data the rms relative deviation is 0.34 percent, about the same as found by Hust and Stewart only by use of the eight-constant power series and by weighting the data and deviations according to their uncertainties. Our deviation was obtained with no weighting, and with fewer arbitrary coefficients.

Approaching the critical point, these oxygen data are extremely precise, enabling us to see that $F_2(x)$ gives a much better representation at $T > 141$ K than does the logarithmic form, $F_1(x)$. This is evident upon comparing deviations via $F_1(x)$ in figure 1 with the corresponding deviations via $F_2(x)$ in figure 2. On these plots $\Delta \equiv 100 \cdot (P/P_{\text{calc}} - 1)$.

TABLE 1. *Fixed-point constants used*

	Nitrogen	Oxygen
T_t.....K...	63.14[10]	54.353[5]
P_t.....atm...	[a] 0.1233	0.00150[5]
P_t.....MN/m²...	.0124934	.0001519875
T_c.....K...	[a] 126.25	154.77[5]

[a] Adjusted to minimize deviations.

TABLE 2. *Some results for equation (3a)*

	Nitrogen	Oxygen	Oxygen
$F(x)$	([a])	([a])	([b])
P_c.....atm...	33.524	50.105	50.139
P_c.....MN/m²...	3.396819	5.076889	5.080334
$(d\ln(P)/d\ln(T))_c$...	5.8775	5.9203	6.0117
ϵ.....	.....	.....	1.633
a.....	5.2149143	7.5955889	5.9479153
b.....	0.5126235	5.1202773	8.2487892
c.....	−.1221435	−2.2994456	−3.7796060
d.....	.6158760	3.2246189	4.8725595
NP.....	89	188	188
RMS.....% ...	0.051	0.060	0.059

[a] $F(x) \equiv -(1-x)^2 \cdot \log (1-x)$.
[b] $F(x) \equiv (1-x)^\epsilon \cdot x$.

Table 3 compares results from (5) with results from (3a) using the nonanalytic form (4b). The last two columns give percent deviations of first and second derivatives via (5) from values obtained via (3a). These are plotted in figure 3. It is interesting to see that the

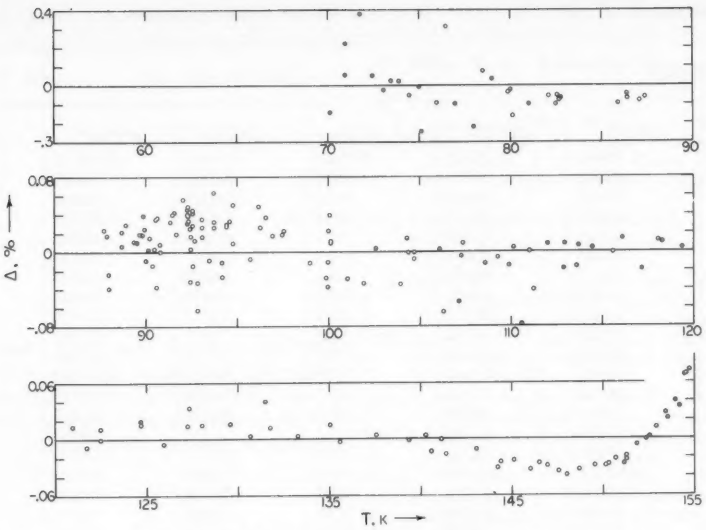

FIGURE 1. *Deviations for oxygen with (3a) and* $F_1(x)$.

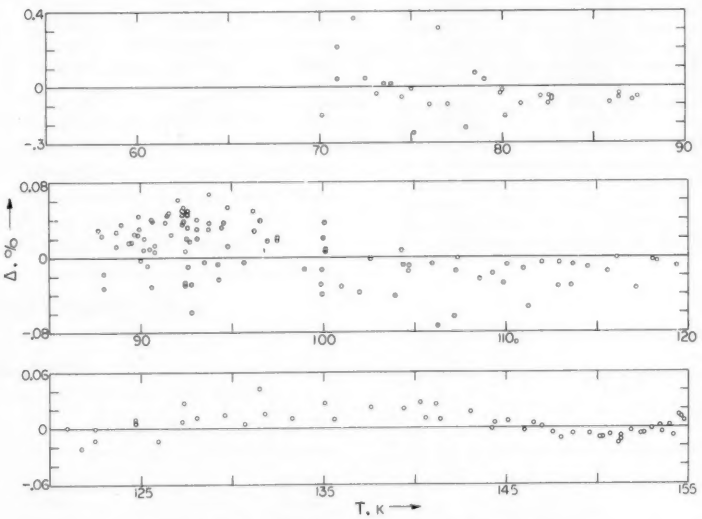

FIGURE 2. *Deviations for oxygen with (3a) and* $F_2(x)$.

number of inversions on these plots corresponds exactly to the number of terms used in the power series (5).

We also may compare the curvature d^2P/dT^2 calculated by (3a) with results derived from our specific heat measurements on the two-phase, liquid vapor system for oxygen [11]. In the thermodynamic relation [2],

$$\overline{C}_v/T = -d^2G/dT^2 + (d^2P/dT^2) \cdot v, \qquad (6)$$

$\overline{C}_v$ is heat capacity of the two phase system at constant volume, G is the Gibbs free energy per mol, and v is the overall, average molal volume. Data for $\overline{C}_v(T)$ at two or more different densities must be interpolated onto isotherms. Equation (6) then gives d^2P/dT^2 as the slope of plots of $\overline{C}_v/T$ versus v. Results have relatively large uncertainties, exceeding those expected from the vapor pressure equation. Table 4 gives this comparison of d^2P/dT^2 from (3a) with results from specific heat data via (6).

As a preliminary measure of the generality of (3), table 5 gives the constants obtained when using $F_1(x)$. These values were derived from results such as those in table 2. Fluorine results are quite preliminary. Constants for all three substances have the same signs and about the same magnitudes.

TABLE 3. *Comparison of oxygen vapor pressure equations*

	Goodwin			Hust-Stewart			Percent	Percent
T, K	*P, ATM*	*dP/dT*	d^2P/dT^2	*P, ATM*	*dP/dT*	d^2P/dT^2	*dP/dT*	d^2P/dT^2
54.353	0.0015	0.00046	0.00012	0.0015	0.00046	0.00012	−0.197	−0.514
60.000	.0072	.00182	.00040	.0072	.00181	.00039	−.448	−.478
65.000	.0230	.00491	.00089	.0229	.00489	.00088	−.373	−.206
70.000	.0616	.01120	.00169	.0614	.01118	.00169	−.198	.042
75.000	.1433	.02241	.00285	.1430	.02240	.00286	−.038	.168
80.000	.2970	.04034	.00438	.2967	.04037	.00439	.058	.168
85.000	.5608	.06674	.00623	.5608	.06680	.00624	.085	.084
90.180	.9997	.10464	.00845	1.0000	.10470	.00844	.062	−.035
95.000	1.6108	.15074	.01072	1.6113	.15077	.01070	.017	−.125
100.000	2.5088	.21056	.01323	2.5092	.21049	.01321	−.030	−.160
105.000	3.7379	.28328	.01587	3.7377	.28311	.01586	−.059	−.112
110.000	5.3640	.36946	.01861	5.3629	.36925	.01862	−.057	.013
115.000	7.4557	.46958	.02145	7.4537	.46946	.02148	−.025	.172
120.000	10.0838	.58410	.02438	10.0818	.58425	.02445	.026	.281
125.000	13.3217	.71364	.02746	13.3214	.71415	.02753	.072	.239
130.000	17.2466	.85906	.03075	17.2494	.85976	.03075	.081	−.017
135.000	21.9410	1.02171	.03438	21.9467	1.02206	.03424	.034	−.395
140.000	27.4959	1.20376	.03857	27.5013	1.20319	.03836	−.048	−.529
145.000	34.0172	1.40910	.04382	34.0178	1.40801	.04391	−.077	.207
150.000	41.6391	1.64619	.05178	41.6383	1.64736	.05255	.071	1.487
151.000	43.3115	1.69914	.05421	43.3123	1.70106	.05489	.113	1.255
152.000	45.0383	1.75483	.05734	45.0413	1.75723	.05751	.137	0.294
153.000	46.8224	1.81427	.06189	46.8277	1.81617	.06044	.105	−2.346
154.000	48.6688	1.87999	.07097	48.6746	1.87824	.06374	−.093	−10.180
154.100	48.8572	1.88716	.07263	48.8628	1.88463	.06410	−.134	−11.744
154.200	49.0463	1.89452	.07462	49.0516	1.89105	.06445	−.183	−13.625
154.300	49.2361	1.90210	.07711	49.2410	1.89752	.06481	−.241	−15.944
154.400	49.4267	1.90997	.08038	49.4311	1.90402	.06518	−.312	−18.911
154.500	49.6181	1.91822	.08505	49.6218	1.91055	.06555	−.400	−22.927
154.600	49.8104	1.92708	.09278	49.8132	1.91713	.06592	−.516	−28.950
154.700	50.0036	1.93710	.11141	50.0052	1.92374	.06630	−.690	−40.487

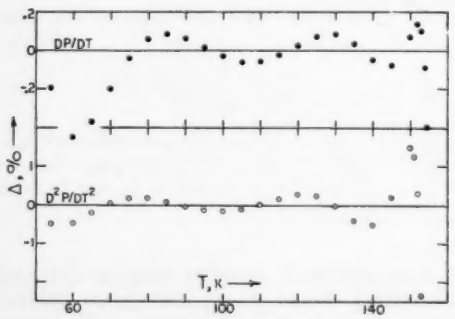

FIGURE 3. *Comparison of derivatives from (5) for oxygen with values from (3a) using (4b).*

TABLE 4. *Comparisons of* d^2P/dT^2 *for oxygen*

$$\overline{C}_v/T = -d^2G/dT^2 + (d^2P/dT^2) \cdot v$$

	d^2P/dT^2, atm/K^2	
T, K	V.P. eq (3a)	Expt'l. $\overline{C}_v$
60.00	0.0004	0.0007 ± 100%
65.00	.0009	.0012
70.00	.0017	.0020
75.00	.0029	.0031
80.00	.0044	.0046
85.00	.0062	.0064
90.18	.0085	.0084
95.00	.0107	.0106
100.00	.0132	.0130
105.00	.0159	.0155
110.00	.0186	.0182
115.00	.0215	.0211
120.00	.0244	.0240
125.00	.0275	.0271 ± 2%

TABLE 5. *Constants for* (3) *with logarithmic* F(x)

	Nitrogen	Oxygen	Fluorine
A	−0.0218	−0.2208	−0.1109
B	3.1969	1.2267	1.2507
C	0.1099	0.3096	0.1913

The oxygen data used here may have a uniquely high precision near the critical point. As (3a) gives an excellent representation of these data, this is good evidence that the vapor pressure formula indeed should be nonanalytic at the critical point, as was suggested by Yang and Yang in 1964.

5. Comments

The following comments have been received, of interest in the rapidly developing theory of critical states. Griffiths and Rushbrooke have proven that if d^2P/dT^2 diverges as $|T-T_c|^{-\theta}$, then $\theta < \alpha' + \beta$ [3b], which brings up the lower limit on ϵ found in the present report for oxygen vapor pressure data.

The scaling laws limit the value of ϵ even further, namely to close to 2. These laws are postulates, not proofs [12]. Recently, a nonanalytic scaling law vapor pressure equation has been used for CO_2 near the critical point [13].

6. References

[1] Miller, D. G., Estimating vapor pressures—a comparison of equations, Ind. Eng. Chem. **56** (3), 46–57 (1964).

[2] Yang, C. N., and Yang, C. P., Critical point in liquid-gas transitions, Phys. Rev. Letters, **13** (9), 303–5 (1964).

[3a] Fisher, M. E., in Critical Phenomena, NBS Miscellaneous Publication 273, M. S. Green and J. V. Sengers, Editors, (U.S. Government Printing Office, Washington, D.C. 20402, 1966).

[3b] Temperley, H. N. V., Rowlinson, J. S., and Rushbrooke, G. S., editors, Physics of Simple Liquids (North-Holland Publishing Co., Amsterdam, 1968).

[4] Straty, G. C., and Prydz, Rolf, The vapor pressure of liquid fluorine, presented at the Cryogenic Engineering Conference, University of California, Los Angeles, June 17, 1969.

[5] Hoge, H. J., Vapor pressure and fixed points of oxygen, and heat capacity in the critical region, J. Res. NBS **44**, 321–345 (1950), RP2081.

[5a] Muijlwijk, R., Moussa, M. R., and van Dijk, H., The vapour pressure of liquid oxygen, Physica **32** (5), 805–22 (1966).

[6] Strobridge, T. R., The thermodynamic properties of nitrogen from 64 to 300 K between 0.1 and 200 atmospheres, NBS Tech. Note 129 (Jan. 1962).

[7] Armstrong, G. T., The vapor pressure of liquid nitrogen, J. Res. NBS **53**, 263–66 (1954), RP2543.

[8] Friedman, A. S., and White, D., The vapor pressure of liquid nitrogen, J. Am. Chem. Soc. **72** (9), 3931–32 (1950).

[9] Hust, J. G., and Stewart, R. B., Private communication, this laboratory, Feb. 16, 1965. Reported by R. B. Stewart, The thermodynamic properties of oxygen, Dissertation, Dept. Mech. Engr'g., Univ. of Iowa, June 1966.

[10] Moussa, M. R., Muijlwijk, R., and van Dijk, H., The vapour pressure of liquid nitrogen, Physica **32**, 900–12 (1966).

[11] Goodwin, R. D., and Weber, L. A., Specific heats of oxygen at coexistence, J. Res. Nat. Bur. Stand. (U.S.) **73A**, No. 1, 15–24 (Feb. 1969).

[12] Vicentini-Missoni, M., Sengers, J. M. H. Levelt, and Green, M. S., Thermodynamic anomalies of CO_2, Xe, and He^4 in the critical region, Phys. Rev. Letters **22**, No. 9, 389–393 (1969).

[13] Sengers, J. M. H. Levelt, Chen, W. T., and Vicentini-Missoni, M., Vapor pressure of CO_2 near the critical point, Bulletin of the Am. Phys. Soc., Series II, **14**, No. 4, 593 (April 1969).

(Paper 73A5–566)

JOURNAL OF RESEARCH of the National Bureau of Standards—A. Physics and Chemistry
Vol. 73A, No. 5, September–October 1969

Some Precise Measurements of the Vapor Pressure of Water in the Range From 25 to 100 °C

H. F. Stimson*

(May 29, 1969)

The vapor pressure of water was measured at seven temperatures in the range from 25 to 100 °C using the boiler and precision manometer with which standard resistance thermometers were calibrated at the NBS in the 1940's. A table gives measured values of pressure, adjusted to even degrees, and indicates estimates of the standard deviations of pressure and of the corresponding temperatures. Except for the measurement at 25 °C, the values of pressure were consistent within one part in 50 000. The temperature measurements had an estimated standard deviation of 0.000 40 degree.

Key words: Manometer; precision manometer; pressure; *p-t* relation; *p-t* relation of water; standard resistance thermometers; temperature; vapor pressure; vapor pressure of water; water.

1. Introduction

One of the fundamental fixed points on the International Temperature Scale of 1948 [1] [1] was the steam point, defined as the temperature of equilibrium between liquid water and its vapor under the pressure of 1013250 dynes per square centimeter. To realize this fixed point precisely at the NBS, the equilibrium temperature was maintained in a boiler and the pressure measured with a precision manometer. The boiler was developed in 1940 by N. S. Osborne and D. C. Ginnings to boil water without bumping. The precision manometer, first made functional in 1941, was being developed for gas thermometry.

In their formulation and tables for the pressure of saturated water vapor, in 1934, N. S. Osborne and C. H. Meyers [2] stated, "In the range below 100 C, . . ., it appears that the spread of the individual results leaves considerable to discretion. . . ." In this range the steam point boiler and the precision manometer could also be used for making reliable measurements of vapor pressure. During January 1942, therefore, C. S. Cragoe and H. F. Stimson made some vapor pressure measurements near 50 °C, 25 °C, 80 °C, and 60 °C in that order. It had been intended to extend the range of these measurements; in particular to obtain reliable values near the ice point, but war emergencies prevented this being done.

The four values obtained in 1942 were used by several authors in compiling tables. These values were known as the Cragoe-Stimson corrections to the Osborne-Meyers formulation and have been mentioned as from a private communication. These corrections were finally published, however, by M. R. Gibson and E. A. Bruges in 1967 [3].

When work was resumed in 1946, a new boiler had to be made for the calibration of standard resistance thermometers at the steam point. This arrangement of the boiler and manometer is shown in part of figure 5 on page 156 of the book *Temperature*, Vol. 2 [4], and is essentially the same as that used in 1942. The descriptions of the manometer and boiler which follow that figure (*q.v.*) furnish many of the details which are relevant here.

From the ice point to 630.5 °C, the International Temperature Scale of 1948 was defined by standard resistance thermometers using the formula which, in the Callendar form, is

$$t=\frac{1}{\alpha}\left(\frac{R_t}{R_0}-1\right)+\delta\left(\frac{t}{100}-1\right)\left(\frac{t}{100}\right)$$

where $\alpha=\frac{1}{100}\left(\frac{R_{100}}{R_0}-1\right)$ and R_0, R_{100}, and R_t were measured resistances at the ice point, steam point, and temperature, t. The δ was to be found from added measurements near the sulfur point.

For certain special thermometers which could not be heated above the steam point, the δ could be found well enough from added measurements at an intermediate temperature which could be determined with standard resistance thermometers.

One place to maintain the intermediate temperature was in the boiler, using the manometer as an indicator for the control of pressure. The manometer at the same time could also furnish data from which to determine

*Retired from the Institute for Basic Standards, National Bureau of Standards, Washington, D.C. 20234. Present address: 2920 Brandywine St. NW., Washington, D.C. 20008.

[1] Figures in brackets indicate the literature references at the end of this paper.

additional values of the vapor pressure of water. Accordingly six series of calibrations were made this way during 1947–1949 by R. E. Wilson, J. L. Cross, and H. F. Stimson. The data relevant to pressure were recorded but the necessary corrections were not applied at that time.

In recent years the author has received urgent requests from several sources for a formal publication of the values of the Cragoe-Stimson corrections. To make such a publication more useful, the values of pressure have now been computed from the 1947–1949 data and are included herein. Some statements are given with these values which may help one to make estimates of their accuracy.

2. Procedures

For the determinations made in January 1942, values of temperature from four platinum resistance thermometers were used. These thermometers were C–21 and C–22, which are known to have been made by H. K. Griffin about 1915; thermometer A–1, which probably was one of that same epoch; and M–2, which was a coiled filament thermometer described by C. H. Meyers in 1932 [5]. All four of these thermometers had alpha coefficients greater than 0.00390, which was considered good at that time. The bridge carried the designation L&N 50953 but it had been rebuilt at the NBS in 1932 by E. F. Mueller and C. H. Meyers with smaller coils thermostated in a metal block of high thermal diffusivity instead of a stirred oil bath. This rebuilt bridge was the prototype for the L&N G–2 bridge.

In the final computation single values of temperature were used from two thermometers near 50 °C, from four thermometers near 25 °C, from three thermometers near 80 °C, and from three thermometers near 60 °C. All values of temperature were actually below the even degrees but none by as much as 0.015 deg. Estimates of the standard deviations of these values are 0.000 28 deg at 50 °C, 0.000 75 deg at 25 °C, 0.000 27 deg at 80 °C, and 0.000 35 deg at 60 °C. The values of pressure have been adjusted to even temperatures by using the slopes, dp/dt, given in the Osborne-Meyers table.

For the determinations made in 1947–1949, four thermometers were used of an improved type which C. H. Meyers developed in 1943. This type is described briefly on page 149 of *Temperature*, Vol. 2 [4]. Their numbers were S–13, S–14, S–15, and S–17 and all had alpha coefficients between 0.003 9256 and 0.003 9261. (Values greater than 0.003 910 were specified in the International Temperature Scale of 1948.)

Six series of measurements were made, each series taking about two days. The first three series were made near 50 °C during May 1947, October 1947, and January 1948. The fourth series was made near 40 °C in July 1948. The fifth series was made near 60 °C in April 1949, and the sixth series was made near 70 °C in July 1949. The values of the actual temperatures were as near the even degrees as those in 1942.

The same bridge, 50953, that had been used in 1942 was used for the first five series. For the sixth series in July 1949 a new bridge, L&N 752448, was used. This bridge was designed by E. F. Mueller after he retired and is described briefly on page 151 of *Temperature*, Vol. 2 [4]. Twenty calibrations of bridge 50953 were made during the interval from April 1947 to May 1949. At no time did the calibrations change enough to affect the values of temperature by more than a few ten-thousandths of a degree.

Calibrations of standard resistance thermometers involve determining the three coefficients, R_0, α, and δ, in the Callendar formula. The δ does not change significantly and in fact all good thermometers have a δ about 1.491 degrees. In some fifteen sets of calibrations of these thermometers during this two year interval, each R_0 was found to increase, the greatest being for S–14, which increased by the equivalent of about 0.01 degree. Some years later, it was demonstrated to the author that a shock, such as letting the thermometer tube hit the table, increases its R_0. This helps to explain why the R_0 increased for all the thermometers and implies that S–14 had a more shocking history than the others.

The values of individual alpha coefficients, on the other hand, were essentially constant and did not vary more than the equivalent of a few ten-thousandths of a degree in a hundred degrees; except for one set of calibrations in late March 1948, where values of all four thermometers were low by the equivalent of over 0.0015 degree. No certain explanation has been offered for this one set but the discrepancy is so large that the values from this set have been discarded from the averages.

To determine a value of an intermediate temperature, a common practice is to compute the value of temperature using the alpha obtained nearest the time when the measurements were made. Because the values of alpha were essentially constant over this period it is now believed that the averages of these alphas are preferable for use here; hence all steam point data in this period were recomputed and the averages taken

The alpha coefficient for each of the four thermometers was determined at least six times during the two year period. The average values are given in table 1 and also estimates of their standard deviations. A change of 39×10^{-9} in the alpha coefficient corresponds to a change of 0.001 deg in 100 deg. The estimate of the standard deviation of the 100-deg interval with these four thermometers is thus 0.000 44 deg.

TABLE 1.

Thermometer	Alpha	Std. dev.
S–13	0.003 925 678	5×10^{-9}
S–14	0.003 926 086	27×10^{-9}
S–15	0.003 926 080	12×10^{-9}
S–17	0.003 925 907	23×10^{-9}

Immediately following the vapor pressure measurements made in January 1942 a triple-point cell was

developed at the NBS to furnish a more reproducible fixed point than the ice point. These cells were used in all subsequent measurements.

All bridge measurements were made with four readings, N–R–R–N (normal and reversed leads), with the thermometer current at 2 milliamperes (mA) and again at 1 mA. These measurements were then extrapolated to get the values of thermometer resistance at zero current. Corrections were made for the bridge zero, the bridge calibration, and, when using the triple point cell, for the extrapolation to 0 °C. Triple-point measurements were made at the end of each day's series and sometimes also during the middle of the day. This practice helped to minimize the errors from changes in R_0 and in part for drifting of the bridge calibrations.

Using the alpha coefficient and the values obtained from R_t and R_0, values of the first term in Callendar's formula were computed and the delta term added. (At 50 °C the delta term is just −0.25 δ. At 40 and 60 °C the term is −0.24 δ and at 70 °C it is −0.21 δ.) These computations gave values of temperature on the International Temperature Scale of 1948, at the level of the thermometer coils in the boiler.

To determine the pressure at this level an account was made for all fluid (both liquid and gas) heads contributing to the pressure. Above the thermometer coils was a head of steam up to the ice-water condenser. Above the condenser up to the dry ice trap was helium with some of the water vapor at the 0 °C saturation pressure. From the dry ice trap down to the laboratory floor was helium at 25 °C. From the floor down to the lower mercury meniscus of the manometer in the cellar there was helium at 20 °C. From the lower meniscus to the upper meniscus was liquid mercury at 20 °C. Finally above the upper meniscus there was mercury vapor pressure at 20 °C (about 1.6 dynes/cm²).

The values for these head corrections were computed for the expected pressure at the even ten degree temperatures, on the assumption that everything in the cellar below the laboratory floor was at 20 °C. This temperature is the temperature at which the gage blocks were calibrated and also was near the temperature of the earth surrounding the cellar. A platinum thermometer and thermocouples were used to measure the departures from 20 °C, several times a day. A "cellar-factor" was applied to these departures to account for the thermal expansion of the gage blocks and for the thermal expansion of all the fluid columns in the cellar contributing to the pressure head. These corrections were small, seldom exceeding a few dynes per square centimeter.

Table 2 gives the values used for these factors, and also values from the Osborne-Meyers table for the dp/dt used to adjust values of pressure to the even temperatures.

TABLE 2. *Correction factors in dynes/(cm² deg)*

Temperature	Cellar-factor	dp/dt
40 °C	12.57	3931
50 °C	21.01	6121
60 °C	33.93	9220
70 °C	53.12	13481

3. Results

Table 3 gives the values of the vapor pressure of water obtained in 1942, adjusted to the even temperatures. The number of determinations of temperature is given in column 2. Column 3 gives the values of pressure in dynes per square centimeter and column 4 gives them in newtons per square meter, which is the unit of pressure in the International System of Units.

TABLE 3. *1942 values for the vapor pressure of water*

Temperature	Number	Dynes/cm²	N/m²
25 °C	4	31 670	3 167.0
50 °C	2	123 386	12 338.6
60 °C	3	199 243	19 924.3
80 °C	3	473 639	47 363.9

Table 4 gives the average values for the vapor pressure of water obtained from each of the six series of measurements made in 1947–1949. The second column gives the month of the series. Column 3 gives the number of computed values of pressure contributing to the average. Column 4 gives the average values of pressure in dynes per square centimeter, and column 5 gives estimates of the standard deviations of these values of pressure.

TABLE 4. *1947–1949 values for the vapor pressure of water*

Temperature	Date	Number	Pressure	Std. dev.
			dynes/cm²	*dynes/cm²*
50 °C	May 1947	16	123 393.7	2.7
50 °C	Oct. 1947	8	123 381.6	1.0
50 °C	Jan. 1948	7	123 383.7	0.3
40 °C	July 1948	24	73 772.7	1.5
60 °C	Apr. 1949	20	199 241.5	1.6
70 °C	July 1949	18	311 661.5	2.2

In this table the value for pressure at 50 °C in the May 1947 series is seen to be higher than the later two. This series took three days. During this time the values of temperature, at the level of the thermometer coils, rose by over a thousandth of a degree but on the third day were still a thousandth of a degree below the values in the October 1947 and the January 1948 series. If it is true that the temperature was low, it should indicate that the pressure was also lower than that computed from the measured height of the mercury column. When adjusted to the even temperature, therefore, the value for pressure would be too high.

It now seems plausible that a bubble of gas was in the mercury column to the upper cell, thus decreasing the fluid head and giving too low a pressure and temperature. A note added to the record book, soon after the May 1947 series, suggests to the author that a gas bubble was suspected then. A similar explanation

might also account for the low values of alpha in the late March 1948 set, mentioned above. The value from the May 1947 series, therefore, has not been included in the final table of values of the vapor pressure of water at 50 °C.

Table 5 gives the combined results from the 1942 and the 1947–1949 periods. In column 4 are the estimated standard deviations of pressure in dynes per square centimeter. Using values for dp/dt gives the corresponding deviations of temperature in the next column. The last column gives the values in newtons per square meter. From the estimates of the standard deviations in table 5 it appears that (except for the 25 °C measurement) the pressure measurements were consistent with each other to one part in 50 000. It also appears that temperatures in this range were measured with a standard deviation estimated to be 0.000 40 degree.

The International Practical Temperature Scale of 1968 (IPTS–68) [6] now replaces the International Temperature Scale of 1948, which has been used for all foregoing temperature computations. In the range between 0 and 100 °C the values of temperature on the new scale are smaller than on the 1948 scale. This makes the values of pressure larger, when adjusted to the corresponding even temperatures. Table 6 gives the even temperatures on the 1968 scale in the first column, the temperature correction in the second column, and the values of pressure adjusted to the even temperatures in the third column.

In conclusion, it appears that the earlier and later measurements agree within experimental error.

TABLE 5. *Summary of measured values for the vapor pressure of water*

Temperature ITS–48	Years	Pressure	Std. dev.	Std. dev.	Pressure
°C		dynes/cm²	dynes/cm²	degrees	N/m²
25	1942	31 670.	1.4	0.000 75	3 167.0
40	1948	73 772.7	1.5	0.000 41	7 377.3
50	1942, 1947, 1948	123 383.0	1.8	0.000 19	12 338.3
60	1942, 1949	199 242.2	1.6	0.000 17	19 924.2
70	1949	311 661.5	2.2	0.000 16	31 166.2
80	1942	473 639.	5.2	0.000 27	47 363.9
100	1947–1949	1013 250.	15.9	0.000 44	101 325.0

TABLE 6. *Values of pressure at temperatures on the IPTS–68*

Temperature IPTS–68	Correction $t_{68} - t_{48}$	Pressure
°C	degrees	N/m²
25	−0.008 54	3 168.6
40	−0.010 34	7 381.3
50	−0.010 37	12 344.6
60	−0.009 57	19 933.0
70	−0.008 05	31 177.0
80	−0.005 89	47 375.2
100	0.000 00	101 325.0

4. References

[1] Stimson, H. F., The International Temperature Scale of 1948, J. Research NBS **42**, 209 (1949).

[2] Osborne, N. S., and Meyers, C. H., A formula and tables for the pressure of saturated water vapor in the range 0 to 374 °C, J. Research NBS **13**, 1 (1934).

[3] Gibson, M. R., and Bruges, E. A., New equations for the thermodynamic properties of saturated water in both the liquid and vapour phases, J. Eng. Sci. **9**, 24 (1967).

[4] Stimson, H. F., Precision resistance thermometry and fixed points, Chapter 9 in Temperature, Its Measurement and Control in Science and Industry, Vol. II (Ed. H. C. Wolfe, Reinhold Publ. Corp., New York, N.Y., 1955). (A photo copy of this chapter appears in NBS Special Publication 300–Volume 2, issued August 1968.)

[5] Meyers, C. H., Coiled Filament Resistance Thermometers, B. S. Journal Research **9**, 807 (1932).

[6] Barber, C. R., The International-Practical Temperature Scale of 1968, Metrologia **5**, 35 (1969).

(Paper 73A5–567)

JOURNAL OF RESEARCH of the National Bureau of Standards—A. Physics and Chemistry
Vol. 73A, No. 5, September-October 1969

The Configurations $(3d+4s)^n 4p$ in Neutral Atoms of Calcium, Scandium, and Titanium*

C. Roth**

(September 5, 1968)

Experimental levels of the configurations $(3d+4s)^n 4p$ for neutral atoms of calcium, scandium, and titanium were compared with corresponding calculated values. The rms errors in the calculated values for Ca I, Sc I and Ti I were 23, 126, and 261 cm^{-1}, respectively.

Key words: Configurations $(3d+4s)^n 4p$; energy levels; first spectra; g-factors; interactions between configurations; iron group.

1. Introduction

Racah and Shadmi [1, 2][1] investigated the configurations $3d^n+3d^{n-1}4s$ in the second and third spectra of the iron group. The configurations $3d^n4p$ in the second and third spectra of the iron group, the configurations $3d^n4p+3d^{n-1}4s4p$ for Sc II, Ti II and V II, as well as the odd configurations of Cu II were investigated by the author [3−6][2].

For neutral atoms of the iron group the only configurations previously investigated were $(3d+4s)^34p$ −Ti I by Rohrlich [7]. However, Rohrlich considered this spectrum in the $L-S$ approximation by taking into account only the interaction between the cores $3d^3$ and $3d^24s$, and that just as a perturbation to the calculated terms. Although for the final result Rohrlich obtained the very high rms error of 1109 cm^{-1}, most of his parameters were taken as starting values for the present investigation. Mainly for this reason the spectrum of titanium was considered first.

2. Ti I −$(3d+4s)^34p$

The configurations $(d+s)^3p$ comprise 92 theoretical terms splitting into 212 levels. In AEL [8], 74 terms splitting into 175 levels are assigned to the configurations $3d^34p+3d^24s4p$. In addition, 11 odd terms splitting into 28 levels are given without a definite configuration designation in AEL. However, in the original paper by Russell [9], only the term $w\,^1$G is given with no configuration designation. Russell suggests that the terms $w\,^3$H, $p\,^3$D, $t\,^3$G, $q\,^3$F, and $n\,^3$D with no configuration designation in AEL, may be attributed to configurations containing a $5p$ electron. The terms $s\,^3$F, $q\,^3$D, and $v\,^1$D Russell assigns as $3d^3(b^2\mathrm{D})p\,s^3\mathrm{F}$, $3d^3(b^2\mathrm{D})p\,q^3\mathrm{D}$ and $3d^3(a^2P)p\,v^1\mathrm{D}$ and $3d^24s(a^2\mathrm{S})4p\,t^3P$ of AEL to the configuration $3d4s^24p$.

Rohrlich also assigns the terms t^3P, o^3D and r^3F to the configuration $3d4s^24p$. In addition, he attributes the singlets v^1D at 43710 and u^1F at 48365 to $3d4s^24p$.

2.1. Initial Parameters

Considering the three configurations $3d^34p$, $3d^24s4p$, and $3d4s^24p$ we obtain [3] from Rohrlich initially:

$$\begin{aligned} A &= 37880 \\ A' &= 30650 \\ A'' &= 45130 \\ B = B' &= 563 \\ C = C' &= 2122 \\ F_2 = F_2' = F_2'' &= 281 \\ G_1 = G_1' = G_1'' &= 306 \\ G_3 = G_3' = G_3'' &= 0 \\ G'_{ds} &= 1381 \\ G'_{ps} &= 4834 \end{aligned} \qquad (1)$$

As did Rohrlich, we made the intitial assumption that the values of the parameters B, C, F_2, G_1, and G_3 are the same for the three configurations. The initial

*An invited paper.
**Present address: McGill University, Montreal, Canada.
[1] Figures in brackets indicate the literature references at the end of this paper.
[2] The reader is referred to these papers for an explanation of the method used, notation and significance of the various parameters.
The numerical values of all levels and parameters are in cm^{-1}.

[3] Unprimed quantities refer to the configuration $3d^34p$, primed quantities to $3d^{n-4}4s4p$ and doubly primed quantities to $3d^{n-4}4s^24p$.

values of the parameters α, J, and K were taken from V II $-3d^34p+3d^24s4p$ [5]

$$x=\alpha'=55$$
$$J'=J=1011 \qquad (2)$$
$$K'=K=3288$$

Here α is the average of α and α' in V II.

From the results of Ti II, V II and Cu II [5], [6], we would expect that the parameter H should have the same sign as J and K. Nevertheless, initially two diagonalizations were performed equal in all respects except for changes in the sign of H. The initial numerical value of 100 was also taken from Rohrlich.

As the effect of the interaction between the configurations $3d^34p$ and $3d^24s4p$ depends on the difference between the heights of these two configurations, the value of A' in (1) was checked by considering as for V II $-3d^34p+3d^24s4p$ [5], the terms ^{5}F and ^{5}G whose electrostatic interaction matrices are of order 2. The electrostatic matrix of ^{5}F was given for V II [5], whereas the electrostatic matrix of ^{5}G is

$$\begin{bmatrix} A-15B-F_2-10G_1-10G_3+12\alpha & \frac{\sqrt{5}}{5}(K-J) \\ \frac{\sqrt{5}}{5}(K-J) & A'-8B'-2G'_{ds}+F'_2-9G'_1-4G'_3-G'_{ps}+12\alpha' \end{bmatrix}$$

Then, by using the centers of gravity for z^5G, z^5F, y^5G, and y^5F, which are 16202, 17046, 26726, and 28767 [8], respectively, we obtain values of A and A', which, in both cases are close to the values of these parameters in (1).

From the small splittings of the terms we note that the spin-orbit interaction is small compared with the electrostatic interaction, [8]. Furthermore, the decomposition of each term into the multiplet levels obeys in general Lande's interval rule. Thus, in order to simplify the initial analysis, we considered first the L-S approximation.

2.2. Discussion and Results

As G'_{ps} is much larger than G'_{ds}, the interaction $p-s$ is stronger than the interaction $d-s$. Thus, the terms of the configuration d^2sp are coupled as

$$d^2(v_1S_1L_1)sp(^{1,3}\mathrm{P})SL$$

and not $d^2s(S_2L_1)p\ SL$ as given in AEL.

Besides the large rms error obtained by Rohrlich, a very disturbing feature of his analysis, is the rejection of six terms, four of which are below 40,000. The experimental terms $y\,^1$D at 27907 and $w\,^3$F at 33683 (note misprint of v instead of w on p. 1384 of Rohrlich [7]), are rejected since they show the very high deviations of 3386 and -3307, respectively. For the experimental terms $u\,^3$F at 37769 and $t\,^3$D at 38721, there are no corresponding calculated terms. However, from an examination of the combinations given by Russell, [9], we obtain the results in table 1 (using the notation for the terms of AEL).

TABLE 1. *Observed transitions from* $y\,^1D$, $w\,^3F$, $u\,^3F$, *and* $t\,^3D$

Term	Combines with	Number of combinations
$y\,^1$D	$a\,^3$F, $a\,^3$P, $a\,^1$D, $e\,^1$D	4
$w\,^3$F	$a\,^3$F, $b\,^3$F, $a\,^3$G, $a\,^3$D	19
$u\,^3$F	$a\,^3$F, $a\,^1$D, $a\,^3$P, $b\,^3$F, $a\,^3$G, $a\,^3$D	22
$t\,^3$D	$a\,^3$F, $a\,^1$D, $a\,^3$P, $b\,^3$F, $a\,^3$D, $a\,^3$P	21

As all four terms are too low to be assigned to configurations containing a $5p$ electron, they must be valid terms of $(3d+4s)^34p$. Thus, initially terms above 40,000 were not inserted into the least-squares in attempts to obtain suitable parameters so that all the lower-lying terms should fit. Since, with the parameters of (1) and (2), the lowest term of ds^2p is at around 43,500, it was necessary to keep A'' fixed at the initial value of 45,130.

From the least-squares fitting performed on the first two diagonalizations (with H positive and negative) it was evident that H should be in phase with J and K.

The agreement bewteen the experimental and calculated terms was steadily improved from iteration to iteration by letting the parameters B, C, and F_2 differ for the configurations $d\,^3p$ and d^2sp. Among the terms still showing high deviations were y^1D, w^3F, u^3F, and $t\,^3$D with deviations of around -1400, -800, -700, and -550, respectively. However, an examination of the theoretical compositions of these terms revealed that their eigenfunctions contained a considerable mixture of ds^2p. Thus a diagonalization was performed so that A'', the height of ds^2p, should have a value of 41,000 instead of the original 45,130. As expected, the deviations for the terms $y\,^1$D, $w\,^3$F, $u\,^3$F, and $t\,^3$D were greatly reduced (with the new A'', the largest deviation of the four terms was -350, for $y\,^1$D). Furthermore, the terms $w\,^3$D at 29814, $y\,^1$P at 35095, and $x\,^1$F at 37623 had deviations of around -500, -700, and -1300, respectively, with A'' fixed at the initial value of 45,130. With the new value of A'', these deviations were reduced to -160, -180, and -250, respectively. Although the term $v\,^3$P at 40,429 was not inserted in the initial least squares, it was apparent that had it been inserted, the resulting deviation would have been around -1000. However, after changing the height of ds^2p and inserting terms up to 44,000, the deviation for $v\,^3$P was 250, since with the new A'', the main contribution to $v\,^3$P is $ds^2p\,^3$P.

In the next variation the parameters J' and K' were allowed to change freely. The rms error was reduced

from 342 to 290 with the following parameters of the interaction between configurations:

$$\begin{aligned} H = H' &= 172 \pm 4 \\ J &= 1128 \pm 41 \\ J' &= 1874 \pm 87 \\ K &= 2595 \pm 49 \\ K' &= 4392 \pm 157 \\ G = G'_{ds} &= 1554 \pm 37 \end{aligned} \tag{4}$$

However, by keeping J and J' equal and letting K' change freely the rms error was increased only to 296. Variations in which G'_1, G'_3, α', and H' were allowed to change freely did not improve the results. Finally, by inserting the parameters of the spin-orbit interaction the rms error was reduced to 261.

In order to ascertain whether a general treatment for the configurations $(d+s)^n p$ of the first spectra is feasible, it is first necessary to obtain all the results under the same conditions. Theoretical investigations of the configurations $(3d+4s)^n 4p$ for all neutral atoms of the iron group were performed. Originally it was hoped that the final parameters would be linear functions of the atomic number analogous to the situation prevailing for singly and doubly ionized atoms [3], [4]. After examining the results of all the spectra investigated,[4] it was decided to have the parameters A, A', A'' (wherever there are levels of the configuration $d^{n-2}\,s^2p$), G'_{ds}, and G'_{ps} change freely. The parameters B, C, F_2, and G_1 were in arithmetic progression for the three configurations, i.e., $B'-B=B''-B'$, etc. The parameters G_3, α, ζ_d, and ζ_p were kept equal for the three configurations. For the parameters of the interactions between configurations H' was kept equal to H, J' to J, and G to G'_{ds}.

From the results of Sc, Ti, and Fe it was found that K' and K should be different with approximately

$$K'\,(d^{n-1}sp - d^{n-2}s^2\mathrm{p}) = K(d^n p - d^{n-1}sp) + 380 + 64n.$$

The parameters β and T had no significance here.

In the least squares of the final iteration in the uniform treatment, 68 experimental terms splitting into 169 levels were fitted by means of 18 free electrostatic parameters and 2 free spin-orbit interaction parameters to yield an rms error of 261. The final parameters with their standard errors are given in table 2.

Below 44,000 cm^{-1} there are 76 experimental terms splitting into 185 levels in AEL. The following 8 terms, which split into 16 levels, were rejected in the final least-squares:

1. $3\,d^24s(b^2\mathrm{P})4p\ y^3\mathrm{S}$ at 35439
2. $w\,^1\mathrm{G}$ at 40883
3. $3\,d^3(a\,^2\mathrm{H})4p\ u\,^3\mathrm{G}$ at $41268_{\mathrm{C.G.}}$
4. $w\,^3\mathrm{H}$ at $41900_{\mathrm{C.G.}}$
5. $p\,^3\mathrm{D}$ at $42300_{\mathrm{C.G.}}$
6. $3\,d^24s(a\,^2\mathrm{S})4\mathrm{p}$: $w\,^1\mathrm{P}$ at 42927
7. $r\,^3\mathrm{F}$ at $43625_{\mathrm{C.G.}}$
8. $v\,^1\mathrm{D}$ at 43710

From table 5, the calculated value of the term $^3\mathrm{P}(^1\mathrm{P})y\,^3\mathrm{S}$ is 34,002. Thus, if the experimental term $y\,^3\mathrm{S}$ were inserted into the least-squares calculations, the deviation would be around 1400. As this deviation is much higher than for the other terms and, furthermore, since the term $y\,^3\mathrm{S}$ has combinations only with the two terms $a\,^3\mathrm{P}$ and $b\,^3\mathrm{P}$ [9], it was not included in the final least-square calculations.

Russell does not attribute to $w\,^1\mathrm{G}$ any definite configuration designation and, furthermore, mentions that "this term depends only on three faint lines and may not even be real." This conclusion seems to be verified by our results since to all the calculated levels in the vicinity of $w\,^1\mathrm{G}$ there correspond other experimental levels.

From the combinations found by Russell for the levels of $u\,^3\mathrm{G}$, it is apparent that $u\,^3\mathrm{G}$ is a valid term. However, if assigned to the theoretical term $(^2\mathrm{H})^3\mathrm{G}$, the deviation would be around -1300. As this deviation is considerably higher than for the other terms and since the experimental term $u\,^3\mathrm{G}$ is high enough in order to conceivably belong to $(3d+4s)^35p$, it was not included.

As the three theoretically predicted terms $^3\mathrm{H}$ of $(3d+4s)^34p$ correspond to $z\,^3\mathrm{H}$, $y\,^3\mathrm{H}$, and $x\,^3\mathrm{H}$, the term $w\,^3\mathrm{H}$ is superfluous. Russell suggests that the terms $w\,^3\mathrm{H}$ may be assigned to configurations containing a $5p$ electron. However, in the configurations $(3d+4s)^34p$, the term $3d^24s(b^2\mathrm{G})4p\ z\,^3\mathrm{H}$ at $31{,}930_{\mathrm{C.G.}}$ is higher by 13,330 than the term $3d^24s(a\,^4\mathrm{F})4p\ z\,^5\mathrm{D}$ at $18{,}600_{\mathrm{C.G.}}$. Thus, $w\,^3\mathrm{H}$ cannot be assigned to $3d^24s(b^2\mathrm{G})5p\ w\,^3\mathrm{H}$, since the experimental term $3d^24s(a\,^4\mathrm{F})5p\ v\,^5\mathrm{D}$ is higher than $w\,^3\mathrm{H}$, [8]. Thus the levels of $w\,^3\mathrm{H}$ probably belong to $3d^24s(a\,^4\mathrm{F})5p\ x\,^5\mathrm{G}$.

In the vicinity of 42,000 there is only one theoretically predicted term $^3\mathrm{D}$. Since the experimental terms $p\,^3\mathrm{D}$ and $q\,^3\mathrm{D}$ are so close it is impossible to decide which term to consider for $(3d+4s)^34p$. However, as Russell suggests that $p\,^3\mathrm{D}$ may belong to configurations containing a $5p$ electron, we assigned $q\,^3\mathrm{D}$ to the theoretical term at 42,700, whose main contribution is $3d4s^24p\,^3\mathrm{D}$. Rohrlich [7], also did not include the terms $w\,^3\mathrm{H}$ and $q\,^3\mathrm{D}$ in his investigation.

The terms $w\,^1\mathrm{P}$, $r\,^3\mathrm{F}$, and $v\,^1\mathrm{D}$ would yield very high deviations if inserted into the least-squares. As these terms may conceivably belong to, or be strongly perturbed by configurations containing a $5p$ electron, they were not included. Similar conclusions hold for most terms above 44,000.

In the configurations $(3d+4s)^34p$, the lowest 6 terms are $(d^2\,^3\mathrm{F}+(sp)\,^3\mathrm{P})\,^{3,5}\mathrm{D, F, G}$. It is conceivable that the terms $u\,^3\mathrm{G}$, $w\,^3\mathrm{H}$, $v\,^5\mathrm{D}$, $p\,^3\mathrm{D}$, $r\,^3\mathrm{F}$, and $t\,^3\mathrm{G}$ belong to the lowest terms of $(3d+4s)^35p$, with the following assignments:

$$\begin{array}{lccc} (^3\mathrm{F}+{}^3\mathrm{P}): & z\,^3\mathrm{D}(p\,^3\mathrm{D}) & z\,^3\mathrm{F}(r\,^3\mathrm{F}) & z\,^3\mathrm{G}(t\,^3\mathrm{G}) \\ & z\,^5\mathrm{D}(v\,^5\mathrm{D}) & z\,^5\mathrm{F}(u\,^3\mathrm{G}) & z\,^5\mathrm{G}(w\,^3\mathrm{H}) \end{array}$$

In parentheses are the corresponding terms with a $5p$ electron.

From table 5 it is evident that the purity of most levels is very low. In many cases, the mixing involves

[4] Results to be published soon.

356-078 O-69—4

eigenfunctions of levels of both configurations $3d^34p$ and $3d^24s4p$, and in some instances even all three configurations. The changes in designation given below were performed. The number in brackets gives the average percentage of the theoretical designation for the term under consideration.[5] A colon after the experimental term indicates that Rohrlich also changed Russell's designation:

1. AEL $d^2s(a\,^4\mathrm{F})p\,y\,^3\mathrm{D}$:→ $(^4\mathrm{F})\,y\,^3\mathrm{D}$ (36)
2. AEL $d^2s(b\,^4\mathrm{P})p\,z\,^3\mathrm{P}$ → $^1\mathrm{D}(^3\mathrm{P})\,z\,^3\mathrm{P}$ (52)
3. AEL $d^3(b\,^4\mathrm{F})p\,x\,^3\mathrm{F}$:→ $^1\mathrm{D}(^3\mathrm{P})\,x\,^3\mathrm{F}$ (57)
4. AEL $d^3(b\,^4\mathrm{F})p\,x\,^3\mathrm{D}$ → $^1\mathrm{D}(^3\mathrm{P})\,x\,^3\mathrm{D}$ (72)
5. AEL $d^3(b\,^4\mathrm{F})p\,y\,^3\mathrm{G}$:→ $^3\mathrm{F}(^1\mathrm{P})\,y\,^3\mathrm{G}$ (55)
6. AEL $d^2s(b\,^4\mathrm{P})p\,w\,^3\mathrm{D}$:→ $^3\mathrm{F}(^1\mathrm{P})\,w\,^3\mathrm{D}$ (27)
7. AEL $d^2s(a\,^4\mathrm{F})p\,x\,^3\mathrm{G}$:→ $^1\mathrm{G}(^3\mathrm{P})\,x\,^3\mathrm{G}$ (71)
8. AEL $d^2s(a\,^2\mathrm{D})p\,v\,^3\mathrm{D}$:→ $^3\mathrm{P}(^3\mathrm{P})\,v\,^3\mathrm{D}$ (71)
9. AEL $d^2s(b\,^2\mathrm{G})p\,w\,^3\mathrm{G}$:→ $(^4\mathrm{F})\,w\,^3\mathrm{G}$ (69)
10. AEL $d^2s(a\,^2\mathrm{D})p\,y\,^3\mathrm{P}$:→ $^3\mathrm{P}(^3\mathrm{P})\,y\,^3\mathrm{P}$ (85)
11. AEL $d^2s(b\,^2\mathrm{P})p\,x\,^3\mathrm{P}$:→ $(^4\mathrm{P})\,x\,^3\mathrm{P}$ (33)
12. AEL $d^2s(a\,^2\mathrm{D})p\,w^3\mathrm{F}$:→ $(^4\mathrm{F})\,w\,^3\mathrm{F}$ (53)
13. AEL $d^2s(b\,^2\mathrm{G})p\,z\,^1\mathrm{H}$:→ $(^2\mathrm{G})\,z\,^1\mathrm{H}$ (58)
14. AEL $d^2s(b\,^2\mathrm{G})p\,x\,^1\mathrm{F}$:→ $ds^2(^2\mathrm{D})\,x\,^1\mathrm{F}^*$ (25)
15. AEL $d^3(b\,^2\mathrm{D})p\,t\,^3\mathrm{D}$:→ $(^2\mathrm{P})\,t\,^3\mathrm{D}$ (34)
16. AEL $d^3(a^2\mathrm{P})p\,w\,^1\mathrm{D}$ → $ds^2(^2\mathrm{D})\,w\,^1\mathrm{D}^*$ (28)
17. AEL $d^3(a\,^4\mathrm{P})p\,s\,^3\mathrm{D}$ → $(\mathrm{A}^2\mathrm{D})\,s\,^3\mathrm{D}$ (56)
18. AEL $d^3(a\,^4\mathrm{P})p\,v\,^3\mathrm{P}$:→ $ds^2(^2\mathrm{D})\,v\,^3\mathrm{P}^*$ (32)
19. AEL $d^3(a\,^2\mathrm{P})p\,r\,^3\mathrm{D}$ → $(^4\mathrm{P})\,r\,^3\mathrm{D}$ (42)
20. AEL $d^3(a\,^2\mathrm{G})p\,y\,^1\mathrm{H}$ → $(^2\mathrm{H})\,y\,^1\mathrm{H}$ (47)

Finally, it is instructive to consider the reasons for the greatly improved results we obtained as compared with those of Rohrlich, [7].

Most importantly, as opposed to Rohrlich, we considered all the three configurations as one problem by inserting the interactions between configurations d^3p-d^2sp, d^2sp-ds^2p, and d^3p-ds^2p explicitly. As a result it is not possible to assign an experimental level to one particular theoretical level. Rather the percentage compositions of most of the theoretical eigenvalues contain a mixture of levels belonging to the configurations d^3p and d^2sp, and in some cases even to all the three configurations.

A second reason for the very high rms error obtained by Rohrlich is due to the fact that he attempted to insert too many high-lying terms which either belong to $(3d+4s)^35p$, or are strongly perturbed by these configurations. Not only did these high-lying terms show large deviations but, also they caused the parameters of $(3d+4s)^34p$ to absorb the perturbations due to configurations containing a $5p$ electron. Thus, also the lower-lying terms assumed unnecessarily high deviations. Excellent examples of this effect are the four low-lying and definitely valid experimental terms of $(3d+4s)^34p$, i.e., $y\,^1\mathrm{D}$, $v\,^3\mathrm{F}$, $u\,^3\mathrm{F}$, and $t\,^3\mathrm{D}$, which Rohrlich rejected.

Thirdly, Rohrlich did not include the $L(L+1)$ correction. As in our initial diagonalization α already had a value different from zero, it is not possible to give an exact quantitative evaluation of the effect of this parameter. However, it can be expected from previous investigations on spectra of the iron group [10–12], where α was very important, that here also the results are improved greatly by considering the $L(L+1)$ correction.

Fourthly, the approximation of Rohrlich that all the electrostatic parameters are equal for the three configurations is not reasonable. By letting the parameters B, C, and F_2 to be in arithmetic progression the rms error was reduced from 461 to 342. The final values of the parameters B, B', C, and C' in table 2 are very similar to those obtained by Racah and Shadmi for Ti II $-(3d+4s)^3$, [1]. The conclusion that F_2 and F_2' are different was also obtained for the configurations $3d^n4p+3d^{n-1}4s4p$ of the second spectra, [5].

The insertion of the spin-orbit interaction, thus treating the configurations in intermediate coupling, had the smallest effect. The rms error was reduced only from 295 to 261. The values of the parameters ζ_d and ζ_p are small, and furthermore ζ_p is not well defined.

Below 44,000 cm^{-1} (the limit of the experimental levels inserted) there are only 7 theoretical levels with no corresponding experimental levels. The lowest of these are the levels $^1\mathrm{D}(^3\mathrm{P})^3\mathrm{P}_0$ and $^3\mathrm{P}(^3\mathrm{P})^1\mathrm{S}$ at 25,713 and 26,170, respectively.

It is interesting to note that the experimental levels $r\,^3\mathrm{D}_3$ and $x\,^3\mathrm{S}_1$ have exactly the same numerical value. However, the combinations of these two levels are quite different [9], and hence the fact that they are coincident is quite accidental. Both levels were inserted into the least-squares calculations.

3. Sc I $-(3d+4s)^24p$

The configurations $(d+s)^2p$ comprise 29 theoretical terms splitting into 70 levels. In AEL [8], 26 experimental terms splitting into 63 levels are assigned to the configurations $3d^24p+3d4s4p$. Of these, the three levels of the terms $3d^2(a^3\mathrm{P})4p\;v^2\mathrm{D}$ and

$$3d^2(a^3\mathrm{P})4p\;z^2\mathrm{S}$$

are given with an uncertainty of y cm^{-1}.

[5] For the theoretical term designations used the reader is referred to section 5 of this paper.

The initial values of the interaction parameters were taken from the final results of Ti I (these are not exactly the values given in table 2, as the latter were obtained after having all the results of the individual treatments, and then deciding on a uniform treatment). Then, initially,

$$\begin{aligned} B &= 560 \\ C &= 1630 \\ G'_{ds} &= 1650 \\ F_2 &= 150 \\ F'_2 &= 280 \\ G_1 = G'_1 &= 280 \\ G_3 = G'_3 &= 20 \\ G'_{ps} &= 5800 \\ \alpha &= 50 \\ H &= 180 \\ J &= 1500 \\ K &= 3000 \\ \zeta_d = \zeta'_d &= 100 \\ \zeta_p = \zeta'_p &= 110 \end{aligned} \qquad (5)$$

The initial value for A was calculated by averaging the values obtained by using the centers of gravity of ^{4}G and ^{2}H, whose electrostatic matrices are of order 1. Then the starting value for A' was obtained by using the result that the trace equals the sum of the eigenvalues on the electrostatic matrices of ^{4}P and ^{4}F, and averaging. Then initially:

$$\begin{aligned} A &= 34658 \\ A' &= 25818 \end{aligned} \qquad (6)$$

The term $d^2(^1S)x^2P_{C.G.}$ is given at 30,662 in AEL. The classification of the term x^2P is obviously wrong, since the term $d^2(^1S)p\,^2$P is the highest and *not* the lowest term of d^2p (diagonal element: $A+14B+7C-2G_1-7G_3$, [13]). As the terms $z\,^2$P and $y\,^2$P correspond to the two predicted terms ^{2}P of dsp, and furthermore, since the lowest term of d^2p is $(^1D)w\,^2$P, we must assign $x\,^2$P to $4s^24p$. This assignment had already been suggested by Racah [14], who also obtained a value of 24,223 for the unperturbed height of $4s^24p^2$P which we use here initially. Also, initially:

$$\begin{aligned} J'(s^2p-dsp) = J(dsp-d^2p) &= 1500 \quad \text{(HELD EQUAL)} \\ K'(s^2p-dsp) = K(dsp-d^2p) &= 3000 \quad \text{(HELD EQUAL)} \\ G(s^2p-d^2p) = G'_{ds} &= 1650 \quad \text{(HELD EQUAL)} \end{aligned} \qquad (7)$$

The only term having a very large deviation in the initial least-squares was $(^1G)w\,^2$F, whose center of gravity is given experimentally at 39,885. (The levels with the uncertainty y cm^{-1} were not considered then). Since the theoretical term $(^1G)^2F_{C.G.}$ was calculated at 43,050, and since from the paper by Russell and Meggers [15], we note that each of the levels of $w\,^2$F is based on only the single combination with $a^2G_{7/2}$, the levels of $w\,^2$F were rejected.

After reaching a stage in the investigation when there was no appreciable difference between the values of the parameters in the diagonalization and in the subsequent least squares, a variation was performed by letting J' and K' vary freely. Then the following values for the parameters of the interaction between configurations were obtained:

$$\begin{aligned} H &= 296 \pm 23 \\ J &= 1398 \pm 239 \\ J' &= 1981 \pm 150 \\ K &= 2628 \pm 118 \\ K' &= 3114 \pm 57 \\ G = G'_{ds} &= 1842 \pm 82 \quad \text{(HELD EQUAL)} \end{aligned} \qquad (8)$$

As expected, the values of J' and K' are greater than J and K, respectively.

As a consequence of this variation the rms error was reduced from 187 to 118. When J' and K' were held equal to J and K respectively, G_3 and G'_3 assumed small negative values, and thus had to be kept fixed at zero. However, when J' and K' were allowed to vary freely, G_3 and G'_3 had the very reasonable values:

$$\begin{aligned} G_3 &= 13 \pm 5 \\ G'_3 &= 22 \pm 9 \end{aligned} \qquad (9)$$

In addition, the agreement of the four experimental Landé g-values was much better after the variation.

Subsequently, a variation was performed by holding J and J' equal and letting K' vary freely. The rms error was only raised to 126, and G_3 as well as G'_3 remained positive. This conclusion is similar to those obtained in Ti I and Fe I, where it was also important to have K' free, but J and J' could be equal without impairing the results greatly.[6]

In the least-squares of the last iteration the levels $(^3P)v\,^2D$ are predicted at 42,420 and 42,437, whereas $(^3P)z\,^2S$ was predicted at 35,567. Thus, either the assignments for the levels $(a^3P)p\ v^2D$ and $(a^3P)p\ z^2S$ are not correct, or they cannot be written with a common uncertainty of y cm^{-1}.

The term $u\,^2D$, given in AEL with no configuration assignment most probably belongs to $(3d+4s)^25p$.

Then neglecting the terms $w\,^2F$, $v\,^2D$, $z\,^2S$, and $u\,^2D$, 58 experimental levels were fitted in the individual least-squares to yield a rms error of 126. The parameters with their standard errors obtained in the individual least-squares of the final iteration in the uniform treatments are given in table 2.

As for Ti II $-3d^24p+3d4s4p$, [5], the experimental term $(^1S)^2P$ is missing and thus α has to be kept fixed. Otherwise there would be more parameters than terms to determine them.

Besides the change $d^2(^1S)p\ x\,^2P \leftrightarrow s^2(^1S)p\ x\,^2P$ mentioned previously, the only other change performed was

$$d\,^2D(^3P)z\,^4D_{5/2} \leftrightarrow d\,^2D(^3P)z\,^2D_{5/2}$$

From table 4, comparing the experimental and calculated energy values, we note that there is considerable sharing of eigenfunctions especially between the three doublets $d\,^2D(^3P)z\,^2P$, $d\,^2D(^1P)y\,^2P$, and $s^2(^1S)x\,^2P$.

Below 40,000 cm^{-1}, there are only 4 theoretical levels with no corresponding experimental levels. The lowest of these is the term $(^3P)^2S$ at 35,567.

The agreement between the experimental and calculated g-factors is very good.

4. Ca I $-(3d+4s)4p$

The configurations $(d+s)p$ comprise 8 terms splitting into 16 levels. For $(3d+4s)4p$, [16] all the predicted levels are given in AEL.

The initial values of the interaction parameters were taken from the final results of Sc I (before the uniform treatment):

$$\begin{aligned} F_2 &= 200 \\ G_1 &= 350 \\ G_3 &= 10 \\ G'_{ps} &= 5800 \\ J &= 1700 \\ K &= 3000 \\ \zeta_d &= 60 \\ \zeta_p &= 100 \end{aligned} \qquad (10)$$

Initially we tried to obtain the values of A and A' from the matrices of ^1P and ^3P, as for Sc II, [5]. However. the results in the two cases were very different. From ^3P, using the fact that the trace equals the sum of the eigenvalues we obtain

$$A+A' = 59{,}560. \qquad (11)$$

From the matrix of ^1P:

$$A+A' = 52{,}624. \qquad (12)$$

Thus the initial value for A was taken as the average of the values obtained by using the centers of gravity of the terms $(dp)^3D$ and $(dp)^3F$. This yields:

$$A = 38{,}100. \qquad (13)$$

As suggested by Professor Racah, the experimental term $4s(^2S)5p\ ^1P$ at 41,679 should be assigned to $3d(^2D)4p\ ^1P$.

Then, from the matrix of ^1P

$$A+A' = 57{,}571. \qquad (14)$$

Now, using (13), (11), and (14), and averaging, we get:

$$A' = 20{,}465. \qquad (15)$$

The final parameters obtained in the uniform treatment are given in table 2.

When G_3 was left to vary freely, it assumed a value of -5 ± 1. Thus in the final variation G_3 was fixed.

The final values of the parameters J and K, and even G'_{ps}, are quite different than expected on the basis of the results from Sc I and Ti I. This indicates that the configurations $(3d+4s)4p$ are perturbed considerably by $4snp$, $n \geq 5$, by $4smf$, $m \geq 4$, and by $4d4p$.

The only change in designation was:

$$4s(^2S)5p\ ^1P \leftrightarrow 3d(^2D)4p\ ^1P.$$

[6] Results to be published soon.

TABLE 2. *Final parameters obtained in the uniform treatment*

Parameter	Ca I $-(3d+4s)4p$	Sc I $-(3d+4s)^24p$	Ti I $-(3d+4s)^34p$
A	37,936 ± 10	35,511 ± 88	37,749 ± 128
A'	21,128 ± 37	25,085 ± 152	31,989 ± 203
A''		25,616 ± 286	40,514 ± 234
B		529 ± 6	554 ± 7
B'			651 ± 7
C		714 ± 69	1,661 ± 33
C'			2,319 ± 57
$G'_{ds}=G$		1,943 ± 68	1,719 ± 56
F_2	128 ± 2	201 ± 8	153 ± 9
F'_2		284 ± 8	286 ± 8
F_2^{β}			419 (Arith. Progress.)
G_{ps}	4,977 ± 19	5,970 ± 82	5,395 ± 97
G_1	394 ± 2	335 ± 9	283 ± 10
G'_1		327 ± 12	288 ± 10
G_1^{β}			293 (Arith. Progress.)
$G_3=G'_3=G''_3$	0 (Fixed)	5 ± 3	10 ± 3
$\alpha=\alpha'$		50 (Fixed)	43 ± 4
$H=H'$		275 ± 18	175 ± 7
$J=J'$	575 ± 20	1,877 ± 96	1,251 ± 53
K	3,795 ± 32	2,551 ± 95	2,415 ± 48
K'		3,059 (Fixed Diff.)	2,987 (Fixed Diff.)
$\zeta_d=\zeta'_d=\zeta''_d$	18 ± 9	58 ± 21	114 ± 29
$\zeta_p=\zeta'_p=\zeta''_p$	87 ± 16	105 ± 56	114 ± 94
rms error	22.8	126.4	261.4

5. Tables of the Observed and Calculated Levels and *g*-Factors

In the column "NAME" the calculated designation of the term is given. Whenever the terms of the parent d^n have different seniorities these are denoted by the letters A and B, the lower calculated term being designated by A. Whenever a calculated term has a corresponding experimental term the small letters $z, y, x, \ldots$, are used as in AEL. The terms of $d^{n-1}sp$ are denoted by $d^{n-1}v_1S_1L_1(sp^{1,3}\mathrm{P})SL$. The terms of d^np are differentiated from those of $d^{n-2}s^2$p by using a star for the latter terms.

The entries in the columns "J", "OBS. LEVEL cm^{-1}", "CALC. LEVEL cm^{-1}", are self-evident. In the column "PERCENTAGE" for each calculated level either the three highest contributions or all those contributions exceeding 5 percent are given.

Whenever the experimental and calculated term designations differ, the experimental designation is entered in the column "AEL", using the notation of C. E. Moore, [8]. In many instances, the exchanges involve complete terms rather than isolated levels. Unless specified otherwise, the entries in the column "AEL" pertain to exchanges in terms.

The columns "OBS. g" and "CALC. g" give the observed and calculated values of the g-factors, respectively.

The entries are in ascending order of magnitude of the calculated terms.

TABLE 3. *Observed and calculated levels of* Ca I 3d4p + 4s4p

Name	J	Percentage	AEL	Obs. level (cm^{-1})	Calc. level (cm^{-1})	O–C	Obs. g	Calc. g
$(^2S)^3P$	0	96		15158	15173	−15		
	1	96		15210	15214	−4		1.500
	2	96		15316	15298	18		1.500
$(^2S)^1P$	1	86 + 14$(^2D)^1P$		23652	23652	0		1.000
$(^2D)^3F$	2	87 + 13$(^2D)^1D$		35730	35726	4	0.754	0.710
	3	100		35819	35807	12	1.076	1.083
	4	100		35897	35889	8	1.245	1.250
$(^2D)^1D$	2	87 + 13$(^2D)^3F$		35835	35877	−42	0.893	0.957
$(^2D)^3D$	1	100		38192	38176	16		0.501
	2	100		38219	38207	12		1.167
	3	100		38259	38251	8		1.333
$(^2D)^3P$	0	96		39333	39337	−4		0.000
	1	96		39335	39345	−10		1.499
	2	96		39340	39327	13		1.500
$(^2D)^1F$	3	100		40538	40556	−18		1.000
$(^2D)^1P$	1	86 + 14$(^2S)^1P$	$4s(^2S)5p\,^1P$	41679	41679	0		1.000

TABLE 4. *Observed and calculated levels of* Sc I $(3d+4s)^2 4p$

Name		Percentage	AEL		Obs. level (cm^{-1})	Calc. level (cm^{-1})	O−C	Obs. g	Calc. g
			Config.	Desig.					
$^2D(^3P)z\,^4F$	3/2	99	$3d4s(a\,^3D)4p$	$z\,^4F$	15,673	15,598	75		0.406
	5/2	99			15,757	15,662	94		1.031
	7/2	99			15,882	15,752	130		1.239
	9/2	100			16,027	15,863	163		1.333
$^2D(^3P)z\,^4D$	1/2	99	$3d4s(a\,^3D)4p$	$z\,^4D$	16,010	15,959	51		0.001
	3/2	99			16,022	15,991	31		1.196
	5/2	98	$3d4s(a\,^1D)4p$	$z\,^2D$	16,023	16,045	−22		1.368
	7/2	99	$3d4s(a\,^3D)4p$	$z\,^4D$	16,211	16,126	85		1.428
$^2D(^3P)z\,^2D$	3/2	95	$3d4s(a\,^1D)4p$	$z\,^2D$	16,097	16,362	−265		0.799
	5/2	95	$3d4s(a\,^3D)4p$	$z\,^4D$	16,141	16,348	−207		1.201
$^2D(^3P)z\,^4P$	1/2	$87+5^2D(^3P)^2P$	$3d4s(a\,^3D)4p$	$z\,^4P$	18,504	18,641	−137		2.401
	3/2	$86+6^2D(^3P)^2P$			18,516	18,644	−128		1.677
	5/2	100			18,571	18,706	−135		1.600
$^2D(^3P)z\,^2P$	1/2	$51+34(^1S)^2P^*+13^2D(^3P)^4P$	$3d4s(a\,^1D)4p$	z^2P	18,711	18,775	−64		0.931
	3/2	$52+32(^1S)^2P^*+13^2D(^3P)\,^4P$			18,856	18,837	19		1.389
$^2D(^3P)z\,^2F$	5/2	94	$3d4s(a\,^1D)4p$	$z\,^2F$	21,033	20,936	97		0.857
	7/2	95			21,086	20,990	96		1.143
$^2D(^1P)y\,^2P$	1/2	$67+21(^1S)^2P^*$	$3d4s(a\,^3D)4p$	$y\,^2P$	24,657	24,606	51		0.667
	3/2	$64+22(^1S)^2P^*$			24,657	24,609	48		1.326
$^2D(^1P)y\,^2D$	3/2	$63+35(^3F)^2D$	$3d4s(a\,^3D)4p$	$y\,^2D$	24,866	24,789	77	0.82	0.807
	5/2	$64+35(^3F)^2D$			25,014	24,925	89	1.17	1.200
$^2D(^1P)y\,^2F$	5/2	$64+27(^3F)^2F$	$3d4s(a\,^3D)4p$	$y\,^2F$	25,585	25,658	−73	0.90	0.857
	7/2	$63+27(^3F)^2F$			25,725	25,771	−46	1.14	1.143
$(^3F)z\,^4G$	5/2	100			29,023	29,102	−79		0.572
	7/2	100			29,096	29,183	−87		0.984
	9/2	100			29,190	29,288	−98		1.172
	11/2	100			29,304	29,416	−112		1.273
$(^1S)x\,^2P^*$	1/2	$34+41^2D(^3P)^2P+18(^1D)^2P$	$3d^2(a\,^1S)4p$	x^2P	30,573	30,576	−3	0.68	0.667
	3/2	$34+40^2D(^3P)^2P+19(^1D)^2P$			30,707	30,680	27		1.333
$(^3F)y\,^4F$	3/2	100			31,173	30,990	183		0.400
	5/2	100			31,216	31,043	173		1.029
	7/2	100			31,275	31,115	160		1.238
	9/2	100			31,351	31,206	145		1.333
$(^3F)y\,^4D$	1/2	99			32,637	32,687	−50		0.000
	3/2	99			32,659	32,706	−47		1.199
	5/2	98			32,697	32,740	−43		1.369
	7/2	98			32,752	32,792	−40		1.427
$(^3F)z\,^2G$	7/2	90			33,056	33,109	−53		0.890
	9/2	90			33,151	33,208	−57		1.111
$(^3F)x\,^2F$	5/2	$54+29^2D(^1P)^2F$			33,154	33,210	−56		0.865
	7/2	$55+30^2D(^1P)^2F$			33,278	33,332	−54		1.143
$(^3P)^2S$	1/2	100				35,567			1.998
$(^3F)x\,^2D$	3/2	$30+28(^3P)^2D+26(^1D)^2D$			33,615	33,597	18		0.801
	5/2	$29+28(^3P)^2D+25(^1D)^2D$			33,707	33,692	15		1.194
$(^1D)^2F$	5/2	$81+15(^3F)^2F$				35,965			0.858
	7/2	$82+14(^3F)^2F$				36,062			1.143
$(^1D)w\,^2D$	3/2	$48+17(^1D)^2P+15(^3F)^2D$			36,934	36,920	14		0.943
	5/2	$66+20(^3F)^2D+13^2D(^1P)^2D$			37,040	37,018	22		1.200
$(^1D)w\,^2P$	1/2	$62+17(^3P)^2P+6(^3P)^4D$			37,126	37,148	−22		0.632
	3/2	$48+18(^1D)^2D+14(^3P)^2P$			37,086	37,097	−11		1.189

TABLE 4. *Observed and calculated levels of* Sc I $(3d+4s)^2 4p$ —Continued

Name	J	Percentage	AEL		Obs. level (cm^{-1})	Calc. level (cm^{-1})	O−C	Obs. g	Calc. g
			Config.	Desig.					
$(^3P)x\,^4D$	1/2	94				37,330			0.038
	3/2	98			37,486	37,361	125		1.202
	5/2	99			37,553	37,426	127		1.371
	7/2	98			37,717	37,522	195		1.428
$(^3P)z\,^4S$	3/2	98			38,180	38,478	−298		1.994
$(^3P)y\,^4P$	1/2	100			38,571	38,611	−40		2.666
	3/2	98			38,602	38,653	−51		1.739
	5/2	100			38,658	38,719	−61		1.600
$(^1G)z\,^2H$	9/2	91			39,153	39,157	−4		0.928
	11/2	100			39,249	39,279	−30		1.091
$(^1G)y\,^2G$	7/2	$90+10(^3F)^2G$			39,393	39,362	31		0.889
	9/2	$82+9(^1G)^2H+9(^3F)^2G$			39,424	39,391	33		1.092
$(^3P)^2D$	3/2	$71+15(^3F)^2D$				42,420			0.800
	5/2	$70+15(^3F)^2D$				42,437			1.200
$(^1G)^2F$	5/2	$87+10^2D(^1P)^2F$				43,400			0.857
	7/2	$87+11^2D(^1P)^2F$				43,342			1.143
$(^3P)^2P$	1/2	$67+23^2D(^1P)^2P$				44,451			0.667
	3/2	$68+23^2D(^1P)^2P$				44,535			1.333
$(^1S)^2P$	1/2	91				48,495			0.667
	3/2	92				48,599			1.333

TABLE 5. *Observed and calculated levels of* Ti I $(3d+4s)^2 4p$

Name	J	Percentage	AEL		Obs. level (cm^{-1})	Calc. level (cm^{-1})	O−C	Obs. g	Calc. g
			Config.	Desig.					
$^3F(^3P)z\,^5G$	2	100	$3d^24s(a\,^4F)4p$	$z\,^5G$	15,877	15,801	76	0.39	0.334
	3	100			15,976	15,889	87	0.93	0.917
	4	100			16,106	16,005	101	1.15	1.150
	5	100			16,268	16,149	119	1.25	1.267
	6	100			16,459	16,320	139	1.33	1.333
$^3F(^3P)z\,^5F$	1	94	$3d^24s(a\,^4F)4p$	$z\,^5F$	16,817	16,723	94	0.00	0.001
	2	98			16,875	16,780	95		1.000
	3	98			16,961	16,866	95	1.26:	1.250
	4	98			17,075	16,981	94	1.34	1.350
	5	98			17,215	17,124	91	1.42	1.400
$^3F(^3P)z\,^5D$	0	94	$3d^24s(a^4F)4p$	$z\,^5D$	18,463	18,455	8		
	1	94			18,483	18,480	3	1.65?	1.498
	2	94			18,525	18,533	−8	1.50	1.497
	3	93			18,594	18,616	−22	1.49	1.498
	4	94			18,695	18,737	−42	1.51	1.497
$^3F(^3P)z\,^3F$	2	$88+8^1D(^3P)^3F$	$3d^24s(a^2F)4p$	$z\,^3F$	19,323	19,343	−20	0.67	0.669
	3	$88+7^1D(^3P)^3F$			19,422	19,437	−15	1.07	1.086
	4	$88+7^1D(^3P)^3F$			19,574	19,583	−9	1.26	1.252
$^3F(^3P)z\,^3D$	1	$84+8^3P(^3P)^3D$	$3d^24s(a\,^2F)4p$	$z\,^3D$	19,938	19,942	−4		0.502
	2	$83+8^3P(^3P)^3D$			20,006	20,023	−17	1.16	1.166
	3	$83+8^3P(^3P)^3D$			20,126	20,155	−29	1.34	1.332

TABLE 5. *Observed and calculated levels of* Ti I $(3d+4s)^3 4p$ – Continued

Name	J	Percentage	AEL		Obs. level (cm^{-1})	Calc. level (cm^{-1})	O – C	Obs. g	Calc. g
			Config.	Desig.					
$^3F(^3P)z\,^3G$	3	95	$3d^24s(a\,^2F)4p$	$z\,^3G$	21,470	21,490	−20	0.75	0.751
	4	95			21,589	21,598	−9	1.05	1.050
	5	95			21,740	21,739	1	1.21	1.201
$^3F(^3P)z\,^1D$	2	$86+10\,^3P(^3P)\,^1D$	$3d^24s(a\,^2F)4p$	$z\,^1D$	22,081	22,615	−534	1.00	1.000
$^3F(^3P)z\,^1F$	3	97	$3d^24s(a\,^2F)4p$	$z\,^1F$	22,405	22,446	−41	1.00	0.999
$^3F(^3P)z\,^1G$	4	94	$3d^24s(a\,^2F)4p$	$z\,^1G$	24,695	24,683	12	0.97	1.006
$^3P(^3P)z\,^3S$	1	$90+7(^2P)\,^3S$	$3d^24s(b\,^4P)4p$	$z\,^3S$	24,921	25,062	−141	1.99	1.988
$^3P(^3P)z\,^5S$	2	93	$3d^24s(b\,^4P)4p$	$z\,^5S$	25,103	25,002	101	1.93	1.984
$^3F(^1P)y\,^3F$	2	$44+25(^4F)\,^3F+23\,^1D(^3P)\,^3F$	$3d^24s(a\,^4F)4p$	$y\,^3F$	25,107	25,062	45		0.668
	3	$43+25(^4F)\,^3F+25\,^1D(^3P)\,^3F$			25,227	25,177	50	1.06	1.084
	4	$41+23(^4F)\,^3F+27\,^1D(^3P)\,^3F$			25,388	25,332	56	1.21?	1.246
$(^4F)y\,^3D$	1	$49+34\,^3F(^1P)\,^3D$	$3d^24s(a\,^4F)4p$	$y\,^3D$	25,318	25,639	−321	0.50	0.562
	2	$28+37\,^1D(^3P)\,^3P+19\,^3F(^1P)\,^3D$			25,439	25,809	−370	1.17	1.330
	3	$32+32\,^3P(^3P)\,^5D+24\,^3F(^1P)\,^3D$			25,644	25,980	−336	1.33	1.391
$^1D(^3P)z\,^3P$	0	$43+38\,^3P(^3P)\,^5D+7\,^3P(^3P)\,^1S$				25,713			
	1	$64+22\,^3P(^3P)\,^5D$	$3d^24s(b\,^4P)4p$	$z\,^3P$	25,537	25,789	−252	1.50	1.493
	2	$49+20(^4F)\,^3D+14\,^3F(^1P)\,^3D$			25,494	25,697	−203	1.47	1.379
$^3P(^3P)y\,^5D$	0	$51+32\,^1D(^3P)\,^3P$	$3d^24s(b\,^4P)4p$	$y\,^5D$	25,605	25,746	−141		
	1	$65+19\,^1D(^3P)\,^3P$			25,636	25,754	−118		1.457
	2	$82+6(^4F)\,^5D$			25,700	25,822	−122		1.470
	3	$56+19(^4F)\,^3D+13\,^3F(^1P)\,^3D$			25,798	25,902	−104		1.438
	4	$87+7(^4F)\,^5D$			25,927	26,004	−77	1.52	1.495
$^3P(^3P)\,^1S$	0	$68+16(^2P)\,^1S+15\,^3P(^3P)\,^1S$				26,170			
$(^4F)y\,^5G$	2	94			26,494	26,614	−120	0.34	0.352
	3	96			26,564	26,701	−137	0.91	0.923
	4	98			26,657	26,817	−160	1.15	1.151
	5	100			26,773	26,961	−188	1.25	1.267
	6	100			26,911	27,130	−219	1.34	1.333
$^1D(^3P)x\,^3F$	2	$58+19\,^3F(^1P)\,^3F+13(^4F)\,^3F$	$3d^3(b\,^4F)4p$	$x\,^3F$	26,803	26,729	74	0.66	0.653
	3	$57+20\,^3F(^1P)\,^3F+14(^4F)\,^3F$			26,893	26,813	80	1.06	1.081
	4	$57+20\,^3F(^1P)\,^3F+15(^4F)\,^3F$			27,026	26,939	87	1.23	1.252
$^1D(^3P)x\,^3D$	1	$78+12\,^3P(^3P)\,^3D$	$3d^3(b\,^4F)4p$	$x\,^3D$	27,355	27,366	−11	0.51	0.516
	2	$73+9\,^3P(^3P)\,^3D+7\,^3P(^3P)\,^5P$			27,418	27,425	−7	1.17	1.210
	3	$64+9\,^3P(^3P)\,^3D+19\,^3P(^3P)\,^5P$			27,480	27,480	0	1.36	1.397
$^3F(^1P)y\,^3G$	3	$56+23(^4F)\,^3G+10(^2G)\,^3G$	$3d^3(b\,^4F)4p$	$y\,^3G$	27,499	27,332	167	0.75	0.750
	4	$55+23(^4F)\,^3G+10(^2G)\,^3G$			27,615	27,474	141	1.05	1.051
	5	$53+24(^4F)\,^3G+10(^2G)\,^3G$			27,750	27,645	105	1.21	1.201
$^3P(^3P)z\,^5P$	1	97	$3d^24s(b\,^4P)4p$	$z\,^5P$	27,666	27,670	−4		2.483
	2	91			27,740	27,739	1		1.788
	3	$79+16\,^1D(^3P)\,^3D$			27,888	27,873	15		1.602
$^1D(^1P)y\,^1D$	2	$32+26(^2D)\,^1D^*+17\,^3P(^3P)\,^1D$	$3d^24s(a\,^2D)4p$	$y\,^1D$	27,907	28,254	−347	0.98	1.000
$(^4F)y\,^5F$	1	98			28,596	28,452	144	0.00	0.001
	2	98			28,639	28,509	130	1.01	1.000
	3	98			28,703	28,595	108	1.24	1.250
	4	98			28,788	28,709	79	1.34	1.349
	5	97			28,996	28,852	144	1.40	1.399
$^3F(^1P)w\,^3D$	1	$33+24(^4F)\,^3D+11(^4P)\,^3D$	$3d^24s(b\,^4P)4p$	$w\,^3D$	29,661	29,811	−150	0.51	0.545
	2	$29+21(^4F)\,^3D+15(^4F)\,^5D$			29,769	29,899	−130	1.16	1.221
	3	$20+35(^4F)\,^5D+15(^4F)\,^3D$			29,912	30,012	−100	1.34	1.385

TABLE 5. *Observed and calculated levels of* Ti I $(3d+4s)^3 4p$ – Continued

Name	J	Percentage	AEL		Obs. level (cm^{-1})	Calc. level (cm^{-1})	O–C	Obs. g	Calc. g
			Config.	Desig.					
$(^4F)x\,^5D$	0	91			29,829	29,837	−8		
	1	$87+7\,^3P(^3P)\,^5D$			29,855	29,881	−26	1.46	1.454
	2	$77+6\,^3P(^3P)\,^5D$			29,907	29,971	−64	1.50	1.445
	3	$55+14\,^3F(^1P)\,^3D+11(^4F)\,^3D$			29,986	30,110	−124	1.49	1.433
	4	91			30,060	30,124	−64	1.49	1.500
$^1G(^3P)x\,^3G$	3	$70+19\,^3F(^1P)\,^3G+6(^2H)\,^3G$	$3d^24s(a\,^4F)4p$	$x\,^3G$	29,915	30,051	−136		1.765
	4	$72+19\,^3F(^1P)\,^3G+6(^2H)\,^3G$			29,971	30,086	−115		1.050
	5	$71+19\,^3F(^1P)\,^3G+6(^2H)\,^3G$			30,039	30,127	−88	1.19	1.200
$^3P(^3P)v\,^3D$	1	$77+16\,^1D(^3P)\,^3D$	$3d^24s(a\,^2D)4p$	$v\,^3D$	31,184	30,927	257	0.51	0.502
	2	$68+15\,^1D(^3P)\,^3D$			31,191	30,937	254	1.17	1.167
	3	$69+14\,^1D(^3P)\,^3D$			31,206	30,952	254	1.34	1.333
$(^4F)w\,^3G$	3	$70+21\,^3F(^1P)\,^3G$	$3d^24s(b\,^2G)4p$	$w\,^3G$	31,374	30,993	381	0.75	0.751
	4	$69+22\,^3F(^1P)\,^3G$			31,489	31,126	363	1.05	1.050
	5	$69+22\,^3F(^1P)\,^3G$			31,629	31,283	346	1.19	1.200
$^3P(^3P)y\,^3P$	0	$85+7(^2P)\,^3P$	$3d^24s(a\,^2D)4p$	$y\,^3P$	31,686	31,779	−93		
	1	$85+6(^2P)\,^3P$			31,726	31,811	−85	1.47	1.499
	2	$85+6(^2P)\,^3P$			31,806	31,878	−72		1.499
$^1G(^3P)z\,^3H$	4	$85+11(^2G)\,^3H$	$3d^24s(b\,^2G)4p$	$z\,^3H$	31,830	31,824	6	0.80	0.800
	5	$86+10(^2G)\,^3H$			31,914	31,891	23	1.04	1.034
	6	$86+10(^2G)\,^3H$			32,014	31,969	45	1.17	1.167
$^1D(^1P)y\,^1F$	3	$36+44(^2G)\,^1F+11\,^1G(^1P)\,^1F$	$3d^24s(a\,^2D)4p$	$y\,^1F$	32,858	32,354	504	0.99 ?	0.999
$^1D(^1P)z\,^1P$	1	$37+29\,^3P(^3P)\,^1P+25(^2P)\,^1P$	$3d^24s(a\,^2D)4p$	$z\,^1P$	33,661	33,083	578	0.94?	1.010
$(^4P)x\,^3P$	0	$33+34\,^3P(^1P)\,^3P+20(^2P)\,^3P$	$3d^24s(b\,^2P)4p$	$x\,^3P$	33,085	33,405	−320		
	1	$33+34\,^3P(^1P)\,^3P+20(^2P)\,^3P$			33,091	33,422	−331	1.46	1.495
	2	$34+34\,^3P(^1P)\,^3P+20(^2P)\,^3P$			33,114	33,438	−324	1.46	1.500
$(^4F)w\,^3F$	2	$54+30\,^3F(^1P)\,^3F$	$3d^24s(a\,^2D)4p$	$w\,^3F$	33,656	33,580	76	0.66	0.667
	3	$53+30\,^3F(^1P)\,^3F$			33,680	33,702	−22	1.09	1.083
	4	$53+30\,^3F(^1P)\,^3F$			33,701	33,853	−152	1.26	1.250
$^3P(^1P)\,^3S$	1	$62+37(^4P)\,^3S$				34,002			1.989
$^1G(^3P)v\,^3F$	2	$81+9(^2D)\,^3F^*$	$3d^24s(b\,^2G)4p$	$v\,^3F$	33,981	34,209	−228	0.63	0.674
	3	$83+9(^2D)\,^3F^*$			34,079	34,198	−119	1.10	1.083
	4	$84+8(^2D)\,^3F^*$			34,205	34,182	23	1.23	1.250
$^3P(^3P)x\,^1D$	2	$56+12\,^3F(^3P)\,^1D+10\,^1D(^1P)\,^1D$	$3d^24s(b\,^2P)4p$	$x\,^1D$	35,035	34,517	518		0.993
$(^2G)z\,^1H$	5	$58+26(^2H)\,^1H+16\,^1G(^1P)\,^1H$	$3d^24s(b\,^2G)4p$	$z\,^1H$	34,700	34,871	−171	1.02	1.000
$^3P(^3P)y\,^1P$	1	$54+26\,^1D(^1P)\,^1P+14(^2D)\,^1P^*$	$3d^24s(b\,^2P)4p$	$y\,^1P$	34,947	35,098	−151		1.005
$(^2G)y\,^3H$	4	$84+13\,^1G(^3P)\,^3H$			35,454	35,247	207	0.79	0.801
	5	$85+12\,^1G(^3P)\,^3H$			35,560	35,369	191	1.04	1.033
	6	$85+12\,^1G(^3P)\,^3H$			35,685	35,515	170	1.17	1.166
$(^4P)w\,^5D$	0	99			35,503	35,481	22		
	1	99			35,528	35,506	22	1.51	1.499
	2	99			35,577	35,557	20	1.53	1.499
	3	99			35,653	35,639	14	1.46	1.499
	4	99			35,758	35,757	1	1.46	1.499
$^1G(^1P)y\,^1G$	4	$45+32(^2G)\,^1G+21(^2H)\,^1G$	$3d^24s(b\,^2G)4p$	$y\,^1G$	36,000	35,750	250	1.00	1.000
$(^4P)y\,^5P$	1	97			36,298	36,308	−10	2.47	2.491
	2	97			36,341	36,367	−26	1.81	1.830
	3	98			36,415	36,455	−40	1.66	1.665
$(A^2D)w\,^3P$	0	$35+35(^4P)\,^3P+23(^2P)\,^3P$			37,091	37,065	26		
	1	$36+35(^4P)\,^3P+23(^2P)\,^3P$			37,173	37,181	−8	1.53	1.499
	2	$33+33(^4P)\,^3P+21(^2P)\,^3P$			37,325	37,362	−37	1.48	1.531

TABLE 5. *Observed and calculated levels of* Ti I $(3d+4s)^3 4p$ – Continued

Name	J	Percentage	AEL		Obs. level (cm^{-1})	Calc. level (cm^{-1})	O−C	Obs. g	Calc. g
			Config.	Desig.					
$(^4P)y\ ^5S$	2	90			37,359	37,178	181	1.99	1.964
$^3P(^1P)u\ ^3D$	1	$42+17(^2P)^3D+13(^4P)^3D$	$3d^34s(b\ ^2P)4p$	$u\ ^3D$	37,852	37,551	301	0.53	0.508
	2	$41+17(^2P)^3D+14(^4P)^3D$			37,977	37,617	360	1.14	1.168
	3	$39+17(^2P)^3D+15(^4P)^3D$			38,160	37,691	469	1.35	1.380
$(^2G)v\ ^3G$	3	$77+7^1G(^3P)^3G+5(^4F)^3G$			37,555	37,583	−28	0.77	0.782
	4	$81+7^1G(^3P)^3G+5(^4F)^3G$			37,618	37,644	−26	1.05	1.058
	5	$85+7^1G(^3P)^3G+6(^4F)^3G$			37,690	37,740	−50	1.20	1.199
$(A^2D)u\ ^3F$	2	$49+20(^2G)^3F+10(^2D)^3F^*$			37,655	37,699	−44	0.65	0.681
	3	$26+14(^2G)^3F+14(^2D)^1F^*$			37,744	37,772	−28	1.08	1.028
	4	$41+26(^2G)^3F+10(^2D)^3F^*$			37,852	37,941	−89	1.24	1.239
$(^2D)x\ ^1F^*$	3	$25+16^1G(^1P)^1F+13^1D(^1P)^1F$	$3d^34s(b\ ^2G)4p$	$x\ ^1F$	37,623	37,841	−218	0.94	1.042
$(^2P)z\ ^1S$	0	$80+18^3P(^3P)^1S$			38,201	38,060	141		
$(^2G)x\ ^1G$	4	$50+29(^2H)^1G+18^1G(^1P)^1G$			38,960	38,200	760	1.02	1.001
$(^2P)t\ ^3D$	1	$37+22(^2D)^3D^*+21(^4P)^3D$	$3d^3(b\ ^2D)4p$	$t\ ^3D$	38,654	38,436	218	0.54	0.503
	2	$32+20(^2D)^3D^*+20(^4P)^3D$			38,700	38,558	142		1.153
	3	$32+20(^2D)^3D^*+22(^4P)^3D$			38,765	38,659	106	1.32	1.329
$(^2H)z\ ^3I$	5	100			38,573	38,454	119	0.81	0.834
	6	100			38,669	38,564	105	1.02	1.024
	7	100			38,780	38,691	89	1.15	1.143
$(^2D)w\ ^1D^*$	2	$28+30(^2P)^1D+24(A^2D)^1D$	$3d^3(a\ ^2P)4p$	$w\ ^1D$	39,266	38,764	502	1.06	1.005
$(^2H)x\ ^3H$	4	93			39,116	39,152	−36	0.882	0.802
	5	$85+12^1G(^3P)^3H$			39,152	39,201	−49	1.02	1.034
	6	$85+12^1G(^3P)^3H$			39,199	39,255	−56	1.18	1.165
$(^2G)t\ ^3F$	2	$58+27(A^2D)^3F+11^3F(^1P)^3F$			38,451	39,257	−806	0.66	0.672
	3	$55+30(A^2D)^3F+11^3F(^1P)^3F$			38,544	39,330	−786	1.08	1.087
	4	$52+34(A^2D)^3F+11^3F(^1P)^3F$			38,671	39,428	−757	1.25	1.250
$(A^2D)x\ ^1P$	1	$73+16(^2P)^1P$			39,078	39,268	−190		1.003
$(A^2D)s\ ^3D$	1	$54+14(^2P)^3D+10^3P(^1P)^3D$	$3d^3(a\ ^4P)4p$	$s\ ^3D$	39,662	39,696	−34	0.52	0.508
	2	$60+17(^2P)^3D+11^3P(^1P)^3D$			39,686	39,774	−88		1.167
	3	$55+20(^2P)^3D+12^3P(^1P)^3D$			39,716	39,910	−194	1.31	1.330
$(^2D)v\ ^3P^*$	0	$37+23^3P(^1P)^3P+18(^4P)^3P$	$3d^3(a\ ^4P)4p$	$v\ ^3P$	40,370	40,129	241		
	1	$24+30(^2P)^3S+14^3P(^1P)^3P$			40,385	40,125	260		1.662
	2	$36+21^3P(^1P)^3P+16(^4P)^3P$			40,467	40,265	202		1.497
$(A^2D)w\ ^1F$	3	$82+7^1D(^1P)^1F$			40,303	40,267	36	1.05	1.007
$(^2P)x\ ^3S$	1	$57+13(^2D)^3P^*+8^3P(^1P)^3P$			40,844	40,286	558		1.827
$(^2H)z\ ^1I$	6	99			40,320	40,342	−22	1.03	1.001
$(^2G)v\ ^1F$	3	$43+31^1D(^1P)^1F+11(^2D)^1F^*$			41,585	41,026	559		1.000
$(^4P)r\ ^3D$	1	$44+22(A^2D)^3D$	$3d^3(a\ ^2P)4p$	$r\ ^3D$	40,556	41,115	−559	0.49	0.502
	2	$43+24(A^2D)^3D$			40,671	41,172	−501		1.165
	3	$40+25(A^2D)^3D$			40,844	41,269	−425		1.328
$(^2H)y\ ^1H$	5	$47+41(^2G)^1H+12^1G(^1P)^1H$	$3d^3(a\ ^2G)4p$	$y\ ^1H$	41,040	41,257	−217	1.03	1.001
$(^2D)s\ ^3F^*$	2	$66+18(A^2D)^3F+6^1G(^3P)^3F$		$s\ ^3F$	41,337	41,307	30	0.66	0.669
	3	$67+19(A^2D)^3F+6^1G(^3P)^3F$			41,458	41,441	17	1.09	1.084
	4	$68+18(A^2D)^3F+5^1G(^3P)^3F$			41,624	41,618	6	1.24	1.250
$(^2P)u\ ^3P$	0	$36+36(A^2D)^3P+9^3P(^1P)^3P$			41,959	41,627	332		
	1	$36+37(A^2D)^3P+9^3P(^1P)^3P$			41,944	41,605	339		1.500
	2	$38+37(A^2D)^3P+9^3P(^1P)^3P$			41,929	41,562	367		1.498

TABLE 5. *Observed and calculated levels of* Ti I $(3d+4s)^3 4p$ – Continued

Calc. *g*	Name	*J*	Percentage	AEL Config.	AEL Desig.	Obs. level (cm^{-1})	Calc. level (cm^{-1})	O – C	Obs. *g*	Calc. *g*
1.964	$(^3H)^3G$	3	$89+7^3F(^1P)^3G$				42,539			0.751
		4	$89+7^3F(^1P)^3G$				42,553			1.050
0.508		5	$89+7^3F(^1P)^3G$				42,581			1.199
1.168										
1.380	$(^3D)q^3D^*$	1	$39+20^3P(^1P)^3D+13(^2F)^3D$		$q\,^3D$	42,146	42,621	−475		0.501
		2	$27+14^3P(^1P)^3D+13(^2F)^1D$			42,207	42,640	−433		1.114
0.782		3	$39+20^3P(^1P)^3D+14(^2F)^3D$			42,311	42,809	−502	1.32	1.333
1.058										
1.199	$(^3P)^1D$	2	$29+16(^2D)^1D^*+12(^2D)^3D^*$				42,799			1.053
0.681	$(^3H)v\,^1G$	4	$30+36(^2F)^1G+29^1G(^1P)^1G$			43,674	43,534	140	0.95	1.000
1.028										
1.239	$(A^2D)u\,^1D$	2	$38+29^1D(^1P)^1D+19(^2F)^1D$			43,800	44,256	−456	0.98:	1.001
1.042	$(^3P)^1P$	1	$37+29(^2D)^1P^*+12^3P(^3P)^1P$				44,480			1.000
	$(^3D)^1P^*$	1	$51+23^1D(^1P)^1P+21(^2P)^1P$				44,818			1.008
1.001	$^1G(^1P)^1H$	5	$72+27(^2H)^1H$				43,356			1.000
0.503	$(^4P)^3S$	1	$59+35^3P(^1P)^3S$				45,555			1.991
1.153										
1.329	$(^2F)^3F$	2	97				46,744			0.667
		3	$86+11(^2F)^3G$				46,731			1.047
0.834		4	$87+10(^2F)^3G$				46,729			1.229
1.024										
1.143	$(^2F)^3G$	3	$87+11(^2F)^3F$				46,954			0.787
		4	$87+10(^2F)^3F$				46,985			1.071
1.005		5	97				47,002			1.200
0.802	$^3P(^1P)^3P$	0	$41+45(^2D)^3P^*$				47,964			
1.034		1	$41+44(^2D)^3P^*$				48,010			1.499
1.165		2	$41+44(^2D)^3P^*$				48,094			1.499
0.672	$(^2F)^1F$	3	$48+24(^2D)^1F^*+15^1G(^1P)^1F$				48,856			1.000
1.087										
1.250	$(^2F)^1D$	2	$67+19(A^2D)^1D+12^1D(^1P)^1D$				49,337			1.000
1.003	$(^2F)^1G$	4	$62+19^1G(^1P)^1G+19(^2H)^1G$				49,392			1.000
0.508	$^1S(^3P)^3P$	0	92				49,646			
1.167		1	91				49,689			1.496
1.330		2	$66+23(^2F)^3D$				49,802			1.406
	$(^2F)^3D$	1	$81+11^3P(^1P)^3D$				49,951			0.504
1.662		2	$58+26^1S(^3P)^3P+8^3P(^1P)^3D$				49,886			1.260
1.497		3	$80+9^3P(^1P)^3D$				49,853			1.333
1.007	$^1G(^1P)^1F$	3	$38+41(^2F)^1F+16(^2D)^1F^*$				53,342			1.000
1.827	$(B^2D)^1P$	1	$47+43^1S(^1P)^1P$				56,958			0.949
1.001	$(B^2D)^3F$	2	$85+11(B^2D)^3D$				57,040			0.724
		3	$78+18(B^2D)^3D$				57,046			1.129
1.000		4	97				57,101			1.250
0.502	$(B^2D)^3D$	1	$86+5^1S(^3P)^3P$				57,154			0.553
1.165		2	$85+11(B^2D)^3F$				57,162			1.111
1.328		3	$78+18(B^2D)^3F$				57,176			1.287
1.001	$(B^2D)^1D$	2	$86+9(^2F)^1D$				57,951			0.999
0.669	$(B^2D)^3P$	0	92				58,656			
1.084		1	91				58,612			1.498
1.250		2	91				58,519			1.498
	$(B^2D)^1F$	3	93				58,886			1.000
1.500										
1.498	$^1S(^1P)^1P$	1	$48+48(B^2D)^1P$				65,788			1.000

The work described in this paper was supported in part by the National Bureau of Standards, Washington, D.C.

The author wishes to acknowledge with everlasting gratitude and appreciation the unremitting kind interest in this work by the late Professor Giulio Racah.

6. References

[1] Racah, G., and Shadmi, Y., Bull. Res. Counc. Israel, **8F**, No. 1, 15 (1959).
[2] Shadmi, Y., Bull. Res. Counc. Israel, **10F**, No. 3, 109 (1962).
[3] Roth, C., J. Res. NBS **72A** (Phys. and Chem.) No. 5, 505 (1968).
[4] Roth, C., J. Res. Nat. Bur. Stand. (U.S.), **73A**, No. 2, 125–157 (1969).
[5] Roth, C., J. Res. Nat. Bur. Stand. (U.S.), **73A**, No. 2, 159–171 (1969).
[6] Roth, C., J. Res. Nat. Bur. Stand. (U.S.), **73A**, No. 6 (1969).
[7] Rohrlich, F., Phys. Rev. **74**, 1381 (1948).
[8] Moore, C. E., Atomic Energy Levels, NBS Circular 467, Vol. I (1949), referred to as AEL.
[9] Russell, H. N., Astroph. J. **66**, 347 (1927), Mt. Wilson Contr. No. 345 (1927).
[10] Trees, R. E., Phys. Rev. **83**, 756 (1951); ibid., **84**, 1089 (1951).
[11] Racah, G., Phys. Rev. **85**, 381 (1952).
[12] Racah, G., Rydberg Centennial Conference, Acta. Univ. Lund, **50**, 31 (1955).
[13] Racah, G., Phys. Rev. **62**, 438 (1942).
[14] Racah, G., Phys. Rev. **62**, 523 (1942).
[15] Russell, H. N., and Meggers, W. F., Sc. Papers Bur. Std. **22**, No. 558, 340 (1927).
[16] Resbey, G., Ark Fys. **37**, No. 18, 231–249 (1968).

(Paper 73A5–568)

JOURNAL OF RESEARCH of the National Bureau of Standards—A. Physics and Chemistry
Vol. 73A, No. 5, September–October 1969

Absolute Isotopic Abundance Ratio and Atomic Weight of Terrestrial Rubidium

E. J. Catanzaro, T. J. Murphy, E. L. Garner and W. R. Shields

Institute for Materials Research, National Bureau of Standards, Washington, D.C. 20234

(June 18, 1969)

An absolute value has been obtained for the isotopic abundance ratio of terrestrial rubidium, using solid-sample thermal ionization mass spectrometry. Samples of known isotopic composition, prepared from nearly isotopically pure separated rubidium isotopes, were used to calibrate the mass spectrometers. The resulting absolute $^{85}Rb/^{87}Rb$ ratio is 2.59265 ± 0.00170 which yields atom percents of: $^{85}Rb = 72.1654 \pm 0.0132$ and $^{87}Rb = 27.8346 \pm 0.0132$. The atomic weight calculated from this isotopic composition is 85.46776 ± 0.00026. The indicated uncertainties are overall limits of error based on 95 percent confidence limits for the mean and allowances for the effects of known sources of possible systematic error.

Key words: absolute ratio; atomic weight; isotopic abundances; rubidium.

1. Introduction

The Analytical Mass Spectrometry Section of the National Bureau of Standards is conducting a long-term program of absolute isotopic abundance ratio and atomic weight determinations, using solid-sample thermal or surface ionization mass spectrometry. Previous elements studied include silver [1],[1] chlorine [2], copper [3], bromine [4], chromium [5], magnesium [6], lead [7], and boron [8]. The present work extends the study to rubidium.

Natural rubidium consists of two isotopes, ^{85}Rb and ^{87}Rb, the latter of which is radioactive with reported half-life values ranging from 47,000 to 50,000 million years [9, 10]. The amount of ^{87}Rb has decreased slightly since the formation of the earth approximately 4550 million years ago but Shields et al. [11] have shown that the present-day $^{85}Rb/^{87}Rb$ ratio is constant in nature within 95 percent confidence limits of 0.15 percent.

A number of other mass spectrometric determinations of rubidium isotopic abundances have been reported in the literature [12, 13, 14, 15, 16] but none of these could be considered absolute.

In the present study, the mass spectrometers were calibrated for bias by the use of samples of known $^{85}Rb/^{87}Rb$ ratio, prepared from chemically pure and nearly isotopically pure ^{85}Rb and ^{87}Rb solutions. The measured biases were then used to correct the raw data obtained on a standard sample of RbCl, yielding an absolute value of $^{85}Rb/^{87}Rb$ for this sample. Bias measurements were made on samples with $^{85}Rb/^{87}Rb$ ratios of approximately 1.0 and 2.6, to double-check the assumption that the bias of each instrument was independent of the isotopic composition.

[1] Figures in brackets indicate the literature references at the end of this paper.

2. Experimental Procedure

2.1. Mass Spectrometry

Isotopic ratio measurements were made on two single-stage solid-sample mass spectrometers which are identical except for very minor differences in the vacuum systems. Each instrument has a 6-in radius of curvature 60° analyzer tube, 48° sector magnet, and a Z lens in the source assembly [17]. Triple-filament rhenium-ribbon (1×30 mils) sources were used. All filaments were prebaked in a vacuum, under a potential field, to eliminate the possibility of significant rubidium background signals from the filament material. Blank filaments which had been prebaked did not show any rubidium ion signals under the standard analytical procedures used in this study.

Two complete sets of samples were prepared. The two sets, prepared from the same parent solutions, had identical isotopic compositions and rubidium concentrations (10 $\mu g/cm^3$) but one set was made up of neutral aqueous solutions while the other consisted of 2 percent HCl solutions. The two operators used different mass spectrometers and different, but isotopically identical, samples, as well as slightly different heating and timing procedures.

One drop of solution (~ 0.2 μg Rb) was placed on each sample filament and dried with a heat lamp and an electrical current of 0.5 A for 10 min. The mass spectrometric analyses were begun when the source pressure was $< 6 \times 10^{-7}$ Torr. An accelerating voltage of 3.8 kV was used and no memory or background signals were ever noted. The relatively low accelerating voltage is necessary because rubidium ions are very efficient producers of secondary electrons. Higher voltages would have defeated the secondary electron suppression components of the collector.

A very small amount of isotopic fractionation, on the order of 0.03 percent, was occasionally noted to occur during the data-taking period (10 min.) of an analysis, but generally the fractionation was not measurable over this small time period. However, preliminary tests showed that fractionation could be a very significant factor between analyses performed with different time, sample-size, and/or heating parameters. In view of this, each operator always performed his analyses in an identical manner; sample-size, heating pattern, and total rubidium ion signals were always kept within strict limits, and data were always taken during the same time interval.

Each analysis consisted of a set of 10 measurements, with base-line readings taken immediately before and after the data. The peak-top data were taken by stepwise changes in the magnet current and each peak-top was monitored for 30 s.

2.2. Purification of the Separated Isotopes

Electromagnetically separated ^{85}Rb and ^{87}Rb isotopes in the form of rubidium chloride were obtained from the Isotopes Division, Oak Ridge National Laboratory of the Union Carbide Nuclear Company. About 2.83 g each of ^{85}RbCl and ^{87}RbCl equivalent to about 2.0 g each of ^{85}Rb and ^{87}Rb were received. The ^{85}RbCl and the ^{87}RbCl were designated Series 144701 and Series 144801, respectively. The certificate of analysis accompanying each sample included a semiquantitative spectrographic analysis which indicated that zinc could be present at the 0.2 percent level and that several other elements could also be present up to the 0.05 percent level. To reduce these impurities to a level low enough so that they could not cause a significant error in the determination of the rubidium ion content in solutions of these isotopes, the separated isotope samples were further purified. The purification method used had been previously found by this laboratory to be effective in removing cationic and anionic impurities from rubidium chloride with the exception of potassium and cesium which co-crystallize with the rubidium.

Each separated isotope sample was treated as follows: The rubidium chloride (about 2.8 g) was dissolved in 50 cm^3 of water in a 100 cm^3 fused silica beaker and 5 cm^3 of "ultra-pure" grade perchloric acid were added. The precipitated rubidium perchlorate, $RbClO_4$, was dissolved by heating the solution almost to boiling and then slowly crystallized by allowing the solution to cool to room temperature. The solution was further cooled to about 5 °C, by placing it in a refrigerator overnight. The crystallized $RbClO_4$ was recovered from the solution by filtering it through a fine porosity polyethylene filter. After the $RbClO_4$ was washed with a cold 80 percent ethanol solution, it was returned to the fused silica beaker and the crystallization process was repeated except that only 2 cm^3 of perchloric acid were added. The recrystallized $RbClO_4$ was again caught on the polyethylene filter and washed with cold 80 percent ethanol. The purified material was dried by passing clean air over the $RbClO_4$ for several hours.

After being transferred to a covered quartz crucible, the recrystallized rubidium perchlorate was placed in an electric furnace and thermally converted to rubidium chloride. This was accomplished by slowly raising the temperature to 600 °C and, to ensure complete conversion, keeping it there for 4 hrs. The crucible was kept covered during this decomposition since a liquid phase eutectic is formed which sprays material on further decomposition. (To avoid isotopic contamination, the decompositions of the $^{85}RbClO_4$ and $^{87}RbClO_4$ were performed in new, separate furnaces which had not been exposed to rubidium salts.) The decomposition proceeds in the following manner [18].

$$RbClO_4 \xrightarrow{\Delta} RbClO_3 + 1/2\, O_2$$

$$RbClO_3 \rightarrow 3/4\, RbClO_4 + 1/4\, RbCl$$

until all of the $RbClO_4$ has been converted to RbCl.

Calculations based on the starting weight of the RbCl and the weight of the recovered RbCl showed that about 95 percent of the rubidium was recovered in each case.

Samples of the purified ^{85}RbCl and ^{87}RbCl were analyzed for potassium and cesium by flame emission spectrometry. The results of these analyses showed that the ^{85}RbCl and ^{87}RbCl contained 120 ± 5 ppm and 100 ± 5 ppm of potassium, respectively; cesium was found to be present at less than 10 ppm in both samples. The samples were also analyzed by spark source mass spectrometry. The results of this analysis showed that no other element was definitely detected at a level greater than 10 ppm.

The effectiveness of this purification procedure was first tested by the purification of natural rubidium chloride to which 0.1 percent each of twelve common cationic impurities had been added. Table 1 shows the results of the analysis of the purified RbCl. Only aluminum was detected at the 10 ppm level. This material was also shown to contain less than 2 ppm of chlorate ion by a test based on the reaction of chlorate with chloride in acid solution to produce chlorine which was detected with *o*-tolidine.

There was no apparent attack of the fused silica crucibles during these decompositions. No change in crucible weights was observed and silicon was not detected at a level greater than 10 ppm in either sample by spark source mass spectrometry. (Platinum

crucibles could not be used since they would be attacked by the decomposition products.)

TABLE 1. *Results of spectrochemical analysis of purified natural rubidium chloride*

Element	Initial concentration	Concentration after purification	Established limits of detection
	ppm	*ppm*	*ppm*
Al	1000	10	5
Ba	1000	.....	2
Ca	1000	.....	4
Co	1000	.....	3
Cu	1000	.....	2
Fe	1000	.....	4
Li	1000	.....	2
Mg	1000	.....	2
Na	1000	.....	20
Ni	1000	.....	4
Si	1000	.....	2
Zn	1000	.....	50

Note: (.....) not detected.

2.3. Preparation and Rubidium Concentrations of the Separated Isotope Solutions

Accurately weighted samples of the purified $^{85}RbCl$ and $^{87}RbCl$ were transferred to 200 cm^3 volumetric flasks whose necks had been cut off so that only about 1 cm remained. The separated isotope samples were dissolved in water and diluted to about 110 cm^3 after the additions of 1 cm^3 of (1+1) hydrochloric acid. After the solutions were thoroughly mixed by swirling the flasks for several minutes, each flask was sealed with a rubber serum septum and left overnight in a balance case to insure thermal equilibrium. The flasks and contents were weighed to ± 0.2 mg and preliminary rubidium concentrations were calculated. The solution of $^{85}RbCl$ was labeled "Rb 85" and the solution of $^{87}RbCl$ was labeled "Rb 87".

Four weighed portions were withdrawn from each separated isotope solution in the following manner. A 4 in platinum needle was inserted through the septum. A short second needle, which just punctured the septum served as a vent. A 10 cm^3 polyethylene hypodermic syringe was attached to the Kel-F hub of the Pt needle and the desired amount of solution was withdrawn. The syringe was then disconnected from the hub and the tip was capped with a polyethylene cap. Any static charge that might be present on the syringe was dissipated by wiping it with a damp paper towel, and the syringe and contents were weighed on a semimicro balance to ± 0.02 mg. The solution was then delivered from the syringe to a tared 15 cm^3 platinum crucible and the syringe was again capped, wiped, and weighed. The weight of the sample was determined from the weights of the syringe before and after delivery of the sample.

About 0.4 cm^3 of "ultra-pure" grade perchloric acid was added to each weighed portion and the solutions were evaporated to constant volume on a hot plate at about 85 °C. A few drops of water were added to each and the solutions were again evaporated to constant volume. The temperature was then raised to 110 °C and held there until fumes of $HClO_4$ were observed. Then the temperature was reduced to about 85 °C; 10 cm^3 of hot water were added to each solution and they were heated to near boiling until the $RbClO_4$ dissolved. The solutions were again evaporated to constant volume and heated to fumes of $HClO_4$ at 110 °C. This process of dissolving the $RbClO_4$ in water, evaporating, and heating to fumes of $HClO_4$ was repeated. The temperature of the hot plate was held at about 110 °C until all of the excess $HClO_4$ had been fumed off.

After fumes of perchloric acid were no longer noted, the samples were again dissolved, evaporated to dryness, and heated at 150 °C. This process was repeated two more times. (The first series of repeated evaporations frees the $RbClO_4$ from chloride. The second series frees the $RbClO_4$ from occluded perchloric acid.)

The crucibles were then covered with platinum covers and transferred to an electric furnace. The temperature of the furnace was slowly raised to 250 °C and the crucibles were kept at this temperature for 16 hr (overnight). Then the covers were removed and the crucibles were cooled and weighed. This procedure of heating, cooling, and weighing was repeated, except that the time of heating was reduced to 6 hr, until a constant weight was obtained, that is, until the weighings agreed to within 5 μg. For simplicity of calculations, the vacuum weight of the rubidium perchlorate was converted to milliequivalents (meq) of rubidium using the 1967 atomic weights for chlorine and oxygen and a calculated atomic weight for the separated rubidium isotope based on the ORNL isotopic analysis. The results of these determinations are shown in table 2.

TABLE 2. *Concentration of rubidium isotope solutions*

Solution	Sample number	Wt solution	Rubidium	Concentration of solution Rb/g soln
		g	*meq*	*meq*
"Rb 85"	1	8.69052	1.359758	0.156465
	2	8.92782	1.397106	.156489
	3	8.33577	1.304329	.156474
	4	8.94403	1.399395	.156461
			Average	.156472
			Corrected for K	[a] .156436
"Rb 87"	1	8.46749	1.409229	.166428
	2	8.25201	1.373551	.166450
	3	8.63473	1.437179	.166442
	4	8.88910	1.479380	.166426
			Average	.166437
			Corrected for K	[a] .166405

[a] The standard error of the average is estimated to be 0.0000085 meq/g soln and the uncertainty of the concentration at the 95 percent confidence level is 0.0000162 meq/g soln.

This method for the determination of the concentrations of the rubidium isotope solutions was adopted after it became apparent that none of the conventional methods for rubidium analysis were capable of yielding precise enough results. It is a valid method as long as the purity of the rubidium chloride is known. As stated previously, the only element detected at the 100 ppm level by spark source mass spectrometry and flame emission spectrometry was potassium. The potassium correction amounted to 0.000036 meq/g sol for the "Rb 85" solution assay and 0.000032 meq/g sol for the "Rb 87" solution assay.

The rubidium concentrations of the two solutions as determined by this method were in good agreement with the preliminary concentrations calculated from the starting weights of rubidium chloride and solution. The "Rb 85" solution was calculated to be 0.156464 meq/g sol and was found to be 0.156432 meq/g sol by this method. The "Rb 87" solution was calculated to be 0.166399 meq/g sol and was found to be 0.166405 meq/g sol.

This method for determining the concentration of rubidium solutions was tested on solutions containing known amounts of rubidium. Seven solutions were prepared from fused high-purity natural rubidium chloride and three solutions were prepared from thermally decomposed rubidium perchlorate (made from the same rubidium chloride). Analysis of this rubidium chloride showed that it contained less than 50 ppm of detected impurities. Four samples containing from 1.2 to 2.0 meq of rubidium were withdrawn from each solution and the rubidium ion concentrations were determined as described above. Analyses of the rubidium perchlorate resulting from the above assay have shown it to contain less than 0.001 percent chloride and less than 0.0002 percent chlorate. The chloride was determined by silver chloride turbidity and the test for chlorate was based on the reaction of chlorate with chloride in acid solution to produce chlorine which was detected with *o*-tolidine. Comparison of the calculated and measured concentration of the ten solutions showed that: (a) the concentration of rubidium ion as determined by this method agreed to within 0.01 percent of the calculated rubidium concentration, (b) systematic errors were negligible, and (c) the analyses of the ten solutions were of equal precision.

From these analyses and from the analyses of the separated isotope solutions, the standard deviation of an individual measurement of the concentration of a rubidium solution was computed to be 0.0000172 meq/g sol, with 36 degrees of freedom. The standard error of the average of four determinations is therefore 0.0000086 meq/g sol and the uncertainty of the concentration is 2.03×0.0000086 or 0.0000162 meq/g sol at the 95 percent confidence level. This corresponds to an uncertainty of 0.010 percent for solutions containing 0.16 meq Rb/g sol.

2.4 Isotopic Analyses of the Separated Isotope Solutions

The separated isotope solutions were analyzed four times each on each instrument. Sources were dismantled, cleaned and reassembled between the analyses of the two solutions, as a protection against the possibility of cross-contamination from the source parts. Except for the sake of complete security, the cleanings were not really necessary. Tests showed that the two separated isotope solutions could be analyzed back-to-back on the same source with no measurable "cross-talk."

The isotopic compositions of the separated isotopes are given in table 3. They have been corrected for mass spectrometric bias, with changes becoming negligible after three rounds of iteration. Instrumental uncertainties, such as recorder dead-zone and nonlinearity, make it highly improbable that any ratio can be measured to better than 0.00002. In view of this, the errors attached to the numbers in table 3 are based on errors of 0.00002 in the ratio determinations, even though the calculated 95 percent confidence limits of the ratio are well below this figure.

TABLE 3. *Isotopic composition of separated rubidium isotopes used in calibration samples*

Separated isotope		Isotopic composition (atom percent)
"Rb 85"	^{85}Rb	[a] 99.8398 ± 0.0020
	^{87}Rb	0.1602 ± 0.0020
"Rb 87"	^{85}Rb	0.8433 ± 0.0020
	^{87}Rb	99.1567 ± 0.0020

[a] The uncertainties are based on a minimum error or 0.00002 for the ratio determinations. The calculated 95 percent confidence limits are well below this value.

The isotopic compositions reported by ORNL are: "Rb 85", 99.85 ± 0.02 atom percent ^{85}Rb and 0.15 ± 0.02 atom percent ^{87}Rb; "Rb 87", 0.84 ± 0.02 atom percent ^{85}Rb and 99.16 ± 0.02 atom percent ^{87}Rb. The ORNL limits quoted express the precision of the measurements. From known sources of systematic errors, the absolute error is estimated by ORNL to be less than 1 percent.

2.5. Preparation of the Calibration Samples

Six calibration samples were prepared by mixing weighed portions of the "Rb 85" and "Rb 87" solutions to produce four ^{85}Rb/^{87}Rb ratios of about 2.6, approximately the natural ratio, and two ^{85}Rb/^{87}Rb ratios of about 1. The portions were withdrawn from the flasks and weighed in the manner previously described. To eliminate any possibility of change in concentration of the isotope solutions with time, the portions for the calibration samples were withdrawn from the flasks on the same day that the samples for determining the rubidium concentrations were withdrawn.

Table 4 shows the composition of these calibration samples. The isotopic ratio of each calibration sample

was calculated from the isotopic analyses of separated isotopes and the meq's of rubidium from each separated isotope solution.

Each calibration sample was thoroughly mixed by stirring and evaporated to dryness on a hot plate. The calibration samples were then taken up in water and diluted so that 1 cm^3 of solution contained 2 mg of rubidium. Portions of these solutions were further diluted so that final solutions contained 10 μg of Rb/cm^3. A second portion of each of the 2 mg/cm^3 calibration standards were diluted with 2 percent hydrochloric acid so that the final solutions contained 10 μg Rb/cm^3. The "neutral" calibration samples were used for one set of analyses and the "acid" calibration samples were used for the other set.

TABLE 4. *Composition of rubidium calibration samples*

Sample number	Isotope solution	Wt soln	Concentration of solution Rb/g soln	Rubidium	Isotopic ratio
	Rb	*g*	*meq*	*meq*	$^{85}Rb/^{87}Rb$
1	85	9.45359	0.156436	1.478882	2.59723
	87	3.44230	.166405	0.572816	
2	85	5.17690	.156436	.809854	1.02142
	87	4.82990	.166405	.803720	
3	85	9.66166	.156436	1.511431	2.63381
	87	3.46884	.166405	0.577232	
4	85	8.54773	.156436	1.337173	2.55500
	87	3.16429	.166405	0.526554	
5	85	4.63494	.156436	.725071	1.01470
	87	4.35317	.166405	.724389	
6	85	9.44640	.156436	1.477757	2.62705
	87	3.40035	.166405	0.565835	

2.6. Preparation of Standard Sample

The standard material used for this work was NBS Standard Reference Material 727, Rubidium Chloride. Solutions of this material were prepared by taking a weighed portion into solution with water and diluting so that 1 cm^3 contained 2 mg of rubidium. One standard solution was prepared by diluting a portion of this solution so that the final concentration was 10 μg Rb/g sol. This standard was used with the "neutral" calibration samples. A second standard solution was prepared by diluting a portion of the 2 mg/cm^3 standard to 10 $\mu g/cm^3$ with 2 percent hydrochloric acid. This standard was used with the "acid" calibration samples.

2.7. Isotopic Analyses of the Calibration Mixes and the Standard Sample

Two complete sets of analyses of the calibration mixes and standard sample were made, one by operator I using instrument #4 and "acid" sample solutions and one by operator II using instrument #5 and "neutral" sample solutions. Each set consisted of 24 analyses of the standard sample made in a simple alternating pattern with four analyses each of the six calibration mixes.

3. Results and Discussion

The results for the six calibration mixes are summarized in table 5. There are no statistically significant differences between any of the values. The slight differences between the 1 : 1 and 2.6 : 1 samples are not significant.

TABLE 5. *Determination of mass spectrometer bias*

Calibration sample No.	Isotopic ratio $^{85}Rb/^{87}Rb$			Correction factor	
	Calculated	Operator I	Operator II	Operator I	Operator II
1	2.59723	2.61022	2.61369	0.995024	0.993704
2	1.02142	1.02638	1.02702	.995172	.994545
3	2.63381	2.64762	2.65195	.994785	.993161
4	2.55500	2.56754	2.57025	.995115	.994066
5	1.01470	1.01948	1.02043	.995312	.994388
6	2.62705	2.64039	2.64445	.994948	.993421
Mean values of correction factors.....				0.995059	0.993881

356-078 O-69—5

The results given in table 6 include the observed and corrected experimental $^{85}Rb/^{87}Rb$ values for the standard sample as well as the final absolute value for this ratio, with uncertainty components.

The calculation of the atomic weight of rubidium is summarized in table 7. Shields et al. [11], detected no variations in the isotopic composition of samples of rubidium from various localities and origins, so the atomic weight of rubidium should be constant within the stated experimental limits. The half-life of ^{87}Rb is sufficiently large so that the decay of this isotope is of no immediate consequence with respect to changes in the absolute ratio and atomic weight of this element with time.

TABLE 6. *Observed and corrected $^{85}Rb/^{87}Rb$ values for the standard sample*

Observed ratios		Correction factor	Corrected ratios
Operator I.....	2.60586	0.995059	2.59298
Operator II.....	2.60827	.993881	2.59231
Mean.....			2.59265 ± 0.00170
Uncertainty components:			
95% confidence limits on ratio determinations.....			± 0.00107
Bounds due to possible systematic error in composition of separated isotopes.....			± 0.00024
Bounds due to possible systematic error in chemical analyses.....			± 0.00039

TABLE 7. *Summary calculations of the atomic weight of rubidium*

Value	Overall limit of error [a]	Uncertainty components		
		Mass spectrometric analytical error	Possible systematic error in composition of separated isotopes	Possible systematic error in chemical analysis
Atomic weight = 85.46776.....	± 0.00026	± 0.00016	± 0.00005	± 0.00005
Nuclidic masses [19] ($^{12}C = 12$)				
$^{85}Rb = 84.911800$.....	± 0.000005			
$^{87}Rb = 86.909186$.....	± 0.000003			
Atomic percent				
$^{85}Rb = 72.1654$.....	± 0.0132	± 0.0082	± 0.0020	± 0.0030
$^{87}Rb = 27.8346$.....	± 0.0132	± 0.0082	± 0.0020	± 0.0030
Isotopic ratios [b]				
$^{85}Rb/^{87}Rb = 2.59265$.....	± 0.00170	± 0.00107	± 0.00024	± 0.00039

[a] The overall limit of error is the sum of the 95 percent confidence limits for the ratio determinations and the terms covering effects of known sources of possible systematic error.
[b] From table 3.

The authors are indebted to Hsien H. Ku for the statistical analysis of the experimental data, to Mrs. Martha Darr for the spectrographic analyses of the purified natural rubidium chloride, to Paul J. Paulsen, Jr. for the spark source mass spectrographic analyses of the separated rubidium isotopes and to Theodore C. Rains for the flame emission spectrographic analyses of the separated isotopes.

4. References

[1] Shields, W. R., Garner, E.L., and Dibeler, V. H., J. Res. NBS **66A**, (Phys. and Chem.), No. 1, 1 (1962).
[2] Shields, W. R., Murphy, T. J., Garner, E. L., and Dibeler, V. H., J. Am. Chem. Soc. **84**, 1519 (1962).
[3] Shields, W. R., Murphy, T. J., and Garner, E. L., J. Res. NBS **68A** (Phys. and Chem.), No. 6, 589 (1964).
[4] Catanzaro, E. J., Murphy, T. J., Garner E. L., and Shields, W. R., J. Res. NBS **68A** (Phys. and Chem.), No. 6, 593 (1964).
[5] Shields, W. R., Murphy, T. J., Catanzaro, E. J., and Garner, E. L., J. Res. NBS **70A** (Phys. and Chem.), No. 2, 193 (1966).
[6] Catanzaro, E. J., Murphy, T. J., Garner, E. L., and Shields, W. R., J. Res. NBS **70A** (Phys. and Chem.), No. 6, 453 (1966).
[7] Catanzaro, E. J., Murphy, T. J., Shields, W. R., and Garner, E. L., J. Res. NBS **72A** (Phys. and Chem.), No. 3, 261 (1968).
[8] Catanzaro, E. J., Champion, C. E., Garner, E. L., Marinenko, G., Sappenfield, K. M., and Shields, W. R., Nat. Bur. Stand. (U.S.), Spec. Publ. 260–17 (1969) in preparation.
[9] Flynn, K. F., and Glendenin, L. E., Phys. Rev. **116**, 744 (1959).
[10] Aldrich, L. T., Wetherill, G. W., Tilton, G. R., and Davis, G. L., Phys. Rev. **103**, 1045 (1956).
[11] Shields, W. R., Garner, E. L., Hedge, C. E., and Goldich, S. S., J. Geophys. Res. **68**, No. 8, 2331 (1963).
[12] Brewer, A. K., J. Am. Chem. Soc. **60**, 691 (1938).
[13] Paul, W., Z. Physik **124**, 244 (1948).
[14] Nier, A. O., Phys. Rev. **79**, 450 (1950).
[15] Herzog, L. F., Aldrich, L. T., Holyk, W. K., Whiting, F. B., and Ahrens, L. H., Trans. Amer. Geophys. Union **34**, 461 (1953).
[16] Packenkov, G. M., Akishin, P. A., Vasilev, N. N., Nikitin, O. T., and Moiseev, S. D., Zhur. Fiz. Khim. **30**, 1380 (1956).
[17] Shields, W. R., editor, NBS Tech. Note 426 (1967).
[18] Markowitz, M. M., and Boryta, D. A., J. Phy. Chem., **69**, 1114 (1965).
[19] Mattauch, J. H. E., Thiele, W., and Wapstra, A. H., Nuclear Physics **67**, 1 (1965).

(Paper 73A5–569)

Fundamental Aspects of Dislocation Theory
A Conference Report with Abstracts

John A. Simmons and Roland deWit

Metallurgy Division, Institute for Materials Research
National Bureau of Standards, Washington, D.C. 20234

and

R. Bullough

Theoretical Physics Division, A.E.R.E.
Harwell, Didcot, Berkshire, England

1. Conference Report

The conference on "Fundamental Aspects of Dislocation Theory" was held under the auspices of the Institute for Materials Research at the Gaithersburg Laboratories of the National Bureau of Standards on April 21-25, 1969.

The purpose of the Conference was to bring together workers active in all fundamental aspects of the theory of dislocations to discuss, evaluate, and contribute to the current state of understanding of these defects in crystalline materials.

The dislocation has been a subject of theoretical study for some 60 years, starting with the investigations reported by Volterra. In the last 20 years there has been a steady increase in sophistication of dislocation theory from the early almost intuitive models to current theories, which range over a large portion of continuum mechanics and solid state physics—from the non-Riemannian geometry of the continuum to anharmonic calculations of atomic configurations and phonon scattering.

A sustained interest in dislocations has existed on account of their anticipated applications, particularly to mechanical properties of materials, but the study of dislocations has received an added impetus over the last 15 years by better correlations with experimental observations made possible by advances in such fields as electron microscopy and crystal growth. With this increase in experimental work recent conferences have been predominantly devoted to experimental results. We felt, therefore, that this was a suitable time for a conference whose scope was limited enough to allow some in-depth treatment of various theoretical developments in the study of dislocations.

A small closed conference of about sixty people was decided upon to insure a high degree of informality and interaction. However, towards the end of our preparations the general interest had exceeded our expectations, so that a little over one hundred participants with forty percent drawn from eighteen different foreign countries finally took part; this produced a gathering of truly international character.

The conference was organized into ten sessions with over seventy contributed papers; the abstracts of the papers are listed alphabetically following this report below. Each chairman organized the papers in his session according to his own views. Two panels punctuated the sessions; these provided some perspective on current opinion of dislocation theory and its relevance to practical problems by aiming at such questions as: "How far have we come?" and "Where do we go from here?" The explicit agenda was as follows:

1) Discrete Dislocations in Continuum Elasticity
   Chairmen: J. D. Eshelby and R. deWit
2) Lattice Theories
   Chairman: R. Bullough
3) Dislocation-Phonon Interactions
   Chairman: J. Lothe
4) Applications of the Geometry of Dislocations
   Chairman: F. R. N. Nabarro
5) Panel on Intrinsic Properties of Dislocations
   Chairman: J. P. Hirth
6) Field Theories, Part I
   Chairman: E. Kröner
7) Field Theories, Part II
   Chairman: J. A. Simmons
8) Thermally Activated Processes and Statistical Theories
   Chairman: A. Seeger
9) Dislocation-Electron Interactions
   Chairman: R. Thomson
10) Panel on Future Directions for Dislocation Theory
    Chairman: A. Seeger

1.1 Discrete Dislocations in Continuum Elasticity

A. K. Head: Discrete Dislocations in Continuum Elasticity

J. Lothe: The Image Force on Dislocations at Free Surfaces. Comments on the Concept of Line Tension

K. Malén: Stability and Some Characteristics of Uniformly Moving Dislocations

G. P. Senkeckyj: Screw Dislocations in Inhomogeneous Solids

D. J. Bacon and P. P. Groves: The Dislocation in a Semi-Infinite Isotropic Medium

D. Kuhlmann-Wilsdorf and R. F. Duncan: Theoretical Considerations on the Extension of 1/2 ⟨110⟩ {111} Dislocations in Isotropic FCC Metals into Shockley Partials

J. Weertman, H. M. Berg, J. E. Bloom, H. Ishii, R. H. Marion, D. E. Pease, D. T. Spreng and J. B. Vander Sande: Subsonic, Supersonic, and Transonic Dislocations Moving on an Interface Separating Two Media of Differing Elastic Properties

J. A. Simmons and R. Bullough: Internal Stress and the Incompatibility Problem in Infinite Anisotropic Elasticity

D. M. Barnett: Series Representations of the Elastic Green's Tensor for Cubic Media

N. Louat: Some Problems Involving Linear Dislocation Arrays

J. C. M. Li: Some Recent Results on Dislocation Pileups

E. Smith: The Behavior of an Elastic Solid Containing Distributions of Free and Fixed Dislocations

M. O. Tucker: The Elastic Interaction Between Grain Boundaries and Screw Dislocation Pile-ups

The session dealt with current research in what may be called "classical dislocation theory," i.e. the theory formulated about 15 years ago in terms of linear elasticity. Two main points stood out: The concept of the force on a straight but finite dislocation segment, and the advantage of using the elastic Green's tensor. The force concept was used by one conferee to derive a surprisingly simple expression for the image force on a dislocation emerging at a free surface, and by another to find a stability criterion for a moving dislocation in an anisotropic medium. The power of the Green's tensor in three dimensions for anisotropic bodies was shown in the context of the general internal stress problem, and a related decomposition theorem (somewhat analogous to Helmholtz' theorem) was presented using projection operators. Then a convenient series representation in terms of the anisotropy factor of the Green's tensor for cubic media was given. This session was so crowded that several interesting papers could not be presented orally, but only discussed from the floor.

1.2 Lattice Theories

N. W. Ashcroft: One Electron Theories of Cohesion on Ion-Pair Potentials in Metals

A. A. Maradudin: Localized Vibration Modes Associated with Screw Dislocations

J. W. Flocken and J. R. Hardy: The Method of Lattice Statics

H. Suzuki: Effect of Zero-Point Motion on Peierls Stress

A. Englert, H. Tompa and R. Bullough: Point Defects and Dislocations in Copper

M. Doyama and R. M. J. Cotterill: Atomistic Calculation of Dislocation in Solid Krypton

A. Hölzler and R. Siems: A Lattice Theory Model for Peierls-Energy Calculations

R. Chang: The Interaction Between a Screw Dislocation and Carbon in Body-Centered Cubic Iron According to an Atomic Model

P. C. Gehlen, G. T. Hahn and A. R. Rosenfeld: The Structure of the ⟨111⟩ Screw Dislocation in Iron

Many of the mechanical and physical properties of dislocations can only be fully understood when we have knowledge of their core structure and energy. To obtain such information demands *a priori* knowledge of the cohesive energy of the crystal lattice, particularly when the atom configuration is far from that of the perfect crystal. In addition the complex topology of the dislocation means that reasonable calculations are only possible if the cohesive energy can be represented in a simple spatial form, such as an analytic pair potential or a simple force constant model.

The session was opened with a survey of the electron theories of cohesion in metals which was a critique of the physical validity of the use of ion-pair potentials in metals. The force constant models were then discussed both in the dynamic situation of phonon scattering (flutter) and in the static situation for the harmonic static configurations—although the latter work was confined to more elementary point defects. Subsequent discussion suggested that the early calculations of

Maradudin on the simple screw dislocation could now be usefully extended to a lattice statics study of the edge dislocation. The problems involved in calculating the Peierls stress and the effects of zero point energy were discussed in relation to the various pair potential models and the session was concluded by a series of research contributions on dislocations in copper, krypton and iron. It was clear that with the rapid developments in computer speed and capacity very ambitious lattice calculations are possible; however it was felt that emphasis should be placed upon the construction of physically valid interatomic potentials and not upon ambitious relaxation procedures.

1.3 Dislocation – Phonon Interactions

T. Ninomiya: Eigenfrequencies in a Dislocated Crystal
P. Gruner: Phonon Scattering by Dislocations and its Influence on the Lattice Thermal Conductivity and on the Dislocation Mobility at Low Temperatures
P. G. Klemens: Phonon Scattering by Cottrell Atmospheres
A. Seeger and H. Engelke: Dragging Forces on Moving Defects by Strain Field Phonon Scattering
J. H. Weiner: Thermal Energy Trapping by Moving Dislocations
J. A. Garber and A. V. Granato: Dislocation Resonance
R. O. Schwenker and A. V. Granato: Dislocation Radiation
C. Elbaum and A. Hikata: The Anharmonic Properties of Vibrating Dislocations
W. P. Mason: A Source of Dissipation that Produces an Internal Friction Independent of the Frequency

This busy session dealt not only with conventional dislocation-phonon interactions but also took up the topic of dislocation drag. It was divided into four subsections, the first two of which treated conventional phonon scattering theories of fluttering and anharmonic scattering.

Dislocation fluttering, which occurs even in a harmonic theory, is produced by the effective inertia of a dislocation which causes impinging phonons to be scattered with a subsequent fluttering of the dislocation line. A review of the perturbations of the eigenfrequencies of a dislocated continuum was presented in this subsession and was related to fluttering for special dislocation configurations.

The second subsession, which was devoted to anharmonic scattering, contained two contributions. A review of scattering in the continuum was given with non-linear elastic effects taken into account. Particular attention was paid to the influence of dislocation configurations and boundary effects on the phonon contribution to thermal conductivity. The second presentation was concerned with the anharmonic effects of Cottrell atmospheres on thermal conductivity particularly after plastic deformation when thermal resistivity can be expected to change as the atmospheres reform by diffusion.

The third subsession turned to the topic of dissipative drag on moving dislocations. Under this title are included such mechanisms as drag by kinks, impurities, or Peierls forces and accoustic radiation from rapidly moving dislocations. Though these topics are not strictly dislocation-phonon interaction processes, the similarity of techniques made the contributions particularly appropriate here. This subsession essentially extended into the fourth subsession which was devoted primarily to the different vibrating string models of dislocations, their experimental applications, and their correlations with dislocation drag.

1.4 Applications of the Geometry of Dislocations

W. Bollman: The Meaning of Dislocations in Crystalline Interfaces
M. H. Yoo and B. T. M. Loh: Structural and Elastic Properties of Zonal Twin Dislocations in Anisotropic Crystals
S. Mendelson: Non-Planar Dissociations of Dislocations
M. J. Marcinkowski: Propagation of Glide Through Internal Boundaries
R. Thomson: Kinks, Vacancies, and Screw Dislocations
W. F. Harris: Topological Restriction on the Distribution of Defects in Surface Crystals and Possible Biophysical Applications
F. R. N. Nabarro: Disclinations in Surfaces
M. Kléman: Aspects in Liquid Crystals Relevant to the Theory of Dislocations
K. H. Anthony: Non-Metric Connexions, Quasidislocations and Quasidisclinations. A Contribution to the Theory of Non-Mechanical Stresses in Crystals
R. deWit: Linear Theory of Static Disclinations

Under this heading there appeared mainly two topics: interfaces and disclinations. The session started with a presentation of dislocations in crystalline interfaces. A generalized development of coincidence sites involving two arbitrary interpenetrating lattices was given using what amounts to the idea of modular arithmetic in each of the lattices. Generalized dislocations in interfaces were described in this context and then further extended to include the concept of secon-

dary dislocations or "super-dislocations" with fractional Burger's vectors which occur in small atomic repeat patterns produced by lattice mismatches at interfaces; such patterns were beautifully illustrated by the use of Moiré patterns. It was then shown that such purely geometrical descriptions of interface dislocations can often be used to calculate relative boundary orientations of two phase mineral systems by employing a geometric measure which ought to vary monotonically with the grain boundary energy. It was suggested in subsequent discussion that such an approach might be applied to predict martensitic habit planes for which there is currently only a strictly phenomenological theory.

Disclinations, which have been under study in isolated localities for some 10 years, were presented in their multifarious forms: in liquid crystals; on surface crystals—with possible biophysical applications—and in ordinary crystals, where their existence is subject to doubt. The discussion of these drastic defects certainly exposed their probable importance in systems of low cohesive energy.

1.5 Intrinsic Properties of Dislocations

Panel Members: J. P. Hirth, R. Bullough, R. deWit, C. Elbaum, J. D. Eshelby, P. Haasen, P. B. Hirsch

The agenda of this panel was as follows:

1) CORE STRUCTURES IN METALS: e.g. Peierls Forces, Atomic Calculations, Nonlinear Elasticity, Adsorption, Faults (bcc), Anisotropic Elasticity.
2) DISLOCATION DRAG MECHANISMS: e.g. Damping, Inertial Effects, Electron Interactions, Thermoelastic, Magnetic (domain wall).
3) CORE STRUCTURE IN COVALENT AND POLAR MATERIALS: e.g. Jogs, Kinks, Diffusion, Interaction with Conduction Electrons and Holes, Interaction with Ionic Defects.
4) EQUILIBRIUM CONFIGURATIONS: e.g. Disclinations, Dipoles, Junctions, Super and Unit Jogs, Grain Boundaries and Interfaces, Nodes, Fault Tetrahedra.
5) CRITICAL CONFIGURATIONS: Cross-slip, Intersection, Bow-out, Peierls, Quasi-Peierls (bcc).

The difficult task of assessing the current status of dislocation theory was undertaken by the panel with skill and enthusiasm.

The physical significance and problems associated with dislocation core studies were reviewed and particular attention was drawn to the dangers of using inadequate ion-ion potentials. It was suggested that meaningful calculations could now be made on aluminum—these would be particularly opportune in view of the recent electron microscope observations of core configurations in this metal. The problem of ensuring complete stability for the body centered cubic lattice with its many possible fault planes was emphasized and a new "third neighbor" potential for iron was presented and discussed. In view of our rather better knowledge of the interatomic potentials for the ionic solids it was suggested that more effort could usefully be put into core calculations in these materials.

The various dislocation drag processes were reviewed and it was concluded that only one—the thermo-elastic damping process—could safely be ignored. It was emphasized that the study of these drag phenomena necessitates a knowledge of both fundamental solid state physics and dislocation theory—a rare combination in one person. The only real hope appears to be for more relevant collaborative studies. The damping due to electron scattering was discussed at length and the theoretical issues distinguishing the two schools of thought on the subject were clearly delineated. Unfortunately the experimental correlation will not be completely clear until someone manages to perform low temperature ultra-sonic attenuation measurements in body centered cubic metals.

The relevance of disclinations to dislocation theory was also assessed. The consensus seemed to be that they were of much more philosophical than practical interest; their energy would be too high in a real crystal. However, in pseudocrystals, such as that made by flux lines, in liquids, two-dimensional crystals, or thin foils, they might play an important role. The evolution of the name "disclination" was revealed by Professor Nabarro: "Well, I think this is just a typical piece of bogus history, but as I remember, F. C. Frank's account of it is that he used the word "disinclination." He then wondered if this was the wisest word, and consulted the Professor of English at the University of Bristol, whose name is forgotten, and he said he was disinclined to use that word." As a companion to the "wedge" disclination, the name "twist" disclination was proposed, in analogy with the well-established names screw and edge dislocation. Discussions followed on whether it would be worthwhile to find the stacking fault energy from anisotropic calculations of the self energy of stacking fault tetrahedra and on whether lattice statics

calculations could provide continuum theory with a better dislocation core cut-off parameter, but no satisfactory answers were given.

At this point the allotted time had been exhausted and the last point of the agenda was skipped.

1.6 Field Theories: Part I

E. Kröner: The Problem on Non-Locality in the Mechanics of Solids: Review on Present Status

E. Kröner and B. K. Datta: Non-Local Theory of Elasticity for a Finite Inhomogeneous Medium—A Derivation from Lattice Theory

I. A. Kunin and A. M. Waisman: On Problems of the Non-Local Theory of Elasticity

K. Kondo: A Non-Riemannian Construction of Variational Criteria for Plastic Manifolds with Special Reference to the Theory of Yielding

M. Mişicu: Derivation of a Continuum Theory of Dislocations on the Basis of an Estimative Analysis of Crystal Lattices

R. Stojanović: The Elastic Generalized Cosserat Continuum with Incompatible Strains

D. M. Barnett: A Note on Admissible Solutions in Non-Local Elasticity

C. Teodosiu: A Dynamic Theory of Dislocations and its Applications to the Theory of the Elastic-Plastic Continuum

C. Teodosiu and A. Seeger: Non-Linear Dynamic Problems for Anisotropic Elastic Bodies in the Continuum Theory of Dislocations

C.-C. Wang: On the Thermodynamics of Inhomogeneous Bodies

C. S. Hartley and M. A. Eisenberg: Elastic-Plastic Plane Bending of a Single Crystal

S. I. Ben-Abraham: Generalized Stress and Non-Riemannian Geometry

The shortcomings of the characterization of dislocations and more complex defects in crystal lattices by means of classical linear elasticity are now accepted. Most of the papers in the first session on field theories were devoted to a re-examination of the transition from a model of an imperfect crystal lattice to a continuum theory encompassing more detailed and sophisticated defect descriptions than are contained in the classical approach.

Long range atomic interactions and lattice dispersion were discussed in the context of non-local continuum theory. In addition, the pitfalls in formulating non-local continuum theory were clearly brought out. These difficulties arise from boundary effects in real finite bodies and the apparent non-existence of Green's functions in linear non-local theory when the Euler-McLauren approach is taken. A possible method for avoiding this latter difficulty by using a formulation based on truncated Fourier transforms was also presented.

The first session concluded with an attempt to combine the techniques of continuously distributed dislocation with those of engineering plasticity to a model of simple glide in a single crystal.

1.7 Field Theories: Part II

T. Mura: The Elastic Field of Moving Dislocations and Disclinations

S. I. Ben-Abraham: Kinematics of Continuously Distributed Dislocations

J. A. Simmons: A Geometric Foundation for the Kinematics of the Imperfect Continuum

A. C. Eringen and W. D. Claus, Jr.: A Micromorphic Approach to Dislocation Theory and its Relation to Several Existing Theories

N. Fox: On the Continuum Theory of Dislocations

The second session was opened by two survey papers on dynamical field theories of dislocations. Dynamic theories are currently in an earlier stage of development than the corresponding theories of static character. Until recently, in fact, research has been separated into general kinematic theories of a geometrical nature and linear elastic field theories and the survey papers presented were devoted to each of these two topics.

New research trends are now appearing, particularly under the impetus of continuum mechanists who are being attracted to dislocation theory. Individual papers of this type were presented in both sessions on such topics as the application of micromorphic mechanics and oriented continua to developing a thermodynamics of the deforming dislocation continuum and on the non-linear elastodynamics of dislocations. Discussion on these topics included an interesting comparison of the oriented continuum approach with the micromorphic approach. The former emphasizes separation of the incompatible lattice distortions from the motion of the points of the continuum at which they are defined, while the latter attempts to treat the continuum as a conglomeration of small elements with microstructure by introducing incompatible deformations into each of these small elements.

1.8 Thermally Activated Processes and Statistical Theories

W. Frank: Dislocation Dynamics in the presence of a Multiple Spectrum of Thermally Surmountable Barriers

U. F. Kocks: Flow and the Arrhenius Equation in the Statistical Framework

A. J. E. Foreman, P. B. Hirsch and F. J. Humphreys: Movement of a Dislocation Through Random Arrays of Point and Parallel Line Obstacles

W. deRosset and A. V. Granato: Strain Rates in Dislocation Dynamics

M. S. Duesberry and P. B. Hirsch: On the Mechanism of Cross-Slip of Dislocations at Particles

H. Engelke: Theories of Thermally Activated Processes and Their Application to Dislocation Motions in Crystals

A. M. Stoneham: The Broadening of Resonance Lines by Dislocations

R. O. Scattergood and U. F. Kocks: Dislocation Pair Interaction in a Finite Body

M. Wilkens: Theoretical Aspects of Kinematical X-Ray Diffraction Profiles from Crystals Containing Dislocation Distributions

J. Holder and A. V. Granato: Thermodynamic Properties of Solids Containing Dislocations

The topics covered by this session included individually thermally activated processes involving dislocations, the statistics of thermal activation, and the statistical properties of static distributions of dislocations. The session was begun by an extensive exposition of the problem of analyzing the effective activation energy for dislocation motion in the presence of a statistical distribution of individual barriers of varying activation and back stress characteristics. Comparison was made between this theory and various other theories describing dispersion hardening, which have generally had the defect of being imprecise or essentially athermal. Following two talks on thermally activated processes, the broadening of resonance lines due to the strain arising from random distributions of static dislocations was discussed. This latter work suggests a possible new experimental technique for probing the dislocation distributions in crystals; it also may provide information on "atmosphere formation" if the resonance centers are themselves mobile and migrate to the dislocations.

1.9 Dislocations—Electron Interactions

P. Haasen and W. Schröter: Charged Dislocations in the Diamond Structure

C. Nourtier and G. Saada: Electronic Effects Associated with Stacking Faults in Normal Metals

R. Thomson: Theory of Surface States on Stacking Faults

C. Elbaum and Hikata: Interactions of Dislocation with Electrons in Metals

C. Elbaum and R. R. Holmes: Electronic Energy States of Dislocations; The Case of Covalent-Ionic Solids

G. P. Huffman and N. Louat: Interactions Between Electrons and Moving Dislocations

The electronic properties of dislocations in semi-conductors have received considerable theoretical attention. The various models were initially discussed and it was clear that the old dangling bond description—at the edge of the extra half plane in the core of an edge dislocation in the diamond structure—provides an inadequate model to explain the recent experimental observations on such deformed materials.

Two contributions on the topical and somewhat controversial subject of electron scattering by dislocation were presented. These treatments contrasted in both approach and results. The one approach using a Boltzmann formalism predicts the dislocation drag to be inversely proportional to the electrical resistivity and therefore to be temperature dependent—although the splitting of dislocations in fcc materials implies a small temperature dependence in that case. The alternate approach involves treating the distortion field of a moving dislocation as a phonon distribution and calculating the associated electron-phonon interactions. This approach produces a drag independent of temperature for any crystal structures. Ultrasonic attenuation experiments at low temperatures have confirmed temperature independence of dislocation drag in fcc materials, but more precise attenuation experiments are required in bcc materials to produce an experimental comparison of the above two approaches.

The session concluded on the optimistic note that perhaps the time is ripe for at last attempting a rigorous quantum mechanical calculation for the electronic states around a dislocation using such techniques as those recently exploited by Calloway for point defects

1.10 Future Directions for Dislocation Theory

Panel Members: A. Seeger, N. W. Ashcroft, A. C. Eringen, E. Kröner, J. Lothe, A. A. Maradudin, J. A. Simmons

Questions submitted to the panel were:

1) What more can be done with classical continuum dislocation theory?
   a) static *vs* dynamic formalisms
   b) discrete *vs* continuous distributions
   c) linear *vs* non-linear theories
2) What are the prospects for fruitful interaction between the ideas of dislocation theory and modern continuum mechanics?
3) What is the future for lattice calculations?
   a) static theories
   b) dynamic theories
4) Are there experimental techniques which can be employed to measure such microscopic phenomena as couple-stresses, non-local effects, disclinations, and incompatibilities, . . . perhaps high resolution microscopy, . . .?
5) Can we extend old analogies or uncover new analogies between dislocation theory and other field theories, particularly electromagnetism, hydro-dynamics, general relativity, quantum mechanics. . . ?
6) What are the prospects for our further understanding of thermally activated processes?
7) What quantum effects are likely to be important in dislocation theory? Conversely, what is the hope of doing more meaningful quantum calculations in dislocation theory?
8) Given an interatomic description, what is the best continuum approximation to it? For instance: If a long-range two body potential suffices in the atomic system what is the appropriate continuum formalism? Or how may many body interactions be incorporated into a continuum framework?
9) What are the prospects of producing a macroscopic plasticity theory based on meaningful microscopic parameters? How soon will we be able to contribute to technologically important subjects such as fatigue, fracture, etc.?

The final session of the Conference was devoted to what the Chairman called "futurology."

In dealing with the future of classical continuum dislocation theory the need for more detailed descriptions of dislocation arrangments was strongly brought out. One approach suggested incorporating some of the ideas of statistical mechanics such as higher order correlation functions for the dislocation distribution and/or thermal vibrations, e.g. by means of phonon representations. The advantage of linear (local or non-local) theories over non-linear theories was pointed out—since superposition allows one to use averaged quantities. Also, the power of Green's function techniques were discussed as well as the need for practical calculations of the anisotropic elastic Green's tensors. The importance of the Indenbom-Orlov approach of reducing three-dimensional elasticity problems to two dimensions was questioned and there was the feeling that attempts should be made to use this method. In contrast the defense was made for the use of non-linear continuum theory to treat physical problems where superposition is violated—such as phonon scattering. In addition it was pointed out that higher order elastic constants are being measured experimentally and that it would be worthwhile using them. (One somewhat different application suggested for higher order elastic constants was to get information on pair-forces in metals.)

When the panel turned to question two there was a query from the floor concerning the physical meaningfulness of the "rather tremendous" amount of work going into the continuum theory. One "continuumist" responded with: "There are so-called 'real' theories and 'unreal' theories. Then there are 'really unreal' theories and 'unreal real' theories. Now, continuum theory is the 'really unreal' theory; sometimes it is called 'phenomenological' in order to give an even more deprecative name to it." However, it was agreed that great possibility exists for fruitful interaction between dislocation physics and continuum mechanics. There is a need to directly develop continuum theories which are internally consistent; these theories, which put restrictions on the form of the possible constitutive laws, will aid physicists in finding generalizations from microscopic to macroscopic phenomena. On the other hand it was felt that more dislocation physics should also be incorporated into the already existing theory of plasticity, so that the engineer would have available a better arsenal of practical theory as well as the know-how to make better materials. For instance, it was noted that a real crystal with a static dislocation distribution is very far from thermodynamic equilbrium so that correct thermodynamic approaches are dif-

ficult. Thus it was concluded that simultaneous development of both approaches was desirable.

Next was the question: What is the future for lattice calculations? This was quickly answered by one panel member: "The future is bright..." The major obstacles to overcome in computerized static lattice calculations are the choice of appropriate boundary conditions and a suitable interatomic potential. Calculations of the change in free energy due to dislocations (for determining Peierl's energy, for instance) and calculation of dislocation-phonon interactions were suggested as feasible research projects.

With regard to experimental techniques for measuring microscopic effects the panel concentrated on the non-local ones. These effects are likely to be important in piezo-electric and ionic crystals; furthermore it was suggested that information about the Fourier transforms of the elastic constants might be obtainable from neutron spectroscopy or from measurements of circularly polarized sound waves in acoustically active crystals.

Finally, turning to question eight, the panel noted that many calculations—such as phonon dispersion—can be carried out in reciprocal space without ever assuming a two-body potential. In fact, it was agreed that even though a two-body potential supplemented by a necessary volume dependent term was useful in many computer calculations, there is no reason for not expecting many-body interactions to be necessary in certain materials, such as some polyvalent metals.

As with the first panel, lack of time necessitated skipping over some questions—in this case questions five, six, seven and nine. It was agreed that question nine was of great technological importance. The session adjourned on the note that "futurology" was by no means exhausted in the two allotted hours.

2. Conclusion

This Conference ended with the expressed hope that it would be followed by another such meeting in about three years. Professors Elbaum, Haasen, and Hartley volunteered to pursue this project.

The written proceedings, "Fundamental Aspects of Dislocation Theory," including the contributed papers, discussions, and panels, will be published as NBS Special Publication 317. This Special Publication should appear in the spring of 1970 and will be available from the Superintendent of Documents, Government Printing Office, Washington, D.C. 20402.

Abstracts

Nonmetric Connexions, Quasidislocations and Quasidisclinations. A Contribution to the Theory of Nonmechanical Stresses in Crystals.

K.-H. Anthony

Institut für Theoretische und Angewandte Physik der Universität, Stuttgart, Germany

Nonmechanical stresses produced for instance by a temperature gradient or by an internal magnetic field are related to an affine lattice connexion, which is nonmetric with respect to the elastic metric. The covariant derivative of the elastic metric with respect to the lattice connexion is regarded as source-function for this kind of internal stresses. It may easily be determined from experimental data. The calculation of mechanical stresses is based on this quantity.

Instead of describing nonmechanical stresses by a nonmetric lattice connexion we alternatively may use an elastic connexion which is metric with respect to the elastic metric. Into the elastic connexion there are involved the tensors of quasiplastic torsion and of quasidisclination-density, which are regarded as source functions of nonmechanical stresses. Both tensors are connected intimately. They are a natural generalization of the quasidislocation tensor in the linear theory of nonmechanical stresses.

From the theory of quasidisclinations we obtain the following statement: In general, nonmechanical stresses cannot be eliminated solely by a dislocation movement. An additional distribution of crystal disclinations is necessary.

One Electron Theories of Cohesion on Ion-Pair Potentials in Metals

N. W. Ashcroft

Laboratory of Atomic and Solid State Physics, Cornell University, Ithaca, New York 14850

The single particle picture of cohesion in metals is briefly reviewed in the light of modern knowledge of their band structures. Periodic components in the electron density distributions (intimately connected with the same band structures) are important in the determination of the effective potential between ions.

In simple metals, defined to be those with tightly bound core states, the net binding of the metallic state is basically a remnant of a competition between kinetic (Pauli principle) and Madelung energies of ostensibly free conduction electrons. Various corrections (for correlation, for exchange, etc.) must be included, and the Madelung energy (which is normally appropriate to a uniform electron gas in a Coulomb lattice of point ions) can be modified as necessary for departures from Coulomb's law. Terms in the total energy also arise from periodic variations in conduction electron density; for perfect lattices these are naturally dependent on the ionic arrangement and will vary in importance from crystal structure to crystal structure. Electronic density variations arising from disorder (e.g. distributions of defects) also introduce corrections into total energy.

The structurally dependent terms in the total energy can be evaluated to second order in the pseudopotential: to this same order the *total* energy may be written as a sum over pair potentials between ions whose form is quite straight forward to evaluate. As with many inter-atomic potentials, the ion-ion potentials demonstate "hard-core" effects at small separation, and are rather weak at large distances.

Extending the simple theory to transition metals or metals exhibiting additional band structure more akin to itinerant narrow-band behavior, can be carried through by incorporating Born-Mayer interactions between tight binding atomic states. This procedure is, of course, only valid in situations where the Bloch method itself is applicable. While the core-core exchange term approximated by the Born-Mayer interaction is quite small in the simple metals it is appreciable for metals like Cu, Ag and Au, and in fact is basically responsible for fixing the equilibrium density. Its addition to the otherwise "simple-metal" like ion pair potentials modifies the behavior at short range.

The Dislocation in a Semi-Infinite Isotropic Medium

D. J. Bacon and P. P. Groves

Department of Metallurgy and Materials Science, The University, Liverpool, England

The displacement associated with an infinitesimal dislocation loop (displacement dipole) or arbitrary orientation in an isotropic, semi-infinite elastic medium has been obtained, and on integration this yields the displacement associated with a finite dislocation loop. The solution for the infinitesimal loop has been obtained by finding the relationship between point forces and displacement dipoles in an infinite medium, and using the same relations with Mindlin's solution for the point force in an elastic half-space. This approach leads to a rather simpler analysis than that of Steketee, and the expressions for the displacements of all the infinitesimal loops near a free-surface are presented here for the first time. The solution is being used to study the stability of a prismatic dislocation loop on a glide prism of square cross-section near a free surface. Preliminary results are presented for the forces on the loop sides and changes in loop energy on rotation for the situation in which the Burgers vector is normal to the surface.

Series Representations of the Elastic Green's Tensor for Cubic Media

D. M. Barnett

Scientific Research Staff, Ford Motor Company, Dearborn, Michigan 48121

Two representations for the cubic Green's tensor components as power series in the anisotropy factor $u = 1 - (c_{11} - c_{12})/2c_4$ are developed, and first order corrections of anisotropy to the Green's tensor and to the interaction energy between two "mechanical" point defects are calculated. It is shown that the best successive approximation scheme is that which constructs the zeroth order (isotropic) approximation to the Green's tensor by identifying the Lamé constants λ and μ as $\lambda = c_{12}$, $\mu = c_{44}$.

A Note on Admissible Solutions in Non-Local Elasticity

D. M. Barnett

Scientific Research Staff, Ford Motor Company, Dearborn, Michigan 48121

In recent years considerable effort has been directed toward incorporating certain features of lattice mechanics within the framework of a continuum description of deforming elastic media. One such theory is non-local elastostatics, developed independently by Kunin, Krumhansl, and Kröner.

The Kunin-Krumhansl non-local scheme is capable of reproducing lattice mechanics exactly by associating a truncated Fourier space with the non-local continuum. The Green's tensor, dislocations, and point defects may be treated rigorously within the framework of this formalism.

Kröner's non-local continuum is associated with a reciprocal Fourier space which need not be truncated. It can be shown that this representation has meaning only if:

(a) The non-local elastic moduli contain a delta function contribution, or, in lieu of this,

(b) The only admissible body force loadings are those which are concentrated over a region larger than that over which the atomic cohesive forces are "appreciable."

Generalized Stress and Non-Riemannian Geometry

S. I. Ben-Abraham

Instituto Technológico de Aeronáutica CTA, São José dos Campos, S. P., Brazil

The general non-Riemannian approach to the geometry of a solid with lattice defects is briefly discussed. Non-Riemannian geometry is applied to the treatment of statics. The "stress" curvature tensor has the meaning of a generalized stress tensor with 27 components, while the associated Einstein tensor represents the classical stress tensor. The "stress" connexion expresses the generalized moment stress having 27 components. Its torsion tensor is the classical couple stress tensor.

The identities of the curvature tensors are identified with the static equilibrium conditions. Using a stress function density instead of a metric tensor, it is shown that the equilibrium conditions can always be identically fulfilled. A consistent theory involving lattice defects must necessarily involve also generalized moment stresses and generalized stresses.

Kinematics of Continuously Distributed Dislocations

S. I. Ben-Abraham

Instituto Technológico de Aeronáutica CTA, São José dos Campos, S. P., Brazil

The general non-Riemannian approach to the geometry of a solid with lattice defects is extended to include the kinematics. The treatment is valid for both the motion of old defects and the creation of new ones. The change in a geometric quantity is described by a corresponding rate. The main quantities dealt with are distortion rates, stretching tensors and connexion rates, and new quantities called fluxions are introduced. In terms of these a fundamental kinematic law and continuity equations for the defect currents are set up and are found to be consistent with earlier results valid in special cases.

The Meaning of Dislocations in Crystalline Interfaces

W. Bollmann

Battelle Institute, Advanced Studies Center, Geneva, Switzerland

The extension of the dislocation concept to arbitrary crystalline interfaces is discussed. It is shown that invariance and continuity of the Burgers vector can be conserved and that in high angle boundaries the function of the standard or primary dislocation is the delimitation of ranges of coordination between the two crystals. In certain relative orientations where the superposition of the two crystals forms a highly periodic pattern (which is energetically favorable such that the crystal tends to conserve it) a slight deviation from that optimum pattern is corrected by a network of secondary dislocations. There is complete balance between the Burgers vectors of primary as well as secondary dislocations.

The Interaction Between a Screw Dislocation and Carbon in Body-Centered Cubic Iron According to an Atomic Model

Roger Chang

Science Center, North American Rockwell Corporation, Thousand Oaks, California 91360

The interaction energy between carbon and a screw dislocation in body-centered cubic iron near the core regions of the dislocation was calculated atomistically using a pair-wise interatomic potential matching the elastic properties of the material. In order to avoid the use of the iron-carbon potential, it was assumed that the iron-carbon octahedron of the Johnson configuration (2 iron atoms separated by 1.225 a_0 in the [100] direction and 4 iron atoms separated by 0.958 a_0 in the (100) plane, a_0 being the lattice parameter) remains undistorted whether it is present in a perfect or a defective lattice. Our first calculations yield, depending on site location, binding energies varying from 0.03 to 1.96 eV. The binding energy is sensitive to changes in hydrostatic pressure and the estimated volume dependence offers a convenient interpretation of the strength-differential effect of martensitic steels via the nonlinear carbon-dislocation interaction mechanism first proposed by Hirth and Cohen.

Strain Rates in Dislocation Dynamics

W. deRosset and A. V. Granato

Department of Physics, University of Illinois, Urbana, Illinois 61801

Since the success by Johnston and Gilman in relating yield phenomena in LiF to direct measurements of dislocation velocities and densities, the Λbv expression for the strain rate has been used almost exclusively, where Λ is the mobile dislocation density, b the Burgers vector, and v is the average dislocation velocity. We note that there are cases for which the strain rate is independent of dislocation velocity. When the velocity is large enough the strain rate is given in a simplified model by $\Lambda b\bar{x}$, where $\bar{x}$ is the average distance traveled by a dislocation. The strain rate is eventually determined, then, by the rate at which new dislocations are created and not necessarily by the rate at which old dislocations expand or by the dislocation velocity.

Linear Theory of Static Disclinations

Roland deWit

Metallurgy Division, National Bureau of Standards, Washington, D.C. 20234

A brief review of compatible and incompatible elasticity theory is given. It is shown how dislocation theory was developed from classical compatible elasticity. Then disclination theory is developed from dislocation theory in an analogous way. The disclination and dislocation density tensors are defined from the plastic deformation. The total deformation satisfies the classical condition of compatibility. By combining these two concepts the geometric basic laws or field equations are found, which relate the elastic deformation to the defect content. The contortion or Nye curvature tensor is found to be a useful equivalent for the dislocation density. Weingarten's theorem motivates the generalization of the Burgers vector and the definition of the analogous rotation vector of disclinations. Finally the dualism between the geometry of disclination theory and the statics of couple-stress theory, and the relation of disclination theory to "motor calculus" are pointed out.

Atomistic Calculation of Dislocation in Solid Krypton

M. Doyama

Argonne National Laboratory and University of Tokyo, Japan

and

R. M. J. Cotterill

Argonne National Laboratory and The Technical University of Denmark, Lyngby, Denmark

The elastic continuum theory treatment usually fails near the core of dislocations. Atomic calculations of edge and screw dislocations in solid krypton were performed very successfully using a pairwise potential. In rare gases, the electron redistribution of the electron density is small, thus, this method is useful to study the properties concerning the core of dislocations.

On the Mechanism of Cross-Slip of Dislocations at Particles

M. S. Duesbery* and P. B. Hirsch

Department of Metallurgy, University of Oxford, England

The effect of the misfit strain field upon the mechanism of cross-slip of dislocations at impenetrable particles in two-phase alloys is considered. The strain field is found to have a profound effect of the activation energy for cross-slip.

The Anharmonic Properties of Vibrating Dislocations

C. Elbaum and A. Hikata

Department of Physics, Brown University, Providence, R.I. 02912

The anharmonic properties of vibrating dislocations are discussed in terms of the nonlinear stress-strain relation and of the higher harmonics of an ultrasonic wave generated when an initially sinusoidal wave propagates in a solid containing (mobile) dislocations. The treatment takes account of both lattice and dislocation contributions to the anharmonic behavior of the solid.

Estimates of the amplitude of the harmonics (these estimates have been confirmed experimentally) indicate that the lattice and dislocation components are comparable for the second harmonic and that the dislocation component is much larger than the lattice component for the third harmonic. Therefore, by investigating the third harmonic, it is possible to obtain detailed information on dislocation dynamics, without the complications of the lattice contribution.

*Now at Division of Pure Physics, National Research Council, Ottawa, Canada

Interactions of Dislocations with Electrons in Metals

C. Elbaum and A. Hikata

Department of Physics, Brown University, Providence, R.I. 02912

Physical arguments are given to show that the interaction of moving (vibrating) dislocations with conduction electrons in metals is independent of temperature. Calculations based on the assumption that the Fourier components of the displacement field of a moving dislocation can be treated as pseudo-phonons give the same result. These conclusions were confirmed by the results of recent experiments.

Electronic Energy States of Dislocations; The Case of Covalent-Ionic Solids

C. Elbaum and R. R. Holmes*

Department of Physics, Brown University, Providence, R.I. 02912

It is shown that electronic energy bands are associated with dislocations in wide-band-gap, compound semiconductors. The eigenvalue problem for the dislocation band edge is solved for CdS-type crystals, and the occupation of the band is calculated. The Fermi energy is then determined for crystals containing many deep-lying discrete levels as well as dislocation bands. It is predicted that when a crystal is illuminated with light of appropriate wavelength and increasing intensity, the thermal activation energy governing the electrical conductivity passes through a series of energy plateaus which are equal to the energy of the discrete levels.In a dislocation-free crystal, these plateaus are connected by step changes, while in a crystal with dislocations they are connected by broad transition regions. The above predictions have been verified experimentally.

Theories of Thermally Activated Processes and Their Application to Dislocation Motions in Crystals

H. Engelke

Institut für Theoretische und Angewandte Physik der Universität, Stuttgart, Germany

Thermally activated processes involving dislocations are usually treated by applying the theory of absolute reaction rates and the string approximation of dislocation. In the first part of this paper the limits of validity of these treatments are discussed. A paper of T. Geszti is briefly reviewed in which it is shown that in processes involving *point defects* deviations from the rate theory must be expected if the energy exchange between defect and lattice waves is slow compared with the average time between jumps, e.g. if localized of quasi-local vibrations contribute essentially to the defect motion. It is pointed out that the localized modes of dislocations may also lead to deviations from the rate theory.

In the second part a treatment of the double kink relaxation (Bordoni relaxation) based on the Kramers-Brinkman diffusion theory of chemical reactions is given. After showing that in f.c.c. metals the influence of the Peierls potential is so small that on dislocation loops only one kink pair must be con-

*Present address: Bell Telephone Laboratories, Whippany, N.J.

sidered explicitly whereas the remaining parts of the loops may be described by the string approximation diffusion equations for the loop motion are derived. Under certain conditions these equations are equivalent to a system of reaction rate equations. Exact solutions of this system are not yet available. However, the behaviour of dislocation loops in the amplitude independent region of internal friction measurements may be extrapolated combining results of two limiting cases: a double well model and a simplified multi-well model.

The relaxation strength and the preexponential factor of the relaxation time calculated have the same orders of magnitude as in measurements of the Bordoni peak. The loop length dependence of the damping peak is in good agreement with neutron-irradiation measurements. The characterisstic half-width of the Bordoni peak may partly be explained using loop length and stress distributions.

Point Defects and Dislocations in Copper

A. Englert,* H. Tompé

Union Carbide European Research Associates, 95, Rue Gatti de Gamond, Brussels 18, Belgium

and

R. Bullough

Theoretical Physics Division, A.E.R.E., Harwell, Didcot, England

A new pair potential for copper has been constructed from a set of ten interpolated cubic polynomials. The form of the potential is such that at short range it agrees with the usual Born-Mayer repulsive potential and is in satisfactory agreement with the available phonon dispersion data and the observed stacking fault energy and vacancy formation energy for copper. The potential has been used to study the atomic configuration associated with various point and line defects in copper. In particular, because of its fit to the stacking fault energy, it provides a consistent result for the degree and nature of the dissociation to be expected for an edge dislocation in copper.

A Micromorphic Approach to Dislocation Theory and its Relation to Several Existing Theories

A. C. Eringen

Princeton University, Princeton, New Jersey 08540

and

W. D. Claus, Jr.

Princeton University and Textile Research Institute, Princeton, New Jersey 08540

Two separate continuum dislocation theories are presented; one dealing with static, incompatible, micropolar dislocations and disclinations, as encountered in initial stress problems, and the other with a dynamical theory of micromorphic solids containing continuous distributions of dislocations.

Relationships between several continuum dislocation theories and micromorphic mechanics are established by providing extensions and new interpretations of the micromorphic theory. First both micromorphic and micropolar theories of elastic solids are summarized, and then the theories of Kröner, Fox, and Berdichevskii and Sedov are discussed in some detail within this framework. In the last section, by use of micromorphic kinematics, dislocation density, strain, and microstrain tensors are introduced and constitutive equations are constructed. Together with the balance laws this constitutes a complete dynamical theory. The theory is intended for predictions of motions and micromotions of a solid containing dislocations undergoing elastic deformations. From the micromotion, the dislocation density and first stress moments can be calculated.

*Visiting Research Associate, Harwell, Summer 1968

356-078 O-69—6

The Method of Lattice Statics

J. W. Flocken and J. R. Hardy

Behlen Laboratory of Physics, University of Nebraska, Lincoln, Nebraska 68508

The formalism of the method of lattice statics for treating the lattice distortions and the formation and interaction energies associated with a defect in a crystal is presented in detail. This approach is based on the Fourier transformation of the set of direct space equilibrium equations to reciprocal space. This results in a set of decoupled equations which can be explicitly solved for the Fourier amplitudes of the displacement field which can then be found by Fourier inversion. A similar approach is used to obtain Fourier transformed expressions for the relaxation and interaction energies associated with the defect.

The solution of the equations of lattice statics for the Fourier amplitudes in the limit of small wave vectors gives expressions for the displacement field identical to those obtained from the theory of continuum elasticity.

Results are presented of recent applications of the method of lattice statics to find the formation energies of Schottky pairs in certain alkali halides. Strain field displacements, relaxation energies and interaction energies associated with vacancies in Na and K are given.

Lattice statics in its asymptotic form has been used to find the displacement field far from cubic point defects and double defects in a number of metals. Displacement profiles about vacancies in Na and K and about a double force defect in Cu are shown. A comparison of the exact lattice statics results to asymptotic results along the ⟨111⟩ direction in K shows that the elastic limit is only attained at about the 19th or 20th neighbor position from the defect.

Movement of a Dislocation Through Random Arrays of Point and Parallel Line Obstacles

A. J. E. Foreman

A.E.R.E., Harwell, Didcot, England

and

P. B. Hirsch and F. J. Humphreys

Department of Metallurgy, University of Oxford, England

The motion of a dislocation through random arrays of impenetrable point and parallel line obstacles is considered. For impenetrable point obstacles the difference in line tension for edges and screws, and the elliptical equilibrium shape of the bowing-out loop are taken into account, and the yield stress for screws and edges is found to be the same. The results of a calculation of the effect of interaction between neighboring segments of the dislocation on the critical breaking angle and on the yield stress are presented. Computer calculations on the motion of dislocations through random arrays of parallel line obstacles show that the dislocations move by the generation and motion of large "kinks." The yield stress is found to increase approximately linearly with the obstacle length. These calculations are relevant to and are compared with the hardening in the early stages of the work hardening curve of dispersion hardened alloys containing small particles, in which rows of prismatic loops are formed at the particles, which act as linear obstacles to the gliding dislocations.

On the Continuum Theory of Dislocations

N. Fox

Department of Applied Mathematics, University of Sheffield, England

The kinematics of an oriented medium is discussed with reference to the contiuum theory of dislocations. The concepts of dislocation density, dislocation flux and slip velocity are introduced and a corresponding constitutive theory is developed.

Dislocation Dynamics in the Presence of a Multiple Spectrum of Thermally Surmountable Barriers

W. Frank

Max-Planck-Institut für Metallforschung, Institut für Physik, Stuttgart, Germany

A theoretical treatment is given of the thermally activated motion of dislocations in the presence of dislocation barriers with different heights. The height of a barrier is allowed to depend on an arbitrary number of characteristic parameters (multiple obstacle spectrum). Under the assumptions which are usually made for the derivation of an Arrhenius equation for the slip rate $\dot{a}$ in the case of a uniform array of dislocation barriers, $\dot{a}$ is calculated for a multiple spectrum of barriers. It is found that even under these conditions the validity of an Arrhenius equation $\dot{a} = \dot{a}_0 \exp\ (-\overline{\Delta G}/kT)$ ($a_0 =$ const., $\overline{\Delta G} =$ mean enthalpy of activation) is preserved. An application of the "spectrum theory" is discussed.

Dislocation Resonance

J. A. Garber and A. V. Granato

Department of Physics, University of Illinois, Urbana, Illinois 61801

At low temperatures in insulators and superconductors, only reradiation of elastic waves should limit dislocation resonance. This effects has been calculated using Eshelby's expression for the reradiation by analogy with radiation damping effects in the electromagnetic case. It is found that the resonance is very sharp, and still persists even when a random distribution of dislocation segment lengths is assumed.

The Structure of the ⟨111⟩ Screw Dislocation in Iron

P. C. Gehlen, G. T. Hahn, and A. R. Rosenfield

Metal Science Group, Battelle Memorial Institute, Columbus, Ohio 43201

The concept of a dissociated a/2 ⟨111⟩ screw dislocation has been invoked to explain the slip behavior in bcc materials and particularly the asymmetry of the critical resolved shear stress. No direct experimental evidence of dissociation has been obtained, but the idea has received some albeit conflicting support from discrete lattice calculations of the atomic positions in the core. Chang, using isotropic elasticity for α-iron, found that the dislocation core has three very narrow intrinsic faults. These

three faults are symmetric with respect to the screw axis. Bullough and Perrin, on the other hand, found that the screw is split with faults on two {112} planes belonging to the zone of the screw axis. The misfit is spread over a distance of about $3b$. On the third {112} plane no splitting was found to occur.

In view of these discrepancies, the calculations were repeated for anisotropic and isotropic elastic boundary conditions and with different interatomic potentials. Excellent agreement was found with Chang's configuration even though a volume expansion term was added to the displacements associated with the dislocation.

It was shown that the final configuration is strongly dependent on the position of the dislocation line with respect to the lattice and at least two metastable positions were found. Even though the atomic arrangment is quite different, their energy is not more than 0.1 eV larger than the energy of the stable one.

Using the Johnson potential unmodified for long-range electronic effects, the dislocation was found to have the following characteristics: core radius, 4-5.5 Å; core energy, 0.20-0.25 eV per atomic plane; and an effective hole radius of 1.35 Å.

It was shown that the final configurations are rather insensitive to the model size and to the boundary conditions used.

Phonon Scattering by Dislocations and its Influence on the Lattice Thermal Conductivity and on the Dislocation Mobility at Low Temperatures

P. P. Gruner

Boeing Scientific Research Laboratories, P.O. Box 3981, Seattle, Washington 98124

On account of the large strains associated with dislocations, the superposition principle is violated. The resulting scattering of phonons limits the lattice thermal conductivity and leads to a friction force which acts on moving dislocations. The phonon-dislocation interaction is treated with non-linear continuum theory. Terms up to the third order in the strains are retained in the Taylor expansion of the elastic energy density. These third order terms contain the phonon-dislocation interaction and the normal three-phonon interactions. In the case of thermal conductivity, the transport problem is solved with the variational method which leads to a system of linear equations for the phonon occupation numbers. The coefficients of this system of equations contain all the information on the scattering mechanisms. The influence on the thermal conductivity of special dislocation configurations such as piled-up dislocations and dislocation dipoles will be discussed.

It will be shown that the friction force which acts on moving dislocations on account of the anharmonicity can be obtained from quantities that are known from the calculations of the phonon conductivity. A one to one correspondence between friction force and thermal resistance exists, however, only if the dislocation velocity is small compared with the sound velocity and if all parts of the dislocation move with the same velocity.

Charged Dislocations in the Diamond Structure

P. Haasen and W. Schröter

Institut für Metallphysik, Universität Göttingen, Germany

The electronic states at dislocations in elemental semiconductors are reviewed in the light of new experimental and theoretical work. Evidence is produced for the existence of a one-dimensional energy band along edge as well as screw dislocations. This explains quantitatively their ability to act as donors as well as acceptors depending on temperature, doping, and dislocation density. The degree of charging has been recalculated from the free energy of a system of charged dislocations screened by free carriers. The dislocation charge limits the Hall mobility in addition to the strain field of the dislocation. Measurements of photo conductivity of deformed semiconductors support the above model of the charged dislocation. The dislocation charge influences the Peierls force and thus the mobility of dislocations in the diamond structure. The occupation limit of the neutral dislocation, measured from the valence band edge, lies at 0.09 eV in germanium, and at 0.3 eV in silicon.

Toplogical Restriction on the Distribution of Defects in Surface Crystals and Possible Biophysical Application

W. F. Harris

Department of Chemical Engineering, Institute of Technology, University of Minnesota, Minneapolis, Minnesota 55455

Many thin biological structures such as some plasma membranes and virus capsids appear to be made up of units packed in two-dimensional lattices. Such structures are termed *surface crystals*. Dislocations and disclinations are observable in some of these crystals. The perfect surface crystal is described by a *pair* of basic vectors and the conventional crystals by a *triplet* of basis vectors; both are regarded as embedded in three-dimensional space. This difference allows the existence of defects which have no counterpart in conventional crystals. The various defects are classified as local or global, intrinsic or extrinsic. Surface crystals that form closed surfaces are considered and it is shown that the sum of the rotation of intrinsic (screw) disclinations in them must equal $2\pi\chi$ where χ is the Euler-Poincaré characteristic of the surface. The biophysical consequences are discussed briefly.

Elastic-Plastic Plane Bending of a Single Crystal

C. S. Hartley and M. A. Eisenberg

Department of Engineering Science and Mechanics, University of Florida, Gainesville, Florida 32601

The elastic-plastic bending of a single crystal beam which deforms by single slip on a plane containing the axis of bending and in a direction normal to the axis of bending is analyzed. Both continuum plasticity and dislocation approaches are used to obtain stresses and/or displacements in the elastic and plastic regions. The relation between the applied bending moment and the curvature of the neutral axis is also obtained. The approaches are compared and correspondences between the two theories are discussed.

Discrete Dislocations in Continuum Elasticity

A. K. Head

Commonwealth Scientific and Industrial Research Organization, Division of Tribophysics, University of Melbourne, Victoria, Australia

As a framework in which to survey some of the current questions in this long-established part of dislocation theory, the problem of the experimental determination of stacking fault energy is considered. Attention is restricted to those methods which observe and measure in the electron microscope a simple dislocation-stacking fault configuration. It is assumed that the configuration is in equilibrium with the forces between the dislocation balancing the surface tension of the stacking fault. The stacking fault energy then follows if these dislocation forces are known from theory for the observed dimensions of the configuration.

Experimental techniques have improved to the point where a reproducibility of 1 to 5 percent standard deviation is claimed. This calls for theory which has at least a similar standard of accuracy. It is doubtful if the theory which is in current use has this accuracy and this is surveyed under the following headings: a) The treatment of the core; b) Elastic anisotropy; c) Zig-zag instabilities; d) The effect of the stacking fault; e) The observation of dislocations by electron microscopy.

Slightly Dissociated Dislocations

R. Hobart

Battelle Memorial Institute, Columbus Laboratories, 505 King Avenue, Columbus, Ohio 43201

A modified Peierls-Nabarro model is used to calculate the relation between the separation of partials and stacking fault energy for an idealized dislocation dissociated into two equal pure screw partials. The resulting expression agrees with the inverse dependence obtained by equating the elastic repulsion of the partials to the attraction of the stacking fault, but unlike that result does not break down at zero separation. Also an argument is given that the width of such a dissociated dislocation should be considered as a complex quantity, with the imaginary part corresponding to the separation of the partials.

Thermodynamic Properties of Solids Containing Dislocations

J. Holder and A. V. Granato

Department of Physics, University of Illinois, Urbana, Illinois 61801

Using thermodynamics and elasticity theory, a unified treatment of the changes in the thermodynamic properties of solids containing dislocations is given. The results are expressed in terms of temperature and pressure derivatives of the formation energy of the dislocations. The required pressure and temperature dependence of the energy is given by the measured pressure and temperature dependence of the elastic constants appearing in the energy expression found at zero pressure and temperature. The method is not restricted to calculations of volume changes, or to isotropic, static or even elastic systems at zero pressure. Changes in entropy, specific heat, thermal expansion and bulk modulus due to dislocations are easily calculated.

A Lattice Theory Model for Peierls-Energy Calculations

A. Hölzler and R. Siems

Institut für Theoretische Physik C der Technische Hochschule, Aachen, Germany

A lattice theory model for a screw dislocation is discussed which is similar to that of Maradudin. For the forces between neighbouring rows of atoms, however, a sinusoidal, not a linear, dependence of their relative displacements is assumed throughout the whole lattice. The displacements are expanded about the elastic theory values. The conditions of equilibrium then yield a system of linear equations for the deviations of the displacements from the elastic theory values, which is solved by an iteration procedure making use of Green's Function for a plane square lattice. For a number of points in the vicinity of the source point and for points in certain symmetry directions simple exact analytical expresssions for the latter are derived, for points at larger distances an asymptotic expansion is given. The displacements thus obtained are then used to calculate the energies of the dislocation at the position of minimum energy and at the saddle point and their difference, the Peierls energy, by direct summation of the interaction energies of neighbouring pairs of atoms.

Interactions Between Electrons and Moving Dislocations

G. P. Huffman and N. Louat,

Edgar C. Bain Laboratory for Fundamental Research, U.S. Steel Corporation Research Center, Monroeville, Pennsylvania 15146

A moving dislocation in a metal induces an electric field which causes currents in the conduction electron gas. The energy dissipation associated with these fields and currents is calculated from the Boltzmann equation in a manner analogous to theories of acoustical attenuation. It is found that the applied stress required for steady motion is proportional to the dislocation velocity divided by the electrical resistivity, in good agreement with low temperature yield and flow stress measurements on bcc metals. The concept of a large electronic component of drag which increases with decreasing temperature is used to give a qualitative explanation of the observed mechanical properties of bbc metals. When one considers electronically damped dislocations impeded by pinning points, it is found that: 1) the dislocation velocity depends only on the mean strength of the pinning obstacles; 2) the stress required to overcome an obstacle dynamically is less than that required statically and is, in fact, the electronic drag stress; and 3) the apparent dislocation velocity should vary rapidly with applied stress. The displacement field of a dislocation is significantly wider and more gradual in a fcc than in a bcc lattice, and this feature can be incorporated into the calculation by assuming that the electronic screening of the positive charge shift of the dislocation is essentially perfect in a fcc lattice. The Boltzmann formation then gives a temperature independent stress or drag coefficient in agreement with experiment and with Holstein's scattering calculation. The problem of a dislocation moving in an applied magnetic field directed along its length and perpendicular to its direction of motion is also treated. Under suitable conditions it is found that the stress or drag coefficients exhibit oscillations of the cyclotron resonance type which could be as large as 10 to 30% of the zero field values.

Identification of the Dragging Mechanisms of Dislocations

V. L. Indenbom

Institute of Crystallography, Academy of Sciences, Moscow, USSR

and

A. N. Orlov

Physico-Technical Institute, Academy of Sciences, Leningrad, USSR

The results of direct investigations of the dislocations movement makes it possible to proceed to identification of the mechanisms, controlling mobility under different conditions and require some revision of theoretical estimations of various mechanisms contribution.

Investigations of high-speed dislocations and amplitude independent internal friction yield data concerning the intensity of energy dissipation which can be explained by the transmission of an impulse from the dislocation to different branches of the spectrum of elementary excitation of the crystal: phonons, electrons, exitons and others.

Most reasonable estimations result from computations of the dynamic Peierls force. In case of even motion of dislocations certain phonon mechanisms do not provide the observed dissipation rate. The accord between theory and experiment improves to a greater extent if the oscillations of the dislocation field due to its movement across the Peierls relief are taken into account.

As temperature falls phonon processes are frozen out and electron mechanisms of dissipation are displayed. Their contribution is clearly exposed in case of superconductors.

Excitations of internal degrees of freedom of a dislocation corresponds to another class of the dragging mechanisms. Creation, movement and interaction of kinks, jogs and other elements of the fine structure of the dislocation core account for microgeometry of a dislocation and its dynamic properties. Elementary mechanisms of this kind are observed in the spectors of internal friction and can be analysed on the basis of the latest observations of dislocation mobility in semiconductors.

Aspects in Liquid Crystals Relevant to the Theory of Dislocations

M. Kléman

Laboratoire de Physique des Solides, Faculté des Sciences, 91 — Orsay, France

A general theory of dislocations in a mesomorphic medium is outlined. On the basis of their symmetry properties, and of viscosity relaxation, it is first shown that perfect disinclinations in nematic crystals may take any shape, are restricted to straight lines in smectic crystals, and that both types exist in cholesteric crystals, where there are two possible axes of rotation. The second part is specialized to the case of cholesteric crystals, for which a mechanism of pairing of dislocations is proposed which allows a multiple disinclination to take any shape, at the expense of a small increase of energy in the faulted ribbon. The observed magnetic instability of these pairs, which constitutes a strong evidence of the proposed model, is explained.

Phonon Scattering by Cottrell Atmospheres

P. G. Klemens

Department of Physics and Institute of Materials Science, University of Connecticut, Storrs, Connecticut 06268

The formation of Cottrell atmospheres can change the scattering of phonons by dislocations and in some cases substantially enhance the lattice thermal resistivity due to dislocations. The strength of the atmospheres can be changed by annealing. This changes thermal conductivity values at high temperatures first, since diffusion through shorter distances is involved. The diffusion coefficient can be determined by means of such annealing studies.

Flow and the Arrhenius Equation in the Statistical Framework

U. F. Kocks

Metallurgy Division, Argonne National Laboratory, Argonne, Illinois 60439

The rate equation of plastic flow and a general work hardening law are combined into a single equation of flow. It degenerates into the Arrhenius law only under certain specified conditions. A single Arrhenius term with temperature insensitive pre-exponential (and entropy) terms adequately describes the rate dependence of dislocation motion through a slip plane studded with obstacles of any spectrum of strengths and spacings. In this case, the mobile dislocation density in the slip plane generally does not enter the flow equation; only the density of slip planes does.

A Non-Riemannian Construction of Variational Criteria for Plastic Manifolds with Special Reference to the Theory of Yielding

Kazuo Kondo

University of Tokyo, Tokyo, Japan

The variational formalism is viewed not as an independent assumption but as a natural consequence following from a more fundamental penetration into the recognition of nature and this is shown in regard to the static aspects of plasticity. The energy is defined as the necessary quantity for the geometrical construction. With the Riemannian and non-Riemannian picture, a bridge is sought between the theory of yielding and the theory of dislocations, as also between the theory of dual yielding

and theory of couple stresses. The standpoint of the theory of yielding and dual yielding is explained constitutively with a statistical construction to reconfirm the formulae which have been proposed. The meaning of the plastic constants involved in the theory is clarified by the construction.

The Problem of Non-Locality in the Mechanics of Solids: Review on Present Status

E. Kröner

Institut für Theoretische Physik, Technische Universität, Clausthal, Germany

The concept of non-locality, in particular with reference to the mechanics of solids, is discussed. A brief report is given on the derivation of the non-local theory of elasticity from atomic lattice theory. In addition some simple solutions of this theory, concerning the interaction of dilatation centers and wave propagation, are quoted. A generalization of the theory which would include dislocations is indicated.

Non-Local Theory of Elasticity for a Finite Inhomogeneous Medium—A Derivation from Lattice Theory

E. Kröner and B. K. Datta

Institut für Theoretische Physik, Technische Universität, Clausthal, Germany

In the linear theory of non-local elasticity the strain energy can be written as a double volume integral summing up the interactions of pairs of mass elements. The properties of the material, in this case, are described by a two-point-tensor function $c_{ijkl}(\mathbf{r}, \mathbf{r}')$. It is found that for finite bodies $c_{ijkl}(\mathbf{r}, \mathbf{r}')$ does not have the symmetries of the (Hooke's) elasticity tensor C_{ijkl} of the local theory. However, the symmetries of this tensor function are sufficient to exclude the rotations from the strain energy expression. It is shown that with the help of the elastic Green's function one can express $c_{ijkl}(\mathbf{r},\mathbf{r}')$ in terms of force constants of the lattice. It is also shown that an infinite homogeneous body is not a suitable model either for the non-local or for the local theory, because in this case $c_{ijkl}(\mathbf{r}, \mathbf{r}')$ as well as C_{ijkl} obey the Cauchy relations.

Theoretical Considerations on the Extension of 1/2 ⟨110⟩, {111} Dislocations in Isotropic FCC Metals into Shockley Partials

Doris Kuhlmann-Wilsdorf

Department of Materials Science, University of Virginia, Charlottesville, Virginia 22903

and

T. R. Duncan

Department of Minerals and Metals Engineering, University of Wisconsin, Madison, Wisconsin 53706

The energy changes and equilibrium separations associated with the extension of 1/2⟨110⟩, {111} dislocations in fcc metals into Shockley partials have been calculated and were found considerably smaller than the previous corresponding values due to Seeger and Schöck. The new results may be shown to be credible on the basis of the following simple estimates.

The theoretical shear fracture strength of a crystal may be written as $\tau_{crit} = G/q$, with G the appropriate shear modulus and the numerical parameter q near 30 for {111} planes in fcc metals. The resolved shear stress required to force the Shockley partials into coincidence at vanishing stacking fault energy, $(\tau_{eq})_{max}$, must approach but cannot exceed τ_{crit} so that $(\tau_{eq})_{max} \simeq G/30$, i.e. much smaller than the value of $\sqrt{6}G/8\pi \simeq G/9$ previously assumed. Similarly, the stacking fault energy cannot exceed the value of $\gamma_{crit} = Ga/\sqrt{6}q$ with a the lattice constant, and the dislocation core energy must be in the order of $E_c \simeq 2r_0\gamma_{crit} \simeq 1/4E_D$ where E_D is the total dislocation energy, and the core radius, r_0, is taken to be that distance from the dislocation axis at which the resolved shear stress on the slip plane would become equal to τ_{crit} in linear elastic behavior. Lastly, D_0, the actual equilibrium separation between the partials must be considerably smaller than D_0^*, the separation calculated from linear elastic theory, as long as $D_0^* < 2r_0$. One finds easily that $D_0^* \leq 2r_0$ for $\gamma \gtrsim \gamma_{crit}/6$ and $\gamma \gtrsim \gamma_{crit}/10$ for edge and screw dislocations, respectively, depending somewhat on Poisson's ratio, so that only in silver will edge dislocations have an equilibrium separation a little larger than $2r_0$, but much less than $2r_0$ in the other common pure fcc metals. For $D_0 = 2r_0$, when the core energy is reduced by about 1/3 according to the rule of the square of the Burgers vectors but the elastic energy is virtually unaffected, and remembering that work $2r_0\gamma$ with $\gamma \simeq \gamma_{crit}/6$ must be done to spread out the stacking fault, the relative energy gain due to the extension of edge dislocations is simply estimated as $(\Delta E/E_D)_\perp \simeq [1/3E_c/4E_c - 1/6\gamma_{crit}/4\gamma_{crit}] \simeq 4\%$ which may be compared to the calculated value of 4.6% in silver.

On Problems of the Non-Local Theory of Elasticity

I. A. Kunin and A. M. Waisman

Institute of Thermophysics, Academy of Sciences, Novosibirsk, USSR

The paper contains new results concerning the linear theory of an elastic medium with non-local interactions:

I. *The structure of the general solution of the equations of motion.* The dependence of the general solution on the distribution of energy operator zeroes. Specific effects of the non-locality: new types of dampled and undamped waves, the existence of a maximum frequency for the latter ones, the space dispersion. The Green's function.

II. *Approximate models.* Two types of approximate models: the long-wave approximations and the first zeroes approximations. Domains of their applicability.

III. *Boundary value problems.* The replacing of the boundary by a boundary layer of width of the interaction radius. Generalized Green's formula. Fundamental boundary value problems, their correct formulation for first zeroes approximations. The comparison with couple-stress theories. Examples of exact and approximate solutions. The existence of new types of surface wave different from Rayleigh waves.

Some Recent Results on Dislocation Pileups

J. C. M. Li

Materials Research Center, Allied Chemical Corporation, Morristown, New Jersey 07960

A few results intended to illustrate the usefulness of orthogonal polynomials and singular integral equations for the problem of dislocation pileups are described. A simple method of solving a few special integral equations is suggested. The usefulness of a Moutier cycle for the calculation of stress concentration is shown.

The Image Force on Dislocations at Free Surfaces. Comments on the Concept of Line Tension.

J. Lothe

Institute of Physics, University of Oslo, Blindern, Oslo, Norway

It is shown that a straight dislocation emerging at a planar free surface is acted upon by a force distributed according to the law $d\mathbf{F}=\lambda^{-1}\,(-E\,\text{cotan}\,\theta+\partial E/\partial\theta)\,d\lambda$. Here θ is angle of inclination to surface, E is dislocation energy factor, and λ is distance from surface along the dislocation. The proof involves use of a slightly generalized version of the energy flow theorem for straight dislocations (Lothe, Phil. Mag. **15**, 9 (1967)). The above formula is the exact linear elasticity law corresponding to the usual approximate line tension result. According to this law there are certain angles of incidence for which the forces vanish so that the dislocation can be straight. Similarly, when only elastic terms are considered, there are certain node orientations for which the forces on the branches vanish so that the branches can be truly straight (Indenbom and Dubnova, Sovj. Phys. (Solid State), **9**, 915 (1967)). In this paper a discussion is given of how core energy terms may modify the results. It is concluded that also for nodes in the characteristic orientation for no elastic forces on the branches, some branch curvature will be present near the node.

Some Problems Involving Linear Dislocation Arrays

N. Louat

Edgar C. Bain Laboratory For Fundamental Research, U.S. Steel Corporation, Research Center, Monroeville, Pennsylvania 15146

Muskhelishvili's inversion formulae for singular integral equations are shown to be special cases of a more general result which is then employed to deal with two types of problems. In the first we consider the distribution of dislocations in a double periodic array of screw pile-ups in an arbitrary stress field. The second type is concerned with screw pile-ups terminating at phase boundaries, again for arbitrary stress fields.

Stability and Some Characteristics of Uniformly Moving Dislocations

M. Malén

AB Atomenergi, Studsvik, Sweden

The stability of uniformly moving dislocations has been studied in the case of elastic anisotropy using computer. The velocity for instability to occur for a screw dislocation in an isotropic medium is so high, 0.98 C_t, with C_t the transverse sound velocity, that it may well be unattainable. Inclusion of anisotropy gives the possibility of more reasonable instability velocities. Some data showing this for Fe, Li and Cr are given.

The stress field around a uniformly moving dislocation has been studied. Increasing the velocity of a dislocation corresponds to some extent to a change in the anisotropy of the crystal.

In uniform motion above the lowest velocity of sound in the direction of motion one can have associated with the moving dislocation 2, 4 or 6 Çerenkov waves, above the next sound velocity 4 or 6 and above the highest sound velocity 6 waves.

The formula developed earlier for the stress field around a uniformly moving planar dislocation loop can be generalized directly to three dimsions using the theorems of Indenbom and Orlov for the fields from three-dimensional sources using data for two-dimensional sources.

The generalization can also be made using the fact that the choice of cut surface is arbitrary.

Localized Vibration Modes Associated with Screw Dislocations

A. A. Maradudin

Department of Physics, University of California, Irvine, California 92664

The dispersion relation for the one-dimensional continuum of localized modes associated with a screw dislocation is obtained in the long wavelength limit, as a function of the wave vector parallel to the dislocation line. The result has the form $\omega^2(q) = s^2q^2 - \omega_0^2 \exp(-\text{const.}/q)$ where s is the speed of sound for transverse acoustic waves, and ω_0 is a typical Brillouin zone boundary frequency.

Propagation of Glide Through Internal Boundaries

M. J. Marcinkowski

Engineering Materials Group and Department of Mechanical Engineering, University of Maryland, College Park, Maryland 20742

It has been shown that when an internal boundary such as a grain boundary is cut by a crystal glide dislocation, a disturbance is left at the boundary. This disturbance closely resembles that about a crystal dislocation with the exception that a) there is no extra half plane associated with the dislocation and b) the Burgers vector associated with this disturbance is a variable which depends on the nature of the internal boundary. These boundary dislocations have been termed virtual dislocations.

The nature of the virtual boundary dislocations have been treated in detail for the symmetrical tilt boundary. Both homogeneous and heterogeneous type glide across these boundaries have in turn been applied to grain boundary crack formation and propagation, grain boundary rotation, preferred orientation etc.

A Source of Dissipation that Produces an Internal Friction Independent of the Frequency

Warren P. Mason

Department of Engineering and Applied Science, Columbia University, New York, N.Y., 10027

Many measurements of the internal friction of metals and other materials such as the earths crust show that there is a component at low frequencies which produces a value independent of the frequency. It has been shown that this component is associated with dislocation motion.

Using a model for which dislocation motion results from the motion of kinks, it is shown that such a loss can be associated with the energy dissipated when kinks cross Peierls barriers. Theoretical calculations have shown that the energy dissipated in mechanical vibrations requires a dissipative force equal to from 0.01 to 0.1 of the Peierls stress to replace the energy lost. At the low stresses used in internal friction measurements, it requires a thermal activation to cause motions of the kinks. The lag of the motion behind the applied stress produces a drag coefficient B proportional to the temperature. The energy due to kink dissipation produces an internal friction to modulus change ratio b, equal to the ratio of the dynamic to the static kink stress. Measurements in copper indicate that this ratio is about 0.04 in agreement with calculations.

Non-Planar Dissociations of Dislocations

S. Mendelson

2660 Somerset Blvd., Troy, Michigan 48084

Non-planar dissociations of dislocations are studied in hcp, fcc, bcc, diamond lattice, tetragonal and orthorhombic crystal structures. The geometric and energetic conditions are shown to be favorable for various dissociations in each crystal structure. A general equation is formulated for dissocations into partials which are glissile on various twin planes of a common zone. The Burgers vector of the twinning dislocations are expressed in terms of orthogonal unit vectors which lie in the "plane of shear" of the twin mode. The twinning dislocations are generally of the "zonal" type, chosen to be consistent with minimum shear-strain and simple atomic shuffling criteria for twinning, and applied in derivations of the twinning elements and shear-strains for various twin modes. The sign of the shear-strain determines the "stress sense" characteristics for dislocation resistance and twinning and are shown to be consistent with behavior in various hcp and bcc metals. The maximum repulsive force on the twinning partials γ_m is computed using anisotropic elasticity, and compared with evaluations of twin lamella energies γ. In many cases it is found that $\gamma_m/\gamma > 1$, leading to an increase in dislocation resistance, locking, or twinning at lower temperatures. In the cases where $0 < \gamma_m/\gamma < 1$ the partialized dislocation model reduces to the "modified pseudo-Peierls-Nabarro model" for dislocation resistance.

Among various effects, the dissociations account for all twin modes in hcp metals and for the extreme difference in the flow behavior of Cd and Zn on one hand and Ti and Zr on the other. The stress dependent activation energies for motion of dissociated 60° dislocations in germanium are computed and compare favorably with the data of Kabler. A "lock" for kinks on 60° dislocations is discribed which can account for dragging points in the model of Celli et al.

Derivation of a Continuum Theory of Dislocations on the Basis of an Estimative Analysis of Crystal Lattices

M. Mişicu

Center of Mechanics of Solids, Academy of Sciences, Bucharest, Rumania

Starting from the non-primitive crystal lattice model, a continuum theory is derived by means of an interpolation procedure which takes into account the variability of kinematic and dynamic fields. The non-holonomy of the fields of displacements, energy and entropy is considered in order to elaborate the analysis of dislocation and irreversible effects.

The Elastic Field of Moving Dislocations and Disclinations

T. Mura

Department of Civil Engineering and Materials Research Center, Northwestern University, Evanston, Illinois 60201

The previous work and the present stage of study on the elastic field of moving dislocations and disclinations are reviewed. Emphasis will be placed upon the general method and approach using Green's tensor functions and Fourier integrals. The previous solutions for individual problems are reviewed as examples of this unified approach.

Disclinations in Surfaces

F. R. N. Nabarro

Department of Physics, University of the Witwatersrand, Johannesburg, South Africa

The screw disclination is essentially a 2-dimensional object. Screw disclinations provide a convenient classification of star polygons. By considering the disclinations in vector fields lying on surfaces, it is possible to relate Euler's theorem for polyhedra inscribed on a sphere (faces − edges + corners = 2) to the fixed-point theorem for continuously-varying small displacements of points on a sphere. The changes in the Euler characteristic produced by the addition of holes, handles and cross caps are related to the disclinations which these singularities introduce into vector fields lying on the surface. These disclinations may be localized into the neighbourhood of their corresponding singularities.

Eigenfrequencies in a Dislocated Crystal

T. Ninomiya

Department of Physics, University of Tokyo, Tokyo, Japan

Dynamical theories of dislocation vibration and interactions with phonons are surveyed. Eigenfrequencies of lattice vibration in a crystal containing a straight dislocation vibration (wave number κ) in each of the intervals of the normal mode frequencies of $k_z = \kappa$ in a perfect lattice. It is also found that there is a band of localized dislocation vibration below the phonon band. The mean squared amplitude of the dislocation vibration is determined by the localized mode for an edge dislocation and by the resonance modes for a screw dislocation. Phonon scattering by the fluttering mechanism is next treated by using the above results and the condition of resonance scattering is given. Finally, the effect of the Peierls potential and the vibration of a dislocation dipole are discussed. In the Appendices the problem of quantization of dislocation vibration and the extension of the above theories to a case of translational motion is briefly described.

Electronic Effects Associated with Stacking Faults in Normal Metals

C. Nourtier

Physique du Solide, Faculté des Sciences, 91 Orsay, France

and

G. Saada

Département de Physique, CUSLA, B.P. 36, 59 − Lille Distribution, France

The authors use a simple pair interaction model to make the following calculations. 1) Stacking fault energy of simple metals. 2) Interaction energy between a stacking fault and an impurity atom or a vacancy, and application to the study of segregation effects. 3) Interaction energy of parallel stacking faults.

Numerical results are given. Consequences of the long range interaction between defects are discussed.

Dislocation Pair Interaction in a Finite Body

R. O. Scattergood and U. F. Kocks

Metallurgy Division, Argonne National Laboratory, Argonne, Illinois 60439

The elastic interaction between dislocations in a finite body shows important features not found in an infinite body. For example, two like dislocations parallel to the axis of a cylinder repel each other only when they are close, but attract each other when their distance is comparable to the cylinder radius. Contours of the pair interaction energy are given for both screw and edge dislocations in a circular cylinder.

These new features appear not only when free surface conditions are demanded on the entire body, but even when approximate stress fields are used that demand some surface tractions, so long as no torques are transmitted through the body.

The relevant torques (bending moments) associated with an edge dislocation in a circular cylinder, which vanish when the mantle is traction free, may be made to vanish in general by a simple modification of the stress field of the edge dislocation.

Dislocation Radiation

R. O. Schwenker and A. V. Granato

Department of Physics, University of Illinois, Urbana, Illinois 61801

Thin walls of mobile dislocations have been produced. These can be excited to emit macroscopic plane sound waves. Calculations have been made to predict the properties of the reradiated waves on the basis of a vibrating string model which neglects dislocation interactions. Measurements of the relative modulus change $\Delta G/G$ and the decrement Δ (real and imaginary part of the response) as a function of frequency permit a check of the Kramers-Kronig dispersion relations. In addition, measurements of the amplitude of the reradiated wave provide another check since the amplitude is proportional to $[(\Delta G/G)^2 + (\Delta/\pi)^2]^{1/2}$.

Dragging Forces on Moving Defects by Strain-Field Phonon Scattering

A. Seeger and H. Engelke

Max-Planck-Institut für Metallforschung, Institut für Physik, Stuttgart, and Institut für Theoretische und Angewandte Physik der Universität, Stuttgart, Germany

An expression for the dragging force on a uniformly moving defect by scattering of phonons at its strain-field has been derived using nonlinear elasticity theory. The quantization procedures and the formulation of the master equation for the phonon distribution follow the techniques developed in the theory of heat conductivity. Numerical calculations have been performed for kinks in screw dislocations in copper. A comparison with numerical results obtained in the theory of heat conductivity shows quite good agreement. The formalism developed should prove useful also for calculations of the electron drag on dislocations in metals.

Screw Dislocations inn Inhomogeneous Solids

G. P. Sendeckyj

School of Engineering, Case Western Reserve University, Cleveland, Ohio 44106

The problem of screw dislocations interactıng with free surfaces and inhomogeneities is reconsidered and a general method is presented for solving a large class of screw dislocation problems. The method is based on knowledge of certain general solutions in the theory of antiplane deformation of elastic solids. It can be shown that all the known screw dislocation solutions for solids undergoing antiplane deformation can be found by using thiss approach.

As an illustration of the method, three new solutions for screw dislocations near inhomogeneities are given. These are the screw dislocation near 1) an elastic elliptic cylindrical inclusion, 2) two circular cylindrical inclusions, and 3) a *curvilinear* cavity or rigid inclusion. The interaction energy between the dislocation and the inhomogeneities is also computed.

A Geometric Foundation for the Kinematics of the Imperfect Continuum

John A. Simmons

Metallurgy Division, National Bureau of Standards, Washington, D.C. 20234

This investigation is concerned with the foundations of the geometry of a continuum approximation to the deformation of an imperfect crystalline solid.

A method of formulating the infinitesimal deformation of a system of particles based on an averaging process is developed. This formulation is based on the construction of a "polyhedral mesh" valid for any system of particles whether or not they lie in a lattice configuration. When the particles lie in a perfect lattice configuration, the mesh formalism is shown to reproduce the kinematics of a classical elastic continuum. If the lattice configuration is not perfect two alternate kinematic descriptions in terms of space-time affine connections are derived by the averaging process. The simpler produces a curvature free formalism corresponding to the distant parallelism formulation of Bilby et al. This formulation is seen to be appropriate when the local elastic energy density is essentially determined by the averaged local lattice distortion such as might be expected in non-polygonized single crystals. The second kinematic description produces an averaged local lattice distortion together with a measure of dispersion of this distortion. This gives rise to a dynamic affine connection with curvature. This type of description is seen to be more appropriate to polycrystalline and polygonized single crystalline materials.

Using these results, the concept of infinitesimal plastic transformation is formulated and it is shown that by assuming the initial state of the material to be described by a spatial affine connection, the entire dynamic description of the mateiral deformation is then given by a four dimensional space-time affine connection whose invariants together with the integrated strain define the state of the material. Equations of continuity for plastic as well as for ordinary elastic deformation are derived. The exterior calculus of E. Cartan is utilized in this section to simplify the computations.

Internal Stress and the Incompatibility Problem in Infinite Anisotropic Elasticity

John A. Simmons

Metallurgy Division, National Bureau of Standards, Washington, D.C. 20234

and

R. Bullough

Theoretical Physics Division, A.E.R.E., Harwell, Didcot, Berkshire, England

Using the language of projection operators, the elastic distortion field of a linear infinite anisotropic body is decomposed into its internal and external components. The kernel of the external projection operator is identified as the elastic field due to force dipoles while that of the internal field corresponds to internal distortion fields due to displacement dipoles.

By integration of the projection operator for the internal distortion field, an alternative description for internal distortion fields in terms of dislocations is given. The Mura-Willis formula as well as the distortion field due to a rational dislocation element (in the sense of Eshelby and Laub) for an anisotropic body are then obtained as integrals of the basic displacement dipole kernel for internal distortions.

Further integration of the displacement dipole kernel provides a description of the internal distortion field due to a rational incompatibility element. The general formula for the stress function due to an incompatibility distribution in a general infinite anisotorpic body is then given and shown to reduce to the formulation given by Kröner for isotropic bodies.

Finally, explicit methods to compute kernels for internal distortions due to incompatibilites are given and discussed.

The Behavior or an Elastic Solid Containing Distributions of Free and Fixed Dislocations

E. Smith

Department of Metallurgy, University of Manchester, England

There are many situations in metal physics where the stresses acting on fixed dislocations have an important bearing on a physical phenomenon, and the paper derives a general expression relating these stresses when fixed edge dislocations are contained within an infinite elastic solid in which there are also free edge dislocations that occupy equilibrium positions.

Special cases are considered in detail, particular attention being given to the situation where all the dislocations are of the same type, the free ones having identical Burgers vectors b while there are two fixed dislocations with Burgers vectors pb and gb; all the dislocations lie in the same plane within an infinite solid. This is the most general model for which the stresses on each dislocation and also the equilibrium positions of the free dislocations may be determined analytically. It is indicated how the model degenerates into all the others that have been discussed analytically in terms of classic polynomial functions.

The results are briefly discussed in relation to the problem of cleavage crack nucleation in crystalline solids.

356-078 O-69—7

The Elastic Generalized Cosserat Continuum with Incompatible Strains

Rastko Stojanović

Department of Mechanics, University of Belgrade, Yougoslavia

Considered is a continuum with deformable directors. Dislocations are regarded as sources of incompatibilities and internal strains. Established are the relations between the dislocation density tensor and the gradients of directors. The conservation law for dislocations (i.e. the law that the dislocation lines cannot end inside a body) appears as the integrability condition for the dislocation density – gradients of directors relation. In a linearly connected space L_3 in which the directors of a dislocated medium represent fields of absolutely parallel vectors the equality of the dislocation density tensor with the torsion tensor of the space L_3 follows as an immediate consequence. It is also proved that the geometry of L_3 is equivalent to the geometry of the linearly connected space L_3 which is defined in terms of the distorsions, introduced in the theories based on the non-oriented continuum models. From the principle of virtual work are derived the general (non-linear) relations for stress and hyperstress. The stress tensor is not symmetric. In the appendix are presented the modified divergence theorem and the expressions for the variations of the gradients of directors in the absence of a displacement field, i.e., in the case when the compatibility conditions for the strain tensor are not satisfied.

The Broadening of Resonance Lines by Dislocations

A. M. Stoneham

Theoretical Physics Division, A.E.R.E., Harwell, Didcot, England and Coordinated Science Laboratory, University of Illinois, Urbana, Illinois 61801

Dislocations and other defects in solids broaden sharp resonance lines in solids, such as spin resonance and optical zero phonon lines. The broadening is a result of the random strain fields produced, and the shape of the resonance line is a measure of the distribution of internal strains. Measurement of line shapes can give information which is different from that given by the more usual mechanical and transport studies of dislocations. We calculate the shapes of the resonance lines in terms of the properties of the individual defects which cause broadening, their density and their statistical distribution. The theory is applied to straight dislocations, infinitesimal loops, dislocation dipoles and to point defects.

Effect of Zero-Point Motion on Peierls Stress

H. Suzuki

Department of Physics, Faculty of Science, University of Tokyo, Bunkyo-ku, Tokyo, Japan

Calculations of the Peierls stress hitherto made are criticized and the following conclusions are obtained. The significant difference in Peierls stress between different materials arises mainly from the difference in crystal structures. The Peierls stress is necessarily high in a rectangular lattice where atoms just above and below the slip plane face each other, while in the lattices where the atoms face alternately along the slip plane it is of the order of one percent of that in the rectangular lattice. The Peierls stress in the body-centered cubic crystal is, however, rather high for a screw dislocation owing to the screw structure of this crystal with the axes parallel to [111] direction. The calculated Peierls

stresses are several times of those expected from experiments. The zero-point motion decreases the calculated Peierls stress through two mechanisms. The one is the difference in frequency spectrum of a dislocation line at the bottom of the potential valley and at the top of the potential hill. The other is due to the change in spring constants of atom pairs around the dislocation through anharmonicity.

A Dynamic Theory of Dislocations and its Applications to the Theory of the Elastic-Plastic Continuum

C. Teodosiu*

Max-Planck-Institut für Metallforschung, Institut für Physik, Stuttgart, and Institut für Theoretische und Angewandte Physik der Universität, Stuttgart, Germany

The starting point of this study is a paper by Kröner (J. Math. Phys., **42**, p. 27, 1963), who proposed the replacement of the loading history variables in the yield criterion and in the work-hardening equation by state variables, such as the dislocation density and the density of dislocation loops.

The first part of the work summarizes the formulation recently given by the author for the dynamic non-linear theory of dislocations in anisotropic media. The relations connecting the continuum kinematic quantities to the discrete dislocation arrangement and to the dislocation velocities are emphasized.

To construct a theory of the elasto-plasticity, the system of kinematic equations is completed by postulating a yield condition and a work-hardening equation, which contain as independent variables the stress, the dislocation density, the density of dislocation loops, and the temperature.

Making constitutive assumptions for the free energy, the specific entropy, and the heat conduction vector, and using the principle of material indifference and the thermophysical restrictions, a definite theory of the elastic-plastic continuum is obtained.

Non-Linear Dynamic Problems for Anisotropic Elastic Bodies in the Continuum Theory of Dislocations

C. Teodosiu* and A. Seeger

Max-Planck-Institut für Metallforschung, Institut für Physik, Stuttgart, and Institut für Theoretische und Angewandte Physik der Universität, Stuttgart, Germany

The non-linear continuum theory of dislocations has been used to solve a number of problems for *isotropic* materials, including the determination of stresses produced by dislocations, the scattering of elastic waves by straight dislocations and kinks, and the small-angle scattering of X-rays by dislocation lines and rings. For the application of these results it is necessary to know the elastic constants of third or higher order entering the constitutive equations. Third-order elastic constants have recently become available for a large class of single crystals with an accuracy that exceeds considerably the earlier polycrystalline data. It appears therefore desirable to develop a formulation of the theory that may be applied to *anisotropic* materials.

The present work aims at developing approximate methods for solving non-linear problems such as the determination of the strains produced by stationary or uniformly moving dislocations in anisotropic media and of their effects on a superimposed infinitesimal motion.

The non-linear problems are solved by reduction to a series of linear problems using expansions in terms of small parameters. Three such parameters appear naturally: the magnitude of the distortion produced by dislocations, the magnitude of the deformation gradient of the superimposed motion, and the ratio between the dislocation and sound velocities. To obtain definite approximation algorithms, hypotheses concerning the relative order of magnitude of these three parameters are introduced.

*Permanent address: Center of Mechanics of Solids, Str. Constantin Mille 15, Bucharest, Romania

Kinks, Vacancies, and Screw Dislocations

Robb M. Thomson

Department of Materials Science, State University of New York at Stony Brook, Stony Brook, New York 11790

A vacancy on a nonsplit pure screw dislocation can dissociate into a set of kinks. This dissociation is demonstrated geometrically for the NaCl lattice, showing that no geometrical constraints are violated by the dissociation. The kinks thus generated also splinter and spread the charge of the vacancy along the line. The effective vacancy association energy on the line is thus much higher than has been supposed hitherto, and is partly due to the delocalization of the charge singularity of the point defect and partly due to the delocalization of elastic singularity. When the Peierls energy is low, the vacancy will always dissociate, while if it is high, the dissociation will occur only when the total kink energy is less than the vacancy energy. Vacancy contributions to both climb and pipe diffusion are discussed in terms of the kink dissociation process. Results are that interstitial pipe diffusion is entirely summetric to vacancy pipe diffusion, no motion energy is needed, and the formation energy for diffusion is related to the Peierls energy.

Theory of Surface States on Stacking Faults

Robb M. Thomson

Department of Materials Science, State University of New York at Stony Brook, Stony Brook, New York 11790

The Slater-Koster method in the Bloch representation is applied to a model for a stacking fault in an idealized crystal leading to a type of Shockley surface state. A series expansion is obtained for the energy which is worked out for the simplified case of a constant matrix element, with the result that for a tight binding nonoverlapping band, there are surface waves which split off from both the top and bottom of the band. Contrary to Shockley's results for external surfaces, and to the Slater-Koster theory of the localized impurity, localized states occur on the stacking fault for a single nonoverlapping band and for arbitrary potential values. A constant matrix approximation is worked out for the case of the simple metals.

The Elastic Interaction Between Grain Boundaries and Screw Dislocation Pile-Ups

M. O. Tucker

Department of Physics, University of Surrey, Guildford, Surrey, England

The configuration of an array of parallel infinitive straight screw dislocations, in equilibrium under a constant applied stress, and pile-up on a plane inclined to a grain boundary at an arbitrary angle is considered. The model used for the grain boundary is the plane interface between two elastically anisotropic half-spaces welded together. Using this approximation of a continuous distribution of infintesimal dislocations the integral equation expressing the equilibrium conditions is solved using a Wiener-Hopf technique and approximate expressions are presented for the stresses near to the tip of the array when the dislocations are parallel to orthotropic symmetry axes in each half-crystal.

On the Thermodynamics of Inhomogeneous Bodies

C.-C. Wang

Department of Mathematical Sciences, Rice University, Houston, Texas 77001

This paper concerns the thermodynamics of inhomogeneous elastic bodies. I adopt the constitutive equations for thermoelastic materials given by Coleman & Noll (1963) and develop a theory for bodies made up of such materials. The general scheme of this theory is based on my paper on Generalized Simple Bodies (1969). The main result is the explicit field equations for the deformation and the temperature on a thermoelastic body.

Subsonic, Supersonic, and Transonic Dislocations Moving on an Interface Separating Two Media of Differing Elastic Properties

J. Weertman, H. M. Berg, J. E. Bloom, H. Ishii, R. H. Marion, D. E. Pease, D. T. Spreng, and J. B. Vander Sande*

Materials Science Department and Materials Research Center, Northwestern University, Evanston, Illinois 60201

This paper examines the problem of a dislocation moving on an interface separating two isotropic elastic media that have differing elastic constants and densities. This problem has application to the phenomenon of diffusionless transformations. Solutions are found for moving screw dislocations, gliding edge dislocations, and climbing edge dislocations. It is assumed that the dislocation velocity lies in either the subsonic, the transonic, or the supersonic velocity region. We have generalized the analysis that was used in a study of the elastic displacements and stress field of subsonic, transonic, and supersonic dislocations moving in an ordinary elastic medium. The results given in the present paper are formally identical to those obtained in that simpler analysis.

Thermal Energy Trapping by Moving Dislocations

J. H. Weiner

Division of Engineering, Brown University, Providence, R. I. 02912

The steady motion of a dislocation along a piece-wise harmonic Frenkel-Kontorowa model is considered. For suitable model parameters there is one localized mode associated with either the stable or unstable dislocation configuration and the remaining modes are non-localized or extended. Because of the piece-wise harmonic character of the model, the set of normal modes of the system changes at discrete instants of time, referred to as transition times, as the dislocation moves along the chain. In particular, the localized modes must move along with the dislocation position and we refer to the localized mode momentum and energy as the dislocation momentum and energy respectively. The particle momentum and energy due to the sum of the extended modes is termed thermal.

At the transition times, it is necessary to expand atomic velocities in terms of the new set of modes appropriate to the forthcoming state of the crystal. It is found that a coordination effect exists between the transition times and the thermal motion such that on the average over many transitions, thermal momentum in the direction of the dislocation motion is transferred to the dislocation momentum.

*Instructor and students of Advanced Dislocation Class at Northwestern University.

The Mean Square Stresses $\langle\sigma^2\rangle$ for a Completely Random and a Restrictedly Random Distribution of Dislocations in a Cylindrical Body

M. Wilkens

Max-Planck-Institut für Metallforschung, Institut für Physik, Stuttgart, Germany

The paper gives a full proof of the author's earlier statement according to which the elastic interaction energy of completely randomly distributed dislocations vanishes. As a consequence the outer cut-off radius in the logarithmic factor of the elastic energy coincides with the external cylinder radius rather than with the mean dislocation spacing. The proof takes into account the elastomechanical boundary conditions which were neglected in the earlier paper. Further it is shown that for a restrictedly random distribution the outer cut-off radius is equivalent to the radius of the areas small compared with the cylinder cross-section, each of which contains the same number of dislocations randomly distributed over the corresponding area. In the special case that each area contains only one dislocation with arbitrary inside the outer cut-off radius degenerates to the mean dislocation spacing.

Theoretical Aspects of Kinematical X-Ray Diffraction Profiles from Crystals Containing Dislocation Distributions

M. Wilkens

Max-Planck-Institut für Metallforschung, Institut für Physik, Stuttgart, Germany

The paper deals with a theoretical study of the Fourier transorm of the X-ray diffraction line profiles from crystals containing dislocation distributions. The theory is based mainly on a calculation of spatial averages of powers of the strains ϵ_n, where ϵ_n means the differential strain perpendicular to the reflecting planes averaged over a certain length n (n = variable of the Fourier transform). The second power average $\langle\epsilon_n^2\rangle$ is calculated in a closed form for a restrictedly random dislocation distribution. However, the result is approximately valid also for other distributions. The contributions of the averages of higher powers of ϵ_n are taken into account in an approximate manner. The expression derived for the Fourier transform depends on the two parameters ρ and R_e, where ρ is the dislocation density. R_e is equivalent to the effective outer cut-off radius which appears for instance in the logarithmic factor of the elastically stored energy. The result which is applicable for $R_e \geq \rho^{-1/2}$ is discussed in comparison with the theory of Krivoglaz and Ryaboshapka, in which a completely random dislocation distribution is assumed, and with the theory of diffraction from distorted crystals mainly developed by Warren and Averbach.

Structural and Elastic Properties of Zonal Twin Dislocations in Anisotropic Crystals

M. H. Yoo and B. T. M. Loh

Metals and Ceramics Division, Oak Ridge National Laboratory, Oak Ridge, Tennessee 37830

A descriptive definition of zonal twin dislocations for compound twin systems is given based on the well-established rational crystallographic elements. Geometric characteristics of zonal twin dislocations in double lattice structures are thoroughly discussed. Equilibrium shapes of an incoherent twin boundary have been analyzed by using the anisotropic elastic properties of edge dislocations. Short-ranged structural properties of zonal twin dislocations are discussed based on a Peierls-Nabarro model. It is found that the "anisotropic parameter," K_eS_{66}, correctly predicts the active mode of crystallographically non-equivalent conjugate twin systems.

JOURNAL OF RESEARCH of the National Bureau of Standards—Physics and Chemistry
Vol. 73A, No. 5, September–October 1969

Publications of the National Bureau of Standards*

Selected Abstracts

Bortner, M. H., **A review of rate constants of selected reactions of interest in re-entry flow fields in the atmosphere,** *Nat. Bur. Stand. (U.S.), Tech. Note 484, 62 pages (May 1969), 60 cents.*
The major reactions normally encountered in flow field re-entry calculations for the oxygen nitrogen system are reviewed and a rate constant value for each reaction is recommended. Collisional ionization processes, charge exchange reactions and attachment-detachment reactions are included. Rate constant coefficients to fit the equation $k = aT^b e^{-c/T}$ are reported in tabular form for the selected rate constant. The data are also graphed as log k vs T(K). In all, over twenty forward and reverse reactions are reviewed. Additionally, a large number of rate constant values for reactions which also effect flow field calculations are given.

Key words: Attachment-detachment reaction; charge exchange reaction; collisional ionization reaction; evaluated rate constants; flow field kinetics; O_2-N_2 systems.

Franklin, J. L., Dillard, J. G., Rosenstock, H. M., Herron, J. T., Draxl, K., Field, F. H., **Ionization potentials, apperance potentials, and heats of formation of gaseous positive ions,** *Nat. Stand. Ref. Data. Ser., Nat. Bur. Stand. (U.S.), 26, 289 pages (June 1969), $4.00.*
This is a compilation of ionization and appearance potentials of positive ions published from 1955 through June 1966. The compilation lists the ion formed, the parent species from which it was formed, the other products of the process, the threshold energy for the formation of this ion, and the method by which this data was obtained. Where feasible, the heat of formation at 298 K of the positive ion has been computed for each entry using auxiliary thermochemical data. From these computed values "best" values have been chosen.

Key words: Appearance potential; compilation; data; heat of formation; ionization potential; ions; positive ions.

Koeser, R. L., Editor, **Report of the 53d National Conference on Weights and Measures, 1969,** *Nat. Bur. Stand. (U.S.), Spec. Publ. 311, 182 pages (Mar. 1969), $1.25.*
This is a report of the proceedings (edited) of the Fifty-third National Conference on Weights and Measures, sponsored by the National Bureau of Standards, held in Washington, D.C., June 17–21, 1968 and attended by State, county, and city weights and measures officials and representatives of the Federal Government, business, industry, railroads, and associations.

Key words: Conference, weights and measures—laws; weights and measures—regulations; weights and measures—technical requirements; weights and measures—history; weights and measures.

LaFleur, P. D., Editor, **Activation Analysis Section: Summary of activities July 1967 to June 1968,** *Nat. Bur. Stand. (U.S.), Tech. Note 458, 109 pages (Mar. 1969), $1.00.*
The facilities used by the reactor, LINAC and neutron generator groups for activation analysis are described. Proposed installation of four new irradiation terminals and a new pneumatic transfer tube system are outlined.
A new 2.5-mA neutron generator has been installed and the biological shield, pneumatic transfer system and the detector assembly modified. Studies of blank problems for oxygen determination and self-absorption corrections in photopeak analysis have resulted in greatly improved precision for Standard Reference Materals. Halide in photographic emulsions, using 14-MeV and 2.6-MeV neutrons, have been determined.
Considerable emphasis has been placed on the development of group radiochemical separations, SRM steel and high purity zinc samples have been analyzed using this technique.
Eighteen different SRMs were analyzed for a variety of elements and a variety of service analyses were performed.
The self-absorption effects of the matrix on irradiation photons were studied and calculations of sensitivities for photon activation analysis were made. Carbon in sulfur, yttrium in rare earth oxides and oxygen in sodium were determined by photon activation.
The extraction of metals by bis(2-ethylhexyl) orthophosphoric acid has been studied, and distribution coefficients are given for many of the transition metals. The results indicate enhanced applicability of this reagent for radiochemical separations.
Updated keys for computer literature searching and a sample output are included.

Key words: Activation analysis; Cockcroft-Walton neutron generator; computer literature searching; extraction; group separations; homogeneity testing; hydrogen bis(2-ethylhexyl) phosphate; matrix effect, molybdenum, NBS LINAC, NBS reactor, photon activation analysis sensitivities; Standard Reference Materials; zinc.

Lee, R. D., **Construction and operation of a simple high-precision copper-point blackbody and furnace,** *Nat. Bur. Stand. (U.S.), Tech. Note 483, 16 pages (May 1969), 30 cents.*
Detailed instructions for the construction and operation of an inexpensive copper-point blackbody and furnace are presented. Such a source may be expected to realize the radiance temperature of 1083.3°C (Int. 48) with an uncertainty of 0.2°C and a variation in successive use of less than 0.33°C. The furnace requires no inert gas or vacuum and utilizes only 225 watts to reach a melt in about an hour after turn on. Melts and freezes last about five minutes each and at least fifty melts and freezes are expected during the lifetime of the furnace.

Key words: Blackbody; optical pyrometry; radiometry.

Mason, H. L., Editor, **Making valuable measurements. Proceedings of the 1968 Standards Laboratory Conference,** *Nat. Bur. Stand. (U.S.), Spec. Publ. 313, 177 pages (May 1969), $1.50.*
The National Conference of Standards Laboratories is a nonprofit, laboratory-oriented organization whose purpose is to promote cooperative efforts toward solving the common problems faced by standards laboratories in their organization and operation. Established in 1961 under the sponsorship of the National Bureau of Standards, NCSL has a membership of more than 200 organizations. Three biennial national meetings have been held previously as well as a number of specialized regional workshops.
The theme of the 1968 Standards Laboratory Conference is "Making Valuable Measurements." The papers presented will attempt to answer the Who? When? Where? How? and Why? of making valuable measurements. The conference provides an opportunity for discussion of problems confronting laboratory managers and calibration personnel.
Representatives of member organizations of the National Conference of Standards Laboratories met at the Boulder facility of the National Bureau of Standards August 25–29, 1968. Major addresses were

given by A. V. Astin and J. L. Sloop. Reports and discussions at eight sessions covered the management of valuable measurements: the management of equipment and data, measurement agreement comparisons, international practices, Defense Department activities, NBS activities. NCSL liaison, and NCSL committee work.

Key words: Metrology management; National Conference of Standard Laboratories; physical measurement.

Rapial, A. S., Daney, D. E., **Preparation and characterization of slush hydrogen and nitrogen gels,** *Nat. Bur. Stand. (U.S.), Tech. Note 378, 43 pages (May 1969), 50 cents.*
An experimental apparatus has been developed for the gelation of slush hydrogen, and slush hydrogen was gelled for the first time. Measurements of the weight-bearing capacity of the gel as a function of mass percent gelant were made for liquid and slush nitrogen and hydrogen. These measurements verify the simple models discussed here for gelled liquid and slush within the experimental accuracy; the models predict a reduction in gelant concentration from 38 mass percent to 25 mass percent in going from Normal Boiling Point liquid hydrogen to slush hydrogen of 0.40 solid fraction for the silica gelant used in this work. Reduction in the mass percent gelant for other gelants should be similar.

Key words: Gels; liquid hydrogen gels; liquid nitrogen gels; liquid-solid hydrogen mixtures; rocket propellants; slush hydrogen; slush hydrogen gels; slush nitrogen gels.

Roberts, B. W., **Superconductive materials and some of their properties,** *Nat. Bur. Stand. (U.S.), Tech. Note 482, 129 pages (May 1969), $1.25 Supersedes and extends Tech. Note 408.*
This is a noncritical compilation of data on superconductive materials that has been extracted from a portion of the literature published up to early 1968. The properties concerned are composition, critical temperature, critical magnetic field, crystallographic data, and lowest temperature tested for superconductivity. The compilation also includes, bibliography, general reference review articles and a special tabulation of high magnetic field superconductors.

Key words: Bibliography; compilation of data; composition; critical field; critical temperature; crystallographic data; low temperature; superconductivity.

Sindt, C. F., Ludtke, P. R., Daney, D. E., **Slush hydrogen fluid characterization and instrumentation,** *Nat. Bur. Stand. (U.S.), Tech. Note 377, 69 pages (Feb. 1969), 65 cents.*
Areas of the slush hydrogen fluid characterization program covered are production, transfer, and storage of liquid-solid mixtures.
An experiment has been performed in which a second component was added to liquid hydrogen to determine the effect on the size of the solid particles produced by the freeze-thaw method. Also, an experiment performed with 4.4% oxygen in nitrogen resulted in particles an order of magnitude smaller in size than those normally observed in freeze-thaw production of pure nitrogen slush.
The friction angle of settled solids of slush hydrogen on several metals was determined for surface finishes ranging from 2 to 110 micro-inches rms. The angle at which solids slide from the surface was found tp be a function of the surface finish.
Data were taken in the flow loop over a range of velocities from 1.5 to 40 ft/sec (0.46 to 12.2 m/s). The friction losses determined from the flow data are compared to losses predicted for Newtonian fluids. Losses with slush of solid fractions from 0.1 to 0.4 were found to be lower than with triple-point liquid hydrogen at the higher Reynolds numbers.
Liquid-solid mixtures of hydrogen with solid fraction of 0.5 were transferred through three types of flow restrictions. The restrictions were a globe valve, an orifice, and a venturi. Losses through the restrictions were essentially the same with the high solid fraction slush as with triple-point liquid.
A brief review of the pumping characteristics of slush hydrogen is presented. A comparison of developed head, efficiency, cavitation constant, and net positive suction head is discussed.
Gelling of slush hydrogen with pyrogenic silica was accomplished with solid fractions from 0 to 0.2. The amount of gelling agent required to gel slush was found to be proportional to the liquid volume of the slush.

Key words: Friction angle; crypgenic; flow restrictions; gel; liquid-solid mixtures; particle size; plug flow; slurry flow; slush hydrogen.

Taggart, H. E., Workman, J. L., **Calibration principles and procedures for field strength meters 30 (Hz to 1 GHz),** *Nat. Bur. Stand. (U.S.), Tech. Note 370, 157 pages (Mar. 1969), $1.25.*
The National Bureau of Standards has been calibrating many types of field strength meters and their related antennas at frequencies up to 1000 MHz for several years. Various techniques of measurement have been investigated regarding accuracy, calibration time, ease of operation, and reliability. This report discusses some of these calibration techniques in detail, and in some cases lists step-by-step procedures for performing the complete calibration. Typical calibration data are used to take the reader from the beginning of the calibration to the completed test report. All measurement setups are clearly illustrated, listing the equipment necessary to perform the calibration. Methods of calibrating two basic types of antennas are described: (1) the loop antenna at frequencies from 30 Hz to 30 MHz and (2) half-wavelength dipole antennas from 30 to 1000 MHz. Two methods of calibrating loop antennas are discussed in detail, the standard-field method and the injection method. The standard-antenna method of calibrating dipole antennas is fully described. Measurement uncertainties of various methods are discussed. This report was written to help technical personnel actively participate in antenna calibration work. Hopefully this information will help people to set up new calibration services and to improve existing calibrating facilities.

Key words: Calibration Procedures, Field Strength Meters, Loop Antennas, Dipole Antennas.

Wachtman, J. B., Jr., Editor, **Mechanical and thermal properties of ceramics. Proceedings of a symposium Gaithersburg, Md., April 1–2, 1968,** *Nat Bur. Stand. (U.S.), Spec. Publ. 303, 266 pages (May 1969), $4.25.*
The proceedings of the Symposium on Mechanical and Thermal Properties of Ceramics, held at the National Bureau of Standards in Gaithersburg, Maryland, on April 1–2, 1968, are presented. The symposium was cosponsored by the American Ceramic Society, the American Society for Testing and Materials, and the National Bureau of Standards. Attention was concentrated upon properties primarily of structural and/or high temperature use including melting points, thermal expansion, thermal conductivity, thermal radiation properties, elasticity, viscoelasticity, inelastic deformation, and fracture. The dependence of these properties upon composition and microstructure was surveyed and the importance of controlling these features of character to insure reliability of ceramics was emphasized. The procedures by which American ceramists formulate standards and specifications to assist in insuring reliability were summarized.

Key words: Ceramics; elasticity; fracture; inelastic deformation; melting point; standards; thermal conductivity; thermal expansion; thermal radiation; viscoelasticity.

Acquista, N., Abramowitz, S., Lide, D. R., **Structure of the alkali hydroxides. II. The infrared spectra of matrix isolated CsOH and CsOD,** *J. Chem. Phys.* **49,** *No. 2, 780–782 (July 15, 1968).*
The infrared spectra of matrix isolated CsOH and CsOD have been observed. Both the CsO stretching mode and the bending mode have been assigned for each isotopic species. ν_1 of CsOH is at 335.6 cm^{-1}, while a value of 330.5 cm^{-1} is found for CsOD. ν_2 is found at 306 cm^{-1} for CsOH and at 226 cm^{-1} for CsOD. The isotope shift observed for ν_2 confirms the essentially linear structure which was indicated by the microwave spectrum.

Key words: CsOH; high temperature; vibrational assignment; molecular geometry; infrared.

Amano, T., Saito, S., Hirota, E., Morino, Y., Johnson, D. R., Powell, F. X., **Microwave spectrum of the ClO radical,** *J. Mol. Spectry.* **30,** *No. 2, 275–289 (May 1969).*
Rotational transitions in the $^2\Pi_{3/2}$ and $^2\Pi_{1/2}$ electronic states have been investigated for both the ^{35}ClO and ^{37}ClO radicals by means of Stark modulated microwave spectrometers. Improved values were obtained for the rotational constants, Λ-doubling parameter and

hyperfine constants of both radicals. It was found necessary to consider the effect of centrifugal distortion in order to determine the dependence of the spin-orbit coupling constant A on the internuclear distance. The distortion constant D_e was found to be 0.077 ±0.016 MHz and the value of $A'=(r\ dA/dr)$ at the equilibrium internuclear distance was 320±60 cm^{-1}, assuming a value for A determined from electron-paramagnetic-resonance data.
The equilibrium internuclear distance r_e was calculated to be 1.569±0.001 Å from the rotational constants B_0 for ^{35}ClO and ^{37}ClO. A detailed analysis of the second order Stark effect of the $F=0\leftarrow 1$ and $F=1\leftarrow 1$ components of the upper series of the $J=3/2\leftarrow 1/2$ rotational transition in the $^2\Pi_{1/2}$ state of ^{35}ClO was performed and the electric dipole moment was determined to be 1.239±0.010 D. This value was confirmed for the $^2\Pi_{3/2}$ state of ^{35}ClO where the Stark effect is first-order for weak electric fields. The indicated uncertainties are three times the standard errors of the reported value.

Key words: Chlorine monoxide; free radical; hyperfine structure; microwave spectrum; rotational transitions; Stark effect.

Bennett, H. S., **Phenomenology of neutron scattering in Heisenberg systems,** *Phys. Rev.* **176,** *No. 2, 650–654 (Dec. 10, 1968).*
The critical magnetic scattering of neutrons from Heisenberg systems is discussed within the rigorous framework of spectral representations for the longitudinal and transverse spectral weight functions, low order moments of these functions, and their sum rules. The spectral weight functions are expressed as functionals of longitudinal and transverse diffusivities. This exact framework leads naturally to a two parameter phenomenological description of the neutron scattering cross section in Heisenberg ferromagnets. It is shown that replacing the diffusivities by two parameter Gaussian functions, which satisfy the first two sum rules, gives reasonable values for the neutron scattering cross section in ferromagnets.

Key words: Critical magnetic scattering; diffusivity; Heisenberg magnets; neutron cross section.

Birmingham, B. W., Flynn, T. M., **National programs and the compressed gas industry,** *(Proc. 55th Annual Meeting of the Compressed Gas Association, New York City, N.Y., Jan. 1968), Chapter in The Future of the Compressed Gas Industry, pp. 39–49 (Compressed Gas Assoc. Inc., New York, N.Y., 1969).*
The object is to discuss a segment of the compressed gas industry, namely the cryogenic industry, and its relation to selected national programs, such as space, health, agriculture, transportation, conservation, and education.

Key words: Agriculture; compressed gases; conservation; cryogenics; education; health; national goals; space; transportation.

Boutillon, M., Henry, W. H., Lamperti, P. J., **Comparison of exposure standards in the 10–50 kV X-ray region,** *Metrologia* **5,** *No. 1, 1–11 (Jan. 1969).*
Direct comparisons of the low-energy x-ray exposure standards of the International Bureau of Weights and Measures (BIPM) and the National Research Council of Canada (NRC), the BIPM and the National Bureau of Standards of the U.S.A. (NBS), were made, using X rays generated by 10, 30, and 50 kilovolts. The half-value layers for these qualities of radiation were 0.03_6, 0.17_6, and 2.25_7 mm aluminum respectively. The results indicate that a direct comparison between two free-air chambers, in the low-energy X-ray region, can be precise to better than 0.3 percent. The uncertainties and errors in the geometric and correction factors used for the comparison measurements, as well as other systematic and statistical errors, were examined in detail and are reported. The results of preliminary work on the definition of the quality of radiation, air attenuation correction, diaphragm comparisons and saturation correction are included.

Key words: Exposure standards; low-energy x rays; direct comparison; correction factors; air attenuation; analysis of uncertainties.

Cassidy, E. C., Cones, H. N., Wunsch, D. C., Booker, S. R., **Calibration of a Kerr cell system for high-voltage pulse measurements,** *IEEE Trans. Instr. Meas.* **IM–17,** *No. 4, 313–320 (Dec. 1968).*
Several techniques for calibration of an electro-optical (Kerr cell) high voltage pulse measuring system are described. Independent calibrations, without reference to pulse divider measurements, are achieved by application of a direct bias voltage to the Kerr cell. After calibration, experiments with voltages as high as 100 kV demonstrate reasonable agreement (to within 1%) between simultaneous Kerr cell and calibrated pulse divider measurements.

Key words: High voltage measurements; pulse measurements; Kerr cell; electro-optical measurements.

Clark, H. E., Young, R. D., **Field emission through single strontium atoms adsorbed on a tungsten surface,** *Surfac Sci.* **12,** *385–389 (1968).*
Measurements of the total-energy distribution and current-voltage characteristics (Fowler-Nordheim curves) are reported for electron emmission through single strontium adatoms. A number of interpretations of these data are considered; resonance tunneling appears to be the most satisfactory.

Key words: Adsorption; energy distribution; field emission; Fowler-Nordheim curves; resonance tunneling; strontium; tungsten.

Czyz, W., Maximon, L. C., **High energy, small angle elastic scattering of strongly interacting composite particles,** *Ann. Phys.* **52,** *No. 1, 59–121 (Mar. 1969).*
Starting from a simple-minded formulation of the Glauber model of the high energy multiple scattering of strongly interacting composite particles, several generalizations and limiting expressions are derived from the elastic scattering amplitudes at small scattering angles. An extensive discussion of the many possible applications to nucleon-nucleus, nucleus-nucleus and other composite hadron elastic scattering processes is given.

Key words: Deuteron-deuteron scattering; elastic scattering; hadrons; high energy scattering; proton-nucleus scattering; strongly interacting particles.

Davis, D. D., Okabe, H., **Determination of bond dissociation energies in hydrogen cyanide. Cyanogen and cyanogen halides by the photodissociation method,** *J. Chem. Phys.* **49,** *No. 12, 5526–5531 (Dec. 15, 1968).*
The photodissociation process yielding CN $B^2\Sigma^+$ from various cyanogen compounds has been studied in the vacuum ultraviolet. Threshold energies of incident photon to produce the CN $B^2\Sigma^+$ are measured by monitoring the fluorescence due to the transition CN $B^2\Sigma^+ - X^2\Sigma^+$. The upper bounds of bond energies can be obtained from these thresholds and the electronic energy of CN $B^2\Sigma^+$. The average heat of formation of CN and its estimated overall uncertainty, $\Delta Hf_0^\circ(CN)=418\pm4$ kJ mol^{-1} (100±1 kcal mol^{-1}), is computed using these bond energies together with various ΔHf_0°. This value is within an estimated error in excellent agreement with the photoionization value recently obtained by Dibeler and Liston. The bond energies based on $\Delta Hf_0^\circ(CN)=418$ kJ mol^{-1} (100 kcal mol^{-1}) for various cyanogen compounds are D(H—CN)=497 (119), D(Cl—CN)=401 (96), D(Br—CN)=343 (82), D(I—CN)=301 (72), D(NC—CN)=531 (127), D(C—N)=765 (183) all in kJ mol^{-1} (kcal mol^{-1}) with an overall estimated error of ±4 kJ mol^{-1} (1 kcal mol^{-1}). Because of the weak fluorescence intensity, no reliable bond energy was obtained for CH_3CN. Other values obtained are D(F—CN) ≤ 464 kJ mol^{-1} (111 kcal mol^{-1}) and $\Delta Hf_0^\circ(FCN) \geq 30.9$ kJ mol^{-1} (7.4 kcal mol^{-1}). A correlation of the dissociation process with the absorption spectrum is briefly discussed. A comparison is made of bond energies obtained by the photodissociation, photoionization, and electron impact methods. Limitations of the photodissociation method to determine bond energies are discussed.

Key words: Bond dissociation energies; photodissociation; vacuum ultraviolet fluorescence; CN; HCN; FCN; ClCN; BrCN; ICN; C_2N_2.

Delaplane, R. G., Ibers, J. A., Ferraro, J. R., Rush, J. J., **Diffraction and spectroscopic studies of the cobaltic acid system $HCoO_2$—$DCoO_2$,** *J. Chem. Phys.* **50,** *No. 5, 1920–1927 (Mar. 1, 1969).*

Cobaltic acid, $HCoO_2$, and deuterated cobaltic acid, $DCoO_2$, have been prepared and studied by x-ray and neutron diffraction techniques, and by infrared spectroscopy and cold-neutron scattering. The materials crystallize in apparent space group D_{3d}^5—$R\bar{3}m$ of the trigonal system with three molecules in a hexagonal cell of dimensions: $HCoO_2$, $a = 2.851 \pm 06$], $c = 13.150 \pm 005$ Å; $DCoO_2$, $a = 2.854 \pm 001$, $c = 13.354 \pm 005$ Å. The O—O distance, as determined by neutron powder studies, of $HCoO_2$ is 2.50 ± 02 Å. On this basis and the fact that there are three O—H—O bonds along the c direction, the O—D—O distance is 2.57 ± 02 Å. Hence, the isotope effect here is as large as in the system $HCrO_2$—$DCrO_2$. Infrared studies at room temperature and at −195 °C over the region 70 to 4000 cm^{-1} may be interpreted in terms of an effectively symmetric O—H—O bond and an effectively asymmetric O—D—O bond. Although the neutron inelastic scattering measurements are not inconsistent with this interpretation, there is an intense band centered at 264 cm^{-1} in the neutron spectrum for $HCoO_2$ that remains unexplained. Model calculations, based on a two-dimensional potential function in which the asymmetric stretching frequency is coupled to the symmetric stretching frequency, were unsuccessful owing to the magnitude of the coupling term required to account for the very large isotope effect.

Key words: Cobaltic acid; crystal structure; hydrogen bond isotope effect, infrared spectra; lattice vibrations; neutron spectra; selection rules.

Deslattes, R. D., **Estimates of x-ray attenuation coefficients for the elements and their compounds,** *Acta Cryst.* **A25,** *Part 1, 89–93 (Jan. 1969).*
Some recent developments leading to improved knowledge of the distribution of oscillator strength in the photoionization continua of atoms are briefly reviewed. Selective comparisons between the experiments and calculations are indicated. Estimates for attenuation by compounds and solids, insofar as they depart from the mixture rule, require an understanding of x-ray fine structure or, at least of its limiting form, which is not yet at hand. Some of the mechanism leading to fine structure in solids and molecules are briefly reviewed.

Key words: X-ray attenuation; absorption fine structure; mixture rule.

Dibeler, V. H., Walker, J. A., **Mass spectrometric study of photoionization. XIII. Boron trichloride and diboron tetrachloride,** *Inorg. Chem.* **8,** *No. 1, 50–55 (Jan. 1969).*
Mass spectra and ion-yield curves for the molecule ions and various fragment ions of BCl_3 and B_2Cl_4 are obtained by means of a combined vacuum ultraviolet monochromator and mass spectrometer. Shapes of ion-yield curves, measured over the wavelength region from threshold to 600 Å, are discussed briefly. Ionization threshold values are used to calculate heats of formation of ions and radicals and to derive bond dissociation energies, including the boron-boron bond dissociation energy, $D_0(Cl_2B—BCl_2) = 3.80$ eV (87.6 kcal mol^{-1}).

Key words: Mass spectrometry; vacuum ultraviolet; bond dissociation energies; heats of formation; ions, radicals, BCl_3; B_2Cl_4.

Dreschsel, D., Maximon, L. C., **Potential model calculation for coplanar and noncoplanar proton-proton bremsstrahlung,** *Ann. Phys.* **49,** *No. 3, 403–444 (Oct. 1968).*
The cross section for proton-proton bremsstrahlung is calculated for both coplanar and noncoplanar events using the Hamada-Johnston and Reid (soft-core) potentials. Agreement is obtained with the experimental data for angular distributions and cross sections integrated over the photon directions. We present a detailed analysis of the kinematics, the phase space and the matrix element in the neighborhood of the kinematic limit of noncoplanarity. We find a rapid decrease of the cross section integrated over photon angles as this limit is approached. This is due, not to a strong variation of the phase space, which is essentially constant, but to the fact that near the kinematic limit for noncoplanarity of the protons, the photon is restricted to angles for which the probability for emission is small. For low energies (< 30 MeV) of the incident proton we give analytic expressions for the scattering amplitude, valid for coplanar as well as the noncoplanar events.

Key words: Proton-proton bremsstrahlung; potential model calculations; noncoplanarity; photon angular distributions; off-the-energy-shell matrix elements; low energy approximation.

Eick, J. D., Hegdahl, T., **Segregation in dental gold casting alloys,** *J. Dental Res.,* **47,** *No. 6, Part 2, 1118–1127 (Nov.–Dec. 1968).*
The purpose of this investigation was to establish a quantitative method for determining the degree of segregation in dental gold casting alloys. The electron micro-probe was employed to analyze concentration differences. A line scan was used to determine the variations in concentration present in the alloy. The nature of the segregation was expressed by the coefficient of correlation and the coefficient of variation. Segregation occurred between Ag and Cu in the Type I alloys. In the Type II and III alloys Ag and Pd segregated together and opposed Cu, while Ag, Cu, and Pt opposed Pd in the Type IV alloys. Au and Zn did not appear to segregate to a significant degree with the other elements. The coefficient of variation was used to define the degree of segregation on a quantitative basis. The degree of segregation between the fine grained alloys and coarse grained alloys of the same type was not significantly different. Pd was found to have the highest degree of segregation, while Au and Pt segregated the least. As the concentration of Cu was increased in the alloy, the degree of segregation decreased.

Key words: Dental gold alloys; composition; segregation; grain size; grain reduction; casting gold; electron micro probe.

Geltman, S., **Topics in Atomic Collision Theory,** *30, 247 pages (Academic Press Inc., New York, N.Y., 1969).*
This book is based on a course of graduate lectures given at the University of Colorado, Boulder, Colorado (U.S.A.) and at University College in London, England. It concerns the application of quantum scattering theory to low-energy atomic collision phenomena. It is divided into the three parts—static field scattering, electron-atom collisions, and atom-atom collisions—and there are ten sections in each of these parts.

Key words: Static field scattering; electron-atom collisions; atom-atom collisions.

Glasgow, A. R., Jr., Ross, G. S., **Cryoscopy, Chapter 88 in Treatise on Analytical Chemistry, Part I, Theory and Practice,** *I. M. Kolthoff, P. J. Elving, E. B. Sandell, ed., 8, 4991–5083 (Interscience Pub., New York, N.Y., 1968).*
The general principles of cryoscopy as applied to purity analysis, molecular weight determination, and phase investigation are described. The phase rule as it applies to both ideal and non-ideal solutions is discussed. The uses and descriptions of various cryoscopic apparatus are described in some detail. The use of resulting data in the calculation of melting point, sample purity, molecular weight, heat of fusion, heat capacity, and phase diagrams is discussed. The chapter primarily centers around the authors' own work in the field, but includes a bibliography of 175 references.

Key words: Calorimetry, cryoscopy, dilatometry, freezing, heat of fusion, melting, melting point, molecular weight, purity.

Gloub, S., Steiner, B., **Photodetachment of $[OH(H_2O)]^-$,** *J. Chem. Phys.* **49,** *No. 11, 5191–5192 (Dec. 1, 1968).*
The relative photodetachment cross section of $H_3O_2^-$ has been measured from threshold near 2.95 eV to 4 eV. The continuously rising cross section is consistent with detachment to a repulsive state of the neutral H_3O_2. An upper limit to the weakest bond is shown to be 1.2 eV.

Key words: Electron affinity; negative ion; photodetachment; water.

Hanley, H. J. M., McCarty, R. D., Sengers, J. V., **Density dependence of experimental transport coefficients of gases,** *J. Chem. Phys.* **50,** *No. 2, 857–870 (Jan. 15, 1969).*
We analyse experimental transport data for several gases as a function of density and temperature. Necessary conditions are proposed to check if the data are consistent with a given density function at fixed temperature. It is found that the theoretically suggested density function, which involves terms logarithmic in the density, satisfies the conditions for the data examined in the temperature

and pressure ranges considered. A power series in the density does not. Based on the analyses, first density coefficients of thermal conductivity and viscosity are reported, together with an estimate of their precision, at reduced temperatures up to $T^* \approx 30$.

Key words: Thermal conductivity; viscosity; density dependence; correlation; kinetic theory; least squares analysis; logarithmic expansion.

Herron, J. T., Penzhorn, R. D., **Mass spectrometric study of the reactions of atomic oxygen with ethylene and formaldehyde,** *J. Phys. Chem.* **73,** *No. 1, 191–196 (Jan. 1969).*
A mass spectrometric study has been made of the reactions of atomic oxygen with ethylene and formaldehyde. The formation of formaldehyde in the ethylene reaction is shown to be independent of the presence of molecular oxygen, and is attributed to a reaction between atomic oxygen and methyl radicals. The formaldehyde reaction has a rate constant at 300 K of 9.0×10^{10} cm^3 mol^{-1} s^{-1}, with an estimated uncertainty of $\pm 3.0 \times 10^{10}$ cm^3 mol^{-1} s^{-1}.

Key words: Atomic oxygen; ethylene; formaldehyde; kinetics; mass spectrometry; mechanisms; rate constant.

Hubbell, J. H., Berger, M. J., **Photon attenuation. Attenuation coefficients, energy absorption coefficients, and related quantities,** *Chapter 4 in Engineering Compendium on Radiation Shielding, R. G. Jaeger, E. P. Blizard, A. B. Chilton, M. Grotenhuis, A. Honig, T. A. Jaeger, H. Eisenlohr, ed. 1, 167–202 (International Atomic Energy Agency, Vienna, Austria, 1968).*
This paper consists of two parts. The first part contains tabulations of the photon attenuation coefficient and the energy transfer coefficient. The values of the attenuation coefficient represent a revision which takes into account new theoretical data on the photoelectric effect and on radiative corrections to Compton scattering and pair production. Rayleigh (coherent) scattering and the photonuclear effect are disregarded, but can be included by use of auxiliary tables. The main tables cover the energy range 10 keV to 100 MeV for 21 and four mixtures. This range is extended to 10 GeV for 16 elements by interpolation from experimental data. The energy transfer coefficient data were taken directly from tabulations in the literature, and cover the energy range 10 keV to 100 MeV. In the second part, information is given on the individual processes (photoelectric absorption, Compton scattering, pair production and other interections of photons with matter) which combine to give the attenuation coefficient. Theoretical and experimental data are reviewed, and numerical tables and approximation formulas are given.

Key words: Attenuation coefficient; Compton scattering; cross section; energy absorption coefficient; gamma rays; pair production; photoelectric absorption; photons, X-rays.

Hummer, D. G., Rybicki, G. B., **Line formation in differentially moving media with temperature gradients,** *Proc. Natl. Center for Atmospheric Research Conf. Resonance Lines in Astrophysics, Sept. 9–12, 1968, Boulder, Colo., pp. 315–330 (National Center for Atmospheric Research, Boulder, Colo., Dec. 1968).*
The line formation problem for two-level atoms scattering with complete redistribution is solved numerically for plane parallel media in which the macroscopic velocity, electron temperature and all other properties of the atmosphere are arbitrary functions of optical depth.

Key words: Radiative transfer, spectral lines, planetary nebulae, velocity fields.

King, R. J., Maley, S. W., Wait, J. R., **Experimental and theoretical studies of propagation of ground waves across mixed paths,** *(Proc. URSI Symp. Electromagnetic Wave Theory, Delft, Holland, Sept. 1965), Chapter in Electromagnetic Wave Theory, J. Brown, ed., pp. 217–224 (Pergamon Press Inc., New York, N.Y., 1965).*
The propagation of electromagnetic ground waves along non-homogeneous paths has received considerable interest in the past three decades. As a result, several empirical and semi-empirical solutions have been developed and proven useful in calculating the portion of a ground wave transmitted across a coast line. These methods generally have been replaced by more rigorous formulations. Experimental results have been rather meager since ground waves are primarily important at low and very low frequencies where the distances involved are large. Furthermore, it is difficult to evaluate the unwanted effects of other nearby terrain and objects. Therefore, the experiments described here have utilized small laboratory models which simulate, as closely as possible, the mathematical model used in the theoretical formulations. In this way, distances and other parameters can be carefully measured and controlled. If the experimental results compare favorably with the theoretical solution, the theory can then be applied to naturally occurring mixed paths with considerably more confidence.

Key words: Electromagnetic ground waves; ground waves; non-homogeneous paths; propagation of ground waves.

Koonce, C. S., Cohen, M. L., **Theory of superconducting semiconductors and semimetals,** *Phys. Rev.* **177,** *No. 2, 707–719 (Jan. 10, 1969).*
A Green's function method is used to derive a superconducting energy gap equation without the assumption that the Fermi energy is much larger than phonon energies. This equation is then approximated using two separate methods. The first method applies when the screened electron-phonon interaction is almost independent of wavevector and the Fermi energy is of the order of, or larger than phonon energies. The gap equation obtained in this way takes account of the variation in the density of electron states with energy. The second approximation method applies when the screened electron-phonon interaction depends strongly on wavelength or when the Fermi energy is small compared to phonon energies. In this case, the gap equation takes account of the wavevector dependence of the interaction, the wavevector and frequency dependence of the electronic screening, the energy dependence of the density of states, and the wavevector dependence of the superconducting energy gap. In addition, the effects of the retardation of the electron-electron interaction are also included.

Key words: Dielectric function; Green's function; semiconductors; semimetals; superconductivity.

Lafferty, W. J., Maki, A. G., Pringle, W. C., Jr., **Comments on "Tow rotational lines of allene C_3H_4",** *J. Chem. Phys.* **50,** *No. 1, 564–565 (Jan. 1, 1969).*
Goertz has claimed to have observed two rotational lines of allene arising from $J = 3 \rightarrow 4$ transitions in the $K = 0$ levels of the vibrational states of allene. A number of theoretical considerations are presented which cast doubt on the validity of Goertz's assignment of these lines to allene. A thorough search of the microwave spectrum of allene in the regions where the lines resulting from the $1 \rightarrow 2$ and the $3 \rightarrow 4$ transitions should fall produced no evidence for the lines observed by Goertz.

Key words: Allene; E vibrational state; microwave spectrum; rotational transitions; Stark effect; vibrational states.

Lang, S. B., Shaw, S. A., Rice, L. H., Timmerhaus, K. D., **Pyroelectric thermometer for use at low temperatures,** *Rev. Sci. Instr.* **40,** *No. 2, 274–284 (Feb. 1969).*
The applicability of pyroelectric thermometry to temperature change or temperature rate measurement at cryogenic levels was studied, with particular emphasis on calorimetry. The pyroelectric coefficients, dc dielectric constants, and volume resistivities of three ferroelectric ceramic materials, Clevite Ceramic B, PZT–4 and PZT–5A, were measured over the temperature range 4.2 to 300 °K. The pyroelectric coefficients were found to be reproducible, but large electric fields, thermal shock, and aging affected the pyroelectric coefficient. Expressions are derived for the temperature responsivity (voltage output per unit temperature change), noise equivalent temperature change (temperature change equivalent to the electrical noise in a pyroelectric thermometer), and figure-of-merit (a parameter characterizing the physical properties of a pyroelectric material). Typical temperature responsivities of 8.0 and 165 volts/ °K, and values of noise equivalent temperature change of 2.5 and 0.12 microdegrees K, at 5 and 300 °K respectively, are calculated. Recommendations concerning the usage of a pyroelectric thermometer in a cryogenic calorimeter are given.

Key words: Calorimetry; cryogenics; dielectric constant; ferroelectric ceramic; pyroelectric coefficient; thermometry; volume resistivity.

Latanision, R. M., Staehle, R. W., **Plastic deformation of electrochemically polarized nickel single crystal,** *Acta Met.* **17,** *307–319 (Mar. 1969).*
Nickel single crystals were deformed in uniaxial tension under active and passive conditions in a 1 *N* H_2SO^4 solution at room temperature. τ_0 increase and Stages I and II are suppressed in the presence of the thin passive film found at 800 mV (SCE). In contrast, surface removal prior to deformation lowers τ_0 in comparison to crystals deformed in the laboratory atmosphere. Continuous surface removal during deformation only slightly affects θ_1, but does increase the extent of easy glide and Stage II. Abrupt changes in the stress for further plastic deformation occur when crystals are unloaded and held at constant potential in interrupted tests. Electron microscope studies of surface replicas show that slip lines formed under dissolution conditions are stronger and more widely spaced than those produced on crystals deformed in air. The spacing and step height on passivated crystals appear to be intermediate between those two extremes. A model of plastic deformation based upon the activation of *near surface* dislocation sources is presented in the context of the above observations.

Key words: Active potentials: critical resolved sheer strees; passive potentials; shear surface dislocation sources; single crystals.

McIntyre, D., Sengers, J. V., **Study of fluids by light scattering,** *Chapter 11 in Physics of Simple Liquids, H. N. V. Temperley, J. S. Rowlinson, G. S. Rushbrooke, Ed., pp. 449–505 (North Holland Publ. Co., Amsterdam, The Netherlands, 1968).*
The manuscript is a chapter written upon the request of Professor Temperley for a book entitled "The Physics of Simple Liquids," edited by Temperley, Rushbrooke and Rowlinson.
After introducing the basic scattering equations, the first part of the paper is devoted to a discussion of measurements of the intensity of scattered light. A survey is presented of the experimental verification of the Einstein scattering equations. Futhermore, the experimental angular dependence of the scattered intensity near the critical point is discussed, in particular for binary liquid mixtures near the critical mixing point.
The second part of the paper is devoted to the spectrum of scattered light. The Landau-Placzek theory, as worked out by Mountain, is discussed in detail for one component fluids and estimates are presented for several characteristic properties of the spectrum as a function of density and temperature. The experimental verification of the Landau-Placzek theory is surveyed. The paper concludes with a discussion of the spectrum of critical opalescence.

Key words: Light scattering, Rayleigh scattering; Brillouin scattering; critical opalescence; fluctuations; gases; liquids.

McKinley, J. D., Jr., **Mass spectrometric investigation of the surface reaction of tungsten with chlorine-oxygen mixtures,** *(Proc. 6th Intern. Symp. Reactivity of Solids, Schenectady, N.Y., Aug. 25–30, 1968), Chapter in Reactivity of Solids, J. W. Mitchell, R. C. DeVries, R. W. Roberts, and P. Cannon, Ed., pp. 345–351 (John Wiley & Sons, Inc., New York, N.Y., 1969).*
The rapid erosive attack of chlorine, oxygen mixtures on hot tungsten has been studied mass spectrometrically. At surface temperatures between 1000° and 2400 °K the major product is gaseous tungsten dioxydichloride. Volatile tungsten dioxide and trioxide also form at lower rates. Oxide desorption exhibits the same pressure and temperatures dependence as in pure oxygen. No evidence was obtained for simple tungsten chloride or for chlorine oxides among the products.

Key words: Tungsten; chlorine; oxygen; reaction kinetics; mass spectrometry; high temperature.

Madden, R. P., Ederer, D. L., Codling, K., **Resonances in the photoionization continuum of Ar i (20–150 eV).** *Phys. Rev.* **177,** *No. 1, 136–151 (Jan. 5, 1969).*
The absorption spectrum of argon in the region 20–150 eV has been studied photographically and photoelectrically, using synchrotron light as a background source and a resolution of 0.06 Å. Many resonances have been observed in the photoionization continuum which are caused by electronic excitation to high autoionizing states of Ar I. In the region between 27 and 40 eV the observed structure is due to two types of electronic excitation: (i) the excitation of a single sub-shell 3*s* electron, resulting in the configuration $3s3p^6np$ and (ii) the excitation of two of the outer 3*p* electrons simultaneously resulting in configurations of the type $3s^23p^4nln'l'$. Between 44 and 59 eV weak structures have been observed in the absorption continuum due to the simultaneous excitation of a 3*s* and a 3*p* electron, resulting in configurations of the type $3s3p^5nln'l'$. All of the observed resonances have been tabulated, and a partial classification has been given. The profiles of the resonances caused by transitions to states $3s3p^6(^2S_{1/2})np\ ^1P^\circ_1$, for $n=4$, 5, and 6, and the two electron excitation states $3s^23p^4(^3D4s(^2P_{3/2})^2p$ and $3s^23p^4(^3P)3d(^2P_{3/2})4p$, have been studied quantitatively. The values of q, ρ^2, and Γ have been determined for each of these resonances, and the continuum cross-section has been measured between 24 and 36 eV.

Key words: Photoionization; argon; absorption spectra; vacuum ultraviolet; absorption cross-section.

Matsumura, C., Lide, D. R., Jr., **Structure of the alkali hydroxides. III. Microwave spectra of RbOH and RbOD,** *J. Chem. Phys.* **50,** *No. 1, 71–75 (Jan. 1, 1969).*
The microwave spectra of gaseous RbOH and RbOD have been measured with a high-temperature spectrometer. The spectra are generally similar to those observed in CsOH and indicate an essentially linear structure for rubidium hydroxide. The variation of rotational constant with excitation of the bending mode shows anomalies similar to those found in CsOH. The Rb—O bond length is found to be 2.30$_5$ Å, while the O—H distance is 0.96$_5$ Å. Analysis of the nuclear quadrupole hyperfine structure give eq Q values of −67.9 Mc/s in Rb^{85} OH and −35 Mc/s in Rb^{87} OH.

Key words: Bond distances; microwave; quadrupole; high temperature; spectra; RbOH, rotational constants.

Mighell, A. D., Reimann. C. W., Mauer, F. A., **The crystal and molecular structure of diaquobis-(2,2′-biimidazole)nickel(II) dinitrate, $Ni(C_6H_6N_4)_2(H_2O)_2(NO_3)_2$,** *Acta Cryst.* **B25,** *Part 1, 61–66 (Jan. 1969).*
The crystal and molecular structure of diaquobis-(2,2′-biimidazole) nickel(II) dinitrate, $Ni(C_6H_6N_4)_2(H_2O)_2(NO_3)_2$, was determined by single crystal X-ray diffraction techniques. This compound crystallizes in the monoclinic system with $a=10.3925\pm0.0004$Å, $b=9.6284\pm0.0004$Å, $c=9.9615\pm0.0003$Å, $\beta=96.308\pm003$Å, space group $P2_1/n$, $\rho c=1.68$ g cm^{-3}, and $z=2$. The indicated uncertainties are the standard deviations of the sets of individual measurements involved. Three-dimensional data (3151 reflections) were used and the structure solved by the heavy atom method. The Ni(biimidazole)$_2$(H$_2$O)$_2$(NO$_3$)$_2$ molecule is centrosymmetric with the nickel atom at the center of an octahedron formed by two oxygen atoms and four nitrogen atoms. The four coordinating nitrogen atoms, two from each biimidazole molecule, form a rectangle (3.193 × 2.711Å) and the water molecules lie above and below this plane. The structure consists of these complex cations linked by hydrogen bonds formed between coordinated water molecules, the noncoordinating nitrogen atoms in the biimidazole molecules and the nitrate anions. One hydrogen atom in the coordinated water is involved in a bifurcated hydrogen bond to two oxygen atoms.

Key words: X-ray structure determination; transition metal coordination complex; biimidazole and water ligands; hydrogen bonding.

Mills, R. M., **Flame inhibition with electron attachment as the first step,** *Combustion and Flame* **12,** *No. 2, 513–520 (Dec. 1968).*
The suggestion is made that combustion inhibition of the type observed with the use of most halogenated hydrocarbons is due to a two-step process: (1) negative ions and free radicals are formed by dissociative electron attachment with the inhibitor molecules, and then (2) these negative ions and/or free radicals react with the free radicals found in flames. Considerable evidence from the literature is presented which supports this idea. It is concluded that, while the evidence is not conclusive, a serious consideration of the idea is justified.

Key words: Flame inhibition mechanism; electron attachment; flame free radicals.

Paabo, M., Bates, R. G., **Standards for a practical scale of pD in heavywater,** *Anal. Chem.* **41,** *No. 2, 283–285 (Feb. 1969).*
The glass electrode has been found to respond to deuterium ion in heavy water solutions as well as to hyrdogen ion in ordinary water. Furthermore, the glass-calomel pH assembly is useful for practical measurements of pD in heavy water. Several standard reference solutions for pD are needed, however, as the response of individual glass electrodes is not constant over the entire useful pD range. A suitable phosphate solution (pD 7.428 at 25 °C) composed of KD_2PO_4 and Na_2DPO_4 (each 0.025 molal) was established in earlier work. This reference has now been supplemented by two other useful buffer solutions, namely 0.05m KD_2 citrate (pD 4.293 at 25 °C) and a mixture of $NaDCO_3$ and Na_2CO_3 (each 0.025 molal) which has a pD of 10.736 at 25 °C. Values have been assigned at 10 temperatures from 5 to 50 °C. The conventional pD scale fixed by these three standards has been shown to have a satisfactory internal consistency.

Key words: Acidity; carbonate; citrate; deuterium oxide; deuterium ion; glass electrode; heavy water; pD; phosphate; standards for pD.

Pool, K. H., Bates, R. G., **Thermodynamics of hydrochloric acid in 95 volume percent (92.41 mass percent) ethanol from e. m. f. measurements at 5 to 50 °C,** *J. Chem. Thermodynamics* **1,** *21–29 (1969).*
Electromotive-force measurements of cells of the type Pt; H_2, HCl(m) in EtOH–H_2O, AgCl; Ag at 10 temperatures from 5 to 50 °C have been used to derive (a) the standard emf of the cell in 92.41 wt. percent ethanol, (b) the activity coefficient of hydrochloric acid, (c) the relative partial molal enthalpy and heat capacity of HCl, and (d) the thermodynamic constants for the transfer of HCl from water to 92.41 wt. percent ethanol. The molality of the acid ranged from 0.0099 to 1.085 mol kg^{-1}. To obtain the standard emf it was necessary to correct for ion-pair formation and to use the extended terms of the Debye-Hückel theory. The ion-size parameter, chosen to minimize the sum of the squares of the deviations, varied only slightly with temperature, from 3.97Å at 5 °C to 4.31Å at 50 °C.

Key words: Activity coefficients; emf measurements; enthalpy; entropy; ethanol-water solvents; hydrochloric acid; thermodynamics.

Shirley, J. H., **Dynamics of a simple maser model,** *Am. J. Phys.* **36,** *Part 1, No. 11, 949–963 (Nov. 1968).*
A simple maser model consisting of a single mode field coupled to N identical two-level atoms is presented. The assumption of negligible statistical correlation between the atoms and the field permits the Heisenberg equations of motion to be replaced by a self-consistent set of ordinary nonlinear differential equations. Relaxation terms and an energy source are introduced phenomenologically. The resulting equations exhibit a threshold, stable and unstable steady states, and relaxation oscillations. The dynamic equations for the hydrogen maser and the rate equations of laser theory are derived as special cases. Also discussed are the master amplifier, locking of a maser to an external signal and the effects of cavity thermal noise.

Key words: Maser dynamics; laser dynamics; maser amplifier.

Sieck, L. W., **Xenon-photosensitized decomposition of methane at 1470 A,** *J. Chem. Phys.* **50,** *No. 4, 1748–1753 (Feb. 15, 1969).*
The xenon sensitized decomposition of methane and methane-ethylene mixtures has been investigated in the vapor phase at 1470 Å.
Quantum yield determinations and analyses of the isotropic composition of the hydrogens and ethanes obtained from CH_4–CD_4 (1 : 1) mixtures under various conditions indicate that sensitization occurs by at least two concurrent mechanisms. The role of internal photolysis by resonating 1470 Å radiation was found to be negligible in all mixtures, and the existence of XeH as an important intermediate was inferred by chemical methods.

Key words: Energy transfer; photochemistry (vacuum ultraviolet) sensitized decomposition; rare gas levels; quantum yields; hydrocarbons.

Steiner, B., **Photodetachment of electrons from SH^-,** *J. Chem. Phys.* **49,** *No. 11, 5097–5104 (Dec. 1, 1968).*
The cross section for photodetachment of electrons from SH^- for the first 0.75 eV above threshold ($\lambda = 534.7$ to 403.0 nm) has been measured in a crossed beam experiment. The cross section rises rapidly in the first 0.15 eV ($\Delta\lambda = 35$ nm) to the value 1.9×10^{-17} cm^2 determined with a total uncertainty of $\pm 0.4 \times 10^{-17}$ cm^2 given by the square root of the sum of the squares of the maximum observed deviation and the allowances for various systematic factors; over the rest of the observed range it is constant. The detailed shape of the cross section vs. λ curve has been employed to derive the SH^- structural parameters (and their upper limits of uncertainty), which are indistinguishable from those of the neutral free radical: $R = 0.135 \pm 0.002$ nm, $\omega_e = 2700 \pm 290$ cm^{-1}, and $B_e = 9.46 \pm 0.32$ cm^{-1}. The electron affinity is identified with the observed photodetachment threshold, 2.319 ± 0.010 eV. These results are in general agreement with the recent calculations of Cade. Evidence is presented for the importance of inclusion of long range forces in dealing with the threshold behavior of photodetachment from heteronuclear diatomic negative ions.

Key words: Electron affinity; free radical; negative ions; photodetachment; SH.

Trembath, C. L., Wait, D. F., Engen, G. F., Foote, W. J., **A low-temperature microwave noise standard,** *IEEE Trans. Microwave Theory Tech.* **MTT-16,** *No. 9, 709–714 (Sept. 1968).*
An X-band thermal noise source is described which consists of a waveguide termination, cooled in a cryogenic environment, along with temperature and pressure monitors and controls. With liquid helium as the cryogen, the effective noise output at the room temperature flange can be set to values around the voiling point of helium (4.2 °K) with an accuracy of ±0.03 °K. With liquid nitrogen as the cryogen, the output temperature can be set to values around 77 °K with an accuracy of ±0.16 °K.
This accuracy is made possible by several unique features. First, the terminating waveguide section is a vapor bulb thermometer with the absorbing load surrounded with the cryogenic liquid. Second, heat exchangers are used to permit an unusually short waveguide transition section between cryogenic and room temperature. Third, and absolute pressure regulator is used to control the cryogen boil-off rate resulting in a temperature stability of 0.002 °K for nitrogen.
At present, the useful accuracy of the standard is limited to ±0.1 °K because of uncertainties in the insertion loss (about 0.001 dB) of mating room temperature flanges.

Key words: Microwave; noise; standard; cryogenic.

Wier, C. E., Piermarini, G. J., Block, S., **Crystallography of some high-pressure forms of C_6H_6, CS_2, Br_2, CCl_4, and KNO_3,** *J. Chem. Phys.* **50,** *No. 5, 2089–2093 (Mar. 1, 1969).*
From single crystal x-ray diffraction at high pressure and room temperature unit-cell and space-group data were obtained for the following materials:
C_6H_6, I–Orthorhombic, $a = 7.17$, $b = 9.28$, $c = 6.65$, Pbca,
CS_2–orthorhombic, $a = 6.16$, $b = 5.38$, $c = 8.53$, Cmca,
Br_2–orthorhombic, $a = 8.54$, $b = 6.75$, $c = 8.63$, Cmca,
CCl_4, I–rhombohedral, $a = 14.27$, $\alpha = 90°$,
CCl_4, II–monoclinic, $a = 22.10$, $b = 11.05$, $c = 25.0$, $\beta = 114°$, Cc or C2/c,
CCl_4, III–orthorhombic, $a = 11.16$, $b = 14.32$, $c = 5.74$, $C22_1$,
KNO_3, III–rhombohedral, $a = 4.31$, $\alpha = 78°54'$,
KNO_3, IV(?)–orthorhombic, $a = 5.58$, $b = 7.52$, $c = 6.58$, $P2_1$ nb or Pmnb.
All unit-cell dimensions are given in Å with estimated uncertainties of ±2 in the last decimal place given and uncertainties of ±0.5 deg. in angles.

Key words: High-pressure; polymorphism; single-crystal; x-ray diffraction.

Weiss, A. W., **Series perturbations and atomic oscillator strengths: The ^2D series of Al II,** *Phys. Rev.* **178,** *No. 1, 82–89 (Feb. 5, 1969).*
A model calculation has been made of the effects of perturbations of the $3s^2nd$ series of aluminum by the $3s3p^2$ ^2D-term. The model employed is the traditional one of configuration interaction among the independent particle model representations of the relevant

discrete states, with Hartree-Fock functions being used to compute the necessary matrix elements. It is found that, while in the Hartree-Fock approximation the $3s3p^2$ term is bound and embedded in the $3s^2nd$ series, the configuration interaction gives rise to a new autionizing state just beyond the series limit. This state, which is approximately 50% $3s3p^2$, is found to have most of the ^2D absorption oscillator strength ($f=1.1$). The general properties of this model of series perturbations are also discussed in some detail.

Key words: Configuration interaction; oscillator strength; series perturbations.

Wiese, W. L., **Systematic trends of atomic oscillator strengths in isoelectronic sequences,** *Appl. Opt.* **7,** *No. 12, 2361–2366 (Dec. 1968).*
The dependence of atomic oscillator strengths (f-values) on nuclear charge, which leads to systematic trends along isoelectronic sequences, is discussed with particular reference to beam foil spectroscopy. The theoretical background for the nuclear charge dependence is given first, and then several characteristic examples are reviewed in detail. The beam foil technique of measuring lifetimes is one of the most important data sources, because it readily permits reliable experimental determinations of f-values over several stages of ionization within isoelectronic sequences. It is shown that experimental data are most urgently needed when f-values are affected by cancellation in the transition integral or configuration interaction effects, since in these cases most theoretical approaches run into great difficulties.

Key words: Atomic oscillator strengths; beam foil spectroscopy; isoelectronic sequences; nuclear charge dependence; systematic trends.

Wims, A. M., McIntyre, D., Hynne, F., **Coexistence curve for 3-methylpentane-nitroethane near the critical point,** *J. Chem. Phys.* **50,** *No. 2, 616–620 (Jan. 15, 1969).*
The coexistence curve for the liquid mixture 3-methylpentane-nitroethane has been obtained using a visual and a float technique. A detailed analysis of the data shows that the composition differences of the coexisting liquid phases are proportional to $(t_c-t)\beta$, where $\beta=0.340$ with a standard deviation of 0.010. As a result of this analysis and an analysis of the earlier work of Rice and Zimm it is shown that the value of β for binary liquids is not significantly different from the value for gas-liquid systems.

Keys words: Coexistence curve; critical phenomena; magnetic suspension desitometer; 3-methylpentane; nitroethane.

Wolfgang, R., Zare, R. N., Branscomb, L. M., **Chemical accelerators,** *Science* **162,** *No. 3855, 818–822 (Nov. 15, 1968).*
This is a brief account of a conference on chemical accelerators held at the University of Colorado March 28–29, 1968, supported by the Advanced Research Projects Agency.

Key words: Chemical accelerators.

Other NBS Publications

J. Res. Nat. Bur. Stand. (U.S.), 73B (3), 191–279 (Jul–Sept. 1969) $1.25.
A table of integrals of the exponential integral. M. Geller and E. W. Ng.
Principal ideals in matrix rings. M. Newman and S. Pierce.
The second orthogonality conditions in the theory of proper and improper rotations. IV. Solution of the trace and secular equations. H. Gelman.
Minimax error selection of a univarite distribution with prescribed componentwise bounds and ranking. A. J. Goldman.
Minimax adjustment of a univarite distribution to satisfy componentwise bounds and/or ranking. A. J. Goldman.
On the application of some interpolating functions in physics. A. J. Jerri.
Commutator groups and algebras. L. Greenberg.
On a class of nonlinear transformations and their applications to the evaluation of infinite series. H. L. Gray and W. D. Clark.

J. Res. Nat. Bur. Stand. (U.S.), 73C (1 & 2), 1–46 (Jan.–June 1969) $1.25.
An interferometer for measuring gradients in both refractive index and thickness of large or small optics. J. B. Saunders.
A Kerr electro-optical technique for observation and analysis of high-intensity electric fields. E. C. Cassidy and H. N. Cones.
Student-t deviate corresponding to a given normal deviate. B. L. Joiner.
A heat loss compensated calorimeter and related theorems. S. R. Domen.
Laboratory measurements of air cavity temperature in a passenger car tire. B. G. Simson and J. Mandel.

Diamond, J. J., Editor, Bibliography on the high temperature chemistry and physics of materials, January, February, March 1969, Nat. Bur. Stand. (U.S.), Spec. Publ. 315–1, 81 pages (Apr. 1969), 75 cents.
Little, J. L., Some evolving conventions and standards for character information coded in six, seven, and eight bits, Nat. Bur. Stand. (U.S.), Tech. Note 478, 30 pages (May 1969), 35 cents.
Oberholtzer, B. L., Publications of the National Bureau of Standards 1966–1967, Nat. Bur. Stand. (U.S.), Spec. Publ. 305, 220 pages (Apr. 1969), $2.00.
Robinson, D. C., Misalinement detector for axial loading fatigue machines, Nat. Bur. Stand. (U.S.), Tech. Note 480, 15 pages (Apr. 1969), 25 cents.
Stabler, T. M., Editor, Specifications and tolerances for reference standards and field standard weights and measures. 1. Specifications and tolerances for field standard weights, Nat. Bur. Stand. (U.S.), Handb. 105–1, 10 pages (Apr. 1969), 25 cents.
White, H. S., Jr., Editor, Implementation of the code for information interchange and related media standards. Hardware standards interchange codes and media, Nat. Bur. Stand. (U.S.), Fed. Info. Process. Stand. Publ. (FIPS Pub.) 7, 12 pages (Mar. 7, 1969), 25 cents. (Supplement to FIPS Pub. 1 through 3).
Anderson, H. J., Brenner, A., Preparation of rhenium hexafluoroacetylacetonate, J. Electrochem. Soc. **116,** No. 4, 513 (Apr. 1969).
Arenhovel, H., Danos, M., Baryon resonances in nuclei: Magnetic moment anomaly in ^3H and ^3He, Physics Letters **28B,** No. 5, 299–301 (Dec. 23, 1968).
Arp, V. D., Kasen, M. B., Reed, R. P., Magnetic energy storage and cryogenic aluminum magnets, Tech. Rept. AFAPL–TR–68–87, 122 pages (Air Force Systems Command, Wright-Patterson Air Force Base, Ohio, Feb. 1969).
Beatty, R. W., Discussion of effect of realizability conditions upon estimated limits of mismatch error in the calibration of fixed attenuators, IEEE Trans. Microwave Theory Tech. **MTT–16,** No. 11, 976 (Nov. 1968).
Bennett, H. S. Diffuse and propagating modes in the Heisenberg paramagnet, Phys. Rev. **174,** No. 2, 629–639 (Oct. 10, 1968).
Berman, H. A., West, E. D., Heat capacity of liquid nitromethane from 35° to 200 °C, J. Chem. Eng. Data **14,** No. 1, 107–109 (Jan. 1969).
Branscomb, L. M., Joint Institute for Laboratory Astrophysics of the National Bureau of Standards and the University of Colorado, Boulder, Colorado, observatory report, Bull. Am. Astron. Soc. **1,** No. 1, 27–33 (Jan. 1969).
Campbell, W. H., Aurora, Encyclopedia of Atmospheric Sciences and Astrogeology, R. W. Fairbridge, Ed., pp. 105–106 (Reinhold Publ. Co., New York, N.Y., 1967).

Clark, A. F., Fickett, F. R., A nonsuperconducting detection system for low level dc voltages, Rev. Sci. Instr. **40,** No. 3, 465–468 (Mar. 1969).
Cole, A. R. H., Lafferty, W. J., Thibault, R. J., Rotational fine structure of the perpendicular band, ν_7, of ethane, J. Mol. Spectry. **29,** No. 3, 365–374 (Mar. 1969).
Creitz, E. C., Construction details and measurements of response of a gas density balance. J. Chromatog. Sci. **7,** 137–144 (Mar. 1969).
Deslattes, R. D., Paretzkin, B., A small set of reference crystals for double-crystal topography, J. Appl. Cryst. **1,** Part 3, 176–178 Sept. 1968).
Driver, L. D., Arthur, M. G., A wideband RF voltmeter-comparator, IEEE Trans. Instr. Meas. **IM–17,** No. 2, 146–150 (June 1968).

Dunn, G. H., Colliding beams, (Proc. First Intern. Conf. Atomic Physics, June 3–7, 1968, New York, N.Y.), Chapter in Atomic Physics, B. Bederson, V. W. Cohen, F. M. J. Pichanick, Ed., pp. 417–433 (Plenum Press Inc., New York, N.Y., 1969).

Ehrlich, M., Influence of irradiation rate on the production of *F* centers in LiF (TLD grade), J. Appl. Phys. **40,** No. 2, 891–892 (Feb. 1969).

Ehrlich, M., Lamperti, P. J., Uniformity of high-energy electron-beam calibrations, Phys. Med. Biol. **14,** No. 2, 305–314 (Sept. 1968).

Enemark, E. A., Gallagher, A., A pockels cell light modulator for wide angle radiation, Rev. Sci. Instr. **40,** No. 1, 40–41 (Jan. 1969).

Engen, G. F., A method of determining the mismatch correction in microwave power measurements, IEEE Trans. Instr. Meas. **IM-17,** No. 4, 392–395 (Dec. 1968).

Ensign, T. C., Chang, T. T., Low temperature optical-EPR sample probe using tunable coaxial coupling, Rev. Sci. Instr. **40,** No. 2, 268–270 (Feb. 1969).

Fatiadi, A. J., Evidence for a chair conformation of certain osotriazoles of inositols, Chem. Ind. **19,** 617–619 (May 10, 1969).

Gadsden, M., Airglow, Encyclopedia of Atmospheric Sciences and Astrogeology, R. W., Fairbridge, Ed., pp. 8–10 (Reinhold Publ. Co., New York, N.Y., 1967).

Gadsden, M., Airglow motions, International Dictionary of Geophysics I, 50–56 (1967).

Gardner, T. V., Jr., Dickson, G., Kumpula, J. W., Application of diffraction gratings to measurement of strain of dental materials, J. Dental Res. **47,** No. 6, Part 2, 1104–1110 (Nov.–Dec. 1968).

Gautier, T. N., Zacharisen, D. H., Use of space and time correlations in short-term ionospheric predictions, First Ann. IEEE Commun. Convention, pp. 671–676 (June 1965).

Grabner, L., Photoluminescence in $SrTiO_3$, Phys. Rev. **177,** No. 3, 1315–1323 (Jan. 15, 1969).

Hanley, H. J. M., Childs, G. E., Interim values for the viscosity and thermal conductivity coefficients of fluid He^4 between 2 and 50 K, Cryogenics **9,** No. 2, 106–111 (Apr. 1969).

Hardy, S. C., Coriell, S. R., Morphological stability and the icewater interfacial free energy, J. Crystal Growth **3,** No. 4, 569–573 (1968).

Hartman, W. J., Feasibility of communication with a satellite by means of tropospheric scatter, IEEE Trans. Commun. Technol. **COM-14,** No. 3, 251 (June 1966).

Hiza, M. J., Duncan, A. G., A simple gas recirculation pump for low flow and high pressure applications, Rev. Sci. Instr. **40,** No. 3, 513–514 (Mar. 1969).

Hoover, T. B., The *N*-methylpropionamide-water system. Densities and dielectric constants at 20–40°, J. Phys. Chem. **73,** No. 1, 57–61 (Jan. 1969).

Hudson, R. P., The delta campaign. An account of the controversy surrounding the temperature scale for CMN, Cryogenics **9,** No. 2, 76–79 (Apr. 1969).

Ito, J., Johnson, H., Synthesis and study of yttrialite, Am. Mineralogist **53,** 1940–1952 (1968).

Judd, D. B., 1964 CIE supplementary observer applied to the colorimetry of rutile and anatase forms of titanium dioxide, J. Opt. Soc. Am. **58,** No. 12, 1638–1649 (Dec. 1968).

Kramer, R. A., Cryoelectronics, Cryogenics **9,** No. 1, 20–25 (Feb. 1969).

Kaufman, V., Radziemski, L. J., Redetermined level values and interaction parameters of S II and Cl II ground configurations, J. Opt. Soc. Am. **59,** No. 2, 227–228 (Feb. 1969).

Keller, R. A., Excited triplet → singlet intersystem crossing, Chem. Phys. Letters **3,** No. 1, 27–29 (Jan. 1969).

Kropschot, R. H., Report on the fourteenth cryogenic engineering conference, Cryogenics **8,** No. 6, 346–348 (Dec. 1968).

Lance, H. W., Metrology and National goals, (Proc. 22nd ISA Conf. and Exhibit, Chicago, Ill., Sept. 11–14, 1967) ISA Preprint No. M4-1-MESTIND-67, 1–14 (1967); excerpt in Meas. Data **2,** No. 2, 68–71 (Mar.–Apr. 1968).

Lashof, T. W., Standardization and application of accuracy and precision statements: TAPPI Standards Committee-ASTM Committee D-6 policy, Tappi **4,** 732–739 (Apr. 1969).

Lee, T. G., A system for continuously monitoring hydrogen chloride concentrations in gaseous mixtures using a chloride ion-selective electrode, Anal. Chem. **41,** 391–392 (Feb. 1969).

Levin, E. M., X-ray determination of the thermal expansion of silver nitrate, J. Am. Ceramic Soc. **52,** No. 1, 53–54 (Jan. 1969).

Lloyd, E. C., Standards for improved measurement of pressure and vacuum (Proc. 4th Intern. Measurement Conf., Warsaw, Poland, July 2–7, 1967), Acta Imeko, pp. 451–468 (Hungarian Academy of Sciences, Budapest, Hungary, 1967).

Lloyd, E. C., Beckett, C. W., Boyd, F. R., Jr., Measurements in high-pressure environment, Science **164,** 860–861 (May 16, 1969).

Maki, A. G., Comment on the fermi resonance constant in ICN, J. Chem. Phys. **50,** No. 5, 2273 (Mar. 1, 1969).

Moore, C. E., Annual report on spectroscopy, Bull. Am. Astron. Soc. **1,** No. 1, 85–86 (Jan. 1969).

Newman, M., Maximal normal subgroups of the modular group, Proc. Am. Math. Soc. **19,** No. 5, 1138–1144 (Oct. 1968).

Norton, R. B., Aeronomy, Encyclopedia of Atmospheric Sciences and Astrogeology, R. W. Fairbridge, Ed., pp. 3–7 (Reinhold Publ. Co., New York, N.Y., 1967).

Oliver, F. W. J., Error bounds for the Laplace approximation for definite integrals, J. Approx. Theory **1,** 293–313 (1968).

O'Reilly, D. E., Tsang, T., Order-disorder transition in ferroelectric ammonium sulfate, J. Chem. Phys. Letter to Editor **50,** No. 5. 2274–2275 (Mar. 1, 1969).

Plummer, E. W., Gadzuk, J. W., Young, R. D., Resonance tunneling of field emitted electrons through adsorbates on metal surfaces, Solid State Commun. **7,** 487–491 (1969).

Quindry, T. L., Transmissibility measurements for the determination of structural damping, (Proc. Vibrations Conf., Philadelphia, Pa., Mar. 30–Apr. 2, 1969). Preprint No. 69-VIBR-36, 7 pages (American Society of Mechanical Engineers, New York, N.Y., 1969).

Roach, F. E., The brightness of the zodical light at the ecliptic pole, (Proc. Symp. Meteor Orbits and Dust, Cambridge, Mass., Aug. 9–19, 1965), Smithsonian Contributions to Astrophysics, F. L. Wripple, Ed., 11, 225–226 (Smithsonian Institution Astrophysics Observatory, Cambridge, Mass., 1967).

Ryan, J. V., Flammable fabrics act and its implementation, Mod. Textiles Mag. L, No. 3, 67–70 (Mar. 1969).

Sanderson, B. T., Romanoff, M., Performance of commercially pure titanium in corrosive soils, Mater. Production **8,** No. 4, 29–32 (Apr. 1969).

Sarachman, T. N., Microwave spectrum of cis-2-butene, J. Chem. Phys. **49,** No. 7, 3146–3149 (Oct. 1, 1968).

Shah, J. A., Huber, M. G., Danos, M., Separability of the nuclear residual two-body interaction, Physics Letters **28B,** No. 6, 381–383 (Jan. 6, 1969).

Smith, R. V., Current developments in cryomedicine, Cryogenics **9,** No. 2, 84–89 (Apr. 1969).

Smith, R. V., Review of heat transfer to helium I, Cryogenics **9,** No. 1, 11–19 (Feb. 1969).

Smith, S. J., Photodetachment, Chapter in Methods in Experimental Physics, Vol. 7, Atomic and Electron Physics, B. Bederson and W. L. Fite, Ed., pp. 179–208 (Academic Press Inc., New York, N.Y. 1968).

Swartzendruber, L. J., Ulmer, F. H., Coleman, J. A., Direct reading instrument for silicon and germanium four-probe resistivity measurements, Rev. Sci. Instr. **39,** No. 12, 1858–1863 (Dec. 1968).

Weisman, I. D., Swartzendruber, L. J., Bennett, L. H., Resonance studies in ferromagnetic Fe_2B and Fe_2Zr, Phys. Rev. **177,** No. 2, 465–471 (Jan. 10, 1969).

Weiss, B. Z., Meyerson, M. R., The effect of mean stress on fatigue crack propagation in plates under extension and bending, J. Basic Eng. **90,** Series D, No. 3, 414–417 (Sept. 1968).

White, H. S., Jr., Data management and standardization, Mod. Data **2,** No. 5, 52–56 (May 1969).

Wiederhorn, S. M., Fracture surface energy of glass, J. Am. Ceramic Soc. **52,** No. 2, 99–105 (1969).

**Publications for which a price is indicated are available by purchase from the Superintendent of Documents, U.S. Government Printing Office, Washington, D.C. 20402 (foreign postage, one-fourth additional). The NBS non-periodical series are also available from the Clearinghouse for Federal Scientific and Technical Information, Springfield, Va. 22121. Reprints from outside journals and the NBS Journal of Research may often be obtained directly from the authors.*

U.S. GOVERNMENT PRINTING OFFICE : 1969 OL—356–078